AN ANALYSIS OF ECM PROCESS FOR ANODE SHAPE PREDICTION

A THESIS
submitted in fulfilment of the requirements
for the award of the degree
of
DOCTOR OF PHILOSOPHY
in
MECHANICAL ENGINEERING

By
V. K. JAIN

DEPARTMENT OF MECHANICAL & INDUSTRIAL ENGINEERING
UNIVERSITY OF ROORKEE
ROORKEE (INDIA)

JULY 1980

CERTIFICATE

Certified that the thesis entitled "AN ANALYSIS OF ECM PROCESS FOR ANODE SHAPE PREDICTION" which is being submitted by Mr. Vijay Kumar Jain in fulfilment of the requirements for the award of DEGREE OF PHILOSOPHY in MECHANICAL ENGINEERING of University of Roorkee, Roorkee, is a record of the candidate's own work carried out by him under the guidance and supervision of the undersigned. The matter embodied in this thesis has not been submitted for the award of any other degree.

This is further to certify that candidate has worked for a period of about thirty three months from October 1977 to July 1980 at this University for preparing this thesis.

(P.C.Pandey)
Professor
Department of Mechanical and
Industrial Engineering,
University of Roorkee,
Roorkee-247 672 U.P.(India)

Roorkee
Dated : July 15,1980

University of Roorkee, Roorkee
Certified th[illegible] Thesis/
Dissertation [illegible] for the
award [illegible] of
Philos[illegible] Engg
Mech. & Industrial
No. Ex/ 150 E191 [illegible] dated 20.1.81
A[illegible]istrar (Exam.)

ACKNOWLEDGEMENT

The author expresses his deep sense of gratitude and indebtness to Dr. P.C.Pandey, Professor in Mechanical and Industrial Engineering Department, University of Roorkee, Roorkee, for his inspiring guidance, encouragement and invaluable help throughout the course of investigation, without which this work would not have been possible.

Author wishes to thank Dr. C.P.Gupta, Professor & Head of Mechanical & Industrial Engineering Department, University of Roorkee, Roorkee, for providing necessary facilities for carrying out this work.

Author also wishes to thank Sri A.S.Upadhyay of M/S Loyd's Register of Shipping, Roorkee, Sri P.K.Jain of Civil Engineering Department and staff members of Mechanical & Industrial Engineering Department, University of Roorkee, Roorkee, for their help at different stages in this work.

Author acknowledges with thanks the cooperation of various laboratories and workshops of Mechanical & Industrial Engineering Department of this University.

Author also thanks to his wife, Mrs Kanti Jain, and children, Anekant and Syadwad, for their patience and forebearance throughout this period.

V.K.Jain

SYNOPSIS

Technical necessities of modern sophisticated industries such as, aerospace, gas turbine, nuclear, etc., have led to the development of high strength, corrosion and heat resistance but difficult to machine metals. Economic machining of such metals is not possible by conventional methods, however, they can be machined satisfactorily by unconventional methods wherein, the metal removal does not take place due to plastic deformation and the formation of conventional types of chips.

Electrochemical Machining (ECM) is one of the most commonly used unconventional type of machining methods mainly because of its adaptability to several types of operations such as turning, drilling, wire cutting, boring, deburring, etc. However, it has been felt that the capabilities of this process have not been exploited fully due to a lack of understanding of the mechanism of metal removal and difficulties experienced in tooling design.

Survey of literature reveals that majority of the researchers have attempted ECM tool design using classical theory of electrochemical machining as proposed by Tipton, or by the use of finite difference technique reported by Tipton, Nilson and Tsuei, Larsson, König, Kawafune, etc.

Analogue method and the use of empirical formulation has been suggested by Tipton, König, Pahl, Degenhardt, Ippolito and Fassolio. In addition nomographic approach has been reported by König, Ganesh, Heitmann, etc. Nilson and Tsuei, Hewson-Browne, etc. applied the complex variables technique to analyse the problems of ECM tool design. However, a comparison of experimental and analytical results in their case reveals large discrepancy. Furthermore, majority of the available analyses pertain to simple cases of plane parallel electrodes based on over-simplified assumptions.

In this thesis the Finite Elements Technique (FET) has been applied to the design analysis of the tools, for use in ECM problems. Main advantage of this method is that it is possible to analyse complex shaped machining problems hitherto considered to be difficult to solve. The technique is also easily applicable for varying boundary conditions and non-linear problems that are likely to be encountered under practical machining conditions.

Uni-dimensional finite element (FE) model (model FET-11), using simplex bar elements, has been developed and the same has been extended (named SGFET-11) for predicting the anode profile in ECM for the case of a rectangular and a cylindrical deep hole sinking operations.

Analysis of complex shaped workpieces viz., cosine wave etc., has also been attempted. Accuracy of the predicted anode profile has been found to depend upon the accuracy with which the overcut in transition zone can be computed. Available analytical and empirical equations fail to predict the overcut in this zone accurately specially when feed rate is low and consequently the equilibrium gap is high. Based on dimensional analysis of large number of experimental data, an equation has been suggested to predict the overcut in transition zone. The model FET-11 can account for the heat transferred to the tool and workpiece during machining.

The model FET-11 has been employed to analyse three types of tools - bare tool, bare tool bit and coated tool bit for three flow modes of the electrolyte such as inward flow, outward flow and side flow. It has been concluded that inward flow would give minimum dimensional variations whereas, the coated tool bit would give theoretically zero overcut for all the three modes of electrolyte flow. However, full appreciation of the TOOL BIT concept in ECM would require more experimental data.

In case of complex shaped workpieces, the electric field potential distribution within the gap does not obey Ohm's law, therefore, two dimensional FE model (FET-22 and SGFET-22) have been developed based on Laplace's equation.

In such cases, use has been made of the simplex triangular elements. This model has also been applied for the anode shape prediction in ECM of complex shaped workpieces.

To analyse ECWC process the ECM theory has been modified and has been named as "Resistances in Parallel" model. A new equation has been derived which can predict the anode shape while machining with zero and finite feed rates. The equation is dependent upon the current density(J), in contrary to the equations suggested by Tipton which predicts infinite interelectrode gap at infinite time.

To verify the proposed models, experiments have been conducted on a ECM machine developed at this University. The tool material selected during experimentation was brass whereas, the work material used was mild steel, cast low alloy steel and forged low alloy steel. Non-passivating electrolyte (i.e. NaCl) solution was used at different concentration levels. Anode profile was measured on the tool maker's microscope by using replica technique.

Comparison of current density, temperature rise, machining accuracy and anode profile between experimental and analytical results has revealed that a good correlation exists between the theory and experimentation.

CONTENTS

Page No.

ACKNOWLEDGEMENT .. i

SYNOPSIS .. ii

CONTENT .. vi

NOMENCLATURE .. ~~xiii~~

CHAPTER 1 INTRODUCTION

1.1 INTRODUCTION .. 1

1.2 ANODE SHAPE PREDICTION IN ECM .. 6

1.3 SCOPE OF THE PRESENT WORK .. 7

CHAPTER 2 SURVEY OF LITERATURE

2.1 INTRODUCTION .. 9

2.2 COMPLEX NATURE OF THE ECM PROCESS .. 9

2.2.1 Parameters Affecting Metal Removal in ECM .. 10

2.2.1.1 Valency of electrochemical dissolution .. 11

2.2.1.2 Effect of passivation film .. 12

2.2.1.3 Gas evolution and bubble formation .. 14

2.2.1.4 Electrolyte conductivity .. 16

2.2.1.5 Overpotential .. 17

2.2.1.6 Temperature gradient .. 18

2.2.1.7 Electrolyte flow velocity .. 19

2.2.2 Surface Finish .. 19

2.2.3 Discussion .. 22

2.3 THEORY OF METAL REMOVAL BY ECM .. 23

2.3.1 Introduction .. 23

2.3.2 ECM Theory .. 24

2.3.3 Optimization of ECM Parameters .. 29

2.4 ANODE SHAPE PREDICTION TECHNIQUES .. 31

2.4.1 Cos θ Method .. 31

2.4.2 Finite Difference Technique .. 32

2.4.3 Analogue Method .. 35

2.4.4 Empirical Approach .. 36

2.4.5 Nomographic Approach .. 39

2.4.6 Complex Variables Approach .. 40

2.4.7 Perturbation Method .. 41

2.5 FORMULATION OF THE PROBLEM .. 44

CHAPTER 3 ECM THEORY AND ITS APPLICATIONS

3.1 INTRODUCTION .. 47

3.2 EVALUATION OF INTERELECTRODE GAP - ZERO AND FINITE FEED RATE .. 47

3.3 OVERCUT IN THE TRANSITION ZONE .. 50

3.4 ELECTROCHEMICAL WIRE CUTTING PROCESS .. 52

3.5 ELECTROCHEMICAL BORING AND DRILLING - CYLINDRICAL HOLES USING TOOL 'BITS' .. 57

3.5.1 Theory .. 57

3.6 HEAT TRANSFER ANALYSIS OF ECM PROCESS .. 62

CHAPTER 4 APPLICATION OF THE FINITE ELEMENT TECHNIQUE TO ECM PROBLEMS

4.1 INTRODUCTION .. 68

4.2 TYPE OF ELEMENTS AND THEIR CHOICE .. 70

4.3 FINITE ELEMENT PROCEDURE IN BRIEF .. 73

4.4 FINITE ELEMENT ANALYSIS OF ECM PROCESSES .. 76

4.4.1 Introduction .. 76

4.4.2 One Dimensional FE Analysis of ECM Processes .. 76

4.4.2.1 ECM with plane parallel electrode (Model FET-11 and Model FET-12) .. 76

4.4.2.2 Electrochemical drilling and boring .. 82

(a) Cylindrical hole .. 82
(b) Rectangular hole .. 83

4.4.2.3 Electrochemical wire cutting process .. 85

4.4.3 Two Dimensional FE Analysis of ECM Process (Model FET-22) .. 86

4.4.4 Three Dimensional FE Analysis of ECM Process (Model FET-33) .. 91

CHAPTER 5 COMPUTER APPLICATIONS TO ECM

5.1 METAL REMOVAL BY EC DISSOLUTION .. 95

5.1.1 Uni-dimensional Case (Model FET-11 and SGFET-11) .. 95

5.1.2 Two Dimensional Case (Model FET-22 and SGFET-22) .. 98

5.2 A BRIEF DESCRIPTION OF SUBROUTINES USED 98

(a) Program SGFET-11 .. 98
(b) Program FET-22 .. 103

CHAPTER 6 EXPERIMENTAL PROGRAMME

6.1 EXPERIMENTAL SETUP .. 105

(a) Power Source .. 105

(b) Electrolyte Cleaning and Supply System .. 107

(c) Tool and Tool Feed System .. 111

(d) Workpiece and Holder .. 112

6.2 EXPERIMENTAL PROCEDURE AND SPECIFICATIONS

(a) Metal Removal .. 113

(b) Shape of the Hole Produced .. 115

6.2.1 Selection of Tool Material .. 116

6.2.2 Selection of ECM Electrolyte .. 117

6.3 DESIGN OF EXPERIMENTS .. 117

6.3.1 Introduction .. 117

6.3.2 Response Surface Evaluation and Design Schemes .. 119

6.3.3 Analysis of Variance .. 123

6.3.4 Design of ECD Experiments .. 124

6.3.4.1 Design of electrochemical drilling with bare tool experiments .. 124

6.3.4.2 Design of electrochemical bit drilling experiments .. 125

CHAPTER 7 ANALYTICAL AND EXPERIMENTAL RESULTS

7.1 ECM WITH PLANE PARALLEL ELECTRODES .. 126

7.1.1 Zero Feed Rate .. 126

(a) Variations in Current Density .. 127

(b) Machining Accuracy .. 127

7.1.2 Finite Feed Rate .. 127

7.1.3 Complex Shaped Electrodes .. 130

7.1.4 Effect of Tool Material on Temperature Distribution in IEG .. 141

7.2 PARAMETRIC STUDY .. 143

7.3 ELECTROCHEMICAL DRILLING WITH BARE TOOL .. 159

7.3.1 Effect of Voltage .. 163

7.3.2 Effect of Tool Diameter .. 168

7.3.3 Machining Efficiency .. 168

7.3.4 Comparison of Experimental and Analytical Anode Profiles .. 168

7.3.5 Experimental Observations .. 176

7.3.6 Overcut in Transition Zone in ECD .. 176

7.4 ELECTROCHEMICAL DRILLING WITH BARE TOOL USING DESIGN OF EXPERIMENT TECHNIQUE 180

7.5 ELECTROCHEMICAL WIRE CUTTING PROCESS .. 180

7.5.1 Zero Feed Rate .. 185

7.5.2 Finite Feed Rate .. 185

7.6 ELECTROCHEMICAL DRILLING WITH BARE TOOL BITS .. 185

7.7 ELECTROCHEMICAL BORING WITH BARE TOOL BITS .. 198

CHAPTER 8 DISCUSSION

8.1 ECM WITH PLANE PARALLEL ELECTRODES .. 200

8.1.1 Zero Feed Rate .. 200

8.1.2 Finite Feed Rate .. 201

8.1.3 Complex Shaped Electrodes .. 202

8.1.4 Effect of Tool Material on Temperature Distribution .. 203

8.2 PARAMETRIC STUDY OF ECM PROCESS .. 204

8.2.1 Zero Feed Rate .. 204

8.2.1.1 Effect of electrolyte flow velocity .. 204

8.2.1.2 Effect of electrolyte flow mode .. 207

8.2.1.3 Interelectrode gap .. 207

8.2.2 Machining with Finite Feed Rate .. 208

8.2.2.1 Effect of feed rate .. 208

8.2.2.2 Interelectrode gap .. 209

8.2.2.3 Electrolyte flow velocity .. 209

8.3 ELECTROCHEMICAL DRILLING .. 210

8.3.1 Effective Voltage and Anode Profile .. 210

8.3.2 Tool Diameter and Anode Profile .. 213

8.3.3 Machining Efficiency .. 215

8.3.4 Analytical and Experimental Anode Profile During ECD .. 215

8.3.5 Presence of Striations on Work Surface .. 219

8.3.6 Overcut in Transition Zone in ECD .. 221

8.3.7 Study of ECD with Bare Tools Using 'Design of Experiments' .. 222

8.3.8 Study of Electrochemical Bit Drilling (ECBD) Using Design of Experiments .. 223

8.4 ELECTROCHEMICAL WIRE CUTTING .. 224

8.4.1 Zero Feed Rate .. 224

8.4.2 Feeding Electrode .. 225

8.5 ELECTROCHEMICAL DRILLING WITH BARE TOOL BIT .. 226

8.6 ELECTROCHEMICAL BORING WITH BARE TOOL BIT .. 227

CHAPTER 9 CONCLUSIONS AND SCOPE FOR FUTURE WORK

9.1 CONCLUSIONS .. 228

9.2 SCOPE FOR FUTURE WORK .. 231

REFERENCES .. 233

APPENDIX-1 (Tables) .. 250

APPENDIX-2 (Computer Programmes) .. 264

APPENDIX-3 (Dimensional Analysis) .. 276

.. ..

NOMENCLATURE

A	Cross sectional area
$[A]$	A matrix of nodal coordinates
$A', a, a_1, a_2, a_i - a_j$	Constants
A_V	Applied voltage
a_g, a_o, a'_s, a_s	Interelectrode gaps (or overcut) (See Fig.3.2)
$B', B_1 - B_5$	Constants
$[B]$	A matrix that contains information related to derivatives of the shape functions.
b_b	Bare length of the electrode (or tool-bit height).
$b, b_i - b_j$	Constants
C_e	Specific heat of the electrolyte
$C_d, c, C, C_i - C_j, C'$	Constants
D	Tool diameter or tool-bit diameter
$[D_m]$	Unitary or elasticity matrix
d_i, d_j	Constants
E	Electrochemical equivalent
E_V	Effective voltage
e_u	Experimental error
F	Faraday's constant
FET	Finite element technique
FDT	Finite difference technique
F_a, F_c	Shape factor for anode and cathode respectively
F_F	Front feed rate
F_s	Feed rate in the side gap
f	Factor

G	Grand total
g	As defined in chapter 4
Gr	Grashof number
H	As defined in chapter 4
H^*	Height
h	Convective heat transfer coefficient
I	Functional
I_c	Electric current
IEG	Interelectrode gap
J	Current density
K	Electrolyte electrical conductivity
$[K]$, K_m	Stiffness matrix or conductance matrix
K_{ij}	Coefficients of stiffness matrix
KIN	An index used to count the number of computational cycles.
k^*	Wave number
k	Thermal conductivity
L^*	Characteristic length
L	Length of the electric resistance
L_e	Element length
l	Level of the factors (or variables)
MRR	Metal removal rate
M	Any metal
m	Metal removed
m_a, m_t	Actual and theoretical metal removed respectively
$[N]$	Shape function matrix

NE	Total number of elements
NN	Total number of nodes
n	Exponent
n_a, n_c	Natural convection for the cases of anode and cathode respectively.
n_1, n_2	Constants
n'	Length of a normal drawn at the anode surface
n_s	Number of sparks per unit length of drilling
P	Electrolyte pressure in the interelectrode gap
P^*	Distance from the centre of the region
P_r	Prandtl number
p	Mean gap between electrodes
Q	Electrolyte flow rate
$[Q]^e$	A matrix that gives initial and applied loads
q^*	Heat transferred to environment
$q(x, y)$	Column vector of displacement at any point (x, y)
R^*	Thermal resistance
R	Electrical resistance
R_{c1}, R_{c2}	Constants
R_{ex}	Reynold's number at any point 'x'
R_g	Gas constant
r	Radius
s	The coordinate that specifies average surface
T	Temperature
t	Machining time
V	Electrolyte flow velocity
v	Volume

W	Width
x	Distance along electrolyte flow direction (or x-coordinate)
x^*	Level of a factor
X	Column vector
y	Coordinate measured in y-direction
Y	Interelectrode gap
Y^*	Response or yield
Z	Valency of EC dissolution
z	Coordinate measured in z-direction
α	Temperature coefficient of electrical conductivity of the electrolyte.
α^*	Level value
α'	Temperature coefficient of thermal conductivity
α_{dis}	Coefficient of the degree of dissociation
α_v	Void fraction coefficient
β	Constant
β^*	A ratio of gas volume to liquid volume
Δ^e	Area of an element
ΔT	Incremental change in temperature
Δt	Computational cycle time
ΔA_v	Over potential
ΔA_{va}	Activation over potential
ϵ^*	Amplitude of surface irregularity
ϵ_a, ϵ_c	Emissivity of anode and cathode respectively
ϵ	Strain
η	Current efficiency or machining efficiency
θ	Angle between the direction of feed and normal to the tool (or work) surface

θ^*	$T_{wall} - T_{air}$
λ	Wave length
λ^*	Constant
ν, ν'	Correction factors
ν^*	Kinematic viscosity
	Constant
ρ	Mass density
ρ_o	Volumetric concentration of hydrogen gas
σ	Stress
σ^*	Stefan Boltzman constant
ϕ	Electric field potential

SUBSCRIPTS

a	anode
BL	Bottom left
b	boring, bare
c	corner; cathode
d	drill tool, drilling
e	electrolyte, element, equilibrium
F	front
FL	front left
FR	front right
fc	forced convection
g	gas
i,j	node number
l	linear, liquid

L	left
m	work material
max	maximum
n,nc	natural convection
o	initial condition
R	right
r	radiation, condition at any point 'r'
s	sparks, spike, side, specific
t	condition at time 't'
TL	top left
tot	total
u	u^{th} observation
v	volumetric, volume
x	condition at any point 'x'

SUPERSCRIPT

e	element
T	transpose of a matrix
(1),(2),etc.	element number

CHAPTER - 1

INTRODUCTION

1.1 INTRODUCTION

Rapidly advancing technology has placed increasingly severe demand upon the metal cutting industries. Three principal types of requirements demanded from the present day metal cutting technology are versatility, accuracy and productivity (154)*. Thus, there is a need for machine tools and processes which are more readily and accurately controlled, and can machine readily (117) even the most difficult materials to intricate and accurate shapes. In order to meet this challenge, a number of newer metal removal processes viz., electrochemical machining (ECM), electric discharge machining (EDM), electron beam machining (EBM), laser beam machining (LBM), ultrasonic machining (UM), etc. have now developed to the stage of commercial utilization. Out of these, electrochemical machining (ECM) appears to have the greatest potential for satisfying (158) the need setforth herewith.

The principle of metal removal by electrochemical dissolution was known (159) to the scientists and engineers as long back as 1780 AD but it is only over the last few years that this method has been used to advantage. ECM (also known (223) as contactless EC forming) has been described (7,8,14,124,185, 226,227), as the process of accelerated, controlled anodic corrosion and is achieved by means of high velocity electrolyte flowing between the anode and cathode (Fig.1.1) subjected to a small d.c. voltage and maintaining a small interelectrode gap (IEG) between them. The electrolyte serves multifarious purposes viz., takes away the heat generated during machining (13,88), allows high rate of metal dissolution, removes the reaction products, etc. Rate and direction of anodic dissolution in the process depends (13,88) upon the applied voltage, electrolyte conductivity, current density, anode material, electrolyte flow velocity, presence of anodic film, etc.

---

*Underlined numbers in the brackets refer to references given at the end.

Over the years, ECM has found wide applications in a number of practical machining operations viz., turning (21,62,86, 165,166,229), trepanning (82,163), broaching (59,229), grinding (122,123,180,188), fine hole drilling (15,100), die sinkings (39,74,176), cavity sinking (108,206), piercing (146,179), deburring (148,192), plunge cutting (82,83), etc. and is being used widely in aeronautics (187,237), nuclear (211), and space industries (110). Some of the typical examples of ECM applications are: machining of turbine blades (158-160,202) made of high temperature and high strength alloys (78,94,111,153,183), copying of internal and external surfaces (102), cutting of curvilinear slots (204), machining of intricate patterns (64,87,124,153,186), production of long curved profiles (143,154,156), machining of

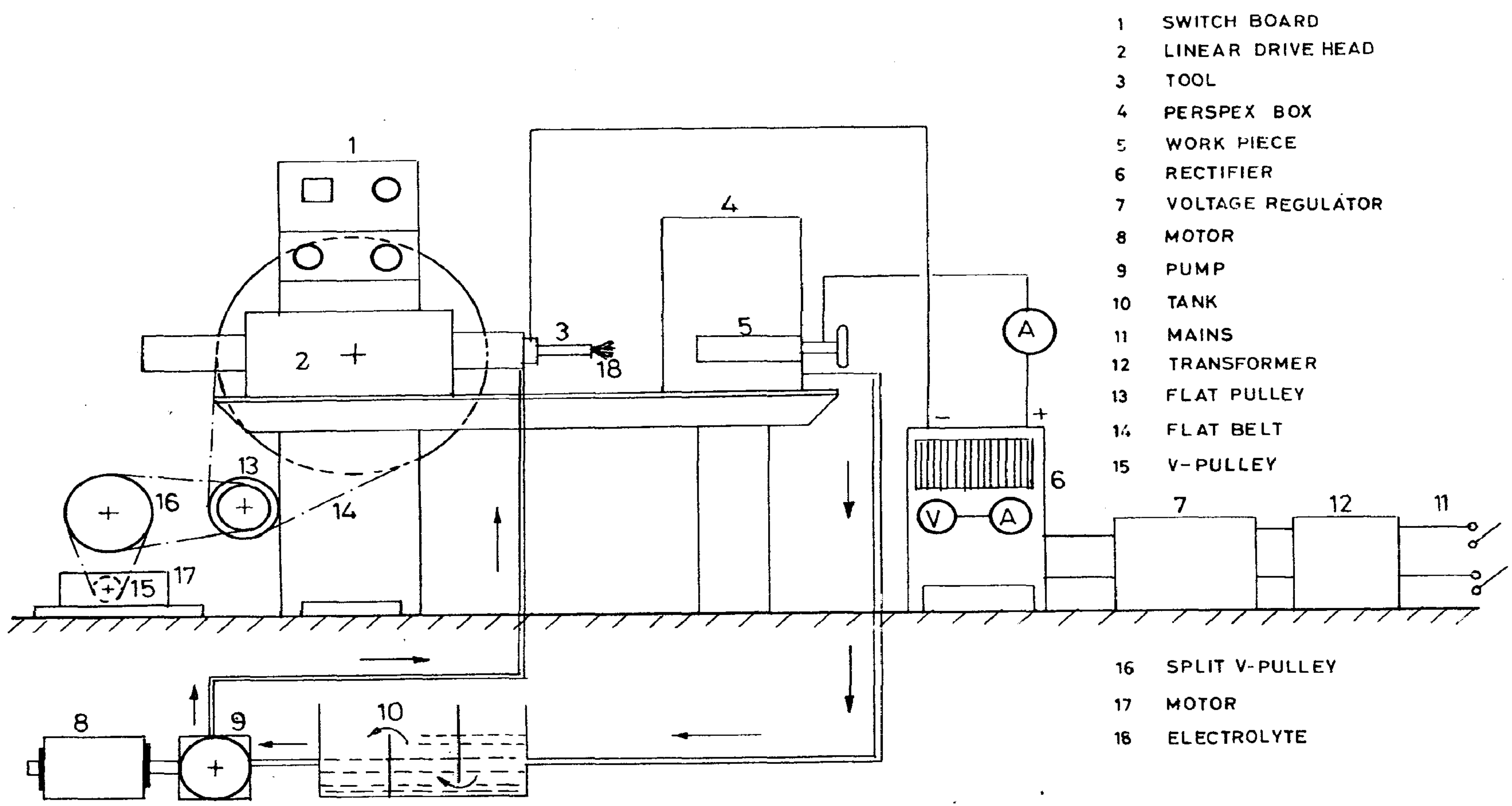
1 SWITCH BOARD
2 LINEAR DRIVE HEAD
3 TOOL
4 PERSPEX BOX
5 WORK PIECE
6 RECTIFIER
7 VOLTAGE REGULATOR
8 MOTOR
9 PUMP
10 TANK
11 MAINS
12 TRANSFORMER
13 FLAT PULLEY
14 FLAT BELT
15 V-PULLEY
16 SPLIT V-PULLEY
17 MOTOR
18 ELECTROLYTE
1
2
3
18
4
5
A
−
+
6
V
A
7
12
11
13
16
14
17
15
8
9
10

FIG. 1.1 SCHEMATIC LAYOUT OF ELECTRO — CHEMICAL MACHINE

gears (30,174), production of integrally bladed nozzle-rings for use in diesel locomotives (202), production of stellite rings and connecting rods (176), machining of thin (80 microns) large diameter diaphragms, etc.

The process has several advantages to offer e.g., machinability of work material is independent of the strength of the material being machined (16,48,105,106,157,163,205), production of stress and burr free surfaces (178,224), comparatively good surface finish (9,58,65,67,140,187,225,228), better corrosion resistance of the parts produced, low overall (158) machining time (e.g. about 20 minutes in ECM and 494 minutes by conventional method in machining a turbine blade) and better working accuracy (33,61,139) independent of the operator's skill (85), However, ECM has its own limitations, that is, it involves high capital investment, and can be employed only for electrically conductive materials (117); machining of materials with hard spots, inclusions, sand and scale present difficulties (158). Production of very sharp corners also presents problems. ECM under certain circumstances has been found to be incapable of producing economically the dimensional tolerances desired on the anode. To overcome this, researchers are constantly and continuously engaged in improving upon the ECM system-technology and equipments.

To meet the accuracy requirements in ECM, whilst machining alloys and metals, a number of new electrolytes have been tried and incorporated in the catalogue of ECM electrolytes (36,42,59,78,85,96,125,146,162) viz., $NaClO_3$, $NaNO_3$, K_2CrO_4, Na_2SO_4, KBr, NH_4F, NH_4NO_3, K_2CO_3, etc. In some cases special additives (8,10,57,80,162) can be added to the electrolyte solution, called as buffers to stabilize the solution pH value, to act as corrosion inhibitors and coagulants. Cogulants assist in settling the sludge and facilitate subsequent purification of the solution. Efforts have also been made to further improve upon the machining accuracy beyond 0.05-0.15 mm in producing through holes and 0.2-0.5 mm in sinking complex shape cavities (163,190). Special purpose ECM machines are (163) also now available for the production of turbine blades. Such machines employ pulse cycle conditions (38,131,163,169) and presently efforts are being made to improve upon their reliability. Machines with NC and adaptive controls (169,195) have also been developed.

Over the last few years, efforts have been continued to present a generalised theory of metal removal by EC dissolution. Some of the areas of research in ECM are, anodic behaviour of metals and alloys using various electrolytes (69,119, 141,188), effects of process parameters on productivity and machining accuracy (121,200), surface quality (10,27), performance characteristics of machined metals and evaluation of machinability, etc. Mathematical models for the EC form generation (191) and tool design, which simulate the actual working conditions satisfactorily have also been developed for simple shaped components.

However, the author feels that the potentials of ECM as a production process, have not been explored fully due to practical difficulties encountered in the design of tools, complex nature (112,113) of the process of metal removal and due to difficulties encountered in prediction of the anode shape obtained under the given set of operating conditions.

1.2 ANODE SHAPE PREDICTION IN ECM

Tool design (3,45,118,148,208,210,213) in ECM deals with the computation of the tool-shape, which under the specified conditions would produce a work having prescribed shape and accuracy. Alternatively, it also deals with the prediction of anode (work) shape (173-184) obtainable from a tool while operating under specified conditions of machining. Majority of the available literature (17), in the field of tool design deals with this latter problem.

For the computation of work shape, obtainable from a tool of known geometry, a number of analytical models are available, these are based on classical ECM theory (212), cos 'θ', method (212,214), analogue method (178,210), empirical formulae (92,110), nomographs, (72,74,110), complex variable analysis (118,170-172) and finite difference technique (90,113, 170,210). Majority of these models do not yield accurate results because they are based on over simplified assumptions and are incapable of analysing geometrically and materially non-linear problems, normally encountered during ECM. They also do not account for the effects of simultaneous variations (i.e. interactions) in important machining parameters. Further, the dependence of anode shape generation, in ECM, on ECM parameters has not been well understood. It has also not been possible to account for the effects of the mode of electrolyte flow, heat transferred to electrodes, microstructure, grain boundary attack, anodic film (40,41), etc., on the accuracy of the workshape produced.

1.3 SCOPE OF THE PRESENT WORK

The work embodied in this thesis has been aimed towards the development of a computer aided method viz., the application of finite element technique for the analysis of EC dissolution processes specifically in ECM, electrochemical drilling (ECD), electrochemical boring (ECB) and electrochemical wire cutting (ECWC) - and for the prediction of anode shape obtained. Computer programmes that have been developed are of general nature and require little input data, most of the data needed for the analysis is generated by the computer itself.

To analyse some of the processes based on EC dissolution principle, modifications to existing classical ECM theory have been suggested. In order to evaluate the overcut in transition zone and to predict the anode profile, new working equations, that are simple and economical to use, have been suggested. For improved accuracy in the analysis of the ECM process, thermal resistance model of process has also been formulated.

In order to check upon the validity of the proposed analytical models, experiments in ECM were conducted and a good agreement between analytical and experimental results has been observed.

CHAPTER - 2

SURVEY OF LITERATURE

2.1 INTRODUCTION

Available literature (8,17) pertaining to electrochemical machining (ECM) research is quite vast and hence it is not possible to review the entire amount of literature available. This chapter presents a brief review of the work done in the area of ECM tool design. Some of the problem areas where more research is needed have been identified and its importance highlighted.

2.2 COMPLEX NATURE OF THE ECM PROCESS

The basic analytical model for the computation of the volume of metal removed in ECM operation, is based on the application of Faraday's law of electrolysis (Eq 2.1)

$$m = \frac{E.I_c.t}{F} \quad .. \quad (2.1)$$

This equation is based on a number of simplified assumptions such as :

(i) metal dissolution efficiency is constant and equal to 100%,

(ii) valency of the work material being machined remains constant throughout,

(iii) the electrolyte properties are uniform over the entire working area and do not change with time,

(iv) overpotential is zero,

(v) metallurgical properties of the work material are uniform and,

(vi) effect of presence of gases evolved during the process, on metal removal is negligible.

The process variables that also influence the rate of EC dissolution, and surface generation in ECM have been discussed by Rourke and Kennedy (123) and are listed below:

Process variables	Process characteristics that are influenced
Voltage	Metal removal rate
Electrolyte viscosity	Process efficiency
Electrolyte pressure	Surface finish
Electrolyte temperature	Surface texture
Electrolyte velocity	Shape : reproducing size
Electrolyte composition	Shape : tolerance of form
Feed rate	
Current distribution	
Electrolyte contamination	
Work material	
Tool material	

2.2.1 Parameters Affecting Metal Removal in ECM

As mentioned earlier, Eq(2.1) is based on a number of simplified assumptions and does not account for the effects of some of the significant process variables. As a result, this equation cannot be expected to yield accurate results under actual working conditions. The following sections briefly examine the effects of electrochemical process parameters on metal removal in ECM.

The MRR in ECM is governed by many factors not accounted for in Eq(2.1) viz., change in valency of EC dissolution during the operation, presence of passivation film (11,37), gas evolution and bubble formation, electrolyte conductivity and temperature variation during the process and along the electrolyte flow path, over potential, etc. Survey of literature shows that extensive information on the above is lacking and contradictory findings have sometimes been reported about their effects on MRR and surface finish.

2.2.1.1 Valency of electrochemical dissolution

It has been reported (59,157,216) that during ECM, a material would not necessarily dissolve at a constant valency throughout. For example, dissolution of iron in NaCl solution may be either in the form of ferrous hydroxide (Fe^{2+}) or ferric hydroxide (Fe^{3+}) depending upon the machining conditions. Copper (148) in chloride solution can dissolve in monovalent state whereas, in nitrate solutions it can assume a divalent form. In machining of En 58J Steel (156,157), dissolution has been found to occur at alternative valency combinations of Fe^{3+} Cr^{6+} or Fe^{2+} Cr^{3+}. Mode of dissolution while machining complex alloys (224,225) is still more difficult to analyse.

In such cases, the differential dissolution of the constituents of the alloys can take place, the mechanism of which is not understood well. In majority of the cases, the preferential valency mode (156) of dissolution has been found to depend upon the electrolyte flow rate, IEG, length of electrolyte flow path and MRR. Incorrect assumption regarding the valency of dissolution can often lead to current efficiency (148,149) values of more than 100% thus introducing appreciable amount of error in the values computed from Eq(2.1).

2.2.1.2 Effect of passivation film

Passivity arises as a result of the chemical and electrochemical behaviour of metals due to the formation of a protective film on their surface. Accordingly it is termed as chemical or mechanical passivity (200). Chemical passivation is caused due to rapid formation of very thin, invisible and imprevious oxide layer having low ionic conductivity during machining. The oxide layer becomes firmly attached to the electrode material and acts as a barrier to the current flow. It can either retard the rate of dissolution or lead to total passivation. Scanning electron microscope studies (217) have revealed the presence of solid film formed by solid state mechanism (27,218) on the anode surface, at potentials prior to electropolishing regime (400 mV). During EC dissolution of copper in NaCl, a film of cuprous chloride is formed while at higher anodic potentials cupric species are produced. Increase in electrolyte flow rate results in film thinning, thus delaying the formation of the film necessary for passivation.

Mechanical passivity is caused due to build up of a protective and comparatively thick layer of excess of metal ions in diffusion layer. Experiments by Chin (41) have revealed that during EC dissolution of 'Fe' in NaCl solution, the rate of film deposition, which is diffusion controlled process, and the film size were found to increase with ferrous concentration, pH of the electrolyte and rotational speed of the platinum ring electrode. The film was found to contain γ-FeOH and is produced as a result of anodic oxidation of the $FeOH^+$ ions in the solution. Presence of the oxide film reduces the active area available to the Fe^{2+}/ Fe^{3+} ions and the oxidation reaction causes the current to decrease. The oxide film is assumed to be porous so as to allow an easy passage to cations through it but hinders the movement of the reaction products and hence reduces the MRR. At higher current densities the film becomes thinner leading to an increase in MRR.

The passivating film is soluble in low pH electrolyte. This condition can be achieved due to presence of oxygen and ferrous or ferric hydroxide in the vicinity of the anode surface. For example, addition of $NaClO_4$ in $NaClO_3$ electrolyte increases the current efficiency and at higher concentrations of $NaClO_4$; it reacts with the oxide film causing pitting and severe grain boundary attack leading to current efficiency values of more than 100%. Low rate of machining observed in case of tungsten carbide (50) is due to the formation of oxide layer which could be blasted off by the intermediate use of reverse polarity.

Thus, it can be seen that a definite relationship, which can correlate the passivation to the MRR does not exist. Further, sufficient data on the extent of passivation caused by the electrolytes, when different materials are machined is not available.

2.2.1.3 Gas evolution and bubble formation

As a result of chemical reaction during ECM, gases are evolved. Equations given below show that during EC dissolution, hydrogen and oxygen are evolved and this leads to low dissolution efficiency specially at reduced current density.

Two kinds of reactions, as described below, occur at the cathode viz; plating of metal ions and evolution of hydrogen gas.

Metal plating:

$M^+ + e^{-1} \rightarrow M$ (M is any metal) .. (2.2a)

Hydrogen gas evolution:

$2H^+ + 2e^- \rightarrow H^2 \uparrow$ (in acid solution) .. (2.2b)

$2H_2O + 2e^- \rightarrow 2(OH)^- + H_2\uparrow$ (in alkaline solution) (2.2c)

Under the given conditions whether plating or hydrogen gas evolution will take place is governed by the electrode potential.

Similarly, two kinds of reactions take place at the anode viz., metal ion dissolution and oxygen gas evolution as follows:

Metal dissolution:

$M \rightarrow M^+ + e^-$ (acidic solution) .. (2.2d)

$M^+ + (OH)^- \rightarrow MOH + e^-$ (in base solution).. (2.2e)

Oxygen gas evolution:

$2H_2O \rightarrow O_2\uparrow + 4H^+ + 2e^-$ (in acid solution) (2.2f)

$4(OH)^- \rightarrow 2H_2O + O_2\uparrow + 4e^-$ (in alkaline solution)(2.2g)

Since part of the current through cell is associated with oxygen evolution at the work surface and therefore, current efficiency is normally below 100%.

During hole sinking by electrochemical methods the side flow region (127) experiences low current density as well as low electrolyte flow velocity. This results into the formation of gas bubbles of small size, however, no practical method is available to observe their presence. Further, it has not been possible to derive a simple quantitative relationship between the gas volume fraction and the cell voltage at different current density values. It has therefore been concluded (206) that the effects of electrolyte flow, hydrogen gas and temperature in the side flow region are negligibly small compared to that prevailing in frontal gap region. Hopenfield and Cole (87) are of the view that the amount of oxygen evolved is too small for realistic considerations; similarly presence of chlorine can be neglected due to its high solubility in water. A two phase flow analysis of the ECM process has been given by Fluerenbrock (71) wherein, it was assumed that the gas and liquid exist at the same pressure and temperature, based on this they derived the balance equation of the process.

2.2.1.4 Electrolyte conductivity

Electrolyte conductivity, (K) is determined by the type and number of the ions present in the electrolyte and their mobility. The degree of dissociation (α_{dis}) of an electrolyte is also important and is defined as the fraction of solute that dissociates into ions that are free to carry current for the given electrolyte concentration. Strong electrolytes have high value of α_{dis} for both low and high concentrations but weak electrolytes (used as additives) yield a value of α_{dis} close to unity at low concentrations and approximately equal to zero at high concentrations. Electrolyte concentration, therefore, is not a true indication of the ability of ions to determine the properties of an electrolyte. α_{dis} is also a function of the electrolyte temperature. In addition, the electrolyte conductivity is influenced by the presence of gases, such as hydrogen in the form of bubbles and due to sludge, etc. In the absence of effective filtration, addition of ionic salts like ferrous or/and ferric hydroxide to the electrolyte could increase the electrolyte conductivity and thereby influencing the accuracy of the results given by Eq(2.1). On the other hand the positive charges in the solution and negative charges in the metal form what has been termed as the double layer. The transfer of ions will clearly cease when the energy required for an ion to dissolve is less than the work done in crossing the double layer.

Electrolyte conductivity, is also a function of electrolyte temperature. Normally, in practice, the temperature distribution (46) obtained in IEG is non-linear. The value of temperature coefficient of electrolyte conductivity, α , varies (135) but for simplification, in majority of the models, it has been assumed to be a constant.

It should also be noted that the bulk of available EC data concerning low current density, low flow velocity and low concentration cannot necessarily be related to ECM.

2.2.1.5 Overpotential

Overpotential ΔA_V can have a significant effect on the MRR and the anode surface finish. It is defined as the difference between the values of equilibrium and working voltages. There are three specific types of overpotentials: activation, concentration and resistance overpotential (148).

Activation overpotential can be calculated from Tafel's Eq(2.3).

$$\Delta A_{va} = A' + B' \log J \qquad \text{..} \qquad (2.3)$$

When the rate of metal dissolution is greater than the rate at which metal ions can diffuse away, a situation is created wherein an ionic concentration gradient develops over a thin layer of the electrolyte adjacent to the electrodes. This layer is called the diffusion layer. The concentration gradient leads to a change in the electrode potential from the reversible value. The numerical difference between the reversible and new value is known as concentration overpotential. However, resistance overpotential (148) is regarded as the potential drop across a thin layer of the electrolyte (or oxide film) on the electrode surface.

Overpotential governs the actual effective working voltage across the IEG as follows:

$$E_V = A_V - \Delta A_V \qquad \text{..} \qquad (2.4)$$

It should be noted that unless the exact value of ΔA_V for the given conditions is known, accurate computation of the MRR is not possible.

2.2.1.6 Temperature gradient

A temperature gradient exists along the IEG (46) mainly due to joule's heating of the electrolyte. As a result of this, the electrolyte conductivity varies. This also leads to variations in IEG along the electrolyte flow direction. Accurate computation of the temperature gradient is difficult, mainly on account of a number of parameters governing the process and hence the predicted results normally differ from the (46,148) corresponding experimental data.

2.2.1.7 Electrolyte flow velocity

ECM is normally applied to all categories of work i.e., simple shaped to highly complex shaped workpieces. The electrolyte flow conditions are normally evaluated assuming that equation of continuity of electrolyte mass flow holds true. However, in case of complex shaped workpieces, this is not true. At the discontinuity in the configuration, electrolyte starvation occurs; due to friction and other losses, flow rate is changed. Further, in practice the flow velocity along and across the flow path is varying and is different from the theoretical one obtained from Eq(2.14). Hence, the use of conformal mapping technique (98,230) has been recommended for an accurate computation of the flow velocity within the IEG.

It should be noted that unless accurate flow velocity distribution within the gap is known, prediction about anode profile and other parameters would not be precise enough.

2.2.2 Surface Finish

In ECM of alloys, differential dissolution of the constituents due to difference between electrode potential may take place. This leads to variations in surface finish obtained under different machining conditions. However, at higher current densities, the difference between the electrode potentials of the constituents is reduced and better surface finish can be expected.

A grain projecting out of the surface being machined (59) may sometimes have a high (or low) electrode potential; under these conditions the material in the vicinity of the grain will be machined (or not machined) leaving the grain protruding (or the formation of a recess) as shown in Fig. 2.1. Recess formation is often known as grain boundary attack. Increased traction forces drag out such grains resulting into roughening of the machined surface.

An irregular (148) anode surface may also cause flow separation between the hills and the valleys of the surface. Around the hills, due to dissolution of both large and small scale irregularities, polished surface is produced. In the valleys, rotating eddy current gives rise to concentration of metal ions, concentration overpotentials and hence etched finish. Surface finish has also been found (34,70,108,129) to depend upon the electrolyte flow velocity and current density. Many times, in ECM configuration with radial outward flow, presence of striations or flow lines have been observed by the author (Fig.2.2). This phenomenon has been explained by Fluerenbrock (71) on the basis of ECM sonic velocity theory; Cole (48) has attributed the formation of streaks or striations to a certain

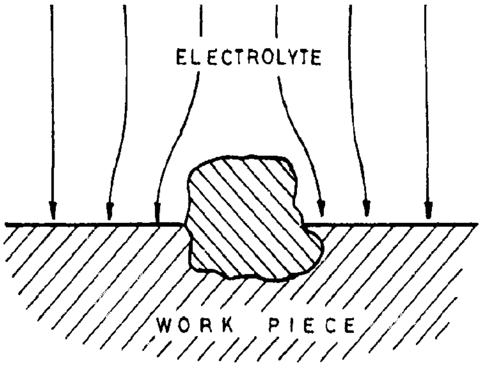
ELECTROLYTE
WORK PIECE

FIG. 2.1 EFFECT OF VARIATION IN COMPOSITION OF WORK PIECE

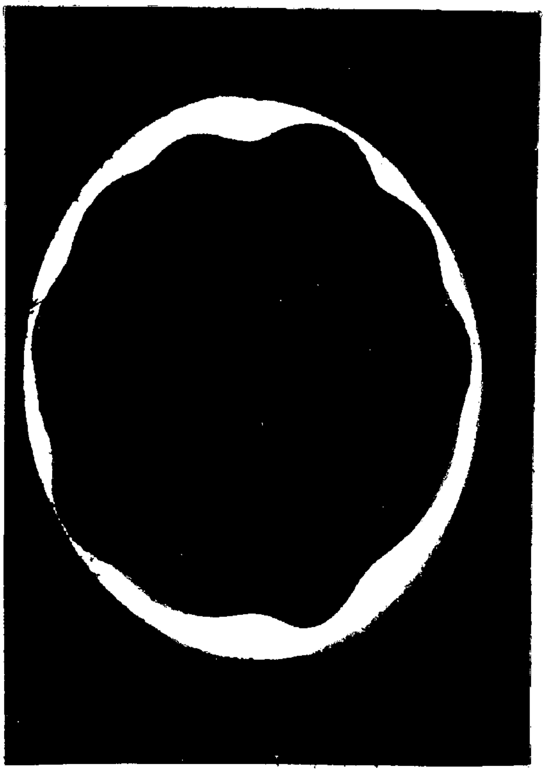

FIG. 2.2 STRIATIONS OBSERVED DURING ECD OF MILD STEEL

combination of electrolyte pressure and flow rate. However, the mechanism of the formation of striation has not yet fully been analysed. Opitz (176) has explained this on the basis of cavitation (196) theory. One of the remedies to overcome the roughening of surfaces due to the formation of streaks is to inject gases such as O_2, N_2, etc., into the electrolyte; this helps in agitating the electrolyte which has beneficial effects. The pH value of the electrolyte, during ECM, also plays an important role in the surface generation. In addition it has also been reported (156,157) that the valency of EC dissolution affects the surface finish produced. For example, presence of Fe^{3+} Cr^{6+} during machining of alloy steels is characterised by the generation of bright polished surface whereas, the formation of Fe^{2+} Cr^{3+} is accompanied by the production of grey rippled surface.

2.2.3 Discussion

From the above it is evident that metal removal in ECM depends upon a large number of interrelated parameters. In order to develop analytical models for the metal removal in ECM, the present state of knowledge is insuffient. Quantification of some of the governing parameters and the manner in which they interact is not well understood. Similarly, the surface finish obtained in ECM is governed by a number of interdependent variables and little work has been done towards the development of analytical models to predict the surface finish in ECM and the related processes.

2.3 THEORY OF METAL REMOVAL BY ECM

2.3.1 Introduction

Trial and error methods are often employed for obtaining the profile of the ECM tools that would produce a work of given dimensions and profile. In such cases, the tool need not be a mirror image of the work shape to be produced and requires certain corrections to its profile. Another alternative is to calculate working gap and account for the same during the tool manufacture. With the availability of high speed computers it is now possible to determine the tool shape that would yield a work of specified geometry, by successive approximation technique. Since the computing time is only a fraction of that required for carrying out the trial and error experiments; analytical correction of the tool is recommended as it saves time and is economical.

Over the years, a number of analytical models for obtaining the anode shape and the design of ECM tools, have been developed. Since the ability to predict the variation in IEG for any given operating conditions is a pre-requisite of a good tool design hence, in successive paragraphs these models are discussed in terms of the equilibrium gap.

2.3.2 ECM Theory

The workshape obtainable from a given tool, under ideal conditions can be computed from the corresponding equilibrium gap. However, as discussed earlier, the results thus obtained are influenced by a large number of parameters (31,32) such as the presence of anodic film (42-44,57,77,130,144,149,187), electrolyte flow rate (157), work-material microstructure (114), intergrannular attack (115,116), change in valency of EC dissolution during cutting (157), type of electrolyte (76,79-85, 95) and the role of additives (10,77), current density (52,56), electrolyte throwing power (126), electrolyte pressure distribution within the IEG (203), stray current attack, passivity (76,83,85), etc. In some cases, the exact influence of the controlling parameters is not very clear.

Fig. 2.3 shows 4 distinct regions of electrolyte flow in EC hole sinking operation. It should be noted that majority of the research (48-50,70,71,75,87,88,91,105-108,110-114,136-138, 150-152,170-172,205-215), pertaining to metal removal by hole sinking tools, deals with front and side gaps only, whereas, scanty or no information is available about the mode of material removal in transient (92,112,113) and stagnation regions (132-134). This information is of practical value as the complete profile of the drilled hole is determined by metal removal in

(i) side gap (Zone 4)
(ii) front gap (zone 2)
(iii) transient region (zone 3)
(iv) stagnant region (zone 1)

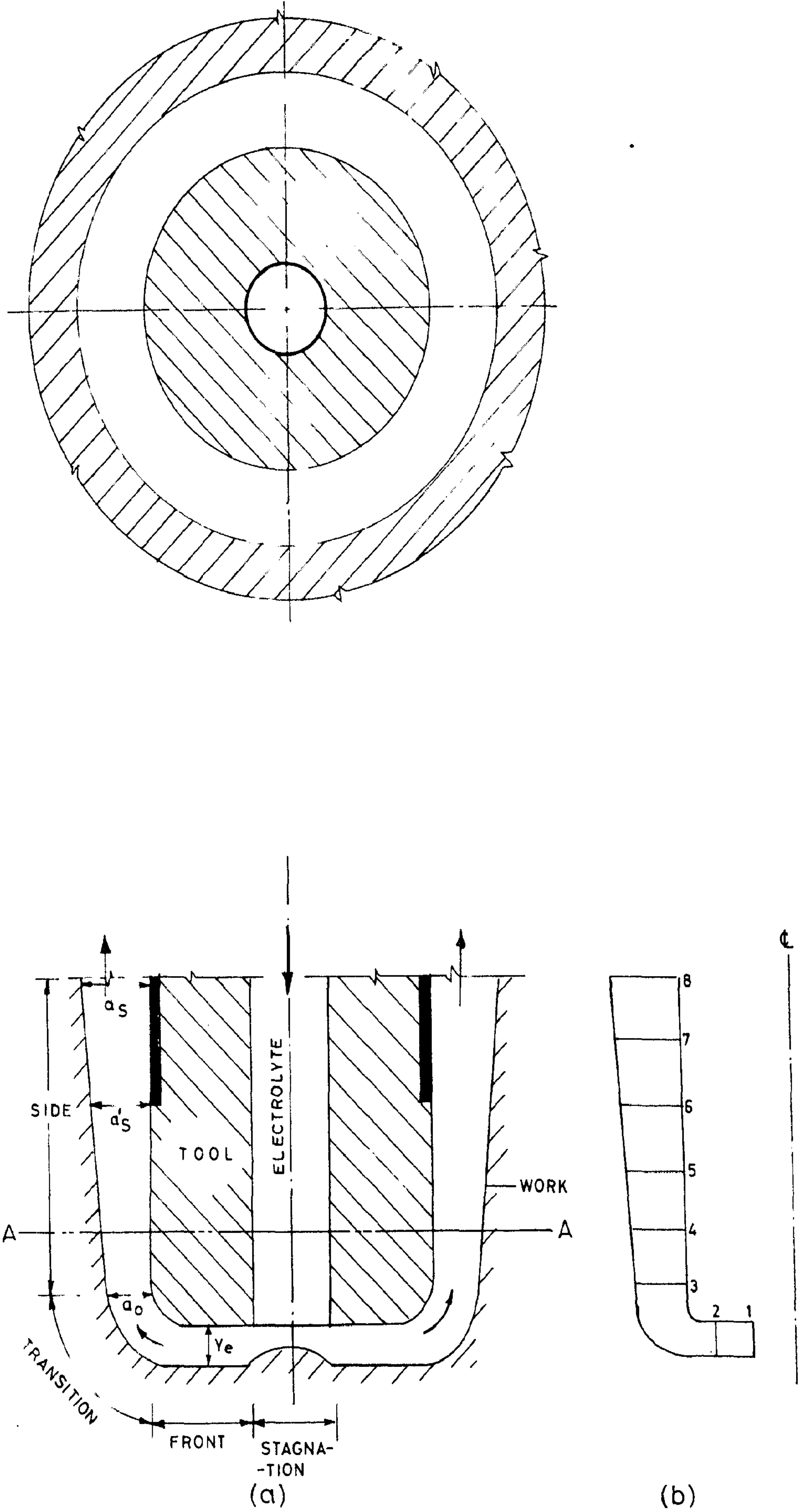
SIDE
a_s
a'_s
TOOL
ELECTROLYTE
WORK
A
A
a_o
Y_e
TRANSITION
FRONT
STAGNA-
-TION
℄
8
7
6
5
4
3
2
1

(a) (b)

FIG. 2.3 ELECTROLYTE FLOW REGIONS IN HOLE SINKING OPERATION

Equilibrium gap (59,148) can be evaluated from Eq(2.5) (for the case shown in fig.2.3)

$$Y_e = \frac{E_V.K.E}{F.F_F.\rho_m.\cos\theta} \qquad .. \qquad (2.5)$$

Eq(2.5) applies to zones 2 and 4 only and when non-passivating electrolytes are used. This equation is based on the assumption that electrolyte conductivity 'K' remains constant during the process. However, K is known (70,71,206,207) to be a function of electrolyte temperature, void fraction, nature of voids distribution within the IEG, electrolyte concentration, efficiency of electrolyte filtration (164), etc. For the computation of K, Eq(2.6) has been proposed (106) which accounts for the effects of electrolyte temperature and hydrogen liberation only.

$$K = K_o(1 + \alpha \cdot \Delta T)(1-\alpha_V)^n \qquad .. \qquad (2.6)$$

In Eq(2.6), Hopenfield and Cole (87) recommend that a value of n=1.5 be used when the void distribution is uniform whereas, for non-uniform distribution specially, when bubbles are concentrated near the cathode, a value of n=2.0 gives better results (70,71,206,207). For the computation of void fraction (α_V) under the given conditions (35,87,88,137,207) the Eq(2.7) can be employed

$$\alpha_V = \beta^* / (1 + \beta^*) \qquad .. \qquad (2.7)$$

where, $\beta^* = Q_g/Q_l$ and

$$Q_g = \frac{I_c.R_g(273 + T + \Delta T)}{Z.F.P.} \qquad .. \qquad (2.7a)$$

Rise in electrolyte temperature (ΔT) during machining (88) is due to chemical reaction occuring in the bulk of the electrolyte, reversible heat of reaction, irreversible heat and the viscous heat generated within the electrolyte, etc. However, the resistance heating of the electrolyte within the IEG is largely responsible for its temperature rise. If all the other forms of heating except Joule's heating is neglected then we can obtain Eq(2.8).

$$\frac{dT}{dx} = \frac{E_V^2 . K}{V . \rho_e . C_e . Y^2} = A'.K \quad .. \quad (2.8)$$

From Eqs(2.5)-(2.8) it is evident that for the case being considered, the IEG would become non-parallel after a time 't' and hence the tool shape used must be corrected to achieve a parallel gap at the end of the cut. Theoretically speaking, EC reaction would attain an equilibrium value after the machining has been in progress for a very long time (i.e., $t \rightarrow \infty$). Based on simplified assumptions, Tipton has suggested the use of Eqs(2.9) and (2.10) for the computation of the IEG while machining with zero feed and finite feed respectively.

$$Y = (Y_o^2 + 2.C.\Delta T)^{\frac{1}{2}} \quad .. \quad (2.9)$$

where,

$$C = \frac{E_V.E.K}{F \rho_m}$$

$$t = \frac{1}{F_F}\left[Y_o - Y_t + Y_e \ln\left(\frac{Y_o - Y_e}{Y_t - Y_e}\right)\right] \quad .. \quad (2.10)$$

If it be assumed that the electrolyte behaves like a pure Ohmic resistance, the current density J can be computed from Eq(2.11)

$$J = E_V . K/Y \quad .. \quad (2.11)$$

This equation is valid over a certain range of experimental conditions (95) only. While machining complicated shaped workpieces the electric field between the tool and workpiece gets distorted and under the conditions use of Ohm's law gives erroneous results. In such cases the current density (J) can be computed (105,106) from Eq(2.12)

$$J = \frac{E_V}{Y}\left(2K_0 \frac{1-\rho_0}{2+\rho_0}\right) \quad .. \quad (2.12)$$

Ippolito (91) has mentioned that the electrolyte conductivity in the IEG is a function of the machining current and score of other parameters and hence the application of Ohm's law in ECM is not justified. He suggested that overall gap resistance be calculated as follows:

$$R_{gap} = R_{elect} + R_{add} \quad .. \quad (2.13)$$

where,

$$R_{elect} = L/AK;$$

$$R_{add} = \xi (1/K)(V^a/I_c)(Q^b/I_c)P^c \quad .. \quad (2.13a)$$

The values of the constants in Eq(2.13a) have been evaluated (91) experimentally, as :

$$a = -0.32,\ b = -0.12,\ c = -0.11 \text{ and } \xi = 0.151$$

Current density distribution within the IEG has been measured experimentally by Kawafune (108). In majority of the cases he found the experimental values to be lower than the analytical. However, in few of the cases (Fig.7.1) experimentally measured current density was observed to be more than the corresponding analytical value. Conflicting nature of the results obtained has been explained on the basis of actual anodic dissolution efficiency (η) and the change in anode material valency of EC dissolution with time, etc.

As the IEG varies continuously along the electrolyte flow direction, the flow velocity also varies from point to point and can be evaluated by the use of continuity equation (2.14)

$$V_1 W Y_1 = V_2 W Y_2 \qquad .. \qquad (2.14)$$

For the case of simple shaped IEG, Eq(2.14) would give satisfactory results, however, for higher accuracy and complex shapes, use of conformal mapping technique (230) is recommended.

2.3.3 Optimization of ECM Parameters

The tool performance in ECM could also be optimized (219) by appropriate choice of the working conditions. The following section describes, in brief, the literature available in this field.

In ECM process, at some limiting tool feed-rate, the state of electrolyte can change over from boiling to non-boiling and choking to non-choking. Thorpe and Co-workers (205,206) have studied the electrolyte flow condition in ECM and have explained this by means of Fig.2.4. In this figure a feed rate value greater than that corresponding to the intersection point 'm' of choke limit and boil limit implies that the flow in the IEG is either choked or the electrolyte is boiling and the maximum MRR is achieved corresponding to the point 'm'. Optimization analysis by Bhattacharyya et al.(25), with MRR as the objective function and electrolyte boiling, hydrodynamic instability and passivity as the constraints, predicted an optimum feed rate, in ECM, of 1.825 mm/min. This analysis does not include the onset of sparking (63) as a constraint but in practice, beyond a certain frequency of sparking the tool damage, on this account, could become significant and make the process uneconomical (133,134). Higher feed rates in excess of the optimum, could result into lower tool-life. For the condition of zero sparking rate, Larsson and Co-workers (133,134) have derived an optimum feed rate of 2.28 mm/min. Thus, the optimum feed rate (25) of 1.825 mm also accounts for the onset of sparking automatically.

2.4 ANODE SHAPE PREDICTION TECHNIQUES

2.4.1 Cos θ Method

This method is based on the computation (212) of equilibrium gap, Y_e, for the given conditions but excludes the consideration of the mode of electrolyte flow, overpotential, electrolyte conductivity, heat transferred to the environment, machining efficiency, etc. In this method equilibrium workshape is computed corresponding to the tool whose profile has to be approximated by a large number of planar sections inclined at different angles. Consider a plane parallel gap inclined to the feed direction so that there is an angle θ between the feed direction and a normal to the tool or workpiece surface (Fig. 2.5). For the case being considered, the equilibrium gap can be evaluated from the Eq(2.5). This theory can be applied to a tool say, with three plane regions inclined at 0^o, θ and $\pi/2$ respectively to the feed direction. The appropriate equilibrium gap is Y_e when the surface of the tool is normal to the feed direction, and $Y_e/\cos\theta$ for the inclined surface (Fig.2.5). For the surface parallel to the feed direction, Eq(2.9) can be applied, since in this case any element on the workpiece experiences zero feed. The resulting work-profile of the surface initially parallel to feed direction would thus attain a parabolic shape after machining. However, this theory is not applicable to regions of the workpiece surface shown by dotted lines in Fig. 2.5. Further, the scope of this method is limited - workshapes with sharp corners cannot be analysed. In general this method is applicable to the situations where $\theta < 45^{o}$ beyond which significant error is introduced in the computed values (Fig.7.5). Furthermore, researchers (212,214) have also expressed conflicting opinions about the choice of reference surface for the measurement of the angle θ. In view of the approximations involved this method is not recommended for complex shaped workpieces.

2.4.2 Finite Difference Technique (FDT)

Cos θ method is based on the assumption that electric current flow lines are straight and normal to the electrode surfaces. This is not true in case of electrodes with small radii. When complex shaped workpieces have to be analysed it is necessary to know the electric field potential distribution within the IEG. This would then determine the current density, MRR, transient and equilibrium anode profile, etc. at each point within the gap. The FDT has been employed (88,168,171, 208,210,211,213) specially for the case of non-passivating electrolyte with constant conductivity and temperature. In such cases electric field flow lines are governed by the Laplace's Eq(2.15) and the boundary conditions (b.c.) as given by Eq(2.16)

$$\frac{\partial^2 \phi}{\partial x^2} + \frac{\partial^2 \phi}{\partial y^2} + \frac{\partial^2 \phi}{\partial z^2} = 0 \qquad .. \qquad (2.15)$$

$\phi=0$ at the cathode and $\phi=E_V=A_V-\Delta A_V$ at the anode .. (2.16)

Eqs(2.15) and (2.16) when solved would yield a set of simultaneous equations that could be solved for ϕ by backward-, forward-, or central-difference technique (147,221); once the potential distribution is obtained the instantaneous current density (210) at the anode surface at any point can be evaluated from (2.17)

$$J = K(\partial\phi/\partial n') \quad .. \quad (2.17)$$

Fig.2.6 shows the tool-work surfaces and IEG drawn in square mesh. The initial potentials at the grid points within the IEG region are set by linear interpolation along the vertical grid lines between the tool and work boundaries. For a point '0' located in the mesh of spacing 'h' (i,j), we can write (210):

$$Q_{ij} = (\phi_{i+1,j} + \phi_{i-1,j} + \phi_{i,j+1} + \phi_{i,j-1})/4 \quad .. \quad (2.18)$$

Eq(2.18) predicts that the potential at any point O(i,j) on the square mesh is equal to the mean of the potentials at the four nearest adjacent points (i.e., the points 1,2,3 & 4 in Fig. 2.6).

For the computation of the potential values within the prescribed tolerances, the work and tool boundaries are at some fixed known potential and therefore, their values are not adjusted during the relaxation process. It should also be noted that, in few of the cases, all the points on the tool and work boundary may not lie on grid points (Fig.2.6) and the regular stars may not be formed; such problems can be attempted (210) by the use of over-relaxation technique. To solve

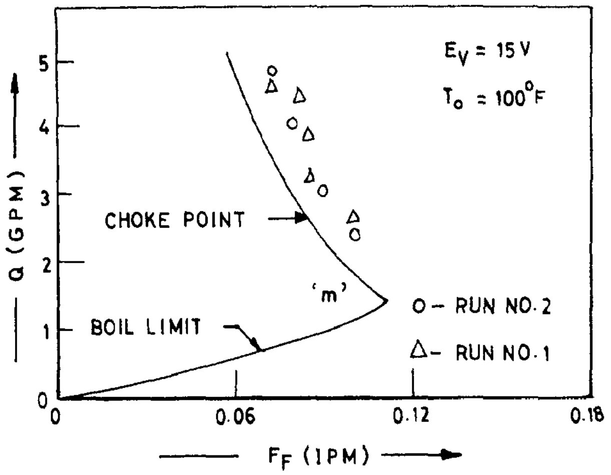

FIG. 2.4 ECM CHARACTERISTIC CURVE

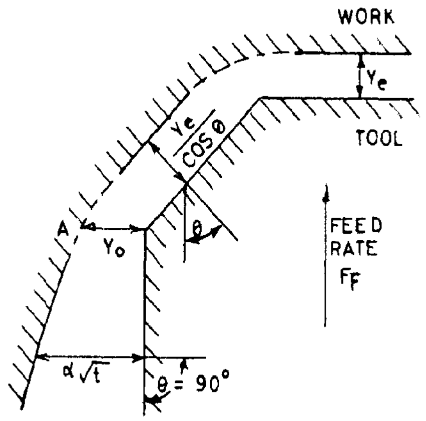
WORK
Y_e
Y_e / COS θ
TOOL
FEED RATE
F_F
A
Y_o
θ
α√t
θ = 90°

FIG. 2.5 THE EQUILIBRIUM GAP FOR THREE ADJACENT REGIONS ON A TOOL

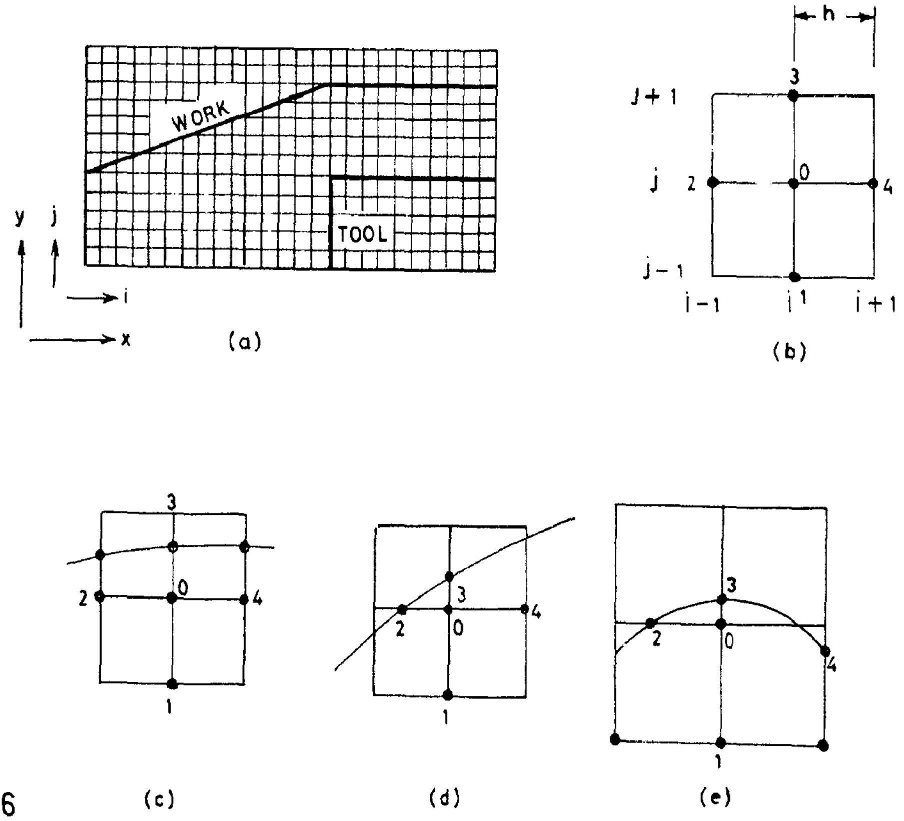
WORK
TOOL
y
j
i
x
(a)
h
J + 1
j
j – 1
i – 1
i 1
i + 1
0
1
2
3
4
(b)
(c)
(d)
(e)

FIG 2.6

(a) DISCRETIZATION IN SQUARE MESHES (b) A SQUARE MESH WITH FOUR EQUIPLACED POINTS (c) IRREGULAR STAR – ONE SHORT ARM-03 (d) TWO SHORT ARMS-02 AND 03 (e) THREE SHORT ARMS – 02, 03, 04 such problems recently, Nanayakkara and Larsson (168) have suggested the use of irregular grids along with regular grids (Fig.2.7). In such a case, a polynomial Eq(2.19) instead of a linear interpolation Eq(2.18) was used to describe the potential distribution in the area around a nodal point including its near neighbour.

$$\emptyset = B_1X^2 + B_2Y^2 + B_3X + B_4Y + B_5 \quad .. \quad (2.19)$$

After each computational interval of Δt seconds, work and tool boundaries have to be moved to new locations, according to the cut and feed vector. For simplicity, Tipton (210) has accounted only for the vertical component of the cut vector which is proportional to the vertical potential gradient at the work boundary. However, for precision in results, movement of the cut vector in both x and y directions should be considered.

It is thus evident that FDT yields only approximate results. Further, in case of complex shaped IEG the tool and work boundaries cannot be matched accurately by the use of square meshes which introduce further approximation.

2.4.3 Analogue Method

Laplace Eq(2.15) has also been solved by the use of conducting paper analogue technique (22,210,221). For obtaining the solution of Eq(2.15) equipotential surfaces representing the anode and cathode, to an approximate scale, have to be drawn on a conducting paper. The work boundary is then segmented to evaluate local current density and then is moved to the position that it would occupy at the end of some time interval, Δt. This could be obtained by finding point to point movement by the vectorial addition of feed rate vector ($F_F \Delta t.\cos\theta$) and cut vector ($K \frac{\partial \phi}{\partial n'} \Delta t$). The method is based on the assumption that feed rate velocity and cut velocities are constant over the time 'Δt'. Before repeating the process, the applied voltage must be adjusted so that the same current values are achieved as earlier. The process has to be repeated until the workshape does not change appreciably between the two successive steps and the final equilibrium shape obtained.

It is thus evident that the analogue method is approximate and cumbersome and its accuracy depends upon the skill of the operator and is not advisable for use when high degree of precision is desired.

2.4.4 Empirical Approach

Exact path of the electric current flow lines, within the IEG, is difficult to determine analytically. Therefore, normally the chordal distance between two stations (156) is taken as the length of current flow line. This assumption, in majority of the cases, is also responsible for the discrepancy between analytical and experimental results. Further, the conformity of the surface radii of the tool and an anode cavity decreases as the angle θ increases. Therefore, empirical equations (48,92,110,112), mostly based on experimental data, have been employed for the evaluation of the IEG and the anode profile.

König and Pahl (110) have suggested an empirical relationship, Eq(2.20), for this purpose

$$a_o = r_c^{0.35}\,(0.35)\left[(10e^*)Y_e\right]^{\frac{1}{2}} \quad .. \qquad (2.20)$$

for $0.15 \leq Y_e \leq 0.6$ mm and $0.5 \leq r_c \leq 5$ mm.

Where, e* is Euler's number. Further, König and Degenhardt (112) have also suggested Eqs(2.21) and (2.22) for the conditions that $1 \text{ mm} \leq r_c \leq 5$ mm.

$$a_o = (0.1 + Y_e)(0.314\, r_c + 1.17) \quad \text{for } b_b = 0 \quad .. \qquad (2.21)$$

$$a_o = 2Y_e + 0.1\left[6.283(r_c - 1)\right]^{0.5} \quad \text{for } b_b \geq 1 \text{ mm} \qquad (2.22)$$

Eqs(2.20)-(2.22) when tested by the author, yielded erroneous results for low feed rates ($F_F \leq 0.006$ mm/s) or when the equilibrium gap was large ($Y_e \geq 1.0$ mm). For low feed rate conditions, the author suggests the use of Eq(3.4), which is based on linear regression analysis of the experimental data.

For the evaluation of a_s' and a_s (Fig.2.3), Eqs(2.24) and (2.25) have been suggested (110).

$$a_s' = (2.b_b.Y_e + a_o^2)^{0.5} \quad .. \qquad (2.24)$$

$$a_s = \left[2.b_b.Y_e + r_c^{0.7}\,(0.123)(10e^*)^{Y_e}\right]^{0.5} + 0.65Y_e \qquad (2.25)$$

Test results (110) predict that the overcut in ECM is a function of the machining parameters only and does not depend on the tool dimensions. However, the experimental data of the author points to the contrary (Chapter 7). It should also be noted that Eqs(2.20)-(2.25) are valid only for the case of non-passivating electrolytes.

Ippolito and Fassolio (92) checked the validity of Equations above and reported that, Eq(2.22) for the case $r_c=0$, gives the upper bound solution whereas, Eq(2.26) gives the lower bound value of the side gap and Eq(2.27) was found to cross the experimental data.

$$a_s' = (2.b_b.Y_e + \nu^2 Y_e^2)^{0.5} \quad .. \quad (2.26)$$

$$a_s' = (2.b_b.Y_e + 2.9\, Y_e^2)^{0.5} \quad .. \quad (2.27)$$

The lateral gap at the end of non-coated zone of the electrode can also be computed from Eq(2.28). This predicts variations in overcut as the conical taper and it was found practically (92) to be independent of the uncoated length, b_b.

$$a_s = a_s' + \frac{2B'Y_e}{D'}\left[\operatorname{arctg}\left(\frac{2X+B'}{D'}\right) - \operatorname{arctg}\left(\frac{B'}{D'}\right)\right] \quad .. \quad (2.28)$$

where,

$$B' = \nu' \frac{E.K.E_V}{F\rho_m} \; ; \quad D' = (4F_F^2\, a_s'^2 - B'^2)^{0.5}$$

ν' is a correction factor for the conductivity and takes into account the effect of non-linearity of the current flow lines and the fact that the work surface is lightly passivated by the presence of the metallic oxides and hydroxides. It is thus evident that, for the evaluation of side and front gaps, Y_e can be used as a basic parameter. In some of the cases, the side gap has been demonstrated to be independent of the machining time which however is not true (Fig.3.1). It is also to be noted that in empirical formulations the effect of mode of electrolyte flow has been neglected. Empirical equations therefore, are normally valid for the specified working conditions only and generalisation in such cases is not possible.

2.4.5 Nomographic Approach

For the evaluation of equilibrium anode shape, a nomographic approach has also been used in few of the cases (72,74,110,112). König (110) has published a nomogram for the evaluation of side gap for the known Y_e, r_c and b_b (Fig.2.8). Heitman (74) has employed nomograms for the evaluation of the electrolyte-temperature rise (ΔT) under specified conditions. Use of nomograms has proved to be advantagenous in planning of ECM operations.

However, the nomograms are often based on a number of simplified assumptions (165,166) and hence cannot be recommended for general use.

2.4.6 Complex Variables Approach

Anode shape prediction in ECM, has also been attempted by the use of complex variables. Collett et al.(49) have determined the IEG in ECM for both completely insulated (sides) and bare and straight sided tools and arrived at Eq(2.29).

$$\text{Overcut at corner/machine gap} = a_o/Y_e \doteq 1.159 \quad .. \quad (2.29)$$

This equation is based on the assumption that the electrolyte conductivity and void fraction remain constant all over the IEG. However, according to PERA research report (238), the ratio defined by the Eq(2.29) should have a value of 1.7. Hewson-Browne (75) have used the conformal mapping technique for the analysis of two dimensional machining problems using straight sided tools with a finite land width, b_b. Assuming that the sides of the insulated tool do not participate in metal removal, they have shown that

$$0.731 \leq \frac{a_o}{y_e} \leq 1.159 \quad .. \quad (2.30)$$

where the lower limit applies to tools with insulated sides and the higher limit to uninsulated tools. The author has found experimentally, that while machining with bare tools, the ratio (a_o/y_e) is a function of machining conditions as well as the tool-work combination and its numerical value varies over a wide range (Fig.7.20). Nilson and Tsuei (170-172) have given a solution to the problem of anode shape prediction by the inverted method, in which the spatial coordinates were selected as dependent variables on the plane of complex potential and the transformed boundary conditions are known explicitely on the free boundary. Known asymptotic solution for the side gap region reduces the size of the field which must be determined.

Thus, use of mathematical models for ECM tool design studies have not been generalized so far. Analysis of machining profiles involving complex shapes and situations where parameters like T,K,J,V,etc., vary during the cut have not been suitably studied for.

2.4.7 Perturbation Method

This method (148,150-152) has been used for the analysis of EC operations like deburring or anode smoothing or shaping when the amplitude of micro-irregularities on the cathode and anode is small compared to IEG. This has limited applications and is based on the simplified assumptions (148) viz., (i) electrolyte conductivity is constant, (ii) effect of joule's heating and gas bubbles are supressed by sufficient agitation of the electrolyte, (iii) machining efficiency is 100%, and (iv) perturbation boundaries change slowly that their motion may be ignored at any instant.

Let us consider a case in which cathode and anode shapes (Fig.2.9) are defined mathematically by Eqs(2.31) and (2.32) respectively.

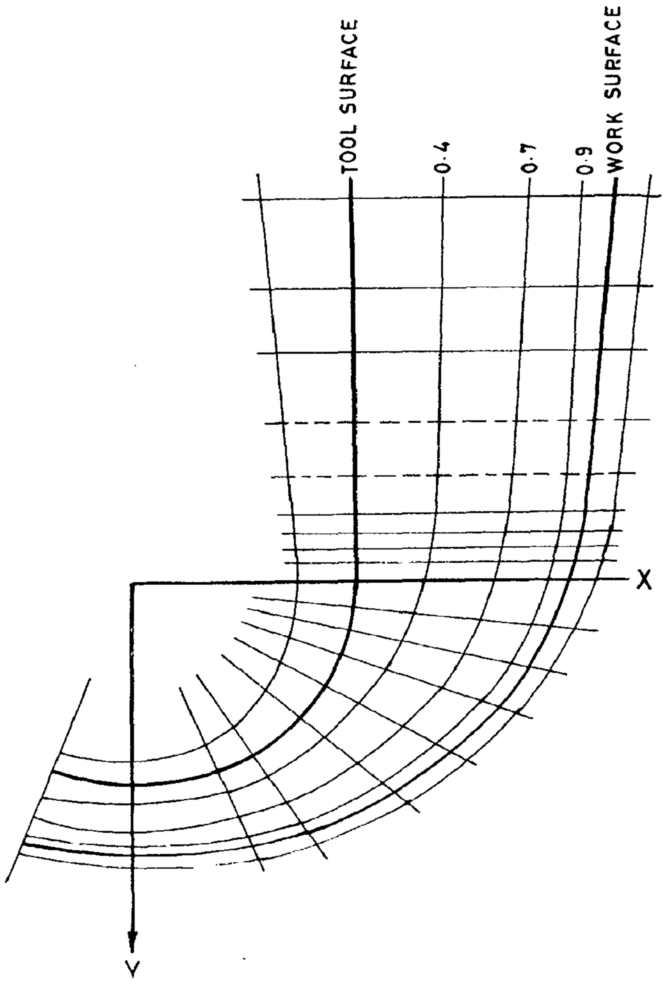
TOOL SURFACE
0.4
0.7
0.9
WORK SURFACE
X
Y

FIG 2.7 DISCRETIZATION OF I E G BY REGULAR AND IRREGULAR GRIDS(168)

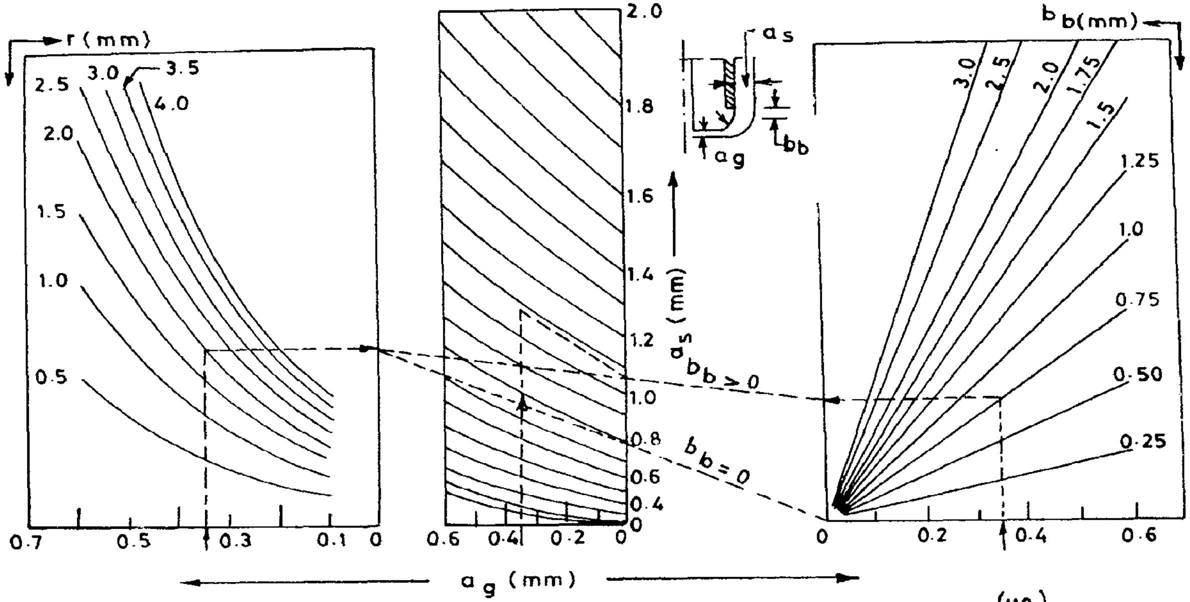

FIG. 2.8 NOMOGRAM FOR EVALUATION OF THE SIDE GAP(110)

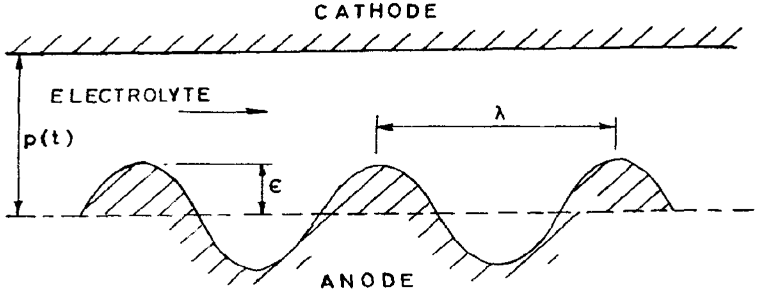
CATHODE
ELECTROLYTE
p(t)
λ
ε
ANODE

FIG. 2.9 CONFIGURATION OF ELECTRODES(148)

$$Y = 0 \quad .. \quad (2.31)$$

$$Y = p + \epsilon^* \sin(k^* x) \quad \text{where } \epsilon^* << p \quad .. \quad (2.32)$$

Laplace's Eq(2.15) for such a case can be solved for the boundary conditions given below, Eq(2.33). Thus, it can be shown (148) that the potential at any point Y is given by Eq(2.34)

$$\phi = 0 \quad \text{on } Y = 0 \quad \text{and } \phi = E_V \quad \text{on } Y = p + \epsilon^* \sin(k^* x) \quad (2.33)$$

$$\phi = \frac{E_V Y}{p} - \frac{E_V \epsilon^*}{p} \cdot \frac{\sin(k^* x) \sinh(k^* y)}{\sinh(k^* p)} \quad .. \quad (2.34)$$

Using Eq(2.34), the set of Eqs(2.35) and (2.36) can be derived which describes separately the behaviours of the anode surface and irregularities respectively.

$$t = \frac{1}{F_F} \left[p_o - p + p_e \ln\left(\frac{p_e - p_o}{p_e - p} \right) \right] \quad .. \quad (2.35)$$

$$\epsilon^* = \epsilon^*_o \, \mathrm{Exp} \left[- ME_V \, k^* \int_{p_o}^{p} \frac{\coth(k^* s)}{ME_V - F_F s} \, ds \right] \quad (2.36)$$

provided $dp/dt \neq 0$. Here, $M = EK/\rho_m F$.

Eq(2.36) has been applied (148) to analyse the irregularities on the anode surface of the type of short wave length, long wave length, arbitrarily shaped and even and arbitrarily shaped. Since this analysis is based on the solution of Laplace's equation hence it accounts for the field concentration effects.

This also explains why more rapid smoothing can be expected in case of irregularities with short wave length than those having long wave length. The analysis can further be extended to more general class of electrode shaping by means of Fourier's Transforms. An equation similar to (2.35) has also been derived by Tipton (212,213) in terms of dimensionless quantities for the case of surface smoothing by ECM.

2.5 FORMULATION OF THE PROBLEM

From the discussions above, it is evident that quantitative data regarding the effects of grain size, grain boundaries, grain boundary density and their orientation, microstructure, heat treatment (182-183), passivation film (42-44,57,126,130,187), etc., on MRR and current density are not available and hence their effects in analytical modelling cannot be incorporated. Also, governing equations that can relate the influence of electrolyte composition to the surface finish (65) and dimensional tolerance achieved (42-44), and the effect of pH of the electrolyte (40) to MRR, are not available. Further, majority of the models do not account for the change in valency of EC dissolution (157) with time. This can often seriously affect the values of machining efficiency (148). It is also evident that available work is mostly based on simplified assumptions like, constant temperature and electrolyte conductivity, zero void fraction, constant current density and do not consider the effects of simultaneous variations in several important machining parameters. The existing models are therefore, incapable of analysing geometrically and materially non-linear problems that are often encountered in practice. A comprehensive analysis of the metal removal and equilibrium gap generation in ECM is also lacking.

To bridge the gap between theory and practice of ECM, an effort has been made in this thesis. The work embodied herein can be described as follows:

(i) A more versatile and accurate analytical tool i.e., finite element technique (FET) has been applied to analyse a group of ECM processes based on the principle of EC dissolution. This analysis has led to better understanding of the effects of the process parameters. Computer programs (known as FET-11, FET-22, SGFET-11 and SGFET-22) for ECD and related processes have been developed to predict the anode shape and other machining parameters.

(ii) Modifications to the classical ECM theory have been suggested so as to improve upon the existing state of knowledge. For this purpose 'resistances in **parallel**' model and new equations for anode shape prediction have been suggested. To account for the effect of electrode - material on anode shape and other machining parameters, a simple thermal resistance model of the ECM process has been proposed. Lastly, using experimental data obtained by the author, working equations, based on regression and dimensional analysis have been formulated so as to predict the over-cut within the transition zone. A single equation, has been developed so as to determine the IEG in ECM that applies to both zero and finite feed rate conditions.

(iii) Proposed analytical models have been verified experimentally and a good correlation between the two has been observed. Experiments were conducted using bare tools and 'tool bits' having different diameter and corner radii. Anode materials selected were mild steel, low alloy steel castings, and low alloy steel forgings. Brass was used as the tool material and NaCl solution of different concentration in water was used as the electrolyte. The experiments were planned in accordance with a statistical analysis technique known as 'design of experiments'.

CHAPTER - 3

ECM THEORY AND ITS APPLICATIONS

3.1 INTRODUCTION

As discussed in chapter 2 the analytical ECM models available till date, do not yield accurate results specially as regards the ECM parameters like, temperature, current density, IEG, etc. This is because, the basic Faraday's Eq(2.1) used for this purpose is not valid in true sense. Secondly, it is difficult to predict the overcut in the transition zone accurately, which has a controlling effect on the anode shape produced. It is also not possible to account for the heat transferred to environment through electrodes or vice-versa. This chapter has been devoted towards the development of the modified ECM theory which has been shown to yield better results as compared to the classical theory as described in chapter 2.

3.2 EVALUATION OF INTERELECTRODE GAP - ZERO AND FINITE FEED RATE

Eq(2.9) when employed for the evaluation of IEG predicts an increase in IEG with time. According to this equation, the IEG would assume an infinitely large value when 't' tends to infinity. However, in reality, the rate of change of IEG diminishes rapidly with time due to the fact that the current density (J) drops as the gap increases. This aspect is not reflected in by the Eq(2.9). The implicit Eq(2.10) in the current form is also independent of the current density. Further, solution of the equation (2.10) is quite tedious and time consuming. The author has therefore, suggested the following modifications to equations (2.9) and (2.10).

For the situation shown in Fig.(2.3), the rate of penetration (dY/dt) of the cathode having unit cross-sectional area is given by Eq(3.1)

$$\frac{dY}{dt} = \eta \frac{JE}{F \rho_m} - F_F = (C' - F_F) \qquad .. \qquad (3.1)$$

Assuming that, during the cut, over a small interval of time (dt) the current density J, machining efficiency η, and electrochemical equivalent E do not change, then Eq(3.1) can be written as,

$$Y = Y_0 + (C' - F_F)\Delta t \qquad .. \qquad (3.2)$$

where,

$$C' = \eta\,(JE/F\rho_m) \text{ and } J = E_v.K/Y$$

Advantage of using the Eq(3.2) is that it is current density dependent and a single equation applies to both the conditions of machining, namely zero and finite feed.

$$Y = Y_0 + C'\Delta t \quad \text{(for zero feed condition)} \qquad (3.3)$$

It is to be noted that in reality feed rate in the side gap, is not zero throughout the operation. As soon as drilled hole gets tapered the feed becomes finite and its value can be evaluated from Eq(3.3a)

$$F_S = F_F/\cos\theta \qquad .. \qquad (3.3a)$$

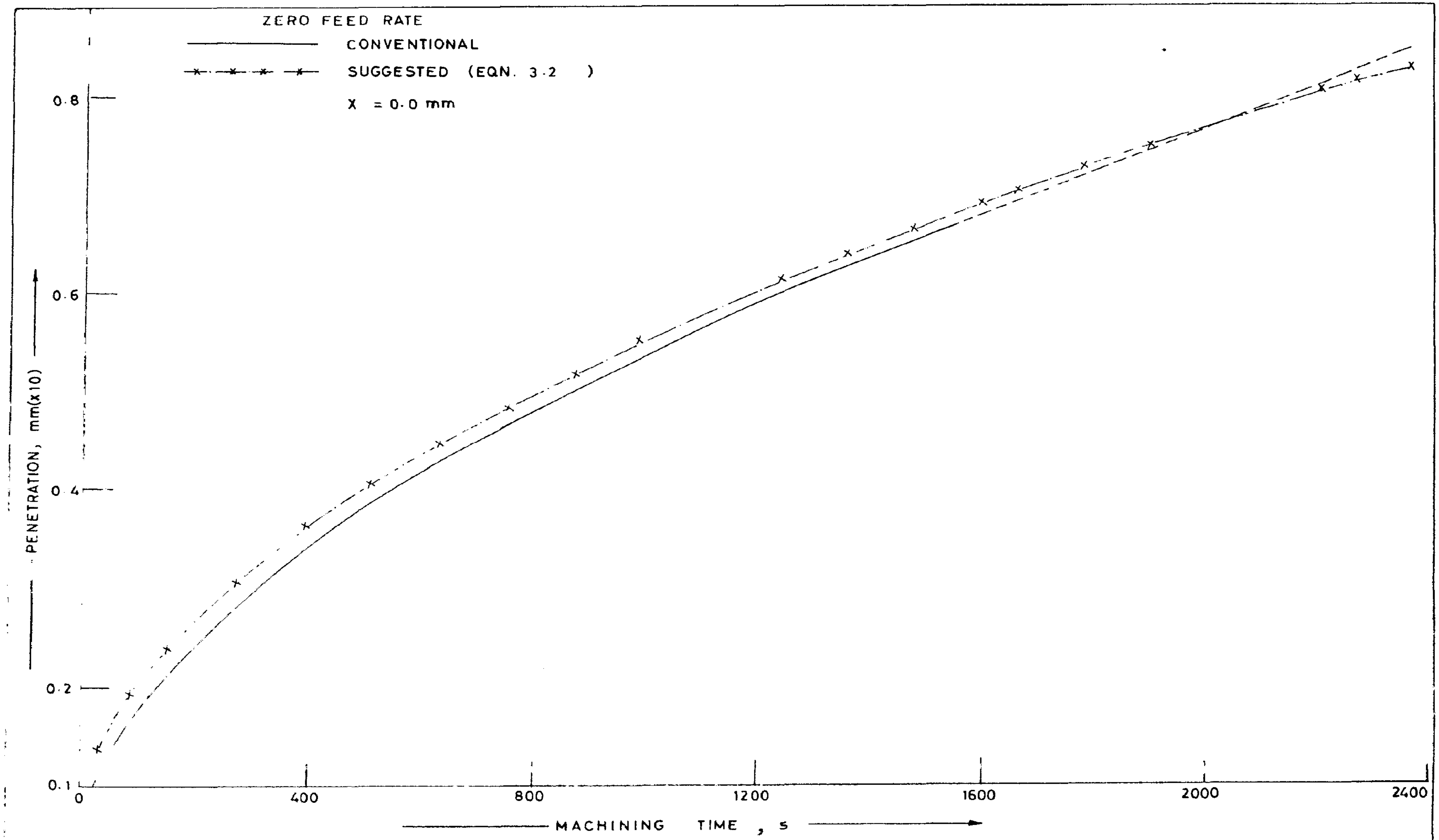

FIG. 3.1 COMPARISON OF CONVENTIONAL EQN. 2.9 AND SUGGESTED EQN. 3.2

3.3 OVERCUT IN THE TRANSITION ZONE

Overcut, a_o in the transition zone has been investigated experimentally by König (110,112) and for the case of machining with partially bare tools an empirical relationship, Eq(2.22), has been suggested. This equation yields inaccurate results (Fig.3.2, for machining conditions - see table 13) specially when equilibrium gap is large while machining at fine feeds.

Assuming that the overcut in the transition zone is a linear function of the equilibrium gap as given by Eq(3.4) where regression line coefficients (101) RC_1 and RC_2 can be evaluated from the exprimental data in Fig.7.20

$$a_o = RC_1 \cdot Y_e + RC_2 \qquad \cdot\cdot \qquad (3.4)$$

The linear relationship (Eq(3.4)) yields a low value of the correlation coefficient in some of the cases hence, it was decided to conduct the dimensional analysis (99,197) of the parameters governing the overcut in transition zone. The parameters considered for this purpose and their dimensions are shown below:

Variables	Dimensions
a_o	L
$\left(\frac{Y_e F_F}{D} \right)$	LT^{-1}
r_c	L
V	LT^{-1}

176617
[illegible] OF ROO[illegible]

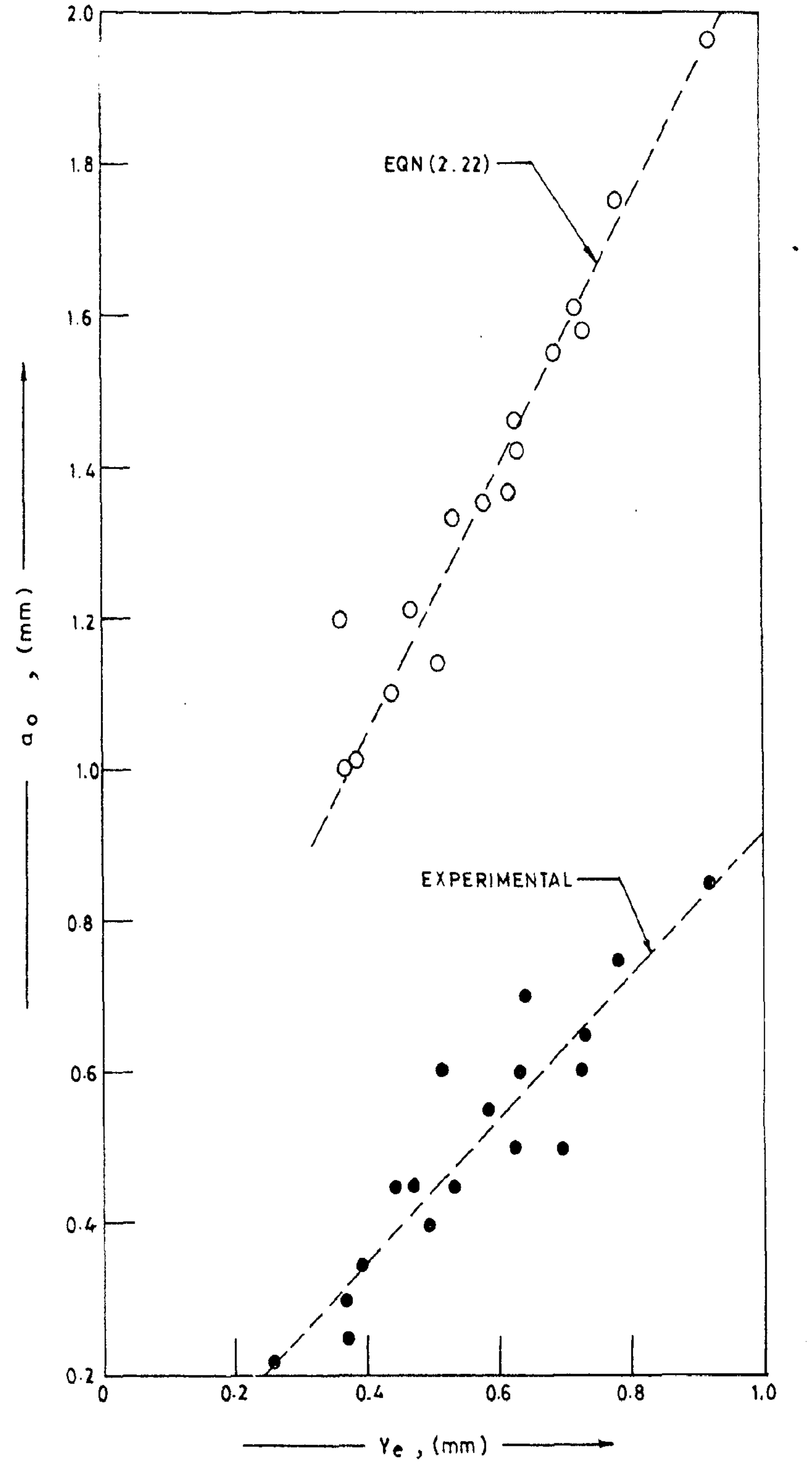

FIG. 3.2 COMPARISON OF EQN. (2.22) AND EXPERIMENTAL RESULTS

Analysis of the parameters yields (Appendix- 3) the following functional relationship;

$$\left(\frac{a_o}{r_c} \right) = C_d \left(\frac{Y_e F_F}{V} \right)^{n_1} D^{n_2} \qquad .. \qquad (3.5)$$

where, C_d, n_1 and n_2 are the functions of tool-work material combination. The values of these coefficients can be evaluated experimentally (See chapter 7).

3.4 ELECTROCHEMICAL WIRE CUTTING PROCESS (ECWCP)

In electrochemical wire cutting process (ECWCP), the material is cut to the desired shape (Fig.3.3) due to EC reaction, using straight or curved wires (220) or tubes (104). This process has several advantages (103) over the conventional ECM specially, when large amount of material is to be removed. This does not necessitate large current supply and high pressure electrolyte flow. Recently (38), wire cutting has also been attempted successfully in stagnant electrolyte (abbreviated as ECMSE) with pulsating current. Pulsating current enables automatic expulsion of reaction products out of the IEG. In ECWCP, like conventional ECM the problem of dimensional control remains unresolved.

Survey of literature (38,103,220) shows that virtually no information is available about the process parametes governing the ECWCP. In the present case a simple case of ECWCP with the scheme of electrolyte supply as shown in Fig.3.4 has been analysed. The analysis is valid under the following assumptions;

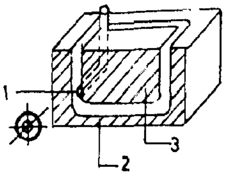

DIAGRAM OF THE FORMATION OF A RECTANGULAR SHAPE USING TUBULAR CATHODE TOOLS.

1. CATHODE TOOL
2. WORK PIECE BEING MACHINED
3. ALLOWANCE BEING REMOVED (COMPONENT)

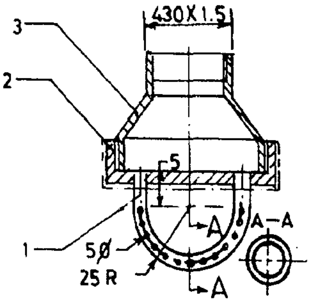

TUBULAR SHAPED CATHODE WITH A RADIUSED PROFILE

1. OPERATING UNIT
2. MAIN BODY
3. ADAPTER

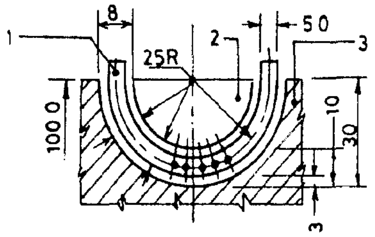

SHAPING A RADIUSED PROFILE WITH A TUBULAR SHAPED CATHODE

1. OPERATING UNIT
2. ALLOWANCE TO BE REMOVED
3. WORK PIECE TO BE ROTATED DURING MACHINING

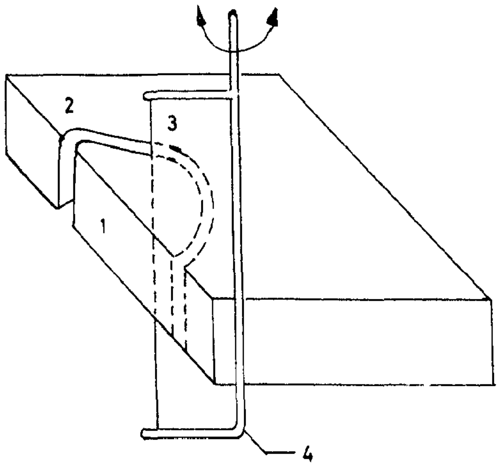

1 ALLOWANCE TO BE REMOVED
2. WORK 3. TOOL ELECTRODE
4. SUPPORT MEMBER

FIG. 3.3 THREE DIMENSIONAL WIRE CUTTING

(1) The electrolyte enters into the IEG from one end and exits at the other. The amount of electrolyte flow is just sufficient to fill up the entire gap (Fig.3.4).

(2) The front and side gaps behave like pure ohmic resistances.

(3) The cutting wire is bare and has uniform rectangular cross-section throughout.

(4) A premachined groove has been provided in the workpiece to initiate the process of cutting.

(5) Mass density of the electrolyte remains unaltered during its flow.

(6) The wire has been assumed to have sharp corners, unless mentioned otherwise.

During ECWCP, cutting takes place in the front as well as side surfaces hence, for the sake of modelling of the cutting process one should consider the resistances R_F, R_L as well as R_R (Fig.3.4). Failure to account any one of these resistances could impair the accuracy of the results obtained. Considering that the resistances are in parallel (Fig.3.4), the equivalent resistance R_{tot} can be evaluated from Eq(3.6).

$$R_{tot} = \frac{Y_F \cdot Y_L \cdot Y_R}{K_F \cdot A_F \cdot Y_L \cdot Y_R + K_L \cdot A_L \cdot Y_F \cdot Y_R + K_R \cdot A_R \cdot Y_F \cdot Y_L} \quad .. \quad (3.6)$$

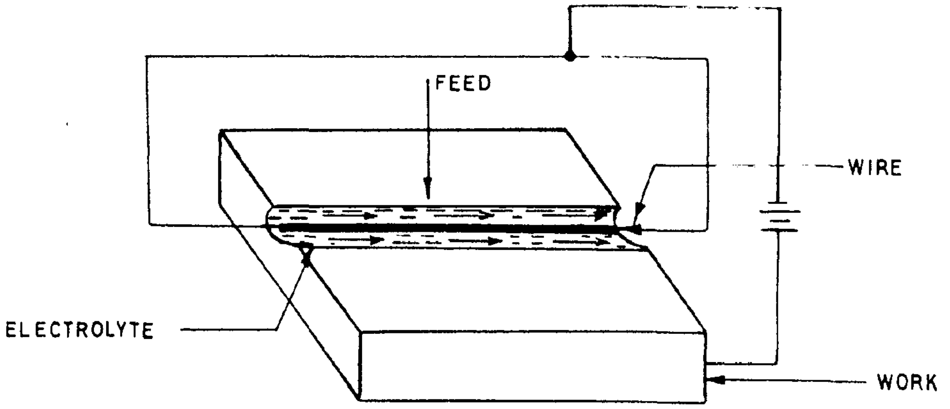
FEED
WIRE
ELECTROLYTE
WORK

(a) SCHEMATIC DIAGRAM FOR ECWCP
(CIRCULAR WIRE)

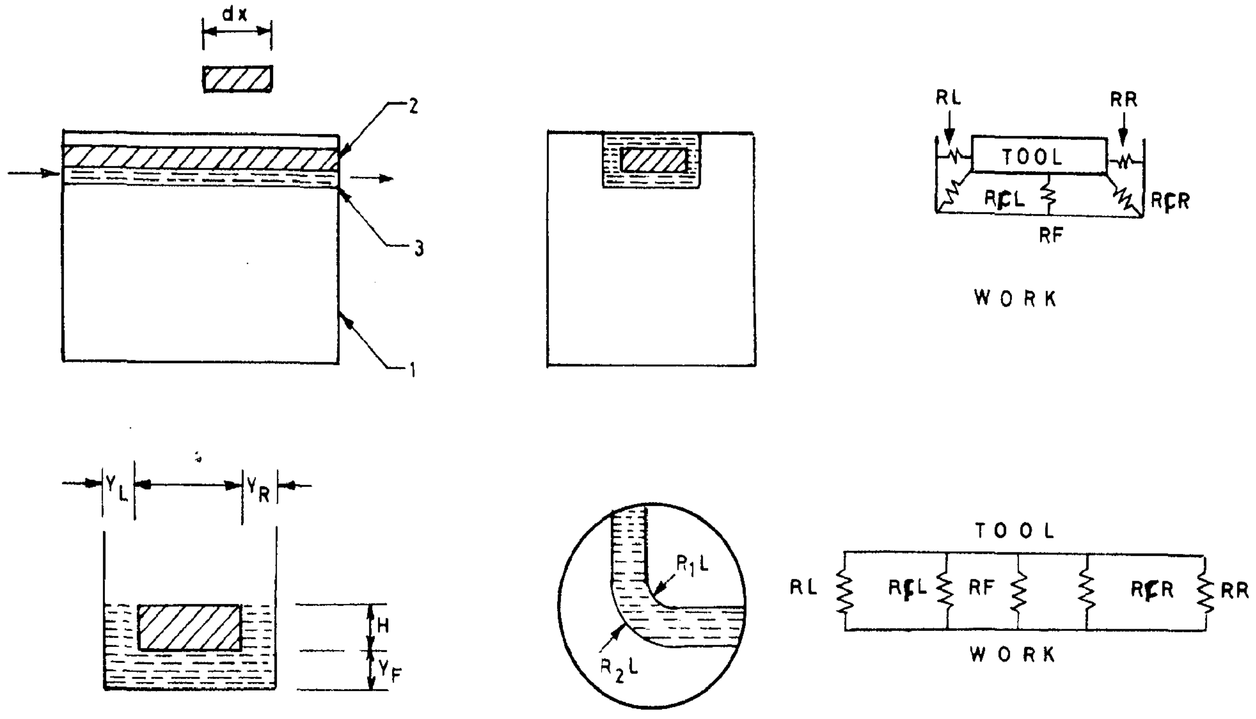
dx
2
3
1
RL
RR
TOOL
RFL
RFR
RF
WORK
Y_L
Y_R
H
Y_F
R_1L
R_2L
TOOL
RL
RFL
RF
RFR
RR
WORK

(b) RESISTANCE MODEL

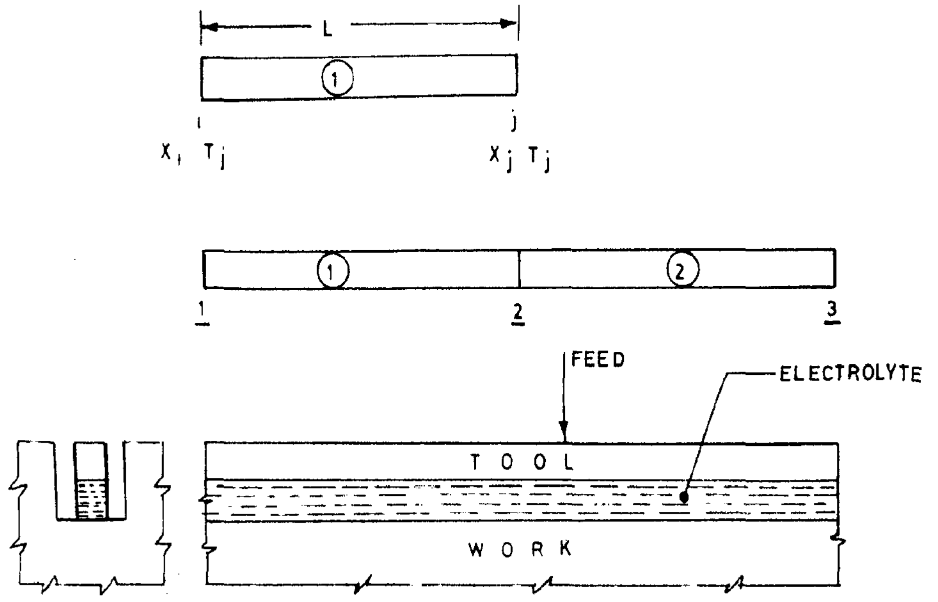
L
1
i
j
X_i T_j
X_j T_j
1
2
1
2
3
FEED
ELECTROLYTE
TOOL
WORK

(c) FINITE ELEMENT MODEL

FIG. 3.4 MODELS OF EC WIRE CUTTING OPERATION

The electrolyte conductivity in the right, left and front sides can be assumed to be equal i.e., if

$$K = K_L = K_R = K_F \qquad .. \qquad (3.6a)$$

hence R_{tot} and the current density, J can be evaluated from the relationships (3.6b) and (3.7) respectively.

$$R_{tot} = \frac{Y_F \cdot Y_L \cdot Y_R}{K(A_F \cdot Y_L \cdot Y_R + A_L \cdot Y_F \cdot Y_R + A_R \cdot Y_F \cdot Y_L)} \qquad .. \qquad (3.6b)$$

$$J = \frac{E_V}{R_{tot} \cdot Area} \qquad .. \qquad (3.7)$$

If the wire corners are not sharp then the above analysis can be modified as follows:

$$\frac{1}{R_{tot}} = \frac{1}{R_i} + \frac{1}{R_j} \qquad .. \qquad (3.8)$$

where,

$$\frac{1}{R_i} = \frac{1}{R_F} + \frac{1}{R_L} + \frac{1}{R_R} \qquad .. \qquad (3.8a)$$

and,

$$\frac{1}{R_j} = \frac{1}{R_{FL}} + \frac{1}{R_{FR}} \qquad .. \qquad (3.8b)$$

The wire cutting analysis with appropriate modifications can also be used to analyse ECD and ECB of rectangular holes (chapter 4).

3.5 ELECTROCHEMICAL BORING AND DRILLING OF CYLINDRICAL HOLES USING TOOL BITS

In this operation, predrilled holes in the workpieces (circular or non-circular) can be enlarged, and finished by correcting the form error, if any. In ECB the effort is also directed towards the removal of taper produced during ECD.

EC drilling using a bare tool invariably results into a tapered hole hence, to overcome this problem normally, an insulated tool is recommended. However, use of such tools presents practical difficulties viz., the coating peels out after some time due to the simultaneous effects of heat and electrolyte pressure. Effectiveness of the insulation depends on the quality of coating and the material used. These tools require frequent reconditioning and hence are uneconomical.

3.5.1 Theory

A new concept in the design of ECM tools would therefore be that, EC boring and drilling tools be used in the form of BITS (Fig.6.4) in place of a single long, bare or the coated tool. Use of tool bits by the author has been found to offer the following advantages;

(i) Absence of taper in the hole produced with coated tool bit in ECD and ECB (Fig.3.5).

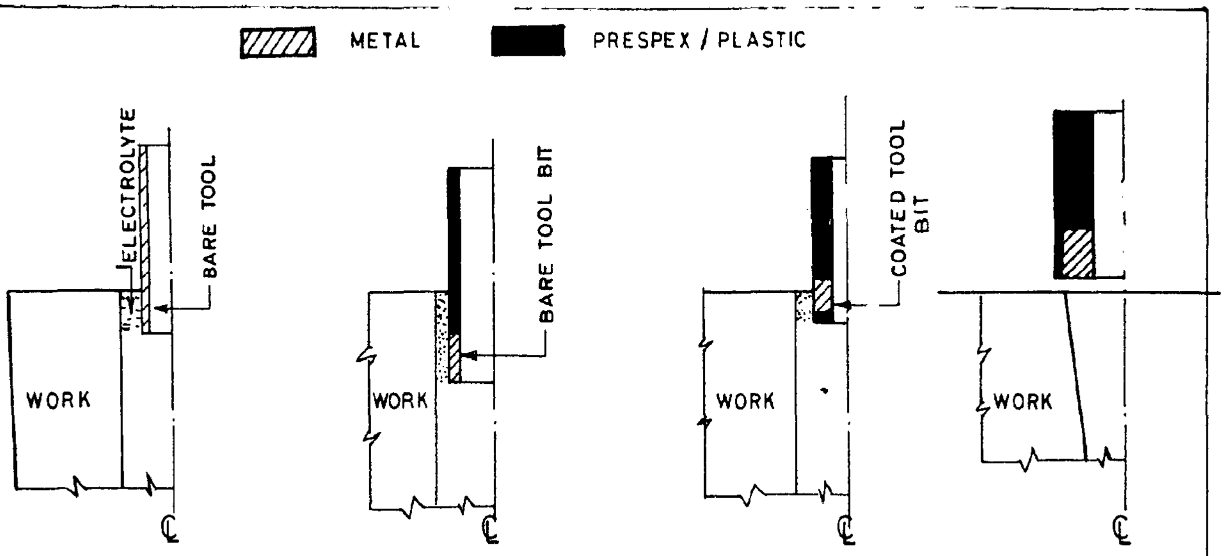
▨ METAL
■ PRESPEX / PLASTIC
ELECTROLYTE
BARE TOOL
WORK
℄
BARE TOOL BIT
WORK
℄
COATED TOOL BIT
WORK
℄
WORK
℄

EC BORING WITH BARE TOOL

EC BORING WITH BARE TOOL BIT

EC BORING WITH COATED TOOL BIT

EC BORING WITH SIDE COATED TOOL BIT

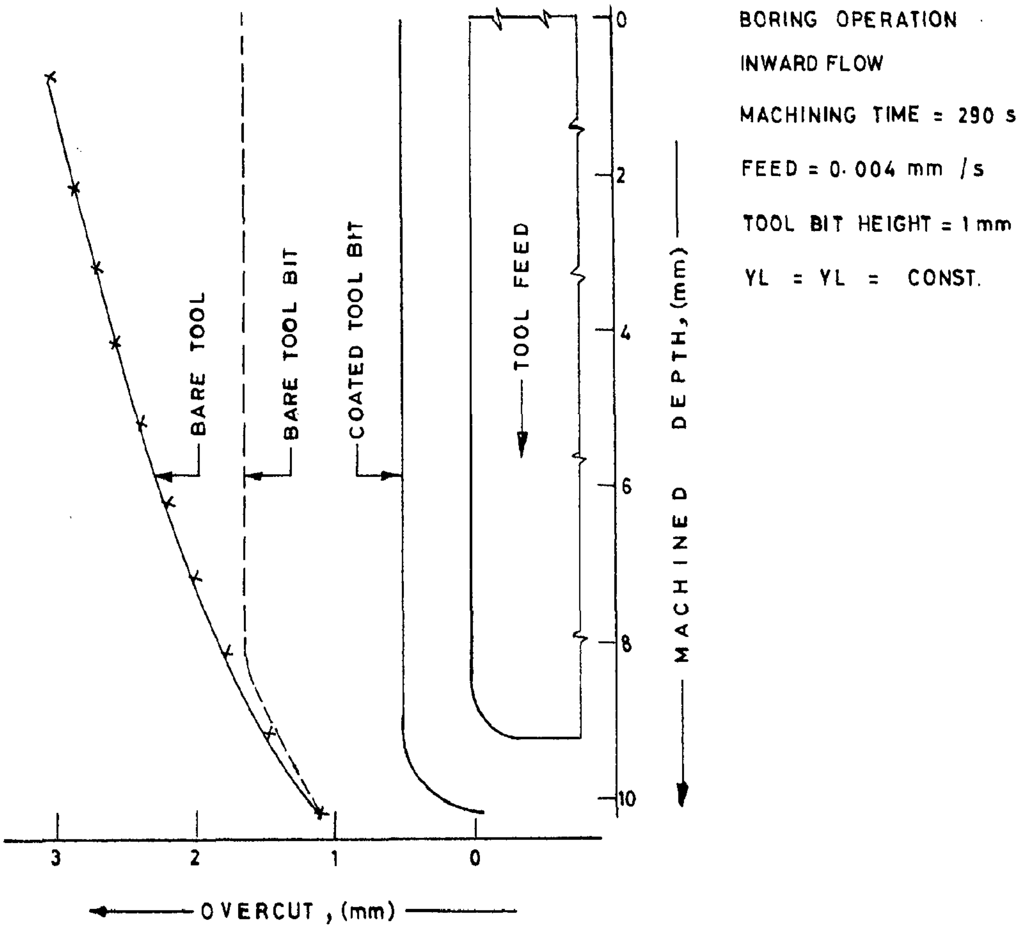

FIG. 3.5 SIDE SURFACE GENERATION DURING EC BORING

(ii) Same tool holder can be used for mounting bits of different shape and size. This ensures a lower tool changing time.

(iii) Material and labour cost are lower as compared to bare tools.

(iv) Tool bits damaged by sparking or otherwise are easily replacable.

(v) Accurate control on the bare land of the tool bit is possible.

(vi) Manufacture of the complex shaped tool bits is easy as compared to the shaping of the full length bared tools.

(vii) Metal removal by the sides of the bits can be varied by changing bare height of the bits.

Fig.3.5 shows a schematic diagram of enlarging a predrilled hole by the method of ECB and the expected anode profiles obtainable when using different tools. For the sake of modelling of the process, the following assumptions have been made.

(i) IEG between the tool and the workpiece behaves like a pure ohmic resistance.

(ii) IEG can be approximated as uni-dimensional continuum.

(iii) Feed rate in the side gap is assumed to be zero, however, using Eq(3.2) in conjunction with Eq(3.3a) the model would as well be valid for non-zero feed rate in the side gap.

(iv) Predrilled hole, which is to be bored has been assumed to have uniform diameter or straight taper over an element of small length, Le.

(v) There is no relative rotary motion between the tool and work electrodes and the tool feed is linear.

(vi) Temperature rise of the electrolyte in boring is predominently due to Joule's heating and heat generated due to chemical reactions, viscous flow of electrolyte, etc. are small and hence negligible.

(vii) Effects of microstructure, grain boundary attack, etc. on the ECM process have been neglected.

IEG at any instant 't' in the side gap can now be computed from Eq(3.9) as;

$$r_2 = r_2' + C' \cdot \Delta t \quad \cdot\cdot \quad (3.9)$$

where,

$C' = EJ/F\rho_m$ and r_2' is hole radius prior machining.

During boring by 'bits' the front face of the bit should be insulated electrically so that there is no stray current attack on the side surfaces of the hole being bored. Bits have also been applied for drilling successfully by the author. It produced the drilled hole surfaces of high precision as will be discussed later. In case of electrochemical bit drilling (ECBD), the IEG, Y, in the front gap can be evaluated as follows;

$$Y = Y_0 + (C' - F_F)\Delta t \quad \cdot\cdot \quad (3.9a)$$

'J' represents the current density at the anode point under consideration. Temperature rise, ΔT can be evaluated using Eq(3.13).

In the present analysis (Eq 3.9), there seems to be no effect of feed rate, F_F on the MRR. This is due to the nature of assumption (iii). It should however, be noted that during computation of r_2 at any point, say 'p', on the drilled hole, computational cycle time, Δt, should not be more than the time for which 'p' had been under actual dissolution. This condition can be described by Eq(3.10)

$$\Delta t_{max} \leq \frac{b_b}{F_F} \quad .. \quad (3.10)$$

For an accurate computation $\Delta t \leq \Delta t_{max}$ and Δt should be an integer multiplier of Δt_{max} i.e. NE should be an integer

$$NE = \Delta t_{max} / \Delta t \quad .. \quad (3.11)$$

Further, for the purpose of FE analysis, b_b can be divided into small elements each of length L_e. If all the elements are of uniform length then;

$$L_e = F_F \cdot \Delta t \quad .. \quad (3.12)$$

Hence, from above

$$b_b = L_e \cdot NE \quad .. \quad (3.12a)$$

Thus, total amount of metal removed in a cut at any point would depend upon the bare length of the bit (b_b) and feed rate (F_F). Their values should be chosen on the basis of boring allowance available.

In case of cylindrical boring, rise in electrolyte temperature and the current density along the flow direction can be evaluated from Eqs(3.13) and (3.14).

$$\frac{dT}{dx} = \frac{2E_V^2 K}{\ln(r_2/r_1)} \cdot \frac{1}{(r_2^2 - r_1^2)\, V.\rho_e.C_e} \quad .. \qquad (3.13)$$

$$J_{r2} = \frac{E_V.K}{r_2 \ln(r_2/r_1)} \quad .. \qquad (3.14)$$

Using these equations, current density, temperature, electrolyte conductivity, etc., in the IEG could be computed and thereby the anode profile obtainable in ECB and ECBD (chapter 7) can be obtained.

3.6 HEAT TRANSFER ANALYSIS OF ECM PROCESS

3.6.1 Introduction

The analyses for ECM, ECD, ECWCP and ECB operations, presented in sections 3.2-3.5, ignore the effect of heat transfer from the electrolyte to the tool and work electrodes. In this section a simple analysis has been presented which could help in the evaluation of heat transfer in ECM. The amount (52,59) of heat generated in ECM is quite large and is mainly due to Ohmic resistance of the electrolyte, reversible and irreversible chemical reaction, viscous flow of electrolyte, etc. The electrolyte is surrounded by electrodes to or from which heat is partially transferred (106), the magnitude of which is governed by thermal properties of surrounding electrodes and machining conditions. The transfer of heat leads to lowering (or increasing) of the electrolyte temperature to a certain extent. Further, metal dissolution is also accompanied by hydrogen and oxygen gases evolution. (148) in the form of bubbles. Dissolution of anode results in precipitation of ferrous and/or ferric hydroxide in the electrolyte. Thus, the electrolyte is a mixture of liquid, gases, solids and precipitate. It is also to be noted that in reality the heat transfer in ECM occurs under transient conditions rather than under steady state conditions. Heat transfer analysis in ECM is thus complicated and involves the considerations of multiphase flow with transient heat and mass transfer. Further if the IEG is of complex shape, it becomes difficult to evaluate the electrolyte flow conditions at each and every point accurately. This further adds to the complexity of the problem.

In view of the difficulties felt in heat transfer analysis in ECM, most of the analytical models, for ECM tooling design, neglect the effect of heat transferred to (or from) electrodes (48,87,154).

Given below is a simplified analysis of the heat transfer, in ECM, from the electrolyte to the environment through the tool and work electrodes. The simplified unidimensional thermal resistance model has been formulated based on the following assumptions:

(i) IEG behaves like a single phase fluid i.e.; steam and gases are not produced and reaction products and solid particles, if any do not find their way to IEG.

(ii) Electrodes used have finite dimensions.

(iii) Electrolyte flow velocity within an element is uniform along and across the section.

(iv) Heat transfer within the IEG occurs under unsteady conditions, however, over a small interval of computational cycle time, $\triangle t$, steady state conditions have been assumed.

(v) Electrodes are assumed at lower energy level and heat transfer through electrodes is assumed to be unidirectional (Fig.3.6).

Temperature gradient and a simplified thermal resistance model for IEG system is shown in Fig.3.6. Transfer of heat from the electrolyte to air would take place in three stages:

(i) Forced convection from electrolyte to the electrodes.

(ii) Conduction through the electrodes, and

(iii) Natural convection and radiation from the electrodes to the surrounding environment.

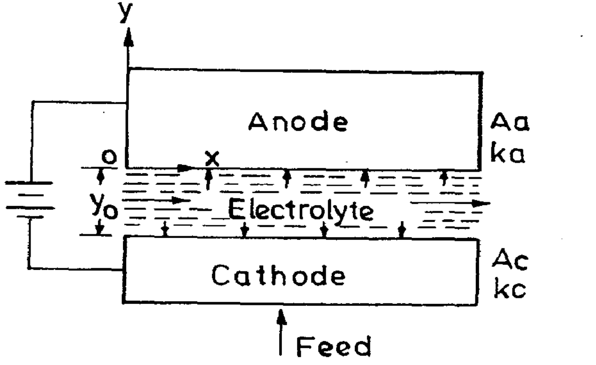
y
Anode
Aa
ka
o
x
y_o
Electrolyte
Cathode
Ac
kc
Feed

SCHEMATIC DIAGRAM OF ECM PROCESS

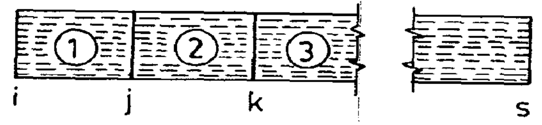

INTERELECTRODE GAP AS AN UNIDIMENSIONAL CONTINUUM

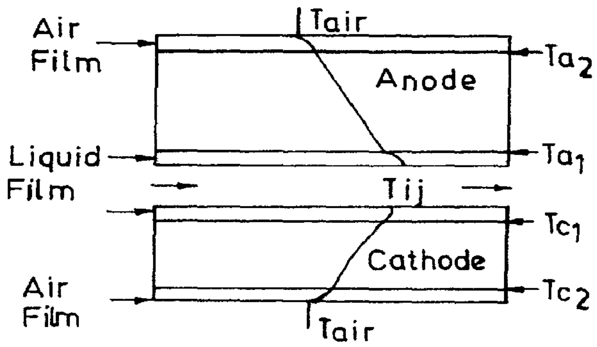
Air Film
Liquid Film
Air Film
Tair
Anode
Ta2
Ta1
Tij
Tc1
Cathode
Tc2
Tair

TEMPERATURE GRADIENT IN TOOL WORK ELECTROLYTE SYSTEM

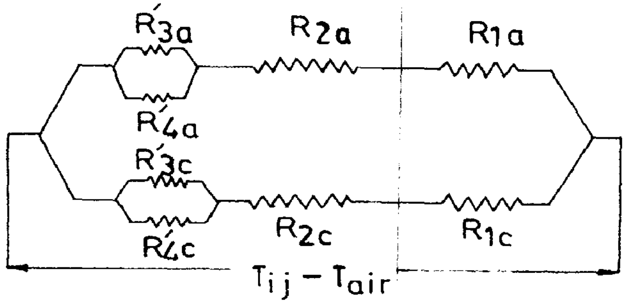
R'3a
R2a
R1a
R'4a
R'3c
R'4c
R2c
R1c
Tij − Tair

THERMAL RESISTANCE MODEL OF IEG IN ECM

FIG. 3.6

Let $*q_a$ and $*q_c$ be the heat transferred from anode and cathode respectively to the air. It can then be shown (73,93) that heat transferred through anode, $*q_a$, would be equal to

$$*q_a = \frac{(T_{ij} - T_{air})}{*R_a} \qquad .. \qquad (3.14)$$

where,

$$*R_a = *R_{1a} + *R_{2a} + *R_{3a} = \frac{1}{A_a}\left[\frac{1}{h_{fa}} + \frac{1}{k_a}\right] + \left(\frac{R'_{3a} \cdot R'_{4a}}{R'_{3a} + R'_{4a}}\right) \qquad (3.14a)$$

Also,

$$R'_{3a} = \frac{1}{A_a \cdot h_{na}} \text{ and } R'_{4a} = \frac{(T_{a2} - T_{air})}{A_a\ \epsilon_a\ \overset{*}{\sigma}_a F_a\ (T'_{a2} - T'_{air})} \qquad (3.14b)$$

where,

T'_{a2} and T'_{air} are the temperatures in Kelvin. Similarly, heat transferred through cathode to the atmosphere is obtained as follows:

$$*q_c = \frac{(T_{ij} - T_{air})}{*R_c} \qquad .. \qquad (3.15)$$

where,

$$*R_c = *R_{1c} + *R_{2c} + *R_{3c} = \frac{1}{A_c}\left[\frac{1}{h_{fc}} + \frac{1}{k_c}\right] + \left(\frac{R'_{3c} \cdot R'_{4c}}{R'_{3c} + R'_{4c}}\right) \qquad (3.15a)$$

Also,

$$R'_{3c} = \frac{1}{A_c\ h_{nc}} \text{ and } R'_{4c} = \frac{(T_{c2} - T_{air})}{A_c\ \epsilon_c\ \overset{*}{\sigma}_c \cdot F_c (T'_{c2} - T'_{air})} \qquad (3.15b)$$

The thermal conductance k_a and k_c of electrodes is a function of the temperature and can be evaluated from Eq(3.16).

$$k_a = k_{ao}\ (1 + \alpha'_a \Delta T) \qquad .. \qquad (3.16)$$

Forced convective heat transfer coefficients for the case of fluid flow over a flat plate can be evaluated (73) from Eq(3.17) and Eq(3.18) for laminar and turbulent modes respectively.

$$h_x = 0.332\, k(P_r)^{1/3} \left(\frac{V_\infty}{\nu^* x}\right)^{\frac{1}{2}} \quad .. \qquad (3.17)$$

$$\underline{h_x = 0.0296\, \frac{k}{x} (P_r)^{1/3} (R_{ex})^{0.8}}$$ ~~(3.18)~~

The natural convective heat transfer coefficient for laminar flow of air at the outer surface of an electrode is given by Eq(3.19).

$$h_n = C'(\theta^*/L^*)^{0.25} \text{ provided } (G_r P_r) < 10^8 \qquad (3.19)$$

where,

$$\theta^* = T_{wall} - T_{air}$$

Now, total heat transferred to the electrodes from the electrolyte can be obtained from (3.20).

$$*q = *q_a + *q_c \quad ... \qquad (3.20)$$

Using equation (3.20) drop in temperature of the electrolyte due to transfer of heat to the atmosphere is evaluated and accordingly the electrolyte temperature is modified.

This analysis has been applied to analyse the effect of tool material on the temperature distribution within the IEG for cases of brass, copper and stainless steel electrodes. Few of the results have been discussed in chapter 7.

CHAPTER-4

APPLICATIONS OF THE FINITE ELEMENT TECHNIQUE TO ECM PROBLEMS

4.1 INTRODUCTION

Finite element technique (FET) has a profound impact in all the spheres of contemporary engineering analysis and design. It is numerical analysis technique which gives approximate solutions (89) to a wide variety of problems rather than exact closed form solution obtainable only in case of simple problems. This technique is based on the principle of going 'from the part to whole' (60,231). The solution region is analytically modelled approximately by replacing it with an assemblage of discrete elements. Through these discrete elements solution to the whole continuum is attained.

Over the years, finite difference technique (FDT) had most commonly been used as numerical analysis method but it does not provide accurate solution to complex shaped problems as is obtainable from FET; square meshes are incapable to discretize the region accurately (Fig.4.1A). FET is capable of analysing all the three types of non-linear problems (i.e., materially non-linear, geometrically non-linear and both materially and geometrically non-linear) including problems with complex varying boundary conditions (60,89). It is possible to vary the properties between as well as within the elements according to pre-selected polynomial pattern (19). But to obtain realistic

Ⓐ

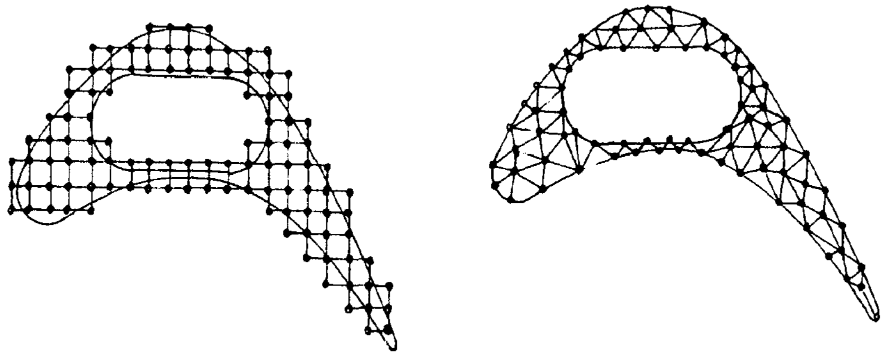

(a) (b)

FIG. 4.1 DISCRETIZATION OF A TURBINE BLADE BY (a) FINITE DIFFERECE (b) FINITE ELEMENT

Ⓑ

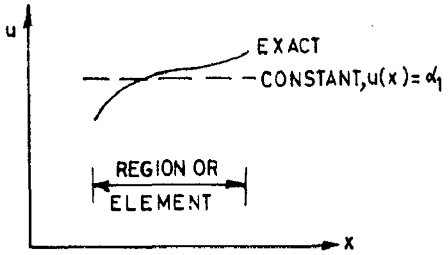
u
EXACT
CONSTANT, $u(x)=\alpha_1$
REGION OR ELEMENT
x

(a) CONSTANT (ONE TERM) POLYNOMIAL

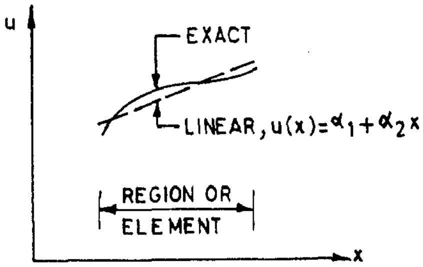
u
EXACT
LINEAR, $u(x)=\alpha_1+\alpha_2 x$
REGION OR ELEMENT
x

(b) LINEAR (TWO TERM) POLYNOMIAL

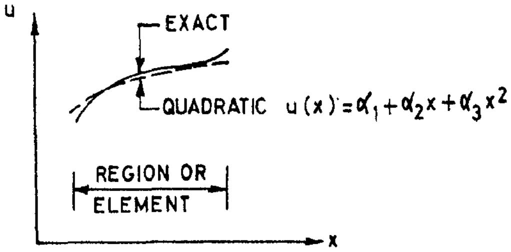
u
EXACT
QUADRATIC $u(x)=\alpha_1+\alpha_2 x+\alpha_3 x^2$
REGION OR ELEMENT
x

(c) QUADRATIC (THREE TERM) POLYNOMIAL

FIG. 4.1 POLYNOMIAL APPROXIMATION IN ONE DIMENSION

results for such complex problems the coefficients or material parameters which describe the basic phenomenon should be accurately known in advance. Another advantage of FET is that only geometrical boundary conditions (b.c.) need to be specified; the natural b.c. are implicitely satisfied in the solution procedure as long as a suitable and valid variational principle is employed. FET has been used extensively to solve a wide variety of problems which can be grouped into equilibrium problems, eignvalue problems and propagation problems (89). A problem can be analysed either in one-, two- or three-dimensions. But majority of the literature deals with one or two-dimensional problems (20). Three dimensional analysis of practical situations is very costly and in many cases it is simply not feasible.

4.2 TYPE OF ELEMENTS AND THEIR CHOICE

Over the last few years, different type of elements have been used in FET and hence a long list of alternative choice of elements exists. However, elements can be classified (2,6) based on (i) element shape such as beam, bar, triangular, rectangular, tetrahedron, etc. (Fig. 4.2); (ii) degrees of freedom; (iii) the completeness of displacement pattern-conforming or non-conforming; (iv) the displacement model used-linear, cubic, etc., (v) the behaviour of the elements-plane stress, plane strain, axi-symmetric, etc.; (vi) nature of the problem one-, two- and three-dimensional (Fig.4.2).

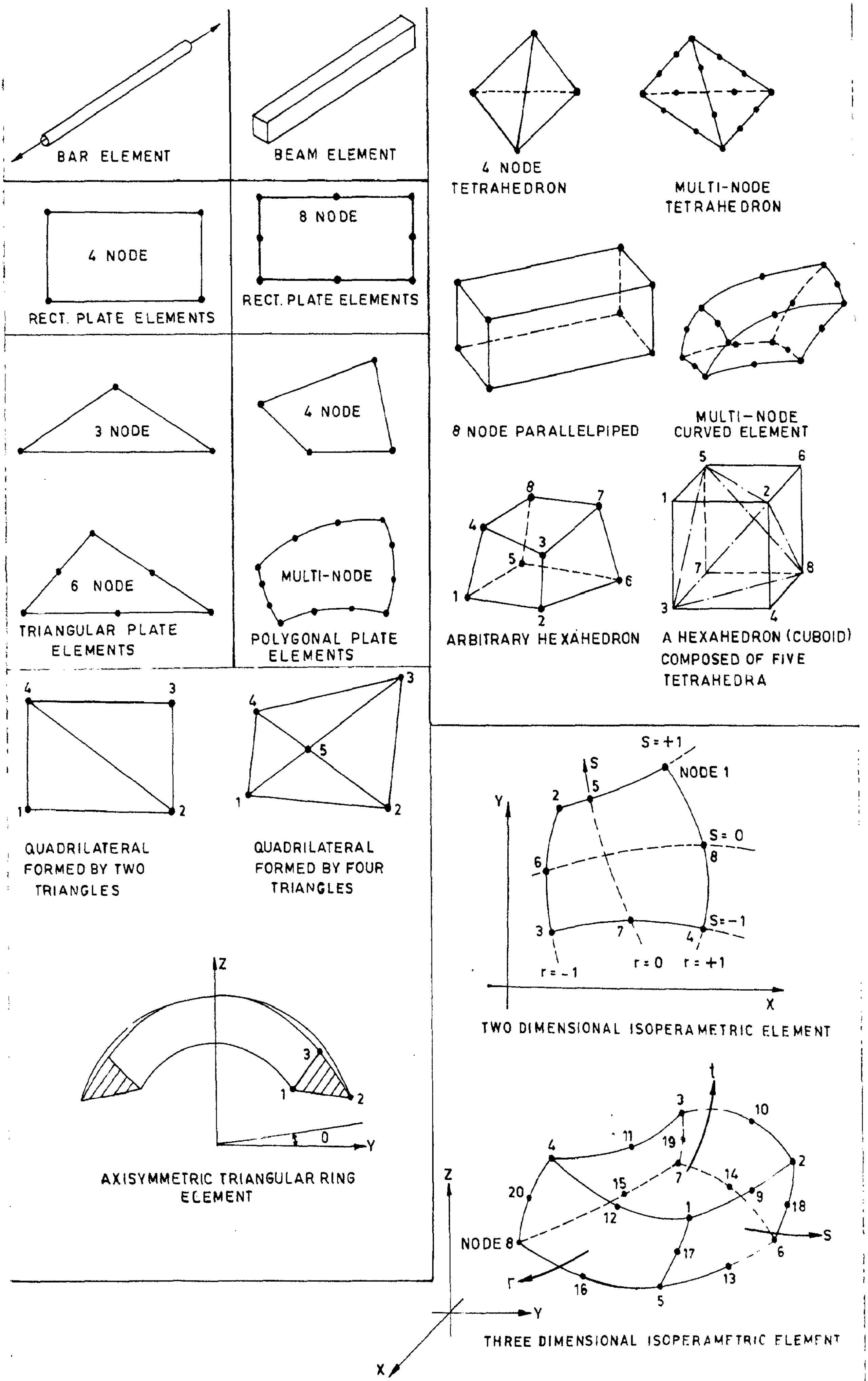
BAR ELEMENT
BEAM ELEMENT
4 NODE
RECT. PLATE ELEMENTS
8 NODE
RECT. PLATE ELEMENTS
3 NODE
6 NODE
TRIANGULAR PLATE ELEMENTS
4 NODE
MULTI-NODE
POLYGONAL PLATE ELEMENTS
4 NODE TETRAHEDRON
MULTI-NODE TETRAHEDRON
8 NODE PARALLELPIPED
MULTI-NODE CURVED ELEMENT
1 2 3 4 5 6 7 8
ARBITRARY HEXAHEDRON
1 2 3 4 5 6 7 8
A HEXAHEDRON (CUBOID) COMPOSED OF FIVE TETRAHEDRA
1 2 3 4
QUADRILATERAL FORMED BY TWO TRIANGLES
1 2 3 4 5
QUADRILATERAL FORMED BY FOUR TRIANGLES
Z
1 2 3
0
Y
AXISYMMETRIC TRIANGULAR RING ELEMENT
Y
S
S=+1
NODE 1
2 5
S= 0
6 8
S=-1
3 7 4
r=-1 r=0 r=+1
X
TWO DIMENSIONAL ISOPERAMETRIC ELEMENT
t
3 10
4 11 19
2
20 15 7 14
9
12 1 18
NODE 8
S
17 6
r
16 13
5
Z
Y
X
THREE DIMENSIONAL ISOPERAMETRIC ELEMENT

FIG. 4.2 TYPES OF FINITE ELEMENTS

selection of a particular type of element and the definition of an appropriate approximating function (i.e., interpolation function) is of utmost importance. Which element provides best alternative in practical usage is judged based on the geometric form of the problem, simplicity of formulation of element properties, versatility of application, computational efforts involved, accuracy obtainable, etc. (2,142).

The size and shape of an element should be selected in such a way that it is capable of simulating accurately, the geometry of the problem. In two and three dimensional analysis an alternative choice of the element is possible. However, a triangular element remains attractive inspite of the developments of a number of other types of elements. With this element it is easy to fit curved boundaries and vary element sizes near stress concentration zones (or higher current density regions near discontinuities and at corners (98) in case of ECM problems). In order to ensure that a small number of elements are able to represent a relatively complex problem, and yield improved accuracy, with the same degree of freedom and reduced data preparation, use of isoparametric elements (19,51,60,231) is recommended. On the other hand, problem formulation with isoparametric elements is more difficult, time required for numerical integration is large and in some cases may result in overall increase in computer time. Reduction in number of complex elements may not be adequate to represent all the local geometries of the real problem. In such cases, often the balance is in favour of the use of simple formulation. Axi-symmetric (or ring type) elements are used when analysing problems which possess axial symmetry in cylindrical coordinates but their forcing functions are also axi-symmetric.

Three dimensional analysis of practical problems is expensive in terms of computation time and effort, in many cases it is simply not feasible. However, tetrahedron and isoparametric elements are more commonly employed elements under such conditions.

4.3 FINITE ELEMENT PROCEDURE IN BRIEF

The solution of the continuum problem can be attained in an orderly and step by step process as follows:

(1) Discretization : The solution region is divided into most suited finite elements. Two or more than two types of element shapes may also be employed in the same solution region.

(2) Field variable model: A field variable may be a scalar, a vector or a higher order tensor. Often polynomials are selected as interpolation functions for the field variable because they are easy to integrate and differentiate. The degree of polynomial chosen depends on the number of nodes assigned (corner nodes, internal nodes and external nodes) to the element, the nature and number of unknowns at each node, and certain continuity requirements imposed at the nodes and along the element boundaries. By truncating an infinite polynomial at different orders, the degree of approximation is varied (Fig.4.1B).

Considering the displacement, q, in a structure that can be expressed by a polynomial $\lfloor f(x,y) \rfloor$ containing one unknown for each degree of freedom possessed by the element. For this case we can write,

$$\{q(x,y)\} = \lfloor f'(x,y) \rfloor \{\beta'\} \qquad .. \qquad (4.1)$$

where $\{q(x,y)\}$ is the displacement at the point (x,y). $\{q\}$ can be expressed in terms of nodal displacement $\{q\}^e$ by substituting nodal coordinates in above equation.

$$\{q\}^e = [A]\{\lambda^*\} \qquad .. \qquad (4.2)$$

where $[A]$ depends upon the nodal coordinates and is known, thus,

$$\{q(x,y)\} = \lfloor f'(x,y) \rfloor \, [A]^{-1} \, \{q\}^e = [N]\{q\}^e \qquad (4.3)$$

Components of $[N]$ are known as 'shape functions' and normally are functions of the position.

(3) Finite element equations: FE equations expressing the properties of individual elements can be derived by either of the four approaches depending upon the nature of the problem. The approaches commonly used are direct approach, variational approach, Galerkin method and Energy balance method. For example, once the displacements are known using Eq(4.3), strains can be evaluated as follows:

$$\{\epsilon(x,y)\} = [\text{diff.of } [N]]\{q\}^e = [B]\{q\}^e \qquad (4.4)$$

Assuming a general elastic behaviour, the stress (σ) and strain (ε) relationship would be linear.

$$\left\{\sigma(x,y)\right\} = \left[D_m\right]\left\{\varepsilon(x,y)\right\} = \left[D_m\right]\left[B\right]\left\{q\right\}^e \qquad (4.5)$$

where $\left[D_m\right]$ is the elasticity matrix and contains the elastic characteristics of the element material.

By imposing virtual displacements and applying the principle of virtual work, the nodal loads are related to nodal displacements as below:

$$\left[Q\right]^e = \left[K\right]^e \left\{q\right\}^e \quad .. \qquad (4.6)$$

where,

$$\left[K\right]^e = \iiint \left[B^T\right]\left[D_m\right]\left[B\right]\, dv \quad .. \qquad (4.6a)$$

(4) Assembly of element properties: To obtain the properties of the overall system modelled by the network of elements, assemble all the element properties derived in earlier section. The stiffness matrix, K, for a complete structure is then obtained as follows:

$$\left[Q\right] = \left[K\right]\left\{q\right\} \quad .. \qquad (4.7)$$

where,

$$\left[K\right] = \sum_{e=1}^{NE} \left[K\right]^e \quad .. \qquad (4.7a)$$

The system equations so obtained, have to be modified to account for the boundary conditions of the problem.

(5) Solution of system equations: Once a set of simultaneous equations is obtained it is solved for unknown nodal values of the field variable. If the equations are linear,

they can be solved by Gaussian Elimination Technique or some other procedure (26,147,194) but solution of non-linear simultaneous equations, is more difficult.

(6) Additional computations: Sometimes, the solution of system equations is needed to calculate other important parameters and should be taken up at this stage.

4.4 FINITE ELEMENT ANALYSIS OF ECM PROCESSES

4.4.1 Introduction

ECM is a highly complex phenomenon. In fact, it is a geometrically and materially non-linear problem, involving a number of interacting parameters varying simultaneously within the interelectrode gap (IEG). In view of the capability of FET to deal with such complex problems, finite element model of ECM has been developed. In this work, basically two types of models have been developed - (i) one dimensional model based on heat transfer phenomenon occuring within the IEG and (ii) two and three dimensional models based on electric potential field distribution within the IEG. However, it is to be noted that the computer program for three dimensional models could not be developed till this time.

4.4.2 One Dimensional FE Analysis of ECM Processes

4.4.2.1 ECM with plane parallel electrode (Model FET-11)

Uni-dimensional FE modelling of ECM process has been based on the following assumptions:

(i) IEG behaves as an uni-dimensional conductor (70,148) (Fig.4.3) i.e. its width and height are negligible compared to the length.

(ii) Heat transferred to the electrodes is negligible and the entire heat energy (only due to joule's heating i.e. I^2R) remains confined within the electrolyte itself. It is further assumed that reversible heat, heat due to chemical reaction, viscous heat and irreversible heat are small and hence negligible(48).

(iii) The electrolyte within the IEG obeys Ohm's law i.e., within the continuum electric current is uniformly distributed over the solution region or in other words the electric current lines flow perpendicular to the tool and workpiece. However, for electric resistance computation, the chordal distance (156) between the two stations has been considered.

(iv) Efficiency of EC dissolution of the anode material is equal to 100% however computer program FET-11 permits to account for actual efficiency.

(v) Effects of anodic films (12,18,42), intergrannular attack (115,116), microstructure (8), change in EC dissolution valency of work material (157), effects of pH value of solution (55) and contamination of the electrolyte on metal removal are small and hence negligible.

(vi) Metal removal is caused due to EC dissolution only and not by disintegration (59) of workpiece material.

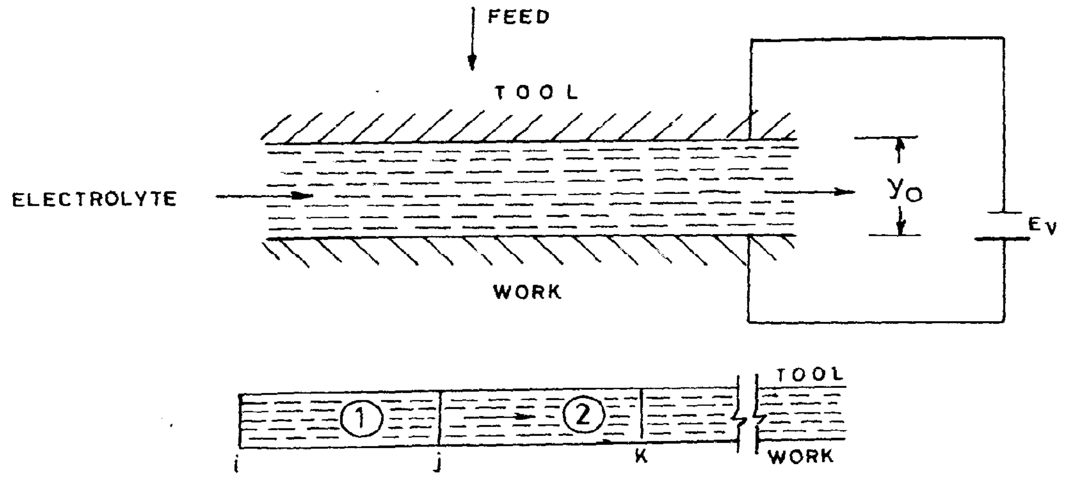
FEED
TOOL
ELECTROLYTE
WORK
y_o
E_v
TOOL
1
2
i
j
K
WORK

FIG.4.3 INTERELECTRODE GAP AS AN UNDIMENSIONAL CONTINUUM
(PLANE PARALLEL ELECTRODE—ECM)

(vii) Temperature of the anode and cathode are equal to that of the electrolyte film in contact with them.

(viii) Within an element, the initial electrolyte conductivity K and IEG, Y are assumed to be known which is later updated to account for varying electrolyte conductivity. However, model FET-12 has been formulated based on varying electrolyte conductivity.

Consider the IEG i.e., electrolyte body acting as an unidimensional continuum (Fig.4.3) and divided into somplex bar elements. The temperature distribution within the IEG has been evaluated as discussed below (142).

For the case under consideration the temperature gradient along the electrolyte flow path is given by Eq(2.8). It can be shown that,

$$T(x) = a_1 + a_2 x = \lfloor 1 \quad x \rfloor \begin{Bmatrix} a_1 \\ a_2 \end{Bmatrix} \qquad .. \qquad (4.8)$$

Also, for x varying between x=xi and x=xj,

$$\delta I = \int_{x_i}^{x_j} \frac{d}{dx}\left(\frac{dT}{dx} \right) \delta T \, dx = 0 \qquad .. \qquad (4.9)$$

and,

$$\frac{dT}{dx} = B T_e$$

where,

$$B = (1/x_{ji}) \lfloor -1 \quad 1 \rfloor$$

From the above we can obtain (142);

$$\frac{dT}{dx}\delta\left(\frac{dT}{dx}\right) dx = \delta\, T_e^T \int_{x_i}^{x_j} B^T B\, T_e\, dx \quad .. \quad (4.10)$$

Using the law of conservation of heat, Eq(4.11) can be obtained for the case of ECM using plane parallel electrodes and with no side surface generation (i.e., where tool is oversized than the workpiece)

$$\frac{dT}{dx} = H^e \frac{D_m}{x_{ji}} \quad .. \quad (4.11)$$

where,

$$H^e = \frac{K \cdot E_V^2}{Y_o} x_{ji} \quad \text{and} \quad D_m = \frac{1}{\rho_e \cdot Y_o \cdot V \cdot C_e} \quad (4.11a)$$

Here, D_m is assumed to be a scalar quantity and x_{ji} is the length of individual element with nodes i-j. From the above,

$$\delta I = \delta\, T_e^T \left[\frac{D_m}{x_{ji}} \begin{Bmatrix} H_i \\ H_j \end{Bmatrix} - \int_{x_i}^{x_j} B^T B T_e\, dx \right] \quad (4.12)$$

since,

$$\delta I = 0 \quad \text{but} \quad \delta T_e \neq 0$$

Therefore,

$$\frac{D_m}{x_{ji}} \begin{Bmatrix} H_i \\ H_j \end{Bmatrix} = \int_{x_i}^{x_j} B^T B T_e\, dx \quad .. \quad (4.13)$$

The conductance matrix (or stiffness matrix) for the case under consideration is given as

$$K_m = \int B^T B\, dx \quad .. \quad (4.14)$$

and could be evaluated to yield the equation below:

$$D_m \cdot H^e = \begin{bmatrix} 1 & -1 \\ -1 & 1 \end{bmatrix} T_e \qquad .. \qquad (4.15)$$

or

$$X = K_m \cdot T_e \qquad .. \qquad (4.15a)$$

For the element 1 let H_1 be the heat generated. Total heat generated within this element can be assumed to be concentrated at node 1 and as the electrolyte flows towards node 2 so does the heat. Heat flowing out of the node is considered to be negative while that flowing towards the node as positive. Assembly of the equations for the two elements gives symmetric, sparse and banded matrix as given below:

$$\begin{Bmatrix} X_1 \\ X_2 \\ X_3 \end{Bmatrix} = \begin{bmatrix} 1 & -1 & 0 \\ -1 & 2 & -1 \\ 0 & -1 & 1 \end{bmatrix} \begin{Bmatrix} T_1 \\ T_2 \\ T_3 \end{Bmatrix} \qquad .. \qquad (4.16)$$

The temperature change in the electrolyte at the entry to element 1 (Fig.4.3) can be taken as zero. Therefore,

$$\Delta T = 0.0 \qquad .. \qquad (4.17)$$

Inserting the boundary conditions (89,142,231) above, the unknown nodal temperatures T_2 and T_3 can be computed.

Model FET-12

In model FET-12, FE formulation has been done based on varying electrolyte conductivity within an element i.e. A'K is not constant in Eq(2.8). Then,

$$\frac{dT}{dx} = A'K_o\left[1 + \alpha(T_j - T_i)\right] = A'K_o(1 - \alpha T_i) + A'K_o\alpha T_j$$

$$= \epsilon_o' + \epsilon_t'$$

Using this equation and following the procedure discussed for model FET-11, it can be shown that for a continuum of five elements, element equations in the assembled form would be given as follows:

$$\begin{bmatrix} 1 & -1 & & & & \\ & 2 & -1 & & \bigcirc & \\ & & 2 & -1 & & \\ & & & 2 & -1 & \\ & & & & 2 & -1 \\ \text{Symmetrical} & & & & & 1 \end{bmatrix} \begin{Bmatrix} T_1 \\ T_2 \\ T_3 \\ T_4 \\ T_5 \\ T_6 \end{Bmatrix} = \begin{Bmatrix} H_1 \\ H_2 \\ H_3 \\ H_4 \\ H_5 \\ H_6 \end{Bmatrix} - \epsilon_o \begin{Bmatrix} -1 \\ 0 \\ 0 \\ 0 \\ 0 \\ -1 \end{Bmatrix}$$

4.4.2.2 Electrochemical drilling and boring

(a) Cylindrical hole; Electrochemically, holes of any shape can be drilled but the analysis presented in this section applies to ECD of cylindrical holes only.

For the case of ECD of cylindrical holes (Fig. 2.3), the resistance R_c of the side gap (59) can be given by;

$$R_c = \frac{1}{2\pi K}\ln(r_2/r_1) \quad .. \quad (4.18)$$

and the current density on the work surface is equal to Eq(4.19)

$$J_{r2} = \frac{E_V K}{r_2 \ln(r_2/r_1)} \quad .. \quad (4.19)$$

With Eqs(4.18) and (4.19), it can be shown that for the case under consideration the values of D_m and H^e in equation (4.11) modify as :

$$D_m = \frac{1}{(r_2^2 - r_1^2)\cdot V\cdot \rho_e\cdot C_e} \quad \text{and} \quad H^e = \frac{2\pi K\, x_{ji}\, E_V^2}{\ln(r_2/r_1)} \qquad (4.20)$$

Eq(4.20) can be used to evaluate column vector X in Eq(4.16). Now, after substituting the b.c. given by Eq(4.17); the set of governing equations thus obtained can be solved by the Gaussian Elimination Technique.

(b) Rectangular hole: Applying 'resistances in parallel' model of ECM in conjunction with the FE technique it is possible to analyse the ECD of rectangular holes (Fig.4.4). In this case, D_m and H^e can be evaluated as follows:

$$D_m = \left[\left\{Y_L(H_L^* + Y_{BL} + Y_{TL}) + H_{TL}^*\cdot Y_{TL} + H_{BL}^*\cdot Y_{BL}\right\}\cdot V\cdot \rho_e\cdot C_e\right]^{-1} \qquad ..\ (4.21)$$

and,

$$H^e = \frac{E_V^2.K.x_{ji}}{R'_{tot}} \quad \text{provided } K_L = K_{BL} = K_{TL} = K \qquad ..\ (4.22)$$

where,

$$R'_{tot} = \frac{\text{cons 1.cons 2}}{\text{cons 1} + \text{cons 2}}\ ; \qquad .. \qquad (4.22a)$$

$$\text{cons 1} = \frac{Y_{TL}\cdot Y_{BL}\cdot Y_L}{\left\{Y_L(Y_{TL}\cdot Y_{BL} + Y_{BL}\cdot H_{TL}^*) + Y_{TL}\cdot Y_{BL}\cdot H_L^*\right\}} \qquad (4.22b)$$

and

$$\text{cons 2} = 2\pi\,\frac{\ln(R_{BL2}/R_{BL1}).\ln(R_{TL2}/R_{TL1})}{\ln(R_{BL2}/R_{BL1}) + \ln(T_{TL2}/R_{TL1})} \qquad (4.22c)$$

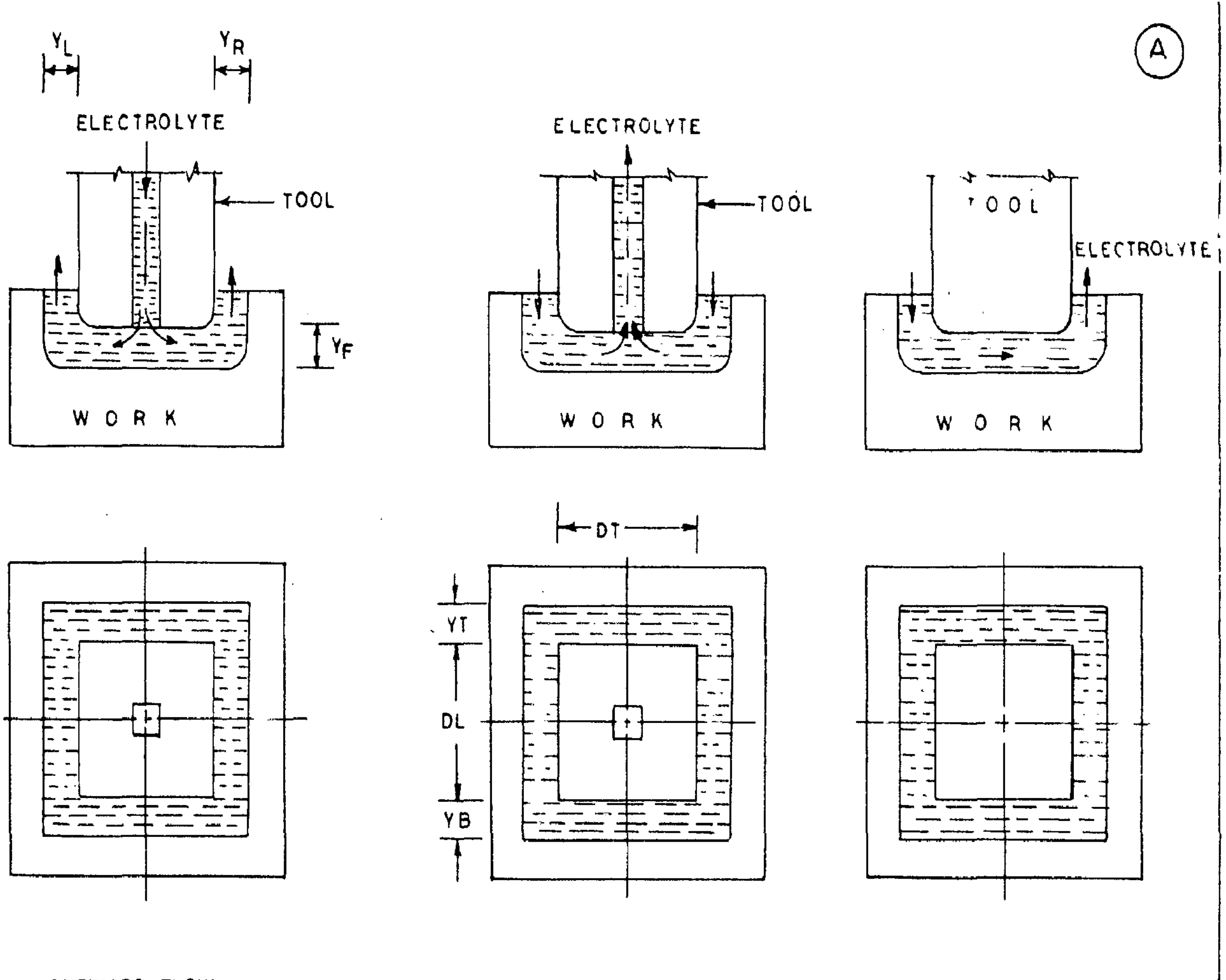
A
Y_L
Y_R
ELECTROLYTE
TOOL
Y_F
WORK
ELECTROLYTE
TOOL
WORK
TOOL
ELECTROLYTE
WORK
DT
YT
DL
YB

OUTWARD FLOW INWARD FLOW SIDE FLOW

FIG. 4.4 E C M SINKING OF RECTANGULAR HOLES USING DIFFERENT MODES OF ELECTROLYTE FLOW

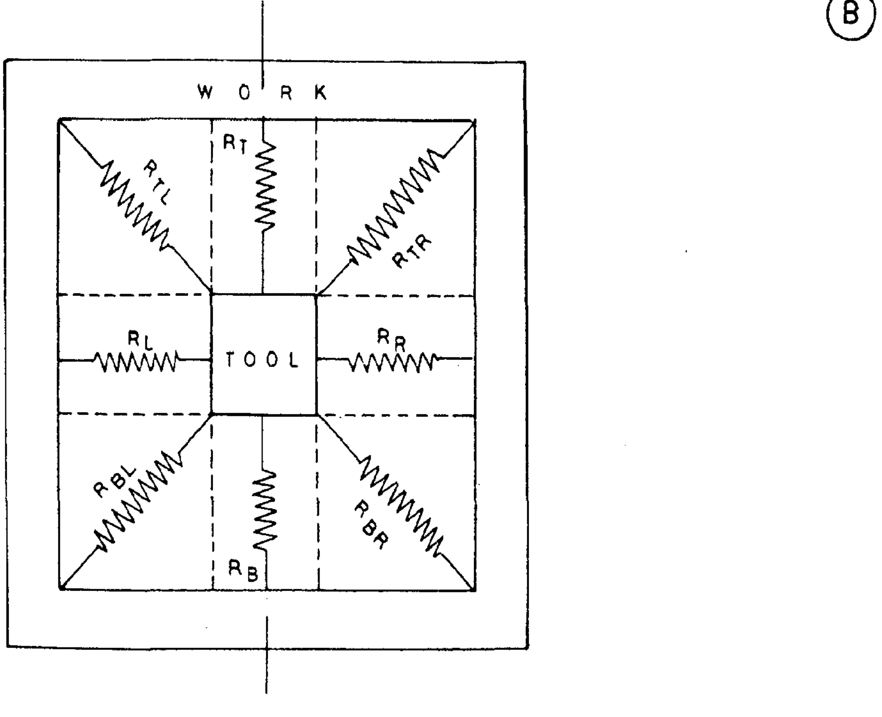
B
WORK
R_T
R_{TL}
R_{TR}
R_L
TOOL
R_R
R_{BL}
R_{BR}
R_B

FIG 4.4 RESISTANCE MODEL OF INTERELECTRODE GAP

Eqs(4.21) and (4.22) have been used to evaluate the resultant vector X in Eq(4.16). Rest of the procedure is the same as discussed earlier.

ECB considered in this thesis is almost a similar in principle as ECD. The type of the tool and workpiece have been assumed to have no rotary motion between them. However, ECD is possible either using a bare tool or 'tool bit' but efficient boring is feasible only with a tool bit. The FE models developed for ECD in this section can well be applied to ECB but will require certain modifications to be incorporated in the scheme of computation as discussed in chapter 3.

4.4.2.3 Electrochemical wire cutting process (ECWCP)

ECWCP can be performed either with rectangular, circular or any other sectioned wire. The FE analysis model discussed for ECD and ECB has been modified so as to apply to the case of rectangular shaped EC wire cutting as well.

For the case being considered the assumptions mentioned in section (4.4.2.1) apply. In addition the assumptions stated in section 3.4 also apply. Based on these assumptions, the D_m and H^e terms in Eq(4.11) would assume the following form:

$$D_m = \left[\left\{Y_F(W + Y_R) + (H^* + Y_F)Y_L + H^*.Y_R\right\} V.C_e\, \rho_e\right]^{-1} \qquad \cdot\cdot \quad (4.23a)$$

and,

$$H^e = \frac{E_V^2 \cdot x_{ji} \cdot K}{R'_{tot}} \qquad \cdot\cdot \quad (4.23b)$$

where, $$R'_{tot} = \frac{Y_F \cdot Y_L \cdot Y_R}{(Y_L \cdot Y_R \cdot A_F + Y_F \cdot Y_R \cdot A_L + Y_F \cdot Y_L \cdot A_R)} \qquad (4.23c)$$

It can be assumed that

$$K_L = K_F = K_R = K \quad .. \qquad (4.23d)$$

Using these equations, X in Eq(4.16) can be evaluated and thereby the unknown nodal temperature can also be determined.

4.4.3 Two Dimensional FE Analysis of ECM Process (Model FET-22)

Uni-dimensional heat transfer finite element model (FET-11), for ECM, was developed earlier based on the assumption that IEG obeys the Ohm's law. This assumption may be true in the early stages of ECM with plane parallel electrodes. It has been pointed out (52,148,210) that the electric field at a point where the curvature of the electrode surface is large and convex is much greater than the electric field at a plane surface (Fig.4.5).

In general the electric field potential distribution within the IEG obeys the Laplace's equation. For a two dimensional case, it can be written as:

$$\frac{\partial^2 \phi}{\partial x^2} + \frac{\partial^2 \phi}{\partial y^2} = 0 \quad .. \qquad (4.24)$$

The field vector ϕ in equation (4.24) should be determined in such a manner that it satisfies the boundary conditions and also minimizes the functional $I(\phi)$ given by Eq(4.25).

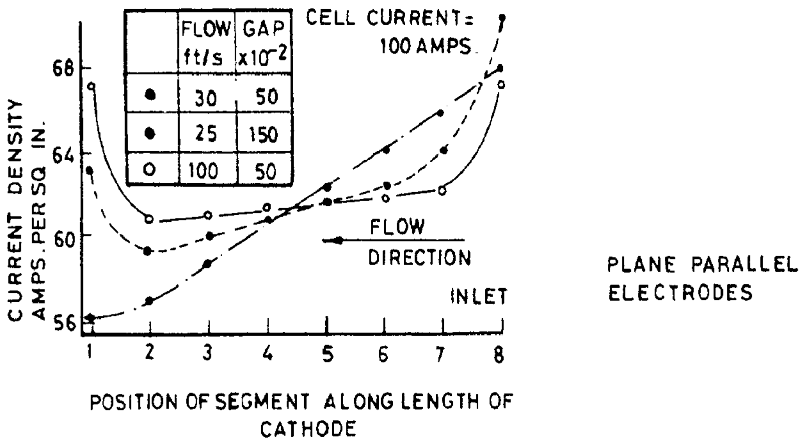

FIG. 4.5 CURRENT DENSITY VARIATION ALONG ELECTROLYTE FLOW PATH

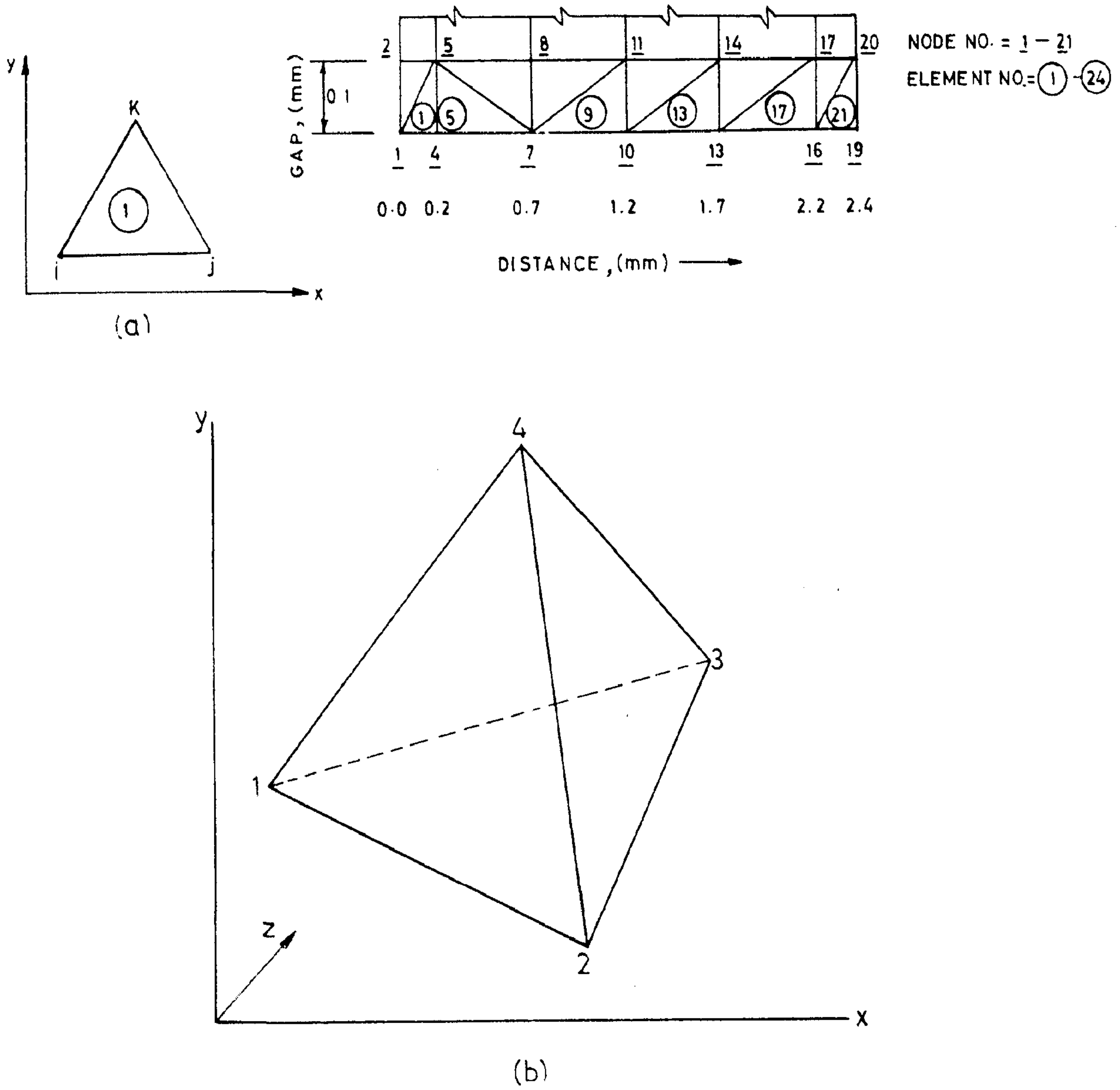
y
K
1
i
j
x
(a)
GAP, (mm)
0.1
2
5
8
11
14
17
20
1
4
7
10
13
16
19
1
5
9
13
17
21
0.0
0.2
0.7
1.2
1.7
2.2
2.4
DISTANCE, (mm)
NODE NO. = 1 – 21
ELEMENT NO.= 1 - 24
y
4
3
1
2
z
x
(b)

FIG. 4.6 FINITE ELEMENTS (a) TRIANGULAR (b) TETRAHEDRON

$$I(\phi) = \iint \left[\frac{1}{2} \left\{ \left(\frac{d\phi}{dx} \right)^2 + \left(\frac{d\phi}{dy} \right)^2 \right\} \right] dx\,dy \quad .. \quad (4.25)$$

Using simplex triangular elements (Fig.4.6a) to represent the IEG, the field variable $\phi(x,y)$ has been assumed to vary linearly (51) within the element throughout the solution domain. For such a case we can write,

$$\phi(x,y) = N_i\phi_i + N_j\phi_j + N_k\phi_k = \lfloor N \rfloor^e \{\phi\}^e \quad .. \quad (4.26)$$

where $\{\phi\}^e$ is the column vector of nodal potentials for element 'e' and the interpolation functions N^e are defined as follows:

$$N_B^e = \frac{a_B + b_B x + c_B y}{2\Delta^e} \qquad \text{where, } B=i,j,k \qquad (4.27)$$

a_B, b_B and c_B are defined as below:

$$a_i = x_j y_k - x_k Y_j; \quad b_i = Y_j - Y_k, \quad C_i = x_k - x_j, \ldots \qquad (4.27a)$$

Similarly, other terms can be evaluated in cylic permutation of the subscripts i,j and k.

To derive element equations, Eq(4.26) has to be substituted into Eq(4.25) and differentiation leads to;

$$\frac{\partial I^e}{\partial \phi_i} = \iint \left[\left\{ \left(\frac{\partial N_i}{\partial x} \right)\phi_i + \left(\frac{\partial N_j}{\partial x} \right)\phi_j + \left(\frac{\partial N_k}{\partial x} \right)\phi_k \right\} \frac{\partial N_i}{\partial x} \right.$$

$$\left. + \left\{ \left(\frac{\partial N_i}{\partial y} \right)\phi_i + \left(\frac{\partial N_j}{\partial y} \right)\phi_j + \left(\frac{\partial N_k}{\partial y} \right)\phi_k \right\} \frac{\partial N_i}{\partial y} \right] dx\,dy$$

$$.. \quad (4.28)$$

similarly, the equations can be derived for nodes j and k of an element. Then the equations for the nodes i,j and k of an element combined together can be written in a standard form as follows:

$$\begin{Bmatrix} \frac{\partial I^e}{\partial \phi_i} \\ \frac{\partial I^e}{\partial \phi_j} \\ \frac{\partial I^e}{\partial \phi_k} \end{Bmatrix} = \left[K_m\right]^e \left\{\phi\right\}^e = \left\{0\right\} \quad .. \quad (4.29)$$

where, K_m is the stiffness matrix with the following coefficients for the element 1.

$$\begin{bmatrix} K_{ii} & K_{ij} & K_{ik} \\ K_{ji} & K_{jj} & K_{jk} \\ K_{ki} & K_{kj} & K_{kk} \end{bmatrix} \begin{Bmatrix} \phi_i \\ \phi_j \\ \phi_k \end{Bmatrix} = \left\{0\right\} \quad .. \quad (4.30)$$

and the coefficients of the stiffness matrix (19,142) are given by

$$K_{ij}^{(e)} = \iint \left(\frac{\partial N_i}{\partial x} \cdot \frac{\partial N_j}{\partial x} + \frac{\partial N_i}{\partial y} \frac{\partial N_j}{\partial y} \right) dx\, dy \quad (4.31)$$

Using the definition of interpolation function, it can be proved that;

$$K_{ij}^{e} = (b_i b_j + C_i C_j)\,(4\Delta^e)^{-1} \quad .. \quad (4.32)$$

The matrices for individual element, say 3, can be assembled together (51) to give the system equations. The system equations assembly procedure is based on insistence of compatibility at the element nodes. It would result into the following stiffness matrix:

$$\begin{bmatrix} K_{11}^{(1)*+} + K_{11}^{(3)} & K_{12}^{(1)} & K_{13}^{(3)} & K_{14}^{(1)} + K_{14}^{(3)} \\ K_{21}^{(1)} & K_{22}^{(1)} + K_{22}^{(2)} & K_{23}^{(2)} & K_{24}^{(1)} + K_{24}^{(2)} \\ K_{31}^{(3)} & K_{32}^{(2)} & K_{33}^{(2)} + K_{33}^{(3)} & K_{34}^{(2)} + K_{34}^{(3)} \\ K_{41}^{(1)} + K_{41}^{(3)} & K_{42}^{(1)} + K_{42}^{(2)} & K_{43}^{(2)} + K_{43}^{(3)} & K_{44}^{(1)} + K_{44}^{(2)} + K_{44}^{(3)} \end{bmatrix} \begin{Bmatrix} \phi_1 \\ \phi_2 \\ \phi_3 \\ \phi_4 \end{Bmatrix} = \{0\}$$

+*Superscripts under bracket mean element number.

.. (4.33)

Reactions at the electrodes cause current density dependent overpotentials (148). Their presence at the electrodes would alter the b.c. as follows:

$$\phi = f^*(J) \quad \text{at the cathode}$$

$$\phi = E_V - g^*(J) \quad \text{at the anode} \qquad .. \quad (4.34)$$

where $f^*(J)$ and $g^*(J)$ are arbitrary functions for the cathodic and anodic overpotentials respectively. For the sake of simplicity it has been assumed that the electrode surfaces are equipotentials, which means

$$\left.\begin{array}{ll} \phi = 0.0 & \text{at the cathod} \\ \phi = E_V & \text{at the anode} \end{array}\right) \qquad .. \quad (4.35)$$

After substitution of the b.c., Eq(4.35), a set of simultaneous equations would be obtained which in the present case has been solved using Gaussian Elimination Technique. Thereafter, other calculations have been made as per method described in chapter 5.

4.4.4 Three Dimensional FE Analysis of ECM Process (Model FET-33)

Laplace Eq(2.15) can also be used for the evaluation of three dimensional potential distribution within the IEG. The problem is then equivalent to finding the distribution of ϕ that satisfies the b.c. and minimizes the functional I.

$$I(\phi) = \iiint \frac{1}{2}\left[\left(\frac{\partial \phi}{\partial x}\right)^2 + \left(\frac{\partial \phi}{\partial y}\right)^2 + \left(\frac{\partial \phi}{\partial z}\right)^2 \right] dx\, dy\, dz \qquad (4.36)$$

or,

$$I(\phi) = \iiint \frac{1}{2} \{g\}^T \left[D_m\right] \{g\}\, dv$$

where,

$$g^T = \left\lfloor \frac{\partial \phi}{\partial x} \quad \frac{\partial \phi}{\partial y} \quad \frac{\partial \phi}{\partial z} \right\rfloor$$

and D_m is an unitary matrix.

$$I = I^{(1)} + I^{(2)} + I^{(3)} + \ldots + I^{NE} = \sum_{e=1}^{NE} I^{(e)}$$

where, $I^{(e)}$ is the contribution of a single element to I. The minimization of I occurs when

$$\frac{\partial I}{\partial \{\phi\}} = \frac{\partial}{\partial \{\phi\}} \sum_{e=1}^{NE} I^{(e)} = \sum_{e=1}^{NE} \frac{\partial I^{(e)}}{\partial \{\phi\}} = 0 \quad .. \qquad (4.37)$$

To evaluate the derivatives $\frac{\partial I}{\partial \{\phi\}}$, integral should be written in terms of nodal values i.e.,

$$\phi = [N]^{(e)} \{\phi\}^{(e)} \quad .. \quad (4.38)$$

Therefore,

$$g^{(e)} = \left\{ \begin{matrix} \frac{\partial \phi^{(e)}}{\partial x} \\ \frac{\partial \phi^{(e)}}{\partial y} \\ \frac{\partial \phi^{(e)}}{\partial z} \end{matrix} \right\}$$

$$= \begin{bmatrix} \frac{\partial N_1^{(e)}}{\partial x} & \frac{\partial N_2^{(e)}}{\partial x} & \cdots & \frac{\partial N_e^{(e)}}{\partial x} \\ \frac{\partial N_1^{(e)}}{\partial y} & \frac{\partial N_2^{(e)}}{\partial y} & \cdots & \frac{\partial N_e^{(e)}}{\partial y} \\ \frac{\partial N_1^{(e)}}{\partial z} & \frac{\partial N_2^{(e)}}{\partial z} & \cdots & \frac{\partial N_e^{(e)}}{\partial z} \end{bmatrix} \left\{ \begin{matrix} \phi_1 \\ \phi_2 \\ \vdots \\ \phi_e \end{matrix} \right\}$$

$$= [B]^{(e)} \{\phi\} \quad .. \quad (4.39)$$

Here, $[B]^{(e)}$ contains information related to derivatives of the shape functions. After simplification it can be shown that,

$$\frac{\partial I}{\partial \phi} = [K_m^e]\{\phi\} \quad .. \quad (4.40)$$

where,

$$K_m = \iiint [B^{(e)}]^T [D_m^{(e)}][B^{(e)}] \, dv \quad .. \quad (4.40a)$$

The final system of equations is obtained by substituting (4.40) into (4.37)

$$\frac{\partial I}{\partial \phi} = \sum_{e=1}^{NE} \left[K_m^{(e)}\right]\left\{\phi\right\} \quad .. \qquad (4.41)$$

Evaluation of stiffness matrix K_m involves the solution of an integral Eq(4.40a) and its value is a function of the type of the element being used. Fig. 4.6b illustrates tetrahedral elements used for the analysis below.

Assuming linear interpolation function, field variable $\phi(x,y,z)$ can be uniquely and continuously represented in the solution domain by Eq(4.42).

$$\phi(x,y,z) = \left[N^{(e)}\right]\left\{\phi^{(e)}\right\} = N_i\phi_i + N_j\phi_j + N_k\phi_k + N_l\phi_l \qquad (4.42)$$

Differentiation of functional I and simplification leads to Eq(4.43).

$$\begin{bmatrix} K_{ii} & K_{ij} & K_{ik} & K_{il} \\ K_{ji} & K_{jj} & K_{jk} & K_{jl} \\ K_{ki} & K_{kj} & K_{kk} & K_{kl} \\ K_{li} & K_{lj} & K_{lk} & K_{ll} \end{bmatrix} \begin{Bmatrix} \phi_i \\ \phi_j \\ \phi_k \\ \phi_l \end{Bmatrix} = \left\{0\right\} \quad .. \qquad (4.43)$$

where, K_{ii}, K_{ij},...,K_{ll} are coefficients of stiffness matrix $K_m^{(e)}$ that can be evaluated as follows:

$$K_{ij}^{e} = \iiint \left(\frac{\partial N_i}{\partial x} \cdot \frac{\partial N_j}{\partial x} + \frac{\partial N_i}{\partial y} \cdot \frac{\partial N_j}{\partial y} + \frac{\partial N_i}{\partial z} \cdot \frac{\partial N_j}{\partial z} \right) dx\, dy\, dz \qquad (4.44)$$

Using the definition of interpolation function, Eq(4.44) can be shown to be reduced as,

$$K_{ij} = \frac{1}{36\,v^2}\left[b_i b_j + C_i C_j + d_i d_j\right] \quad \cdot\cdot \quad (4.45)$$

where, a,b,c and d are constants for an element and can be computed (60).

The analysis presented above would give three dimensional potential distribution within the IEG from which current density, metal removal rate, temperature distribution, etc., could be computed in a manner similar to that in FET-22.

CHAPTER-5

COMPUTER APPLICATION TO ECM

This chapter describes in brief, the development of generalized computer programs for the computation of anode profile, metal removal, etc., in ECM. The results obtained have been employed for the analysis and parametric study of ECM and related processes. The computer simulation was conducted on an IBM 1620, IBM 360 and IBM 370 computer systems at different stages of the work.

The 1st section of this chapter describes briefly the computer programs and the subroutines. For the sake of clarity the logic diagrams (or flow charts) have also been included. Listing of the main program and some important subroutines of SGFET-11 and FET-22 are also given in the Appendix-II.

5.1 METAL REMOVAL BY EC DISSOLUTION

5.1.1 Unidimensional Case (Models FET-11 and SGFET-11)

This refers to the case of idealisation of the IEG by unidimensional continuum and the computation of anode profile generation in ECD. The program generates the element properties and stiffness matrix itself. The logic diagram of the proposed programme is given in Fig.5.1. With slight modifications, this program can also be applied to solution of problems by FET-11 (Flow chart in Fig.5.2).

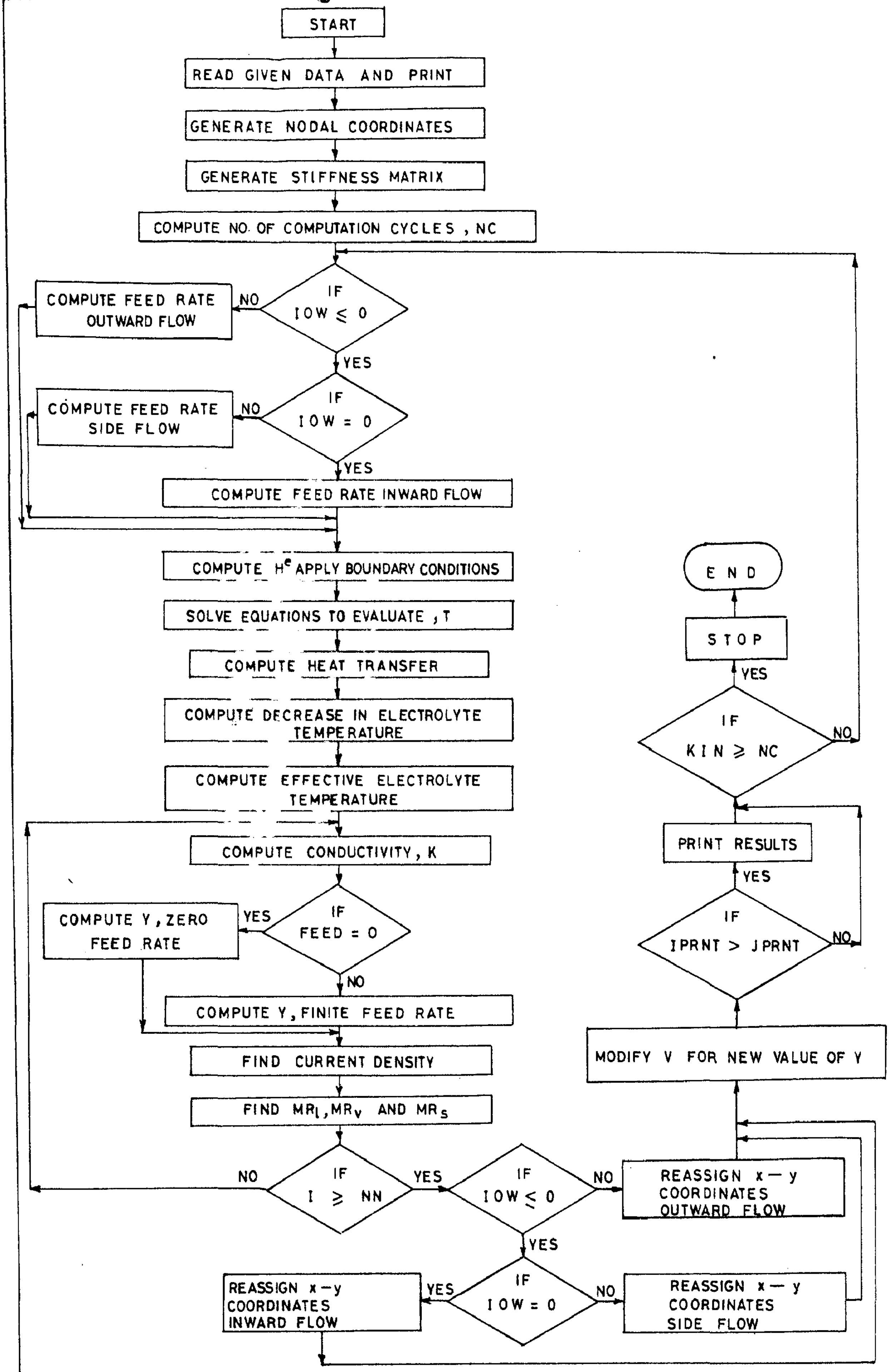
START
READ GIVEN DATA AND PRINT
GENERATE NODAL COORDINATES
GENERATE STIFFNESS MATRIX
COMPUTE NO. OF COMPUTATION CYCLES , NC
IF IOW ≤ 0
NO
COMPUTE FEED RATE OUTWARD FLOW
YES
IF IOW = 0
NO
COMPUTE FEED RATE SIDE FLOW
YES
COMPUTE FEED RATE INWARD FLOW
COMPUTE H^e APPLY BOUNDARY CONDITIONS
SOLVE EQUATIONS TO EVALUATE , T
COMPUTE HEAT TRANSFER
COMPUTE DECREASE IN ELECTROLYTE TEMPERATURE
COMPUTE EFFECTIVE ELECTROLYTE TEMPERATURE
COMPUTE CONDUCTIVITY, K
IF FEED = 0
YES
COMPUTE Y, ZERO FEED RATE
NO
COMPUTE Y, FINITE FEED RATE
FIND CURRENT DENSITY
FIND MR_l, MR_v AND MR_s
IF I ≥ NN
NO
YES
IF IOW ≤ 0
NO
REASSIGN x — y COORDINATES OUTWARD FLOW
YES
IF IOW = 0
YES
REASSIGN x — y COORDINATES INWARD FLOW
NO
REASSIGN x — y COORDINATES SIDE FLOW
MODIFY V FOR NEW VALUE OF Y
IF IPRNT > JPRNT
YES
NO
PRINT RESULTS
IF KIN ≥ NC
YES
NO
STOP
END

FIG. 5.1 COMPUTATIONAL SCHEME USED IN MODEL SGFET- 11

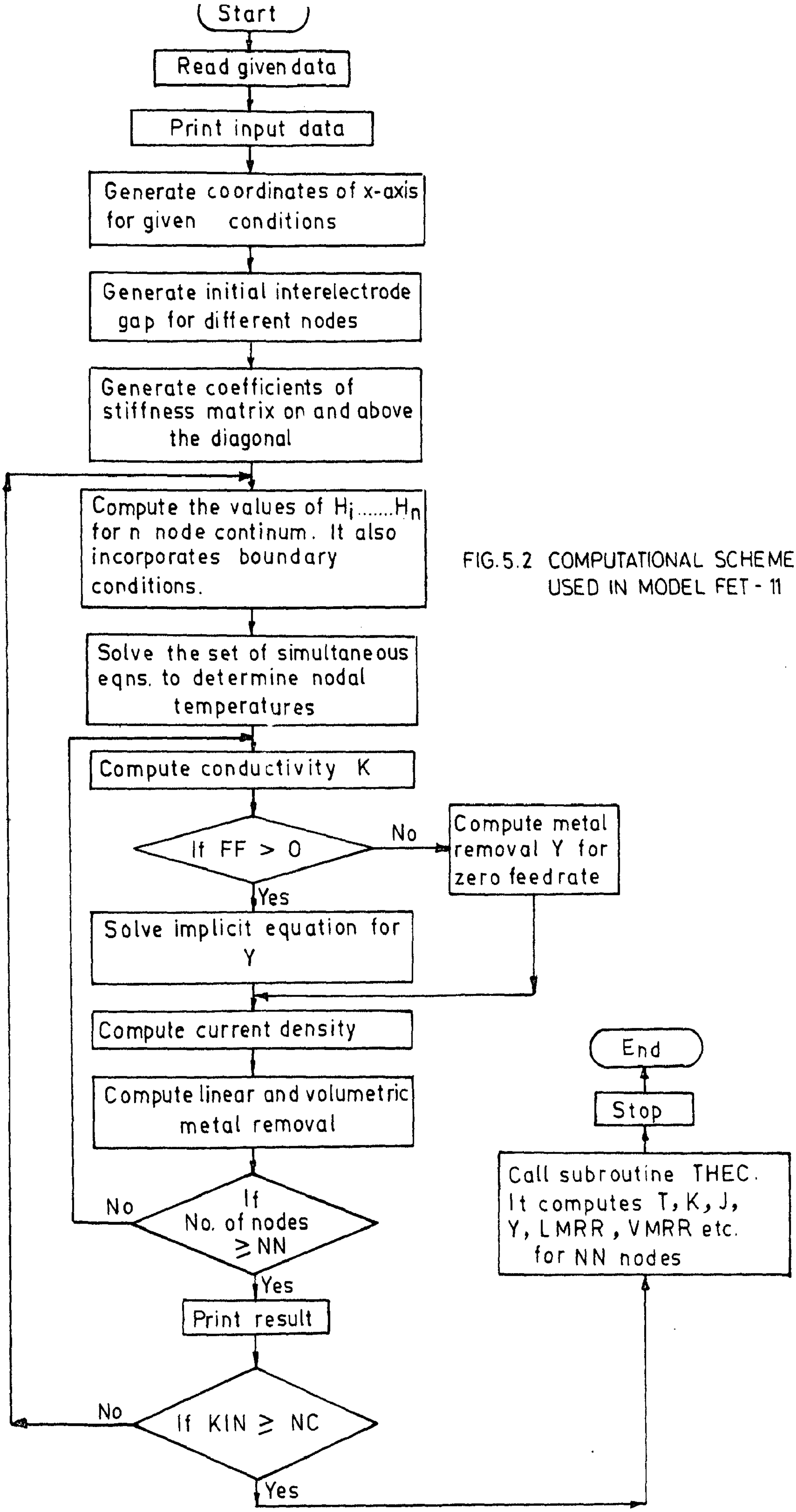
Start
Read given data
Print input data
Generate coordinates of x-axis for given conditions
Generate initial interelectrode gap for different nodes
Generate coefficients of stiffness matrix on and above the diagonal
Compute the values of H_i.......H_n for n node continum. It also incorporates boundary conditions.
Solve the set of simultaneous eqns. to determine nodal temperatures
Compute conductivity K
If FF > 0
No
Compute metal removal Y for zero feedrate
Yes
Solve implicit equation for Y
Compute current density
Compute linear and volumetric metal removal
If No. of nodes ≥ NN
No
Yes
Print result
If KIN ≥ NC
No
Yes
Call subroutine THEC. It computes T, K, J, Y, LMRR, VMRR etc. for NN nodes
Stop
End

FIG. 5.2 COMPUTATIONAL SCHEME USED IN MODEL FET - 11

5.1.2 Two Dimensional Case (Model FET-22 and SGFET-22)

This program refers to FE idealization of two dimensional ECM process. For this purpose, simplex triangular elements have been used. This program is capable of generating automatically the global stiffness matrix in assembled form, apply the prescribed boundary conditions and store the stiffness matrix in the banded form. The governing equations have been solved by the use of Gaussian Elimination Technique. It should be noted that the potential distribution within the IEG, in this case, has been obtained by solving Laplacian equation (2.15). The flow chart for the scheme of computation by FET-22 is given in Fig.5.4. With slight modifications the program can also be applied to predict anode profile by model SGFET-22 (Fig.5.3).

5.2 A BRIEF DESCRIPTION OF SUBROUTINES USED

Computer programs mentioned above, make use of a number of subroutines some of which have been described here in brief.

(a) Program - SGFET-11 ;

(i) Subroutine AGNC

This subroutine permits 'automatic generation of the nodal coordinates' of the elements. For the given length of the domain, total number of nodes, elements and their length has to be specified. In this case, use of unequal elements is also possible.

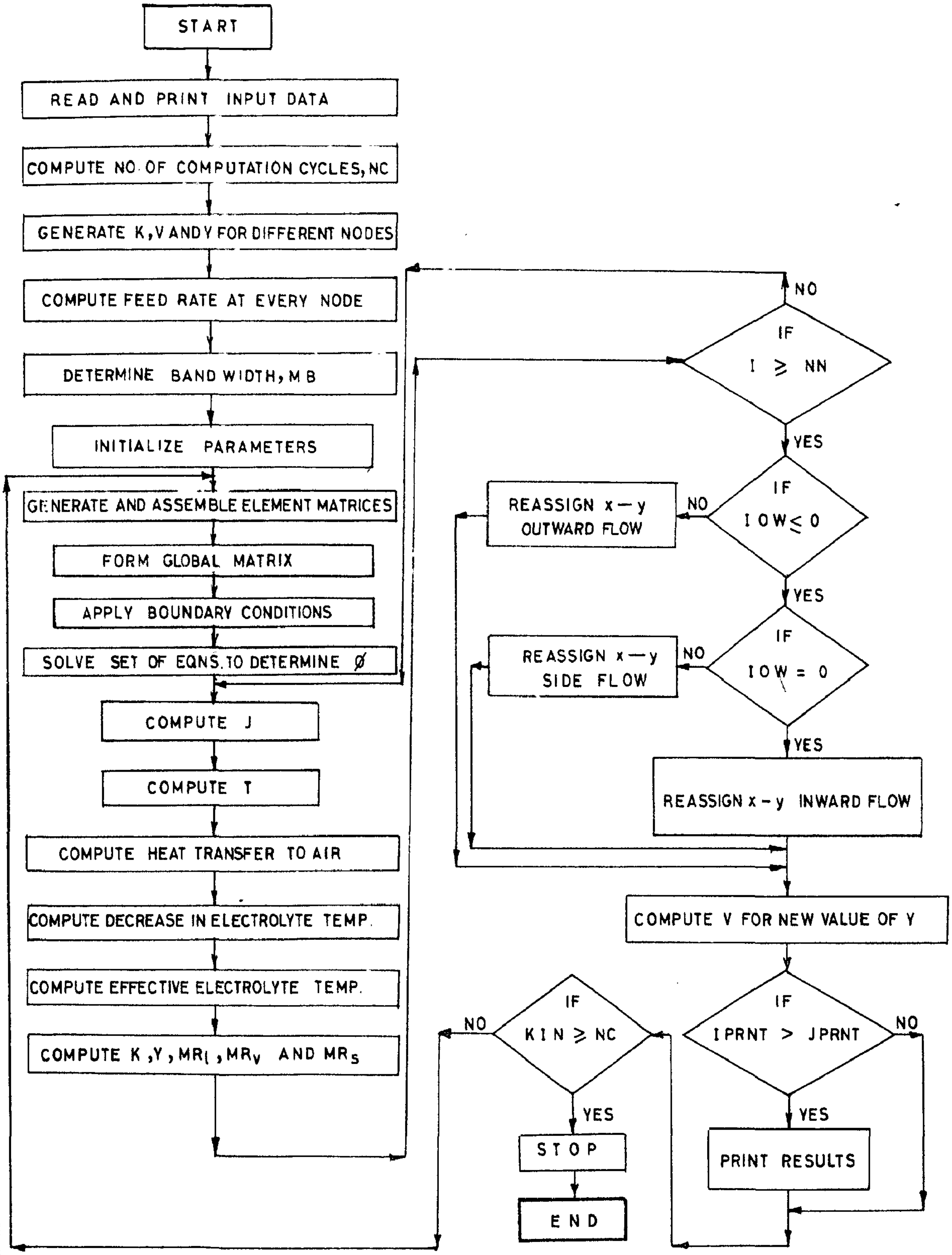
START
READ AND PRINT INPUT DATA
COMPUTE NO OF COMPUTATION CYCLES, NC
GENERATE K,V AND Y FOR DIFFERENT NODES
COMPUTE FEED RATE AT EVERY NODE
DETERMINE BAND WIDTH, MB
INITIALIZE PARAMETERS
GENERATE AND ASSEMBLE ELEMENT MATRICES
FORM GLOBAL MATRIX
APPLY BOUNDARY CONDITIONS
SOLVE SET OF EQNS. TO DETERMINE Ø
COMPUTE J
COMPUTE T
COMPUTE HEAT TRANSFER TO AIR
COMPUTE DECREASE IN ELECTROLYTE TEMP.
COMPUTE EFFECTIVE ELECTROLYTE TEMP.
COMPUTE K, Y, MRl, MRv AND MRs
IF I ≥ NN
NO
YES
IF IOW ≤ 0
NO
REASSIGN x−y OUTWARD FLOW
YES
IF IOW = 0
NO
REASSIGN x−y SIDE FLOW
YES
REASSIGN x−y INWARD FLOW
COMPUTE V FOR NEW VALUE OF Y
IF IPRNT > JPRNT
NO
YES
PRINT RESULTS
IF KIN ≥ NC
NO
YES
STOP
END

FIG.5.3 COMPUTATIONAL SCHEME USED IN MODEL SGFET – 22

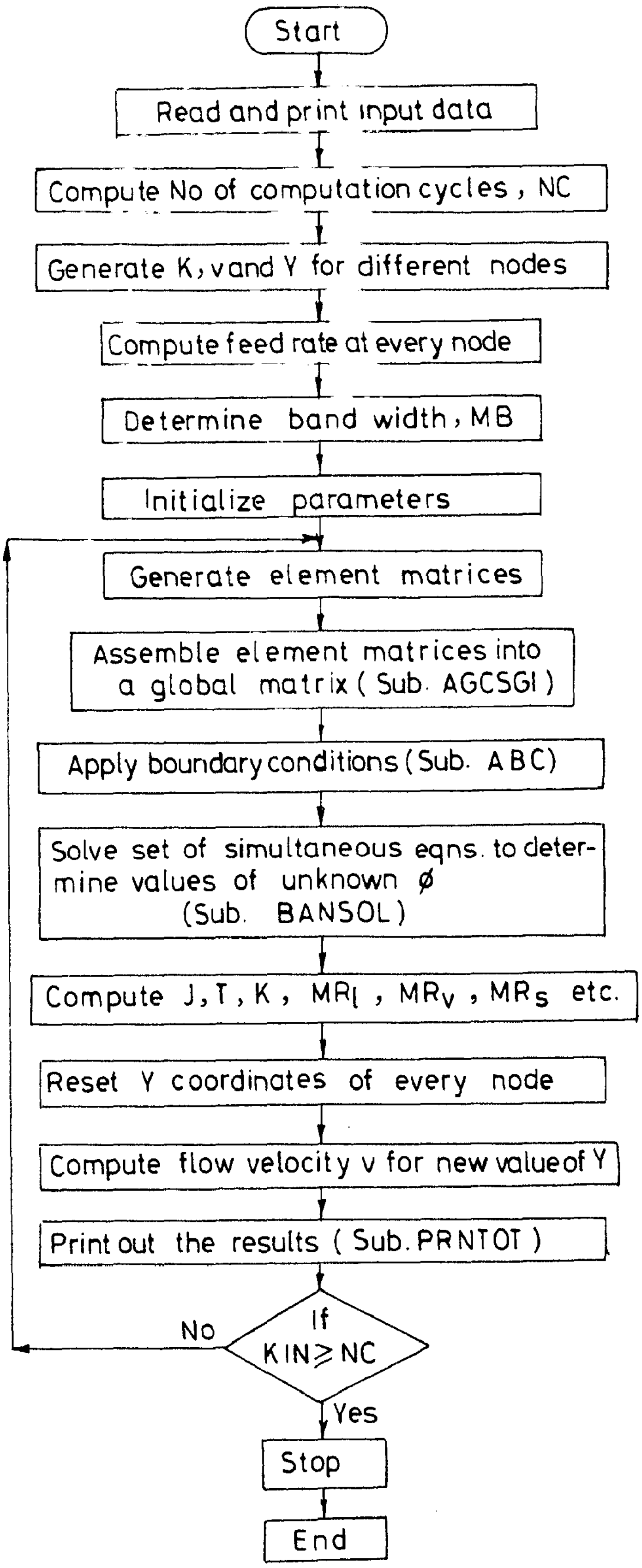
Start
Read and print input data
Compute No of computation cycles, NC
Generate K, v and Y for different nodes
Compute feed rate at every node
Determine band width, MB
Initialize parameters
Generate element matrices
Assemble element matrices into a global matrix (Sub. AGCSGI)
Apply boundary conditions (Sub. ABC)
Solve set of simultaneous eqns. to determine values of unknown ø (Sub. BANSOL)
Compute J, T, K, MRl, MRv, MRs etc.
Reset Y coordinates of every node
Compute flow velocity v for new value of Y
Print out the results (Sub. PRNTOT)
If KIN ≥ NC
No
Yes
Stop
End

FIG. 5.4 COMPUTATIONAL SCHEME USED IN MODEL FET-22

(ii) Subroutine AGCSM

This permits 'automatic generation of the coefficients of stiffness (or conductance) matrix' and takes into account the b.c. of the nature discussed earlier (chapter 4). With this subroutine it is possible to generate the coefficients only on and above the diagonal and upto half band width of the conductance matrix.

(iii) Subroutine GET

This subroutine solves banded, sparse and symmetric matrix which comprises a set of governing equations of the type (4.16). It is based on the philosophy of Gaussian Elimination Technique(26).

(iv) Subroutine BIR

This subroutine solves the implicit equations used to compute the IEG for the case of finite feed rate by applying the technique of 'Bisection Method for Real Roots" (147).

(v) Subroutine DATIN

The subroutine reads in and prints out (punches out or writes out) the input data.

(vi) Subroutine THEC

This subroutine has been developed to compute the theoretical results by applying the exact formulae (named as model-1).

(vii) Subroutine REVEC

This subroutine supplies the values of resultant vectors (or force vectors or column vectors) X for each node.

(viii) Subroutine FETCL

This calculates the electrolyte conductivity, current density, MRR and IEG obtained.

(ix) Subroutine PRNTOT

This subroutine prints out the desired results in the specified format.

(x) Subroutine INFLO

This subroutine reassigns the nodal coordinates and modifies the number of nodes and elements under active EC dissolution for the case of radial inward flow mode of electrolyte.

(xi) Subroutine SIDFLO

It performs the same function as INFLO but applies to the case of side flow mode of electrolyte.

(xii) Subroutine OUTFLO

This performs the similar functions as INFLO with the difference that it applies to the case of radial outward flow mode of the electrolyte.

(b) Program FET-22:

Some of the subroutines used in this program are described below, in brief.

(i) Subroutine ABC

This subroutine is concerned with the application of exact boundary conditions of the problem.

(ii) Subroutine BANSOL

This solves the sparse, banded and symmetric matrix and gives the field potential distribution within the IEG.

(iii) Subroutine CDTC

This subroutine calculates the current density, temperature and electrolyte conductivity after obtaining the electric field potential distribution within the IEG.

(iv) Subroutine INELGP

This calculates the IEG for the case of zero and finite feed rate conditions for a node at any instant of time 't'.

(v) Subroutine METR

A subroutine that evaluates linear, volumetric and specific MRR.

(vi) Subroutine BWD

A subroutine that determines the value of band width and supplies the same to the main program.

(vii) Subroutine ZER

A subroutine that initialises the matrix.

This program also contains the subroutines like DATIN and PRINTOT performing the same type of functions as mentioned earlier in program SGFET-11.

CHAPTER-6

EXPERIMENTAL PROGRAMME

6.1 EXPERIMENTAL SETUP

To verify the analytical models developed in chapters 3 and 4, experiments were conducted on an ECM system. Fig. 6.1 shows an overall view of the experimental setup used. The experimental setup has been described, in brief, under the following heads:

a) Power source
b) Electrolyte cleaning and electrolyte supply system
c) Tool and tool feed system
d) Work and work holder.

(a) Power source :

This consisted of a rectifier unit (13) to convert 3 phase a.c. power supply into a low voltage d.c. supply, a transformer (21 & 22) along with a voltage regulator (19) so that the desired input d.c. voltage could be obtained across the electrodes. Since, ammeter (14) and voltmeter (15) built in the power unit have coarse range, therefore, fine ranged ammeter (17) and voltmeter (not shown) were used. During experimentation the workpiece (2) was made as the anode whereas the tool (1) was made as the cathode.

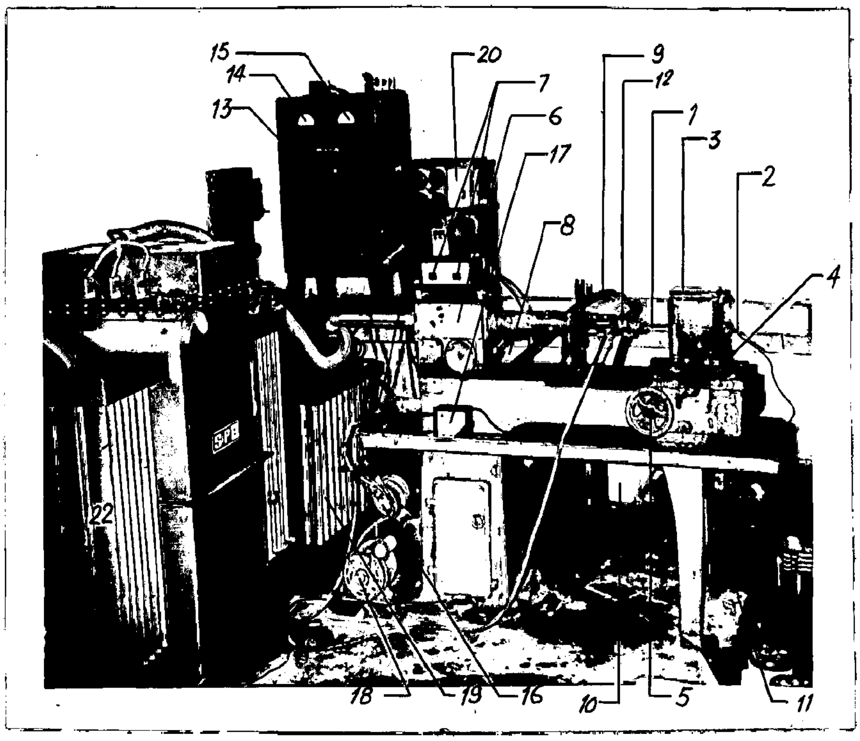

Fig.6.1: Experimental setup used for ECM
1 Tool 2 Workpiece 3 Plastic box 4 Wheel for transverse movement 5 Wheel for axial movement 6 Feed gear box 7 Feed direction change knobs 8 Feed selector 9 Electrolyte supply pipe 10 Overflow pipe 11 Outflow pipe 12 Cable for connecting tool with power terminal 13 Rectifier unit 14 Ammeter 15 Voltmeter 16 Cone pulley 17 Fine range voltmeter 18 Electric motor to drive feed mechanism 19 Variac 20 Electric connection board 21&22 Main transformer.

The specifications and other details of the power unit used in the setup are as follows:

Transformer		Rectifier unit	
Phase	- Three	Phase	- Three
Output current	100 amps/line	Secondary current	500 Amps DC
Input voltage	415 V	Secondary voltage	100 Volts DC
Output voltage	0-415 V	Type	RSC 100/500

(b) Electrolyte cleaning and electrolyte supply system:

As discussed earlier in chapter 2, during ECM of metals, metallic hydroxides are formed and when allowed to lodge between tool and workpiece can lead to sparking, an undesirable feature of ECM process. Hence electrolyte cleaning (145) is very important. In practice, a combination of the following methods may be used;

i) Filtration
ii) Centrifugal separation
iii) Cyclone process
iv) Semimentation and,
v) Floatation

It should be noted that the selection of electrolyte purification/clarification system (120) is normally based on the degree of contamination, degree of separation needed and expenses that can be tolerated. In the present case, electrolyte cleaning was achieved by filtration and sedimentation processes.

With the above in view, to minimise variations in electrolyte conductivity due to contamination by reaction products, a large sized electrolyte tank with three compartments (Fig.6.3) was used. The electrolyte passage from one compartment to the other is shown by arrows. Major part of the reaction products is left in the form of the foam at the top in the compartment I while the suspended reaction products and electrolyte enter to the compartment II through its bottom. Due to natural sedimentation, part of the reaction products settle down at the bottom and rest of the foreign elements are filtered out during their journey to the compartment III. A fine wire filter was also provided at the pump inlet.

In order to control the rate of electrolyte flow through the working gap, a bypass valve was provided in the pipe line (Fig.6.2). By suitable adjustment of the opening of this valve it was possible to achieve the required flow rate. After chemical reaction in the IEG, the reaction products and electrolyte through out-flow-pipe(11) enter in the compartment I of the tank. The bypassed electrolyte through 'bypass pipe'(10) also goes to the compartment I. The specifications of the pump and motor used are as follows:

Type	Induction motor	Make	Crompton Greaves
H.P.	2	Phase	3
Current	3.5 A	Frequency	50 HZ
Speed	1405 R.P.M.	Power	1.5 KW

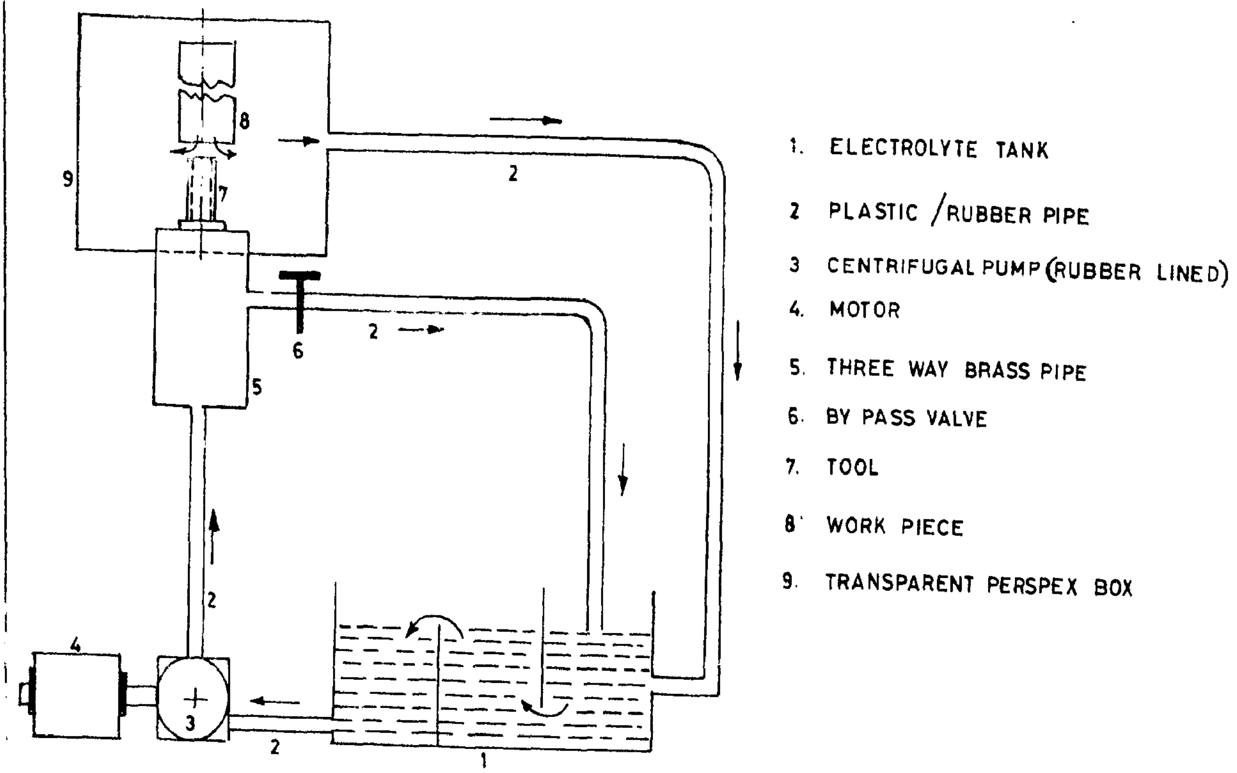
9
8
7
5
6
2
2
2
4
3
2
1
1. ELECTROLYTE TANK
2 PLASTIC /RUBBER PIPE
3 CENTRIFUGAL PUMP (RUBBER LINED)
4. MOTOR
5. THREE WAY BRASS PIPE
6. BY PASS VALVE
7. TOOL
8 WORK PIECE
9. TRANSPARENT PERSPEX BOX

FIG.6.2 SCHEMATIC DIAGRAM OF ELECTROLYTE FLOW PASSAGE

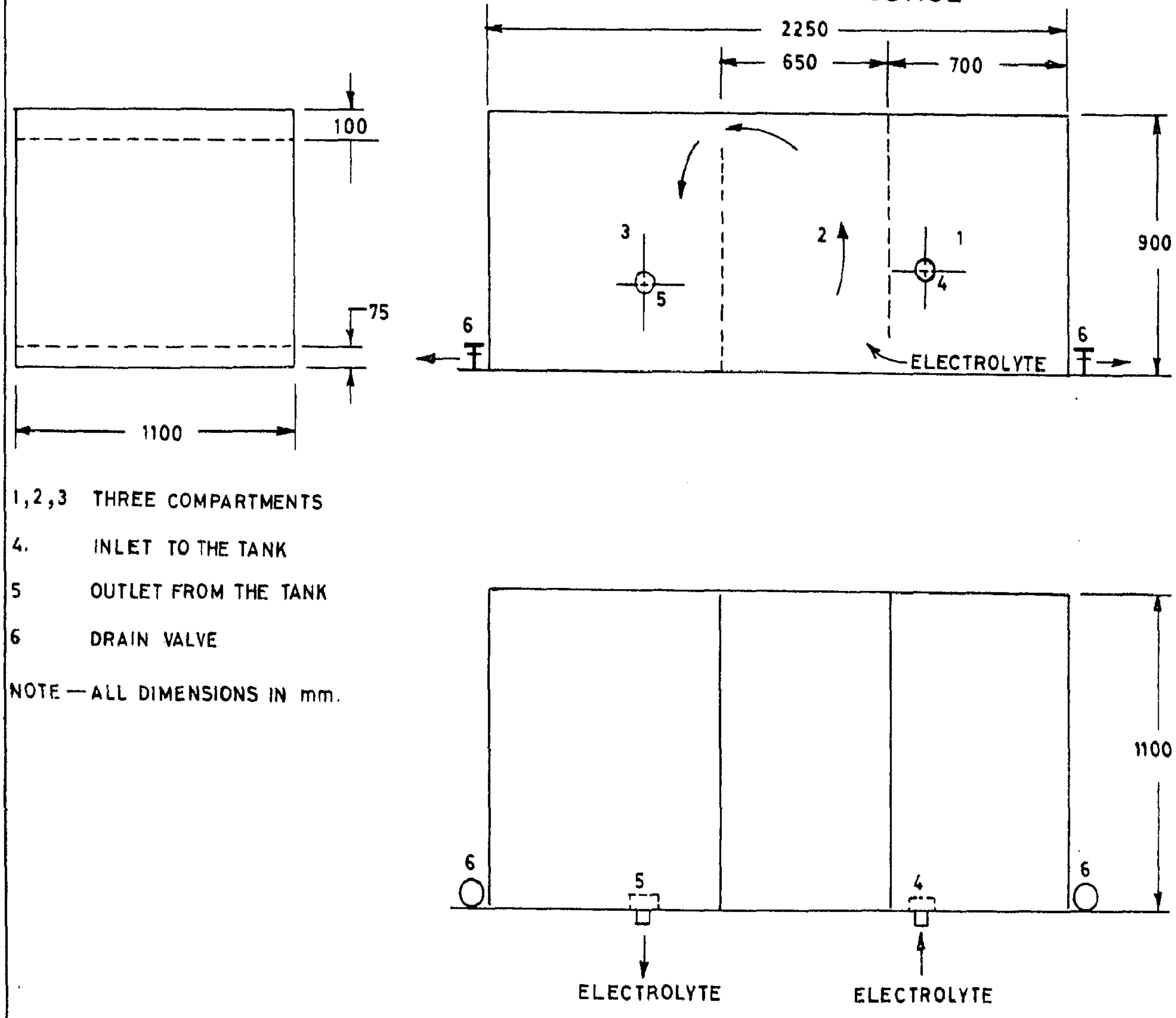
2250
650
700
100
75
1100
900
3
2
1
5
4
6
6
ELECTROLYTE
1100
6
5
4
6
ELECTROLYTE
ELECTROLYTE
1,2,3 THREE COMPARTMENTS
4. INLET TO THE TANK
5 OUTLET FROM THE TANK
6 DRAIN VALVE
NOTE — ALL DIMENSIONS IN mm.

FIG.6.3 ELECTROLYTE TANK USED FOR ECM TESTING

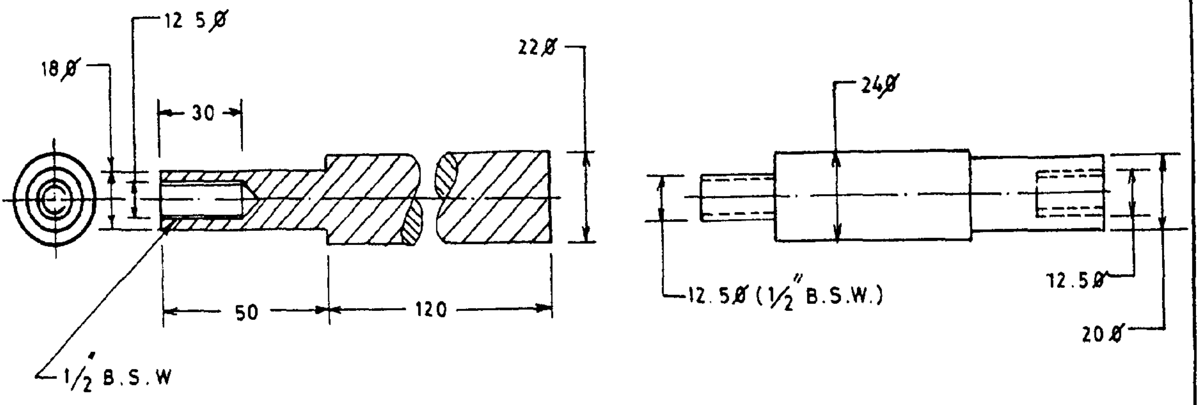
12 5Ø
18Ø
30
22Ø
50
120
1/2" B.S.W
24Ø
12.5Ø (1/2" B.S.W.)
12.5Ø
20Ø

(a) WORK PIECE (b) WORK PIECE HOLDER

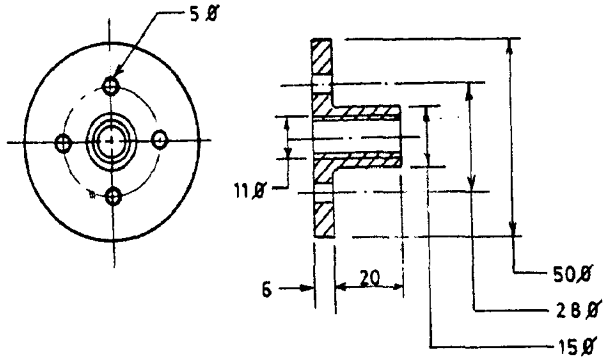
5Ø
11Ø
6
20
50Ø
28Ø
15Ø

(c) TOOL HOLDER

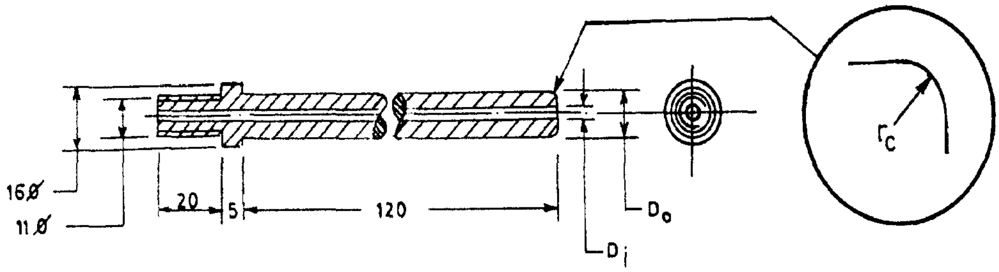
16Ø
11Ø
20
5
120
D_o
D_i
r_c

(d) DRILLING TOOL

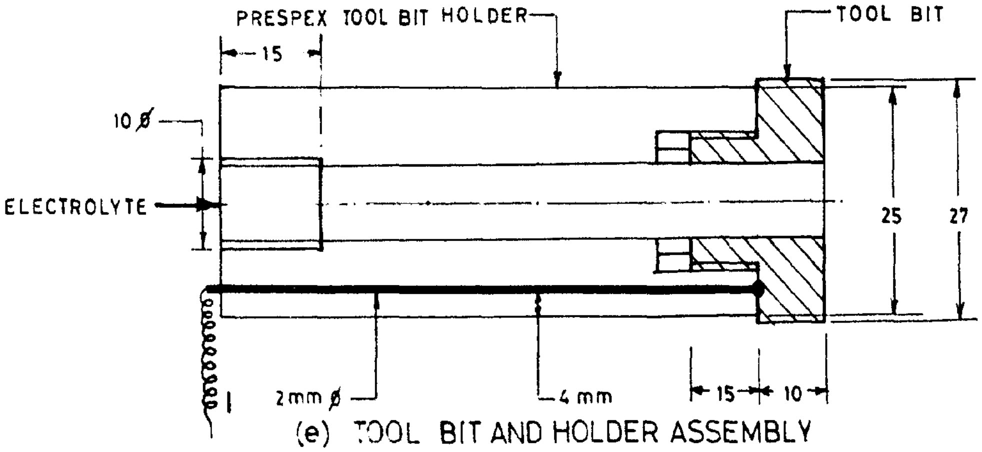
PRESPEX TOOL BIT HOLDER
TOOL BIT
15
10Ø
ELECTROLYTE
25
27
2mm Ø
4 mm
15
10

(e) TOOL BIT AND HOLDER ASSEMBLY

FIG.6.4 DETAILS OF WORK PIECE, WORK PIECE HOLDER, TOOL (OR TOOL BIT) AND TOOL HOLDER

The mode of electrolyte flow that can be achieved in the present setup are - outward, inward, side or complexed flow (4,120) but during experimentation we had used only outward mode of electrolyte flow.

(c) Tool and tool feed system:

The ECM tools for experimentation were provided with a central hole bored through them (Fig.6.4). This would facilitate the supply of electrolyte into the cutting zone. These tools could be clamped to the tool holder by means of a nut and screw system as shown.

The tool feed was provided by means of a specially designed gear box. The kinematic scheme of the feed drive system is shown in Fig.6.5. The gear box used to provide the

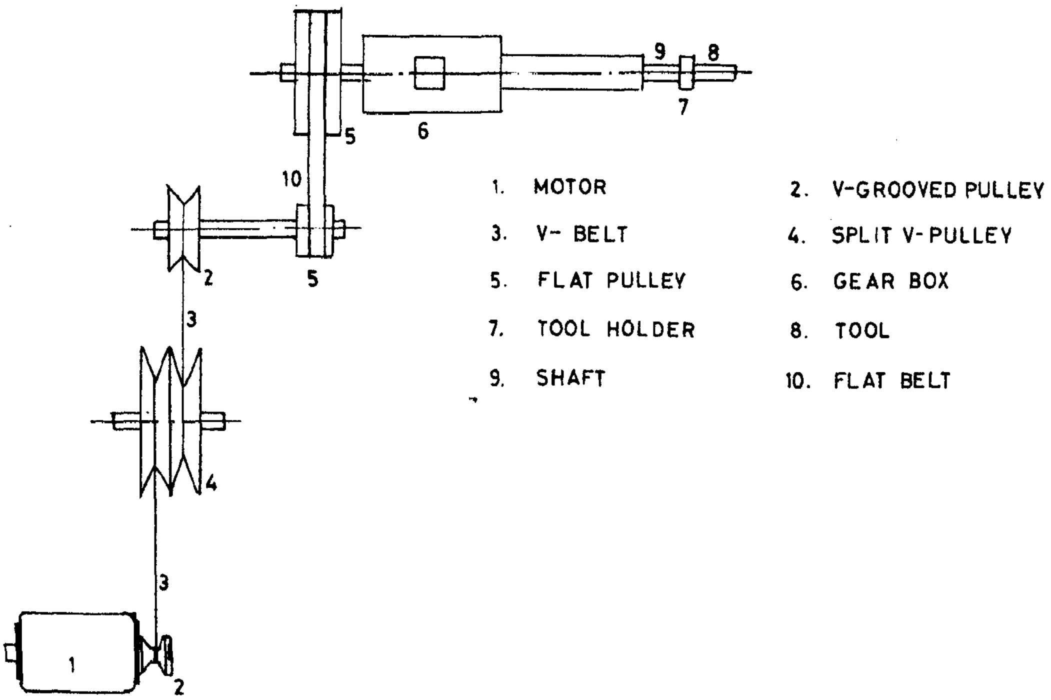
9
8
7
5
6
10
2
5
3
4
3
1
2
1. MOTOR
2. V-GROOVED PULLEY
3. V- BELT
4. SPLIT V-PULLEY
5. FLAT PULLEY
6. GEAR BOX
7. TOOL HOLDER
8. TOOL
9. SHAFT
10. FLAT BELT

FIG. 6.5 KINEMATIC SCHEME OF FEED DRIVE

tool feed motion could achieve an overall reduction of 1640:1. Further, reduction in the range of 3:1 to 8:1 was also possible through a split pulley arrangement (177). Thus, enabling us to obtain tool feed over a wide range. The feed mechanism was driven by means of a single phase, $\frac{1}{2}$ H.P., 230 volts, 1440 RPM, AC induction motor.

(d) Workpiece and holder :

During EC machining, the workpiece was kept stationary whereas, the tool was provided with the linear feed movement. The workpiece was held in a specially designed fixture as shown in Fig.6.4. The work holder design, in the present case, was based on the consideration of accurate location, high ridigity, ease of clamping, etc. The work-holder was made of the brass and the +ve terminal of the power supply was connected to the workpiece through work holder. Both the work and work holder were housed inside a perspex box. The perspex box acted as a close chamber and the entire machining took place within the chamber itself. This helped in restricting the electrolyte splash all over. IEG was set by giving transverse and longitudinal movements to the workpiece with the help of two separate hand wheels (4) and (5) respectively.

In order to prepare the test-pieces, outer skin of the castings or forgings was removed by machining and the dimensions and surface finish of the workpieces were controlled accurately within a narrow range. The hardness (BHN) of the workpieces used was also measured and is given in Table-2. Table-3 gives the chemical composition of different types of work materials used. The microstructures of different materials used during experimentation are shown in Fig.(6.6).

6.2 EXPERIMENTAL PROCEDURE AND SPECIFICATIONS

Experiments were conducted to study the following in ECD and ECB operations using different types of tools, workpieces and operating conditions.

a) Metal removal and

b) Form accuracy.

(a) Metal removal :

In order to measure the work-material removed during the test, loss in weight of the workpiece was adopted as the criterion. The weight measuring accuracy throughout was maintained at 0.25 mg. The time of machining was measured by means of a stop watch with a least count of 0.01 second.

Conditions under which the tests were performed are summarised in Table-4.

It was observed that during a cut, the working voltage has a tendency to vary. In order to improve upon the computational accuracy, the variations in operating voltage (or effective voltage) was recorded at intervals of 30 s or 60 s or 300 s during the test. The average electrolyte flow rate was

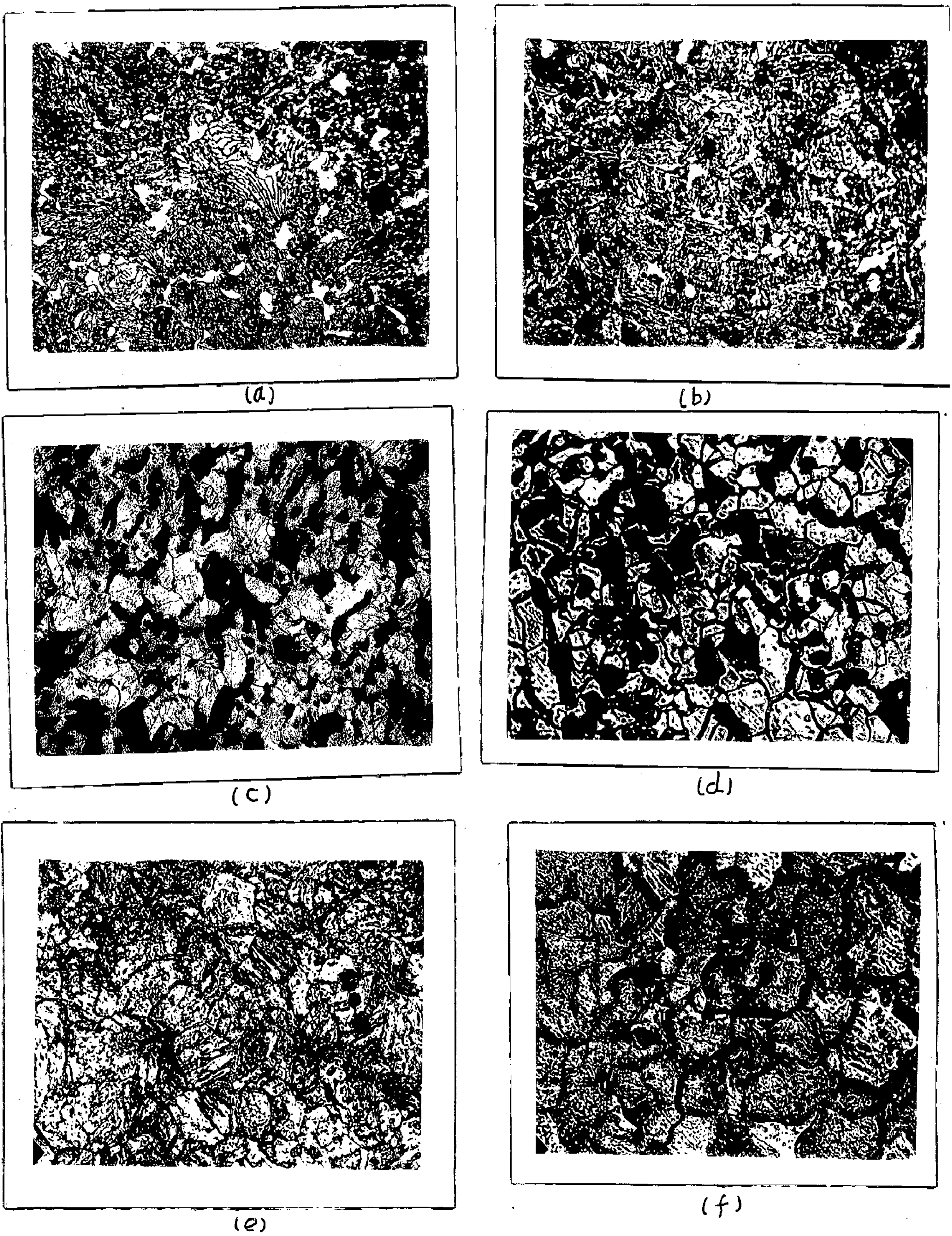
(a) (b) (c) (d) (e) (f)

Fig.6.6: Microstructure of work materials. Test pieces series numbers (a) 700 (b) 600 (c) 500 (d) 400 (e) 200 (f) 100

measured by means of a conductivity meter having the following specifications:

Conductivity Measuring Bridge

Make	Philips
Type	P R 9500/90
Measuring range	0.5 Ohms to 10 M Ohms
Bridge supply(internal)	50 Hz or 1000 Hz
Inertialess electronic indicator	

(b) Shape of the hole produced:

The shape and dimensions of the hole produced were measured in each case by the use of replica technique. For this purpose plaster of paris replicas were prepared and their dimensions measured by means of a CZ large tool maker's microscope (least count 0.01 mm). The measurement of replica dimensions at any point along its length would give the magnitude of radial overcut at that particular location using the following relationships for the cases of drilling and boring:

$$(\text{Overcut})_d = (\text{Drilled hole diameter} - \text{Tool diameter}) \times 0.5 \qquad (6.1)$$

$$(\text{Overcut})_b = (\text{Bored hole diameter} - \text{Initial dia. of hole}) \times 0.5 \qquad (6.2)$$

It is to be noted that before electrochemical boring tests were started, the predrilled hole profile was recorded. Dimension of the machined anode was measured at an intervals of about 0.25 mm or 0.5 mm in zones 1-3 and at an interval of about 0.5 mm or 1.0 mm in zone-4 (i.e. side region). The tool-corner radii were measured by the replica technique.

6.2.1 Selection of Tool Material

Selection of an appropriate tool material in ECM is very important and is governed by its electrical resistivity, stiffness, machinability and heat conductivity. Most widely used tool-materials have been compared in table-5 and from there it is evident that copper or brass would form a good choice. However, in case of slender tools, stainless steel is preferred due to higher stiffness requirement.

Copper as well as brass is also preferred for the conditions where tool damage is expected in the event of minor electrical short circuits. Since their thermal conductivity is high, this helps in removal of much of the heat from local area of shorting and thus reducing the volume or the size of the pit formed. On the other hand, under similar conditions stainless steel or titanium tools get damaged to such an extent that a major repair would be needed before they can be used again. Also tool-surface preparation (removal of nicks, notches, scratches, lines, etc.) and preservation is comparatively easy for the case of copper and brass. Except in respect of thermal conductivity, brass is superior to copper hence it was used as the tool material for the work reported in this thesis.

6.2.2 Selection of ECM Electrolyte

ECM electrolytes have been classified into three categories i.e., neutral, acidic and basic. Nautral electrolytes, say NaCl, produce insoluble sludge while others do not produce such sludge but their composition alters as the machining proceeds and plating out of the metallic ions takes place. Alkaline and acidic solutions are normally not recommended in practice because, they may attack the machine parts, are harmful to the personnel and are comparatively costly. Further, alkalies tend to passivate most of metals used as anode causing the machining to be either impossible or non-uniform. Hence, NaCl was selected as the electrolyte for the present experimental work.

6.3 DESIGN OF EXPERIMENTS

6.3.1 Introduction

Survey of literature shows that a very large number of applications of the design of experiments can be found in chemical, agriculture and related experiments. However, its theories are applicable to almost any type of industrial research (54,181). A good experimental design is one (53) which furnishes the required information with the minimum of experimental effort. During an experiment, random errors may be appreciable hence a certain minimum number of observations is required to give the necessary precision. If the magnitude of errors expected in various measurements during experimentation, is known it becomes relatively easy to forecast the number of observations required to determine any parameter with a given degree of precision. If an experiment is under designed, false conclusions may be drawn and if overdesigned it would lead to wastage of money, time and efforts without yielding extra information. The factorial design used in this case offers the advantage that it contains a large degree of 'hidden replication' (181); for example in a 2^5 experiment each effect is estimated with the precision of an average of 16 comparisons of pairs of observations.

Normally scientific investigations are planned to know the effects of a number of different factors on some property or process. A properly planned experiment would not only give the effect of the individual factors but also the manner in which each effect depends on the other factors (i.e., interactions). In the factorial design the effect of a factor is estimated at several levels of the other factors, hence the conclusions hold over a wide range of conditions. It is also possible to state on theoretical grounds which factors are likely to interact and which may safely be ignored (47). Such full factorial designs require that l^f number of experiments be conducted, f is the number of factors involved and 'l' is the number of levels under investigations. For higher levels and large number of factors, full factorial design require very large number of experiments. This has led to the development of fractional factorial design which reduce the size of an experiment to a fraction of that required for full factorial experiment and providing all the important informations. Fractional factorial design (1,54) or fractional replicates is based on the principle of 'confounding'. When large number of experiments are involved it may not be possible to carryout experiments under uniform conditions, say, on one homogeneous batch of raw materials, etc. Confounding is the division of experimental data into smaller blocks in such a manner that the main effects of the factors and their more important interactions are investigated under uniform conditions; while the heterogenity introduced in consequence of the size (66) of the experiment is allowed to affect only interactions which are likely to be unimportant.

6.3.2 Response Surface Evaluation and Design Schemes

If all the factors represent quantitative variables then the yield (or response) Y^* can be represented as a function of the levels of these variables

$$Y_u^* = \emptyset^*(x_{1u}^*, x_{2u}^*, \ldots, x_{\ell u}^*) + e_u \qquad (6.3)$$

$$Y_u^* = x_{0u}^* + x_{1u}^* + x_{2u}^* + \ldots + x_{\ell u}^* + e_u \qquad (6.4)$$

where $u=1,2,\ldots,N$ represents N observations in the factorial experiment and x_{iu}^* represents the level of the i^{th} factor in u^{th} observations. The function $\emptyset^*$ is called the response surface; e_u measures the experimental error of the u^{th} observation. In the absence of a knowledge of mathematical form of $\emptyset^*$, it can be approximated satisfactorily, within the experimental region, by a polynomial in the variables x^*_{iu}. However, it is to be noted that polynomials are untrustworthy when extrapolated. The solution of Eq(6.4) is obtained (28,29,47,53) by treating it as a particular case of multiple linear regression.

To obtain an idea of interactions and higher order effects, second order designs (Eq 6.5) are preferred instead of first order design (Eq 6.4) as discussed above. Such quadractic type of design are used when responses are not expected to be linear in the experimental space and the design is needed to yield estimates of the curvature aspects of each response (199).

$$Y^*_o = \beta_o + \underbrace{\beta_1 x^*_{1u} + \beta_2 x^*_{2u}}_{\text{Linear terms}} + \underbrace{\beta_{11} x^{*2}_{1u} + \beta_{22} x^{*2}_{2u}}_{\text{Square terms}} + \underbrace{\beta_{12} x^*_{1u} x^*_{2u}}_{\text{Cross-product terms}} + \underbrace{e_u}_{\text{Error term}} \quad .. \quad (6.5)$$

To estimate the magnitudes of the coefficients in the above polynomial, each variable x^*_{iu} must take atleast three different values. This suggests the use of factorial design of 3^k series with levels coded as -1, 0, 1, however, 3^k design would become quite large with more than three x^*-variables. Also, with such design the precision (28) of the coefficients of squared terms is relatively low.

Box and Wilson (28) therefore developed the central composite design by adding (2f+1) additional factor combination to 2^f factorial (i.e. $2^f + 2f + 1$). Such designs were originated to fit second order response surfaces.

Later, this design was modified and named as non-central composite design (47), useful for the situations when maximum response is nearer to one of the other factor combination than to the centre.

Rotatable designs are quite useful in practice and belong to a series that are also central composite design. To explain the concept of rotatability, let the point (0,0,...,0) represent the centre of the region in which 'Y^*' and 'x^*' is under investigation. Let Y_u^* be the estimated response at a point on the fitted second order surface as given by equation below;

$$Y_u^* = b_0 + \sum_{i=1}^{f} b_i x_{iu}^* + \sum_{i=1}^{f} b_{ii} x_{iu}^{*2} + \sum_{i<j} b_{ij} x_{iu}^* x_{ju}^* \quad .. \quad (6.6)$$

In a rotatable design the standard error is the same for all points that are at some distance P^* from the centre of the region.

In such a case,

$$x_{1u}^{*2} + x_{2u}^{*2} + \ldots + x_{fu}^{*2} = P^{*2} = \text{constant}$$

Central composite design (Fig.6.7) can be subdivided into three parts; (i) points related to 2^f design, (ii) extra points n_2 included to form a central composite design with α^*, and

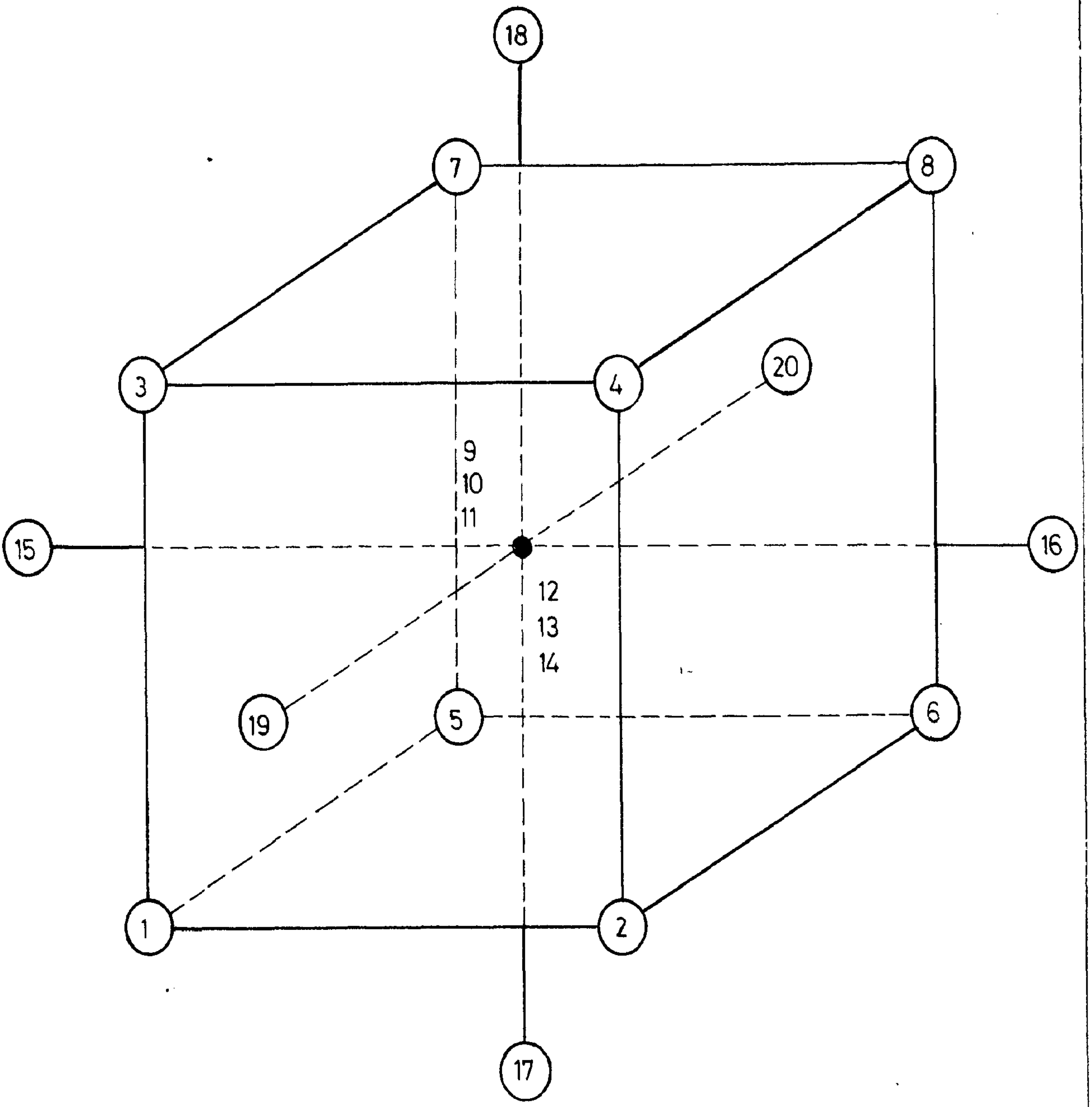
18
7
8
3
4
20
9
10
11
15
16
12
13
14
19
5
6
1
2
17

FIG. 6.7 GEOMETRIC REPRESENTATION OF CENTRAL COMPOSITE ROTATABLE DESIGN

(iii) few more points n_1 added at the centre to give roughly equal precision for Y^* (i.e., true value of yield) within a circle of radius 1. $n_1 \geqslant 1$ however, if $n_1 > 1$ i.e., many replications of the centre point, the standard error of Y^* is low at the centre and increases rapidly as we move away from the centre.

It is to be mentioned that $\overset{*}{\alpha}$ must be equal to $2^{f/4}$ in order to make the design rotatable. With larger number of variables, the experiment size is reduced by using a half replicate of the 2^f factorial. With half replicate, $\overset{*}{\alpha}$ becomes $2^{(f-1)/4}$.

6.3.3 Analysis of Variance

It is usually of interest to partition the sum of squares of the Y^*'s into the contribution due to a first order (linear) equation, the additional contribution due to the second order terms, a 'lack of fit' component which measures the deviations of the responses from the fitted surface, and finally a measure of the experimental errors, obtained from the replicated points at the centre.

General formulae used are as follows:

	Sum of squares	d.f.
(1) First order term.	$\sum_{i=1}^{f} b_i(iY^*)$	f

(2) Second order terms	$b_0(0Y^*) + \sum_{i=1}^{f} b_{ii}(iiY^*)$ $+ \sum_{i<j} b_{ij}(ijY^*) - G^2/N$	$\frac{f(f+1)}{2}$
(3) Lack of fit	Found by substraction $[(5)-(1)-(2)-(4)]$	$n_2 - \frac{f(f+3)}{2}$
(4) Experimental error	$(Y^*_{iu} - \bar{Y}^*_1)^2$	$n_1 - 1$
(5) Total	$\sum_{u=1}^{N} Y^{*2}_u - G^2/N$	n_1+n_2-1

Here, G is the grand total, N- the number of points and Y^*_{1u} represents the responses at the central points, with mean $\bar{Y}^*_1$.

6.3.4 Design of ECD Experiments

6.3.4.1 Design of electrochemical drilling (ECD) with bare tool experiments

To evaluate the effects of following five ECD parameters (or variables) on the metal removal rate (i.e., yield), central composite rotatable design with half replicate was selected (199). This design seems to be the most useful in this type of application. Levels for different factors were selected as per scheme given below:

Factor name		Levels				
		+2	+1	0	-1	-2
Electrolyte conductivity, $\mho$ mm^{-1} ($x 10^{-1}$)	x_1^*	0.030	0.040	0.0493	0.0590	0.069
Initial inter-electrode gap(mm)	x_2^*	2.1	1.7	1.3	0.9	0.5
Feed rate, mm/s, ($x10^{-3}$)	x_3^*	7.917	7.080	6.187	5.330	4.500
Tool corner radius(mm)	x_4^*	3.976	3.16	2.298	1.53	0.75
Tool diameter(mm)	x_5^*	12.06	11.04	10.03	8.99	7.95

The complete design of the experiment (47) in coded level form and the responses are given in Table-6 and the values of these factors at different levels are given above. The solutions of the response surface equations for central composite design are obtained from the equations given alongwith the Table-6.

6.3.4.2 Design of electrochemical bit drilling (ECBD) experiments

To evaluate the effects of feed rate and tool bit - bare height on metal removal rate, the experiments were conducted in accordance with the Design given in Table-7 and the corresponding factor levels values are given below.

Experimental Conditions Used During ECBD of Forged Low Alloy Steel.
$K_o = 0.007 \mho mm^{-1}$ $t = 2400$ s

Factor	Abbreviation	Levels				
		-2	-1	0	+1	+2
Feed rate(F_F), mm/s($x10^{-3}$)	x_1^*	3.2	3.7	4.5	5.30	5.63
Tool bit height (b_b) mm	x_2^*	2.556	3	4	5	5.414

CHAPTER - 7

ANALYTICAL AND EXPERIMENTAL RESULTS

This chapter presents the analytical and experimental results obtained by the author. The experimental study consisted in drilling and boring of different workpieces using several tools and tool bits and electrolytes having different concentration. In order to test the validity of the proposed models experimental data has also been borrowed from the available literature. It should be noted that the analytical results reported in this chapter have been obtained by FET unless otherwise mentioned.

7.1 ECM WITH PLANE PARALLEL ELECTRODES

7.1.1 Zero Feed Rate

Generation of side surfaces, in ECM, can normally be considered to be equivalent to machining under zero feed conditions. This would correspond to a situation when the feed direction and normal at tool (or work) surface are at right angles to each other. Majority of the available experimental data, in literature, relates to zero feed rate in the front gap only. The model FET-11 has been employed to compute the analytical values of the ECM process parameters for the experimental data with zero feed rate. Computation in this case was done at intervals of 30 seconds each, Current density has been calculated using Eq(2.11) and the results compared with the experimental data.

(a) Variations in current density

For the case of zero feed machining, with using NaCl as the electrolyte, Kawafune (106) conducted extensive experimentation (Table-8). For the conditions in Table-8, the current density along the electrolyte flow path has been evaluated analytically using FET-11 (Figs 7.1A and 7.1B). The computed values in this case are based on the assumption of 100% current efficiency and void fraction as zero due to absence of sufficient reliable data in this regards. The current density along the electrolyte path was evaluated by knowing the total current flowing in the segmented electrodes I1 to I5 and their areas.

(b) Machining accuracy

Figs (7.1A and 7.1B) also show a comparison of experimental and analytical values pertaining to machining accuracy obtained by the use of FET-11. For these cases, the same machining conditions as given in Table-8 are true.

7.1.2 Finite Feed Rate

In ECM with finite feed the rate at which the tool is fed is equal to front feed, F_F, if the normal to the work surface coincides with the feed direction otherwise, the cosine component of the feed should be employed. Validity of the model FET-11 for finite feed conditions has also been checked

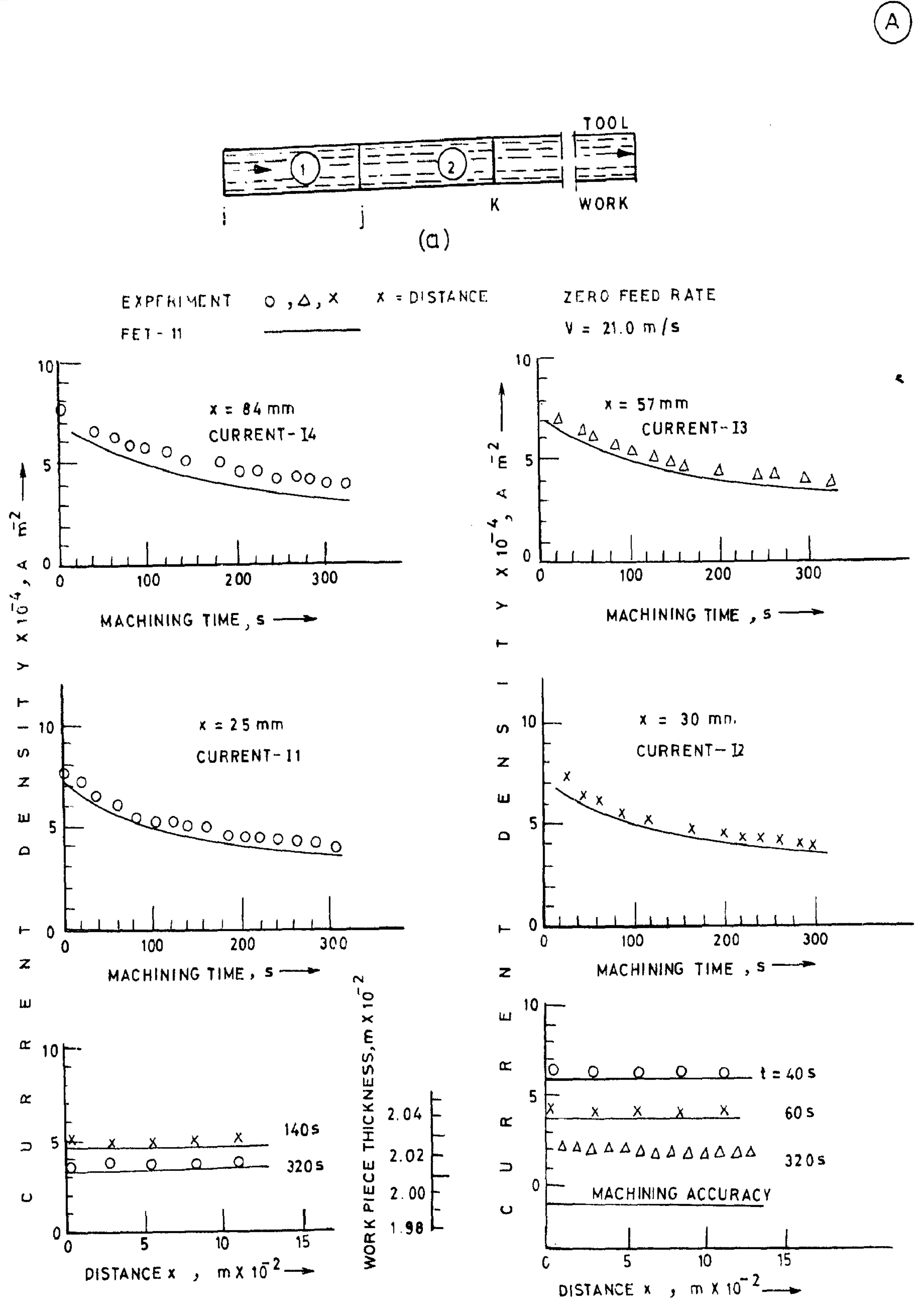

FIG. 7.1 COMPARISON OF THEORETICAL FET-11 AND EXPERIMENTAL RESULTS

Ⓑ

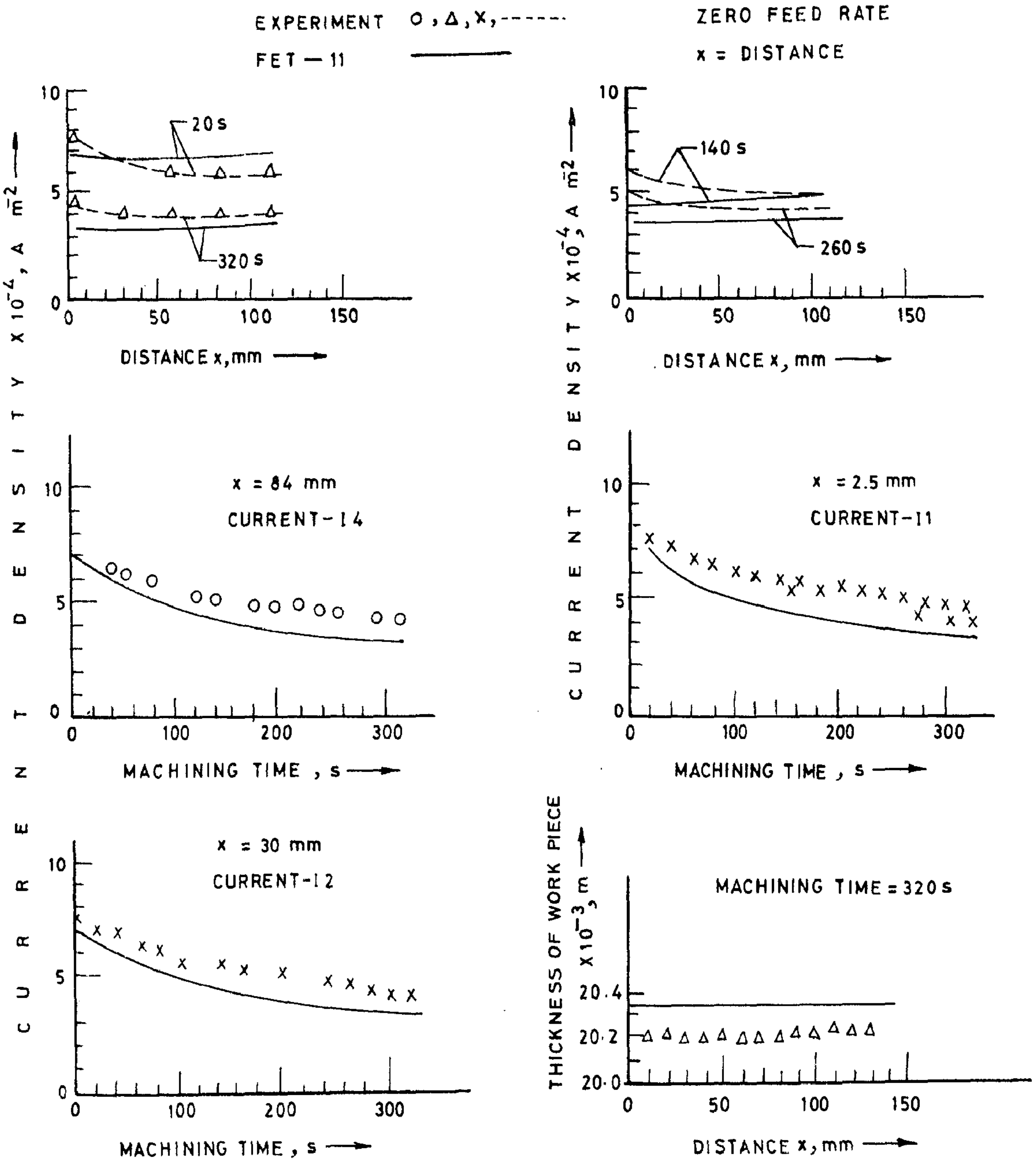

FIG 7.1 COMPARISON OF THEORETICAL (FET-11) AND EXPERIMENTAL RESULTS

using experimental data (23) and the results are given in Figs.(7.2A-7.2D). For the computation of metal removal a current efficiency of 100% and void fraction as zero have been assumed in the absence of availability of reliable data for evaluation of void fraction constant. A computation interval of 30 seconds was used.

Experimental validity of the model FET-22 was also verified (Figs.7.3A-7.3C). Fig.4.6a shows the discretization of two dimensional IEG and the computation of ECM parameters, in this case, was done as per computer programme already discussed. For this purpose a computational interval of 30 seconds was chosen.

For the sake of testing the validity of the model FET-22, for one of the test conditions (23), results about variation in J, K, IEG, etc. are given in Fig. 7.4.

7.1.3 Complex Shaped Electrodes

Applicability of model FET-11 and FET-22 for the case of complex shaped workpieces has been tested by analysing the complicated problems shown in Figs. 7.5A and 7.5B respectively. The machining conditions for which these problems have been analysed are given in Tables-9 & 10 respectively.

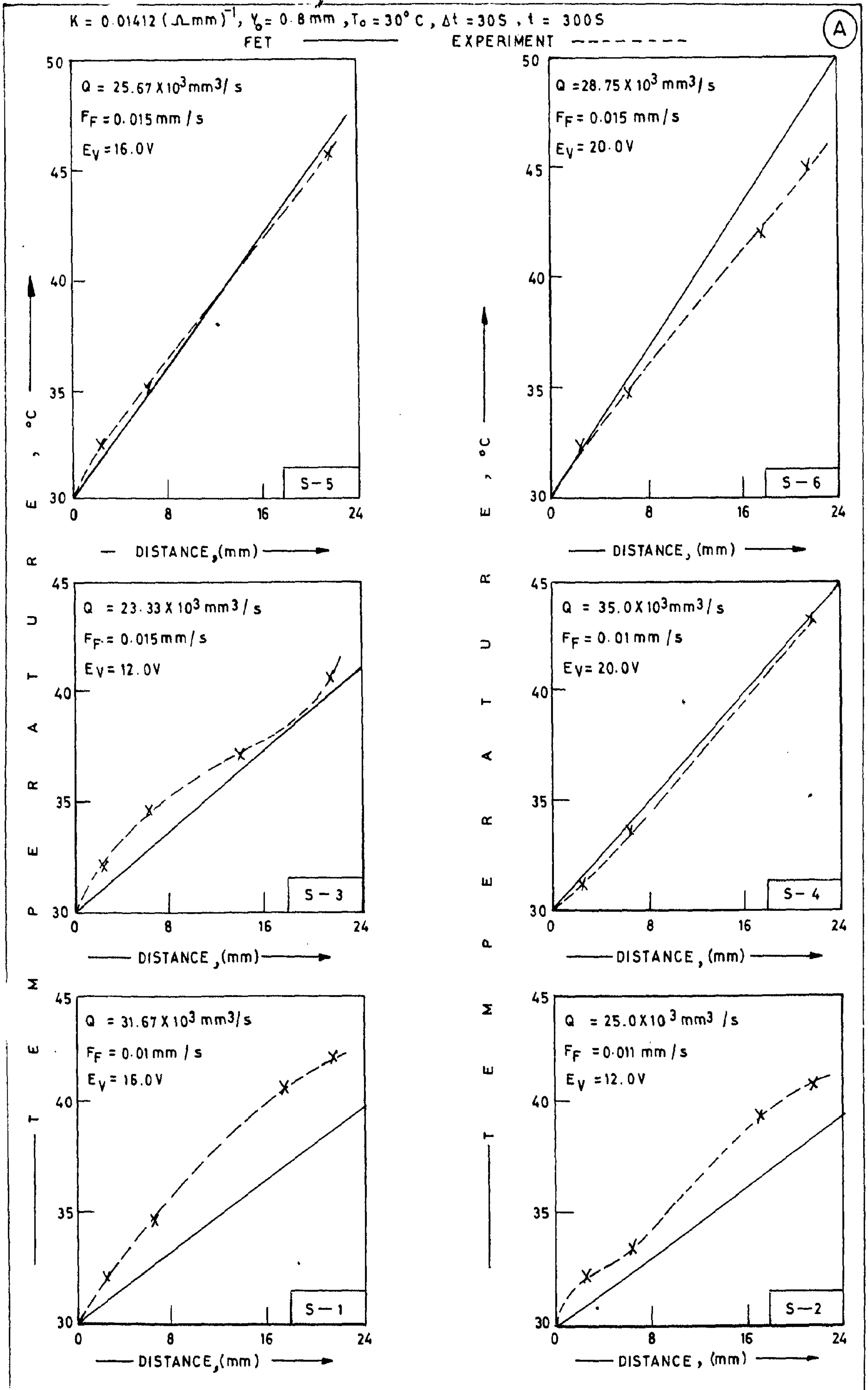

FIG.7.2 COMPARISON OF MODEL FET-11 AND EXPERIMENTAL RESULTS

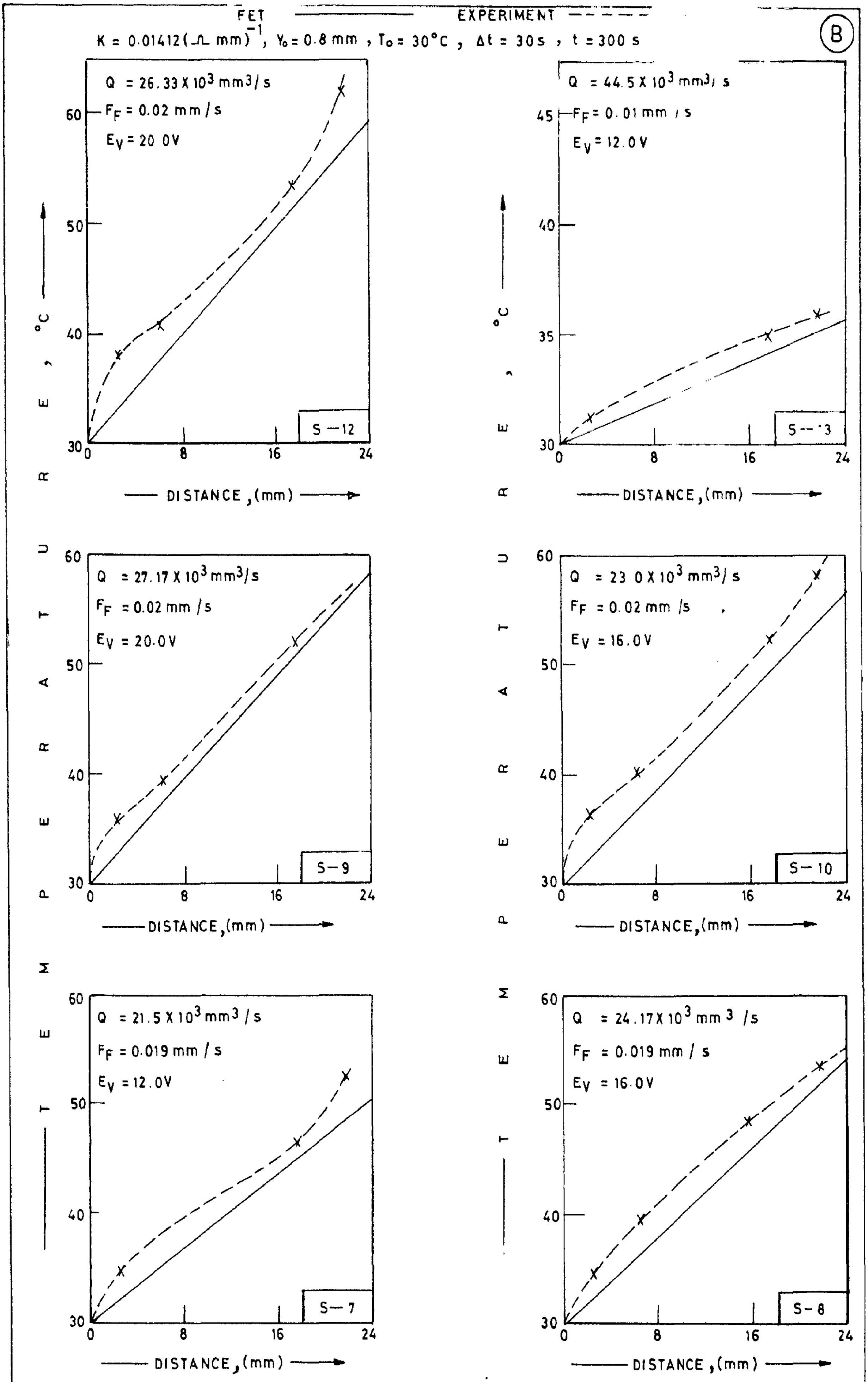

FIG.7.2 COMPARISON OF MODEL FET-11 AND EXPERIMENTAL RESULTS

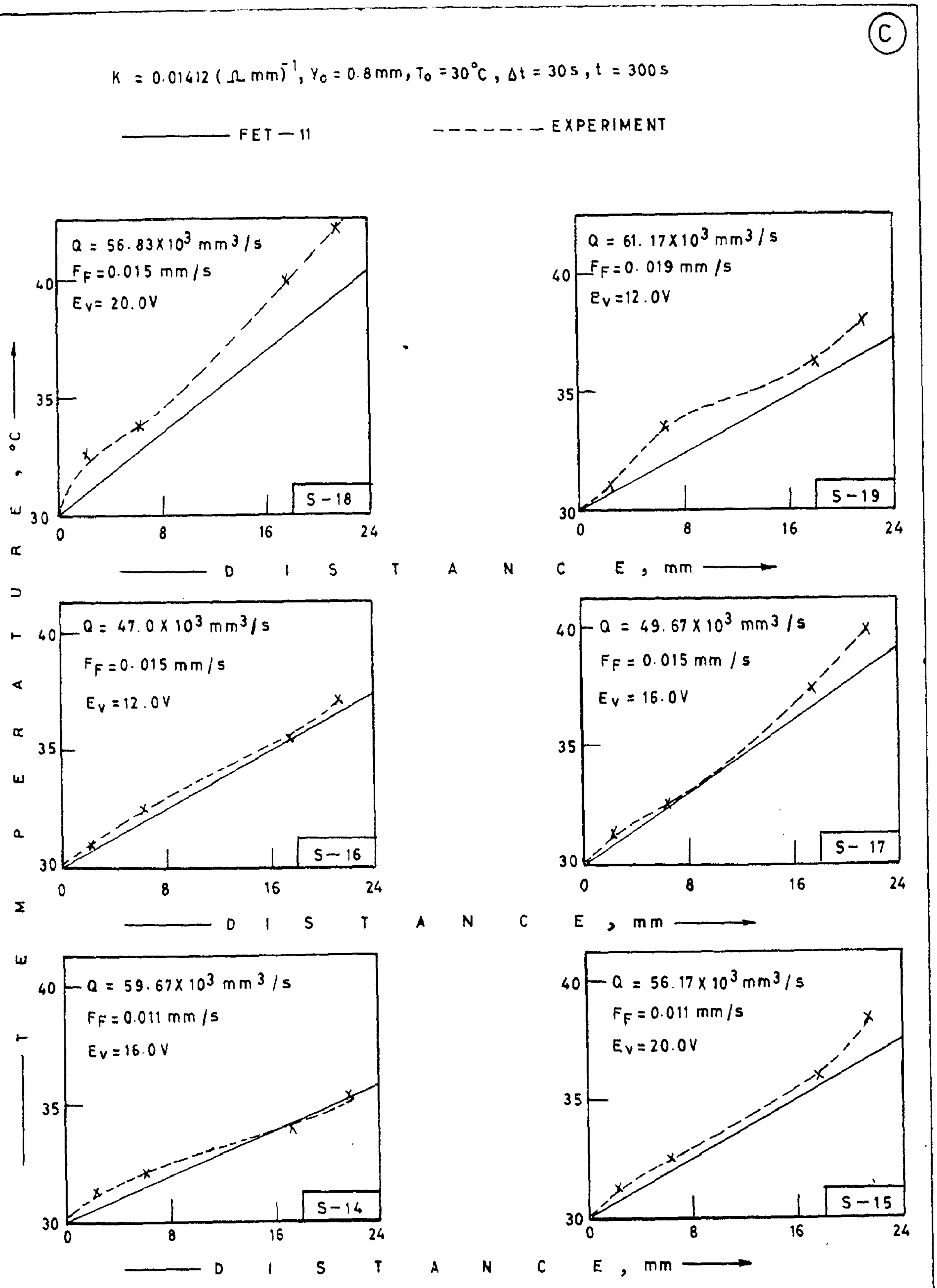

FIG. 7.2 COMPARISON OF MODEL FET-11 AND EXPERIMENTAL RESULTS

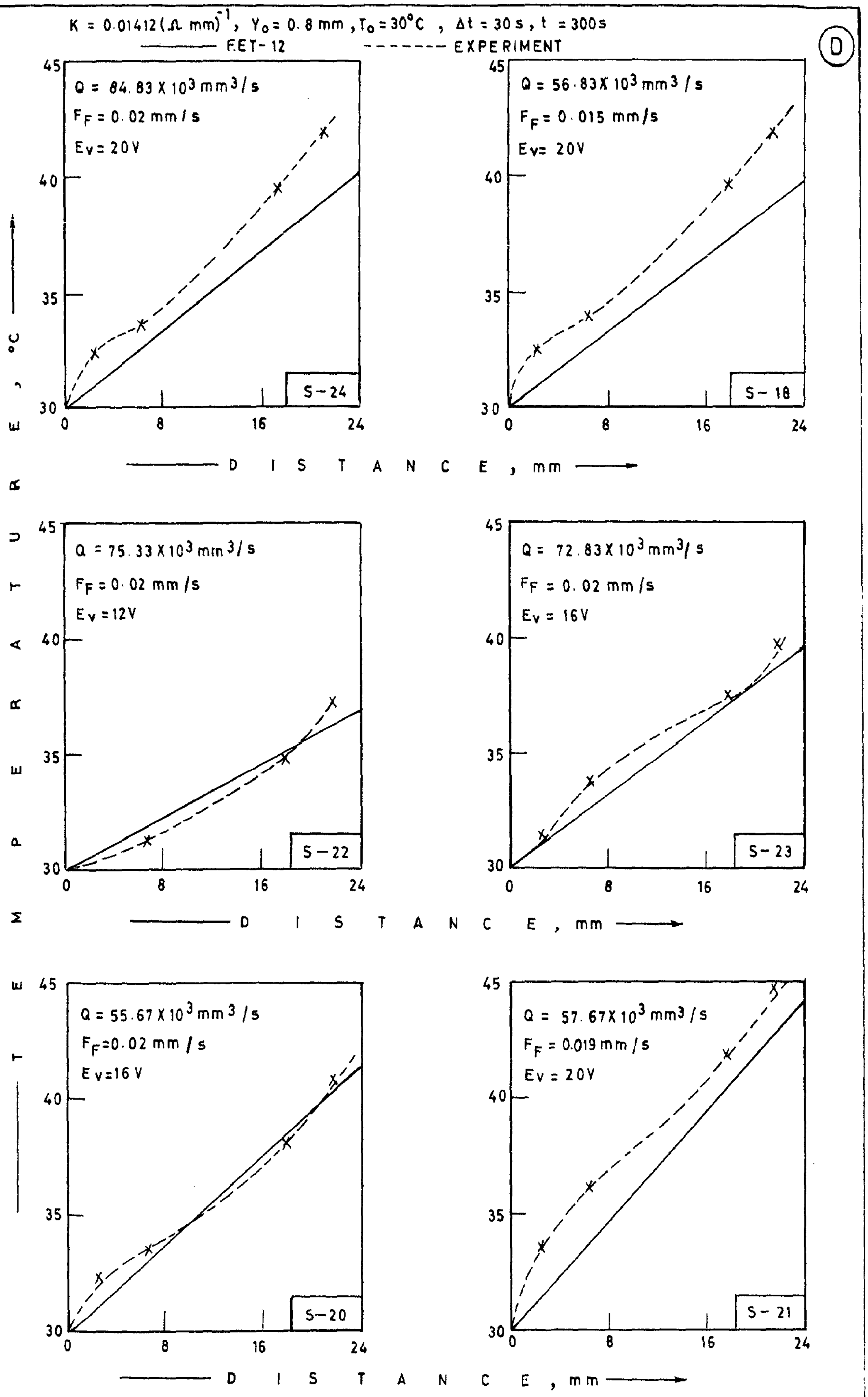

FIG. 7.2 COMPARISON OF MODEL FET-12 AND EXPERIMENTAL RESULTS

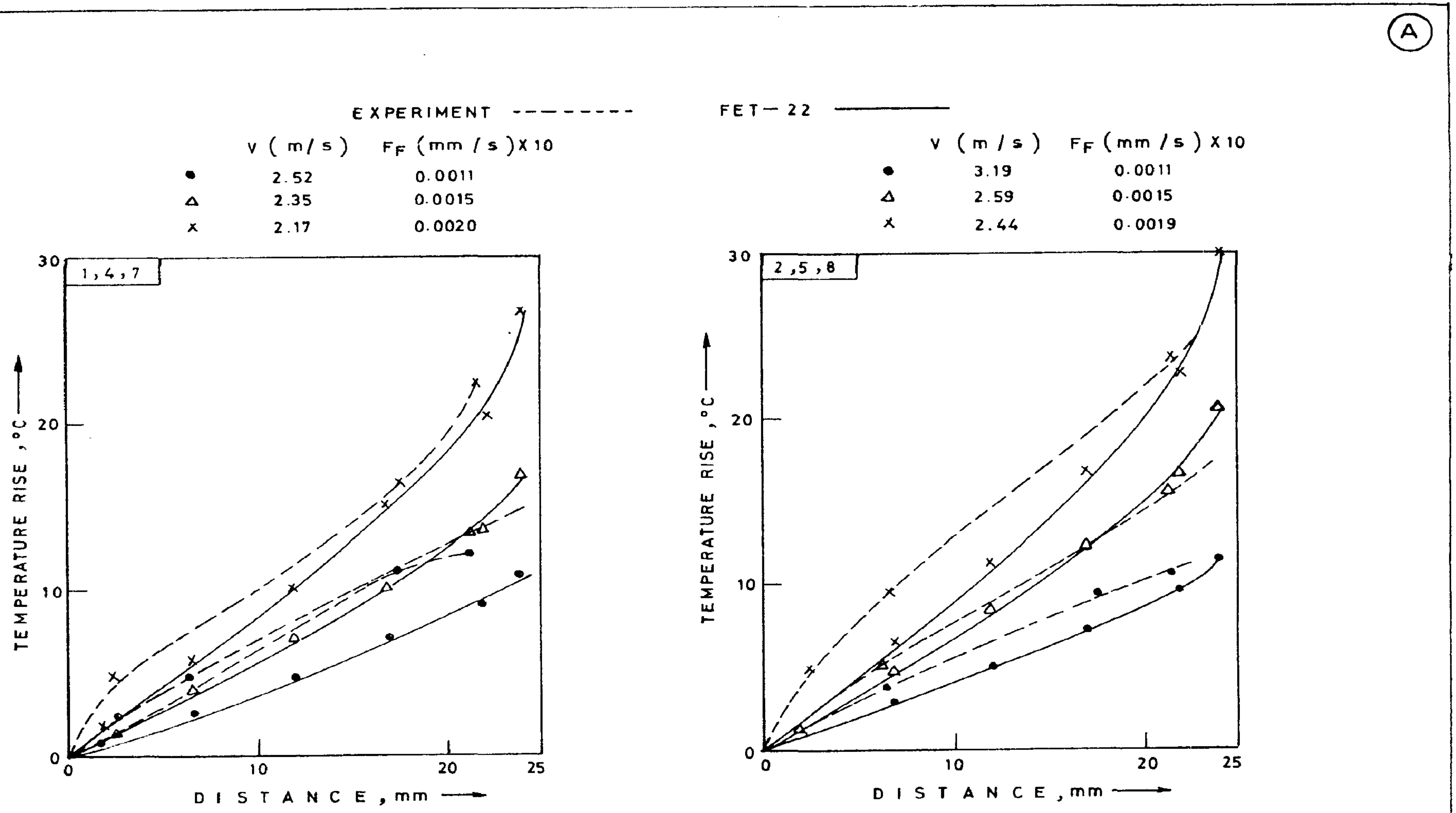

FIG. 7.3 COMPARISON OF THEORETICAL (FET-22) AND EXPERIMENTAL RESULTS

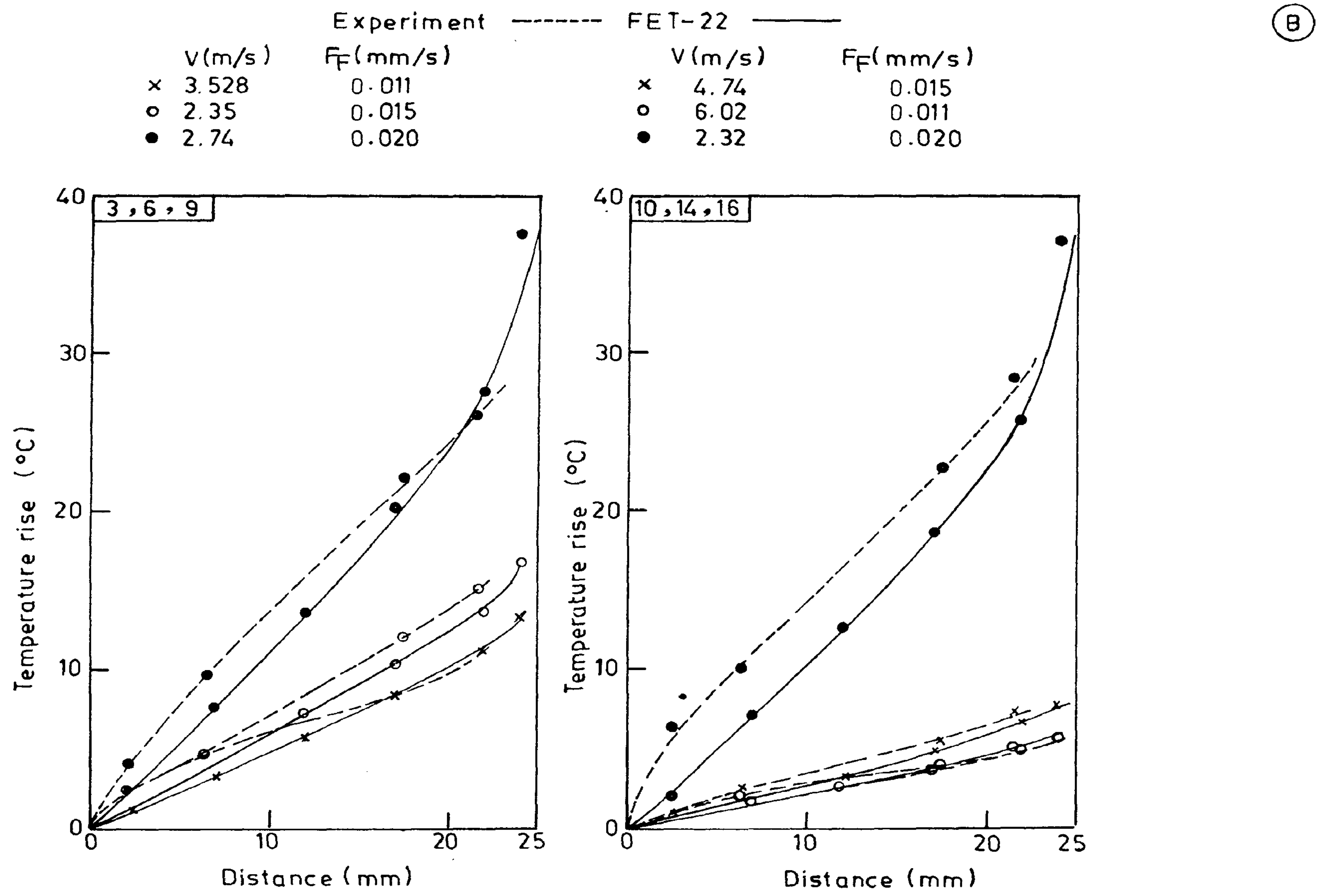

Fig.7.3 Comparison of theoretical (FET-22) and experimental results

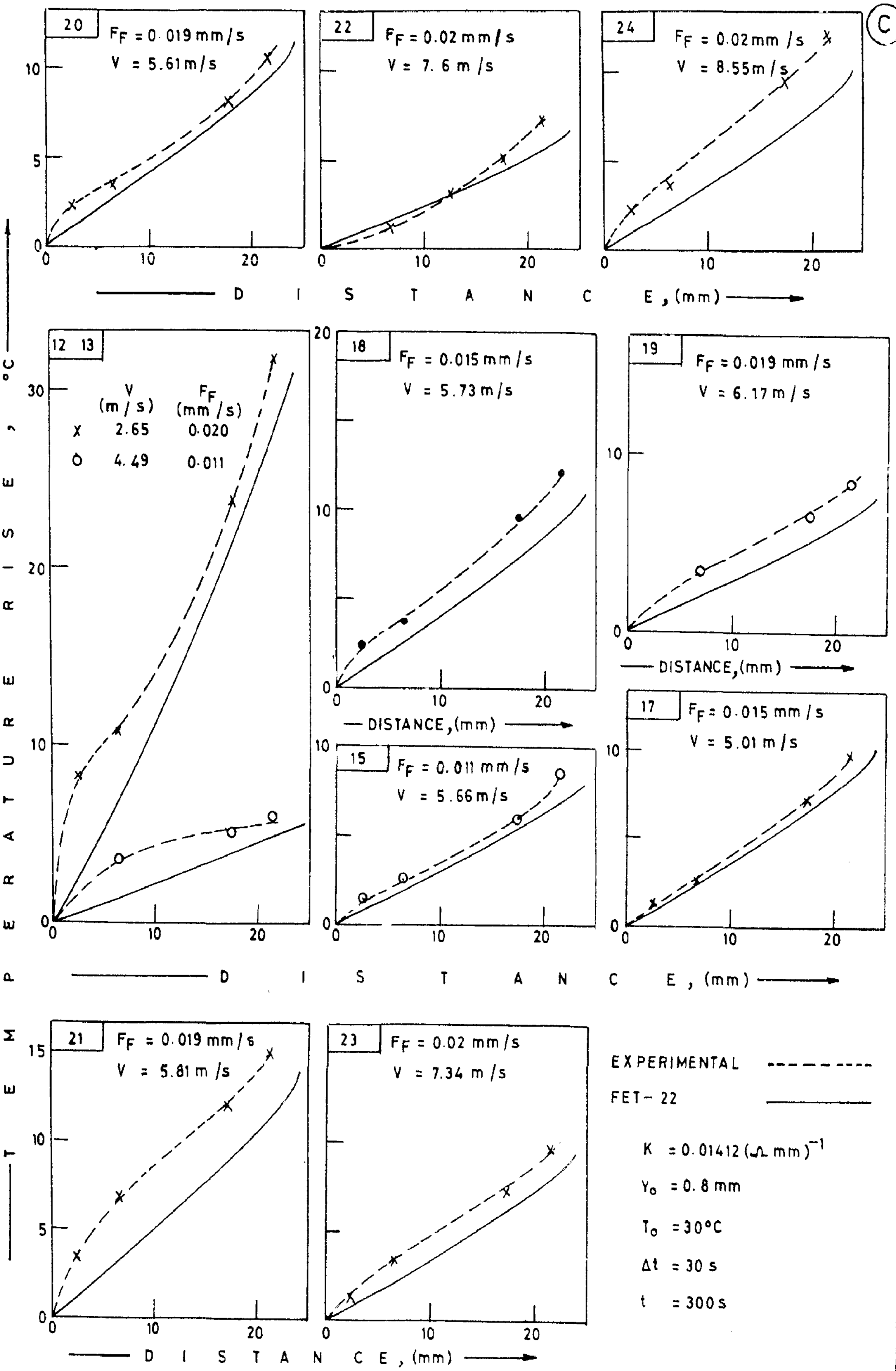

FIG.7.3 COMPARISON OF ANALYTICAL (FET-22) AND EXPERIMENTAL RESULTS

Ⓐ

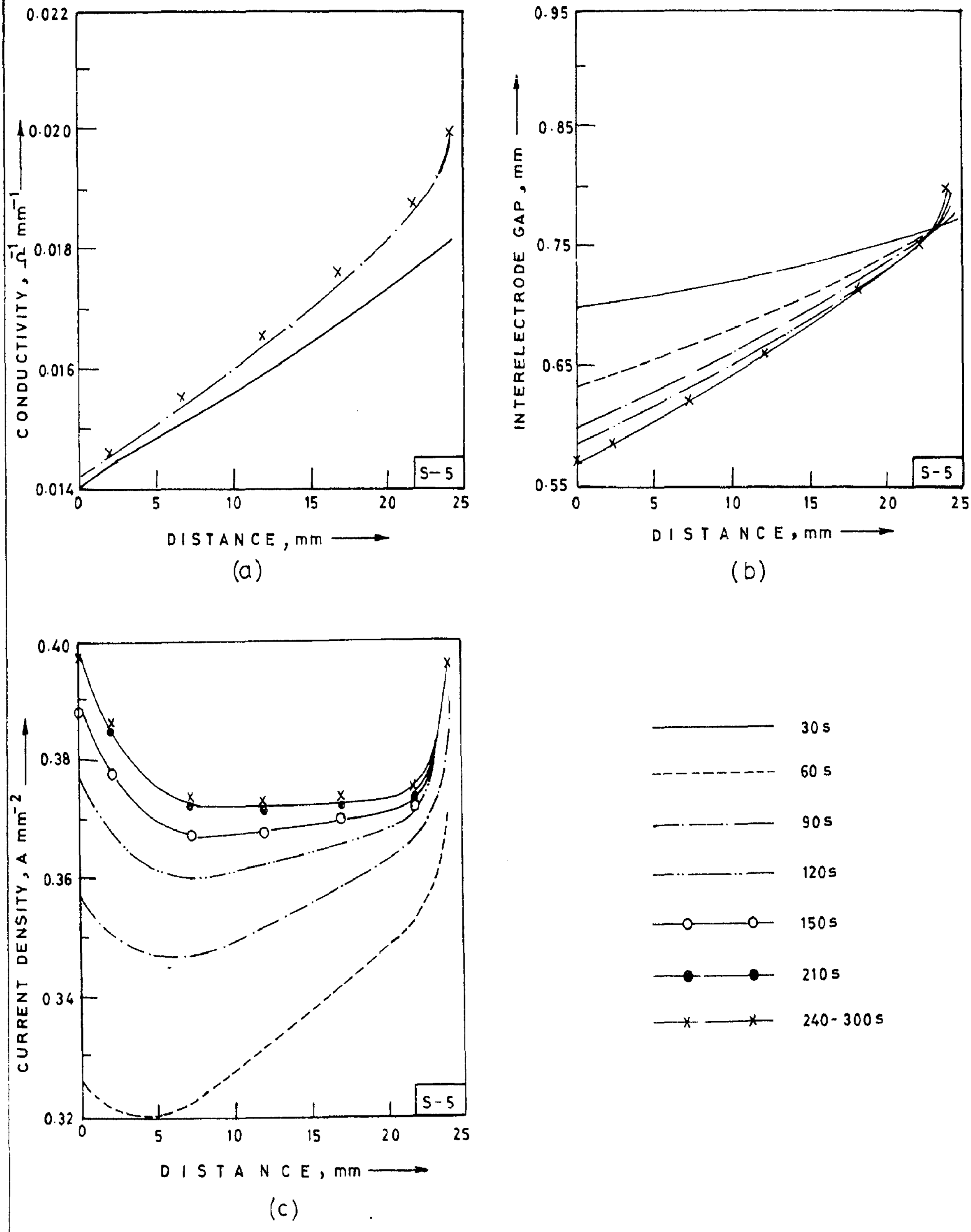

(a)

(b)

(c)

FIG. 7.4 VARIATIONS IN ECM PARAMETERS WITH FLOW DISTANCE (MODEL FET-22)

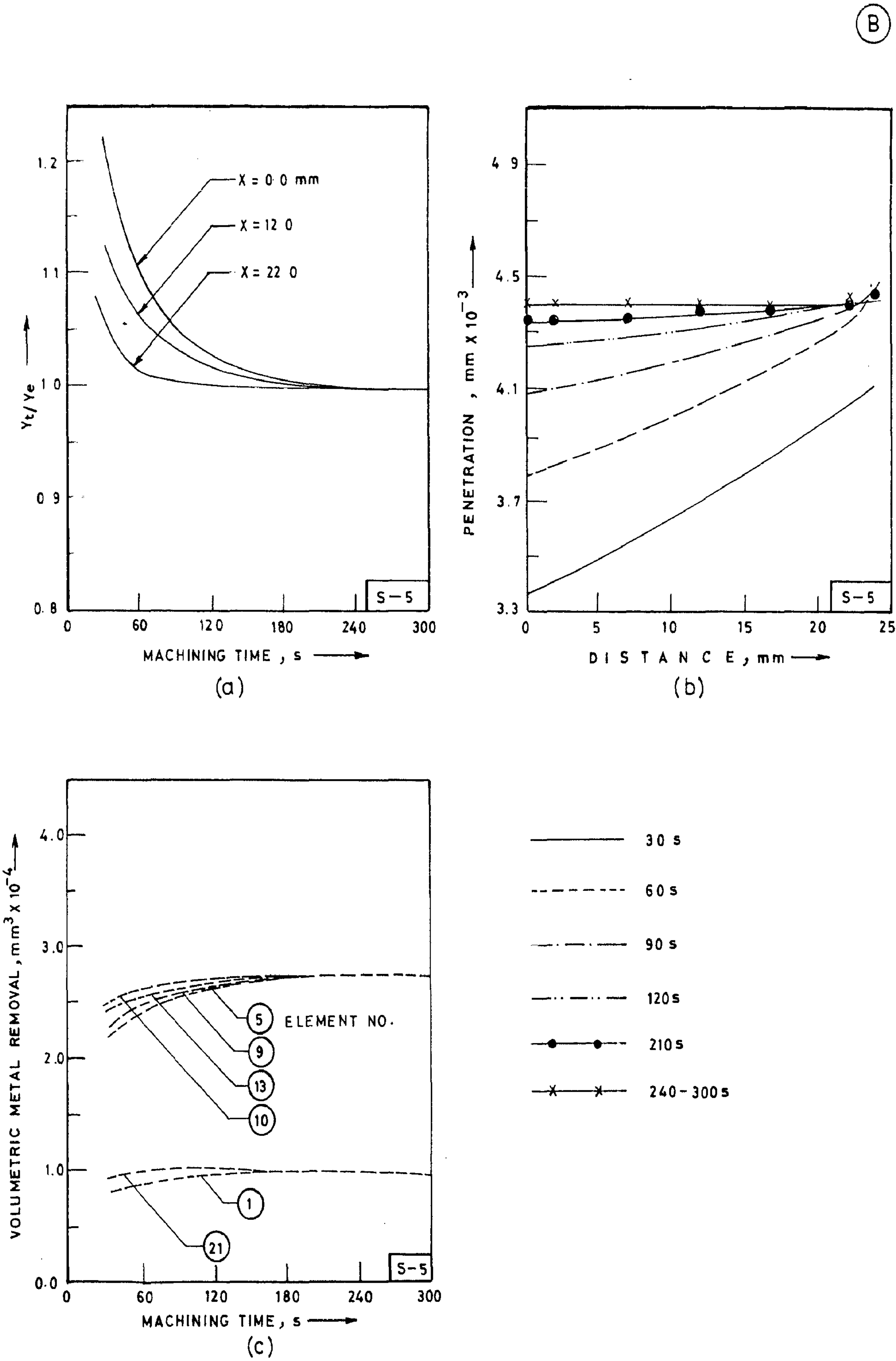

(a)

(b)

(c)

FIG. 7.4 VARIATIONS OF MACHINING PARAMETERS WITH FLOW DISTANCE OR MACHINING TIME (MODEL FET-22)

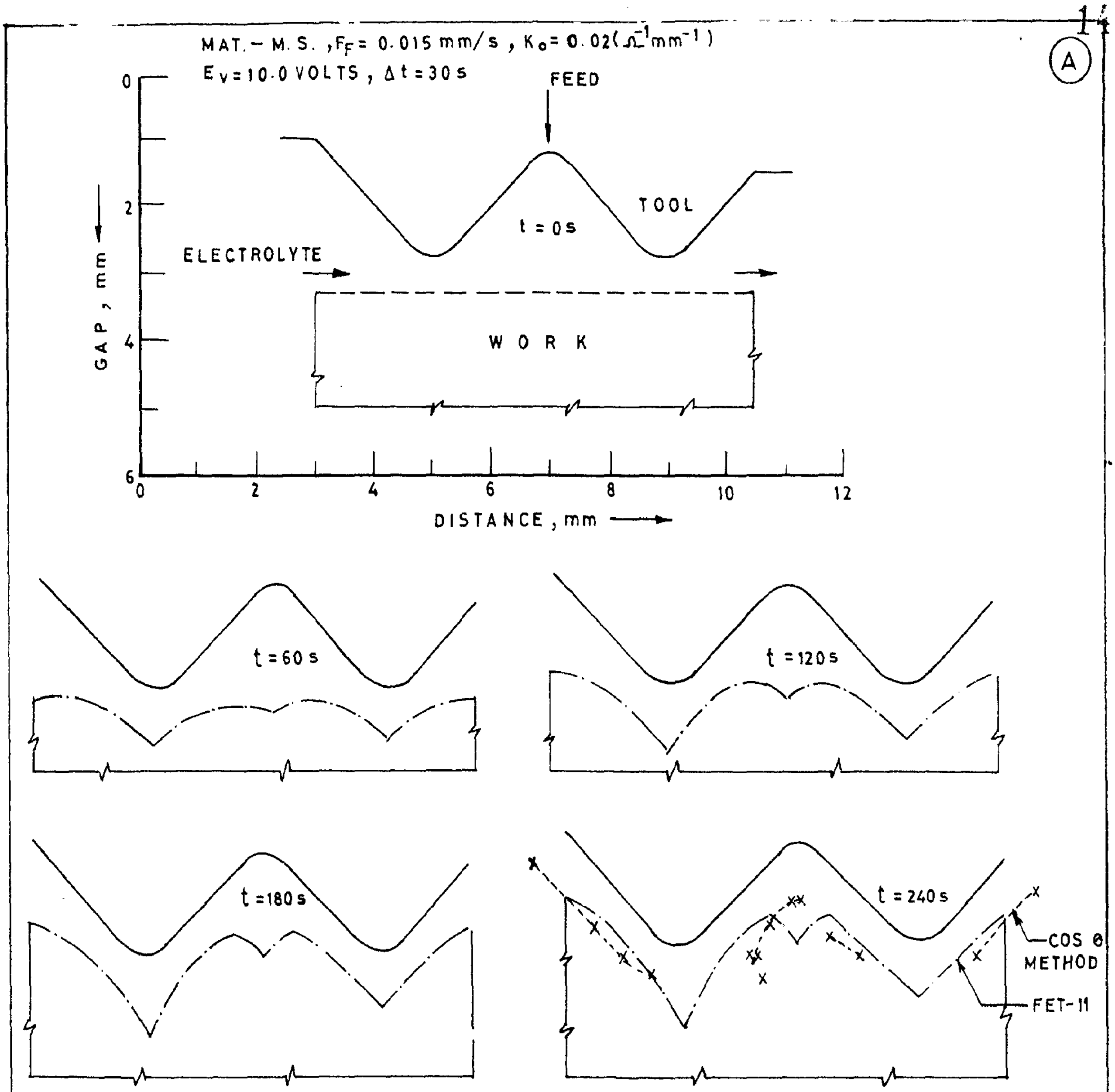

FIG. 7.5 PROGRESSIVE SURFACE GENERATION DURING ECM

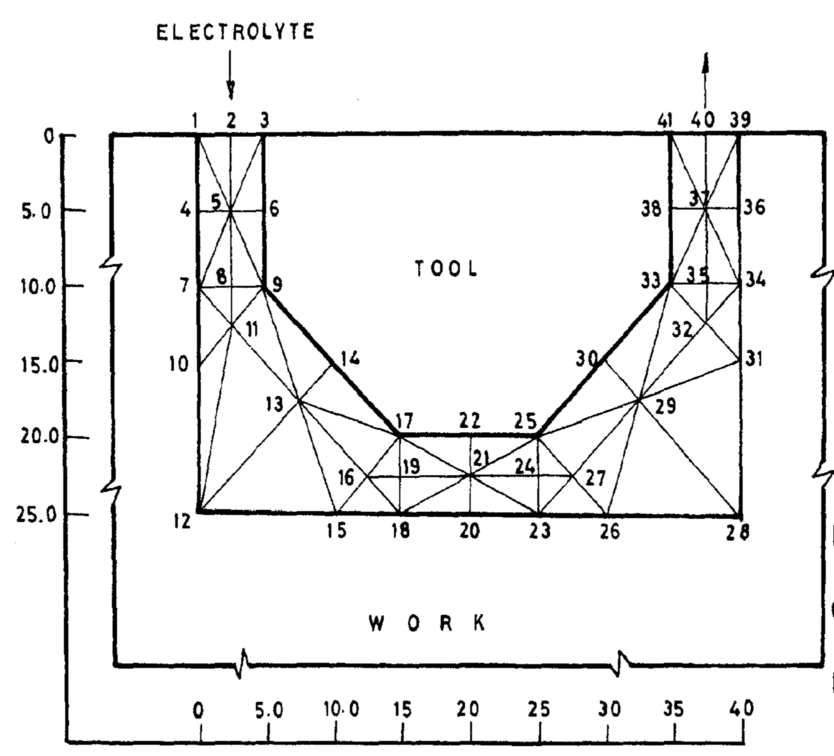
B
ELECTROLYTE
1
2
3
4
5
6
7
8
9
10
11
12
13
14
15
16
17
18
19
20
21
22
23
24
25
26
27
28
29
30
31
32
33
34
35
36
37
38
39
40
41
TOOL
WORK
0
5.0
10.0
15.0
20.0
25.0
0
5.0
10.0
15
20
25
30
35
40

FIG. 7.5 TWO DIMENSIONAL DISCRETIZAION OF A COMPLEX SHAPE INTERELECTRODE GAP

7.1.4 Effect of Tool Material on Temperature Distribution in IEG

In ECM, the frontal gap normally experiences a larger temperature rise as compared to the side gap. Due to large temperature difference, greater amount of heat is transferred from the electrolyte to the electrodes in the front gap. The total heat generated is partially conducted away to the tool and work electrodes and the balance amount stays within the electrolyte itself. This would mean that temperature rise of the electrolyte would be caused due to part of the I^2R loss in the IEG. The remainder heat is dissipated into the environment.

Considering that the entire heat generated(I^2R) within the IEG is taken up by the electrolyte, the temperature rise can be evaluated by the model FET-11 assuming uni-dimensional heat transfer. Due to heat transfer to the tool and work electrodes, the equilibrium temperature of the electrolyte would be lower than that obtained by FET-11. This has been computed as follows:

$$\begin{matrix}\text{Heat transferred} \\ \text{to the environment} \\ \text{through the electrodes}\end{matrix} = \begin{matrix}\text{Heat lost} \\ \text{by the} \\ \text{electrolyte}\end{matrix} \quad .. \qquad (7.1)$$

Computation has been carried out assuming 100% and 95% current efficiencies for three different cathode materials viz., copper, brass and stainless steel (Fig.7.6). For computation purposes, the thermal properties of the electrodes have been obtained from standard data book (73).

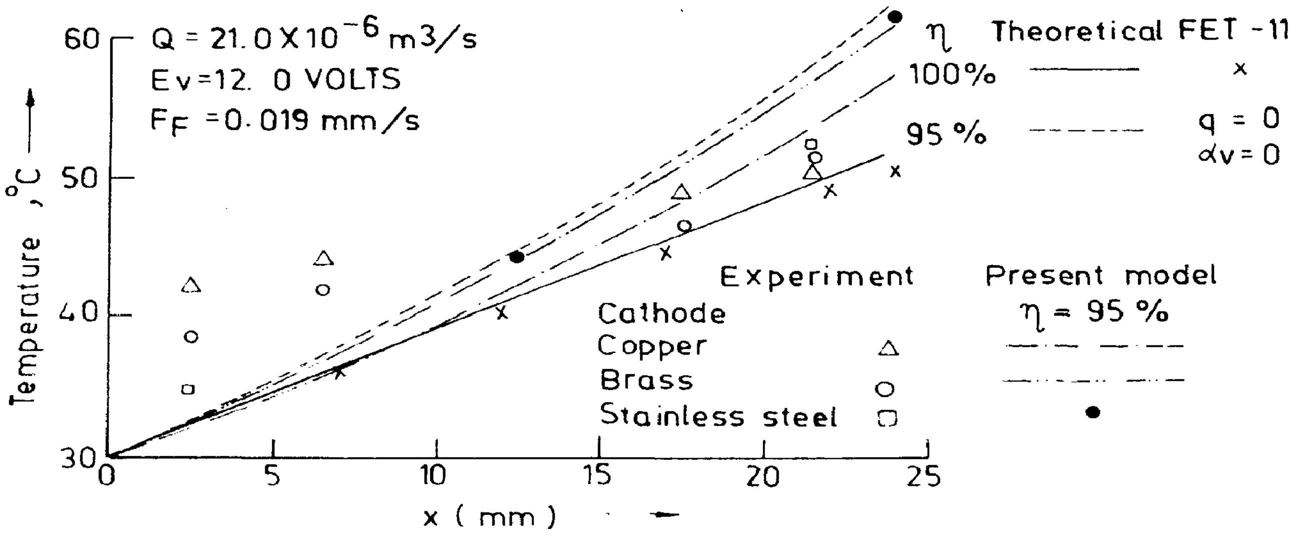

FIG. 7.6 COMPARISON OF ANALYTICAL AND EXPERIMENTAL RESULTS

7.2 PARAMETRIC STUDY

A parametric study of the ECM process would help in a better understanding of the type of inter-relationship between the tool feed rate, electrolyte flow velocity, IEG, temperature distribution, electrolyte conductivity, current density, etc. For this purpose the analytical results obtained by FET-11 and evaluated for the machining conditions given in Table-11 have been given in Figs. (7.7-7.9) for zero feed rate conditions and in Figs.(7.10-7.12) for finite feed rate conditions.

For zero feed rate, effects of electrolyte flow velocity (Fig.7.7), electrolyte flow mode (Fig.7.8) and IEG (Fig.7.9) have been considered. For finite feed rate condition, effects of feed rate (Fig.7.10), interelectrode gap (Fig.7.11) and electrolyte flow velocity (Fig.7.12) have been analysed. It should be noted that the anode profile in this case has been calculated on the assumption that the overcut in the transition zone remains same throughout. Further it is to be noted that linear MRR at each node, and the volumetric and specific MRR within each element can be computed from Eqs(7.1a), (7.1b) and (7.1c) respectively.

$$MR_l(i) = \Delta t.F_F + Y_{(i)} - FPY_{(i)} ; \quad \text{if KIN=1, } FPY_{(i)} = YI \qquad (7.1a)$$

$$\text{if KIN} > 1, \; FPY_{(i)}(KIN) = Y_{(i)}(KIN-1)$$

$$MR_v(i) = W\left[\left\{(MR_l(i) + MR_l(i+1)\right\} . \frac{x(i+1) - x(i)}{2}\right] \qquad (7.1b)$$

$$MR_s(i) = \left[MR_v(i) \Big/ \left(\frac{J(i+1) + J(i)}{2}\right)\right] \qquad (7.1c)$$

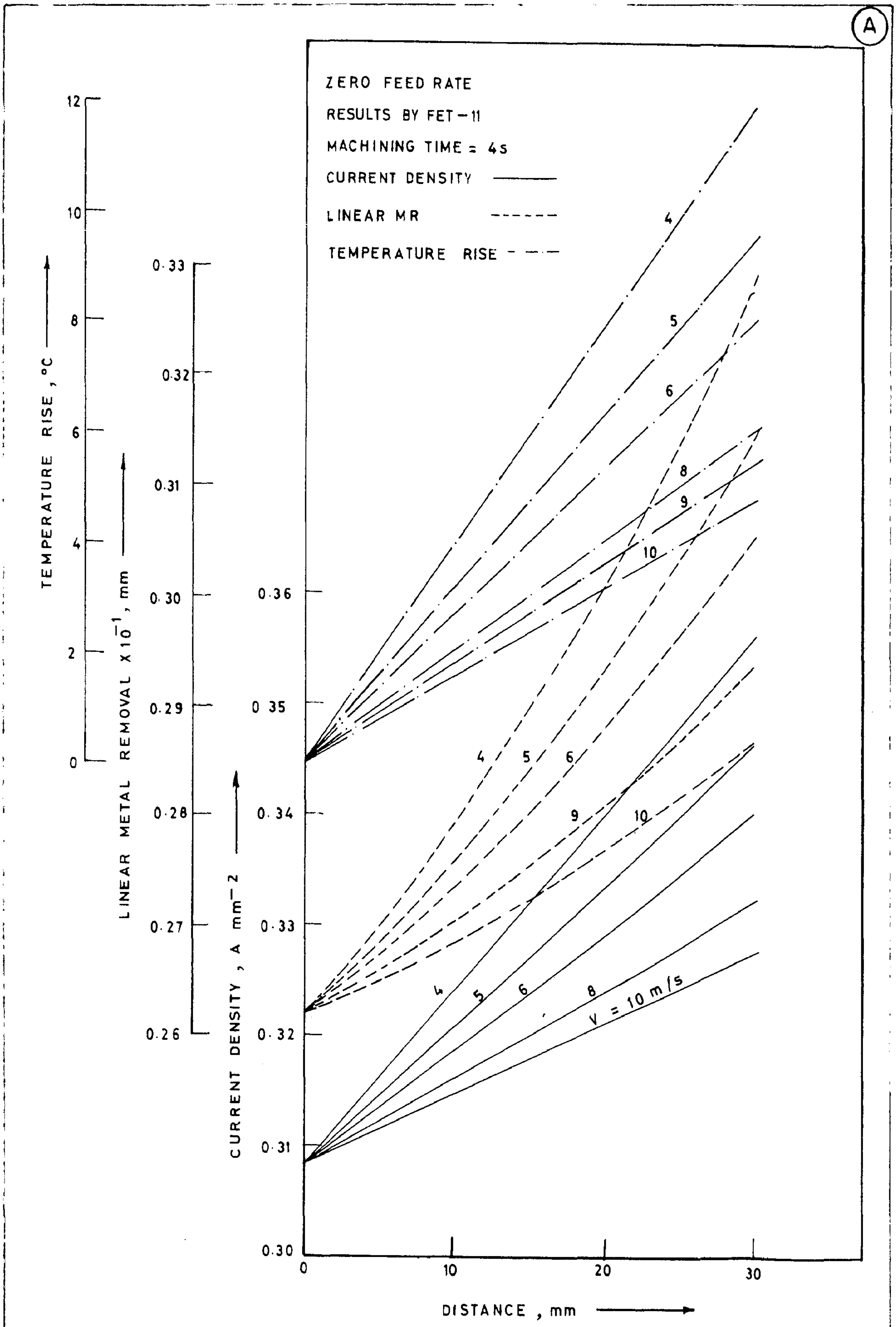

FIG. 7.7 EFFECT OF ELECTROLYTE FLOW DISTANCE ON CURRENT DENSITY, LINEAR METAL REMOVAL AND TEMPERATURE RISE AT DIFFERENT FLOW VELOCITIES

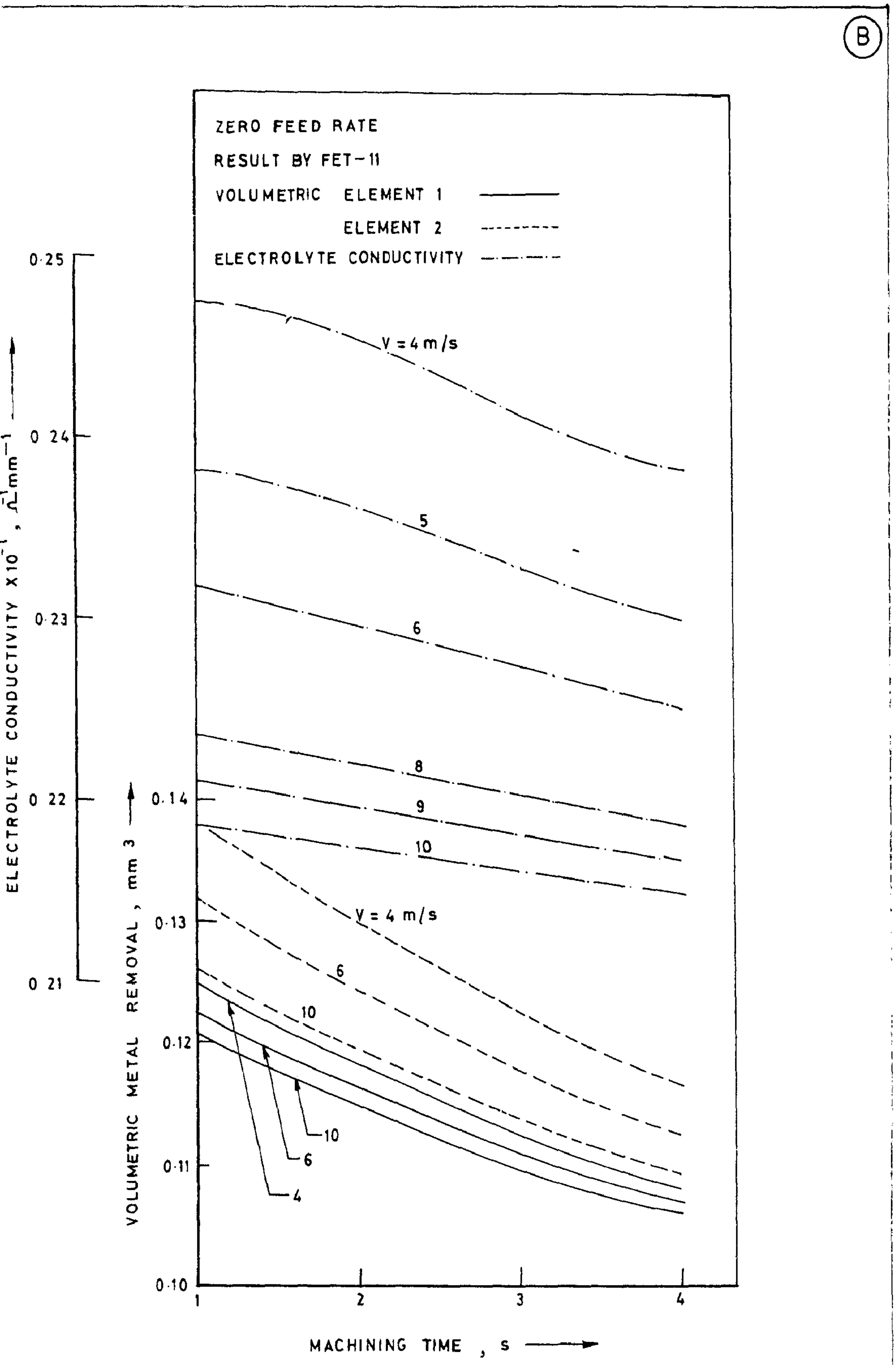

FIG 7.7 EFFECT OF MACHINING TIME ON VOLUMETRIC METAL REMOVAL AND ELECTROLYTE CONDUCTIVITY AT DIFFERENT FLOW VELOCITIES

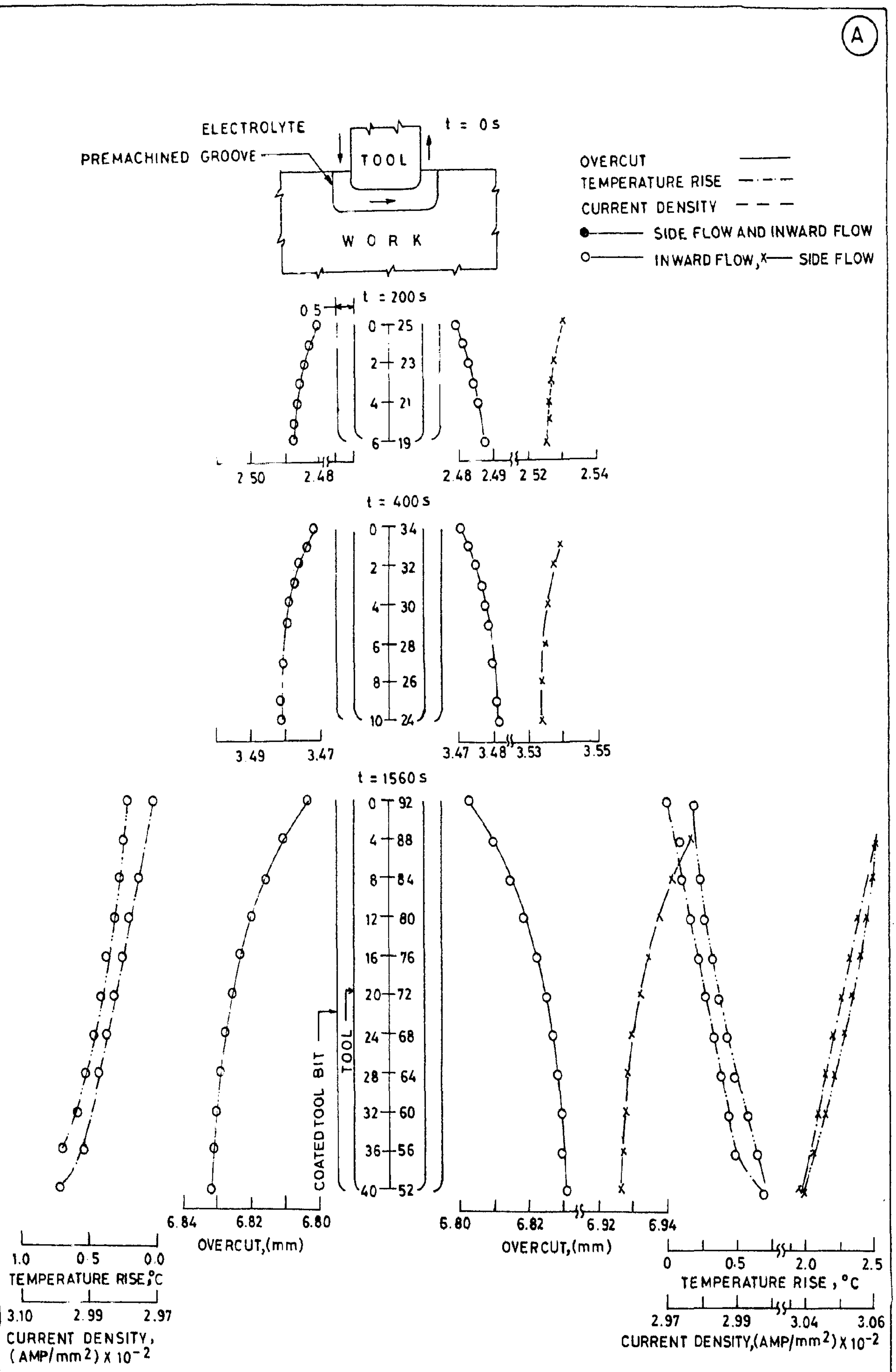

FIG. 7.8 SURFACE GENERATION DURING EC DRILLING

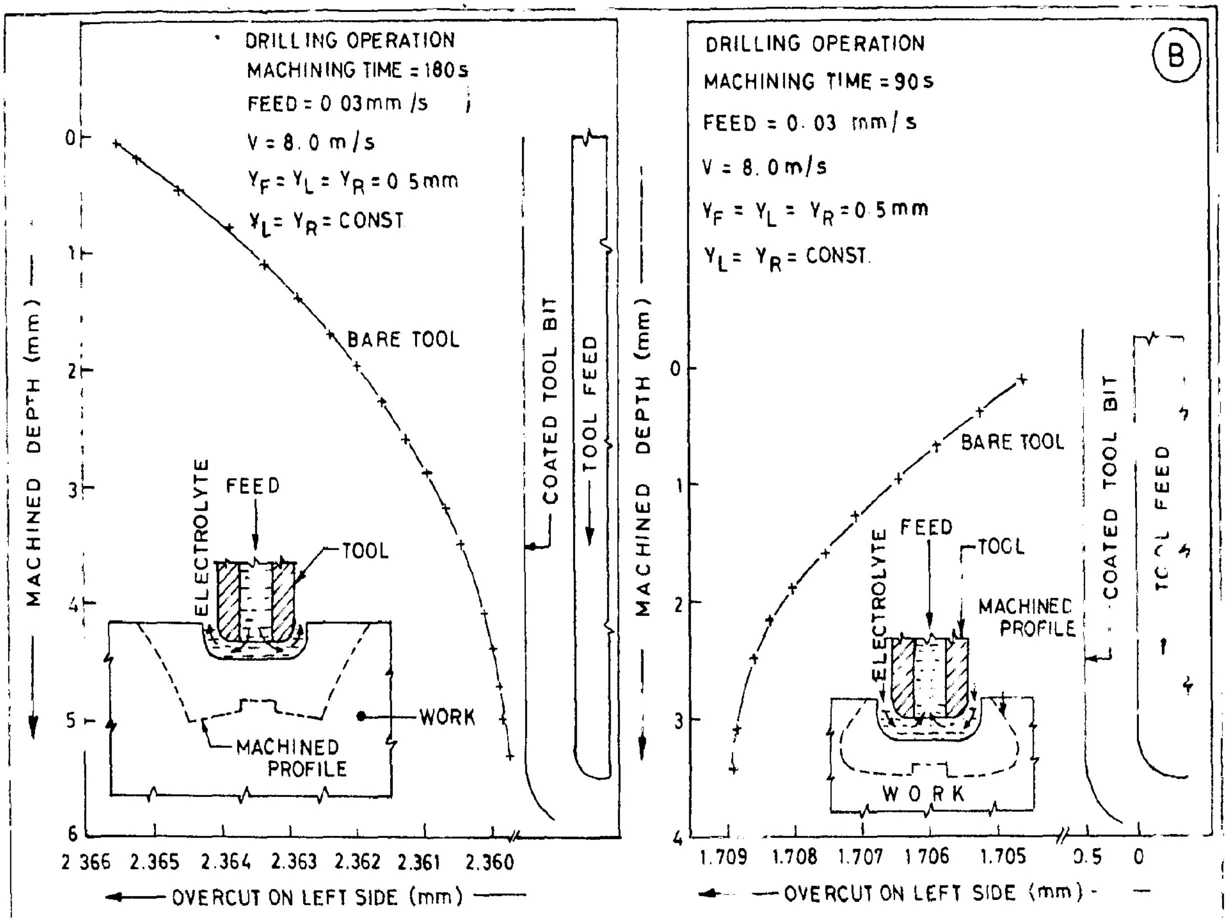

OUTWARD FLOW INWARD FLOW

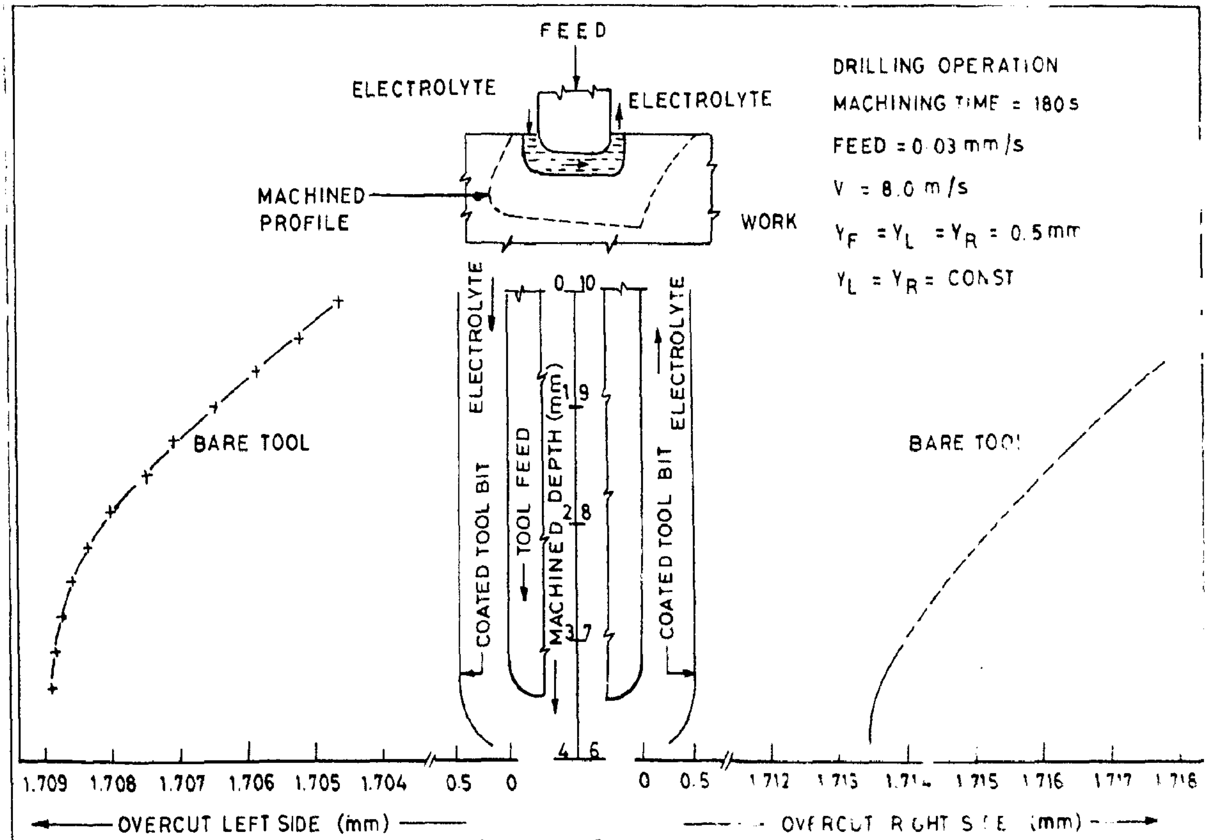

SIDE FLOW

FIG. 7.8 SIDE SURFACE GENERATION DURING EC DRILLING USING DIFFERENT MODES OF ELECTROLYTE FLOW

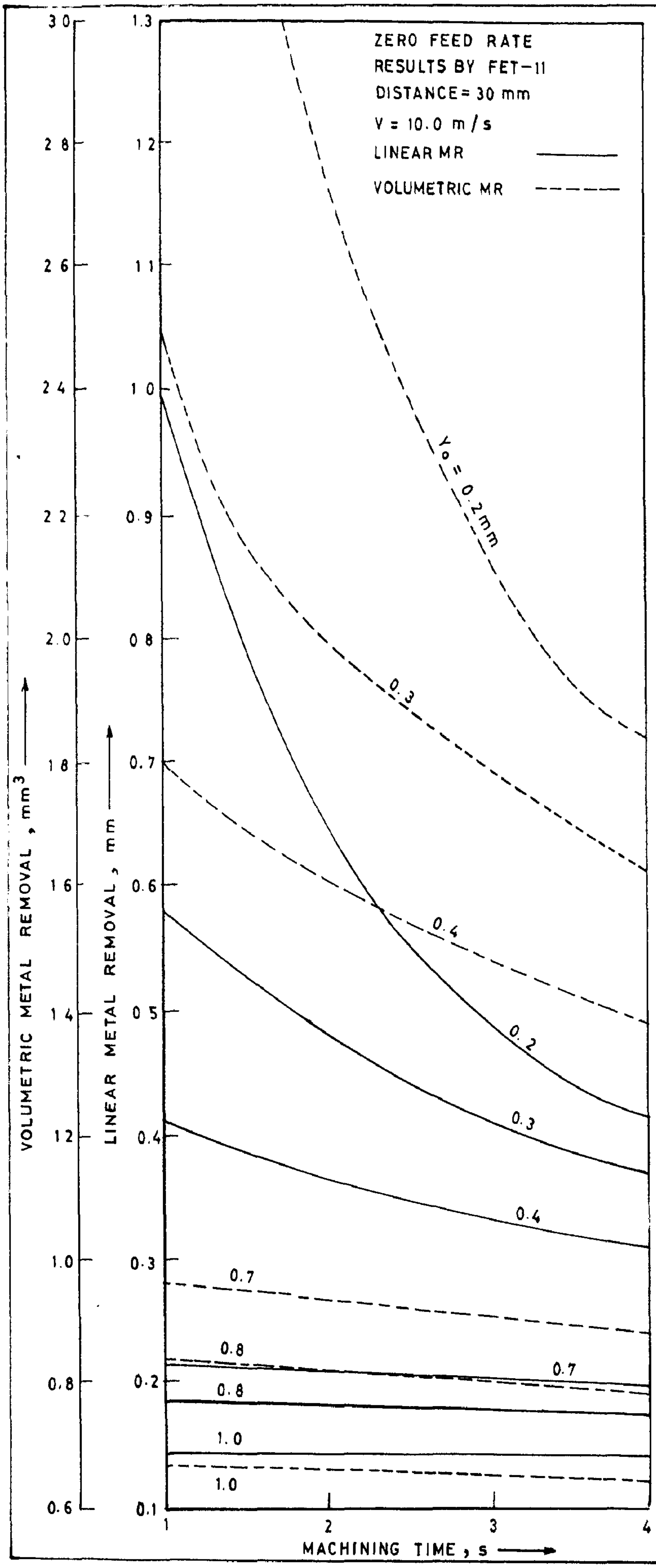

FIG.7.9 EFFECT OF MACHINING TIME ON LINEAR AND VOLUMETRIC METAL REMOVAL AT DIFFERENT INTERELECTRODE GAPS

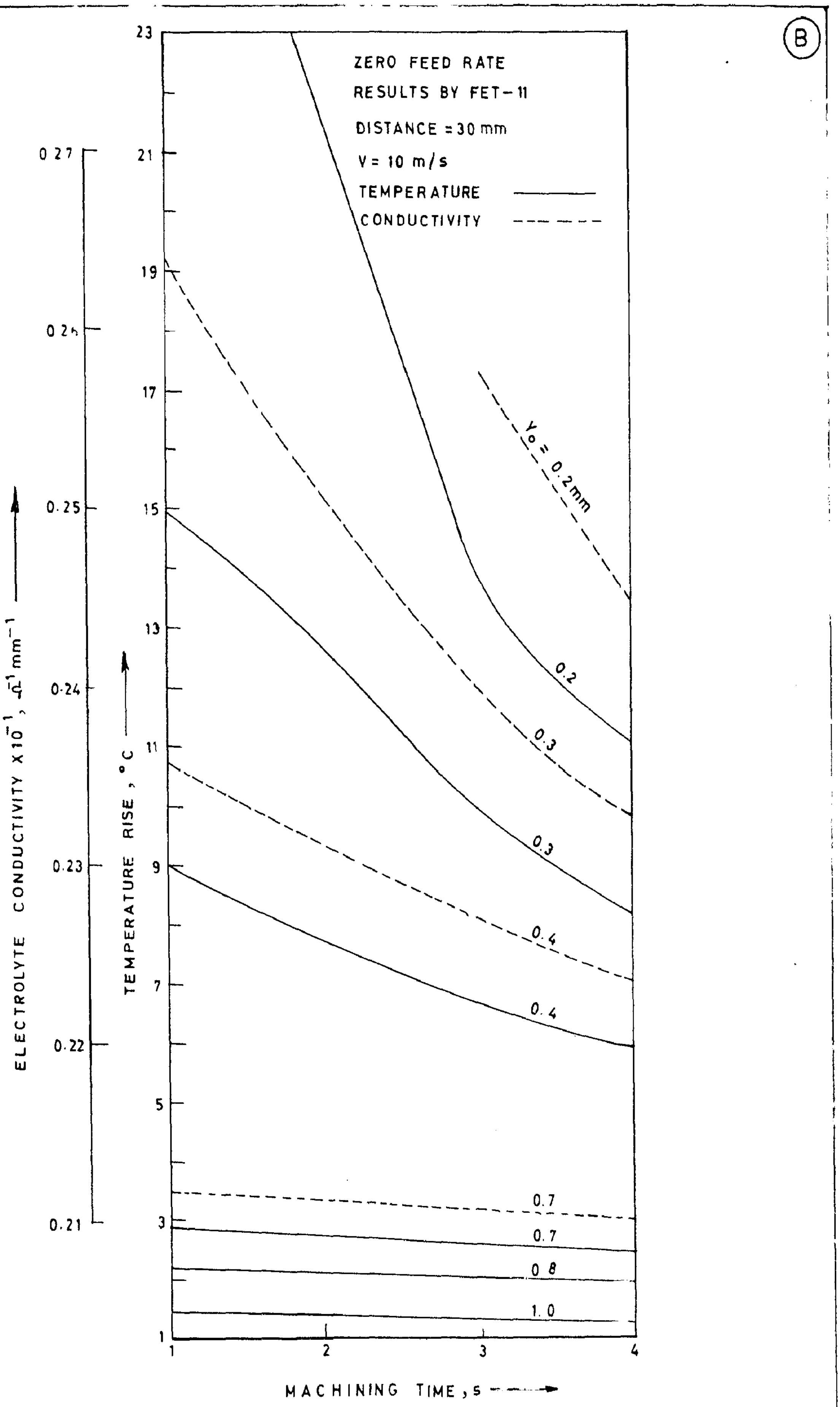

FIG.7.9 EFFECT OF MACHINING TIME ON ELECTROLYTE CONDUCTIVITY AND TEMPERATURE RISE AT DIFFERENT INTERELECTRODE GAPS

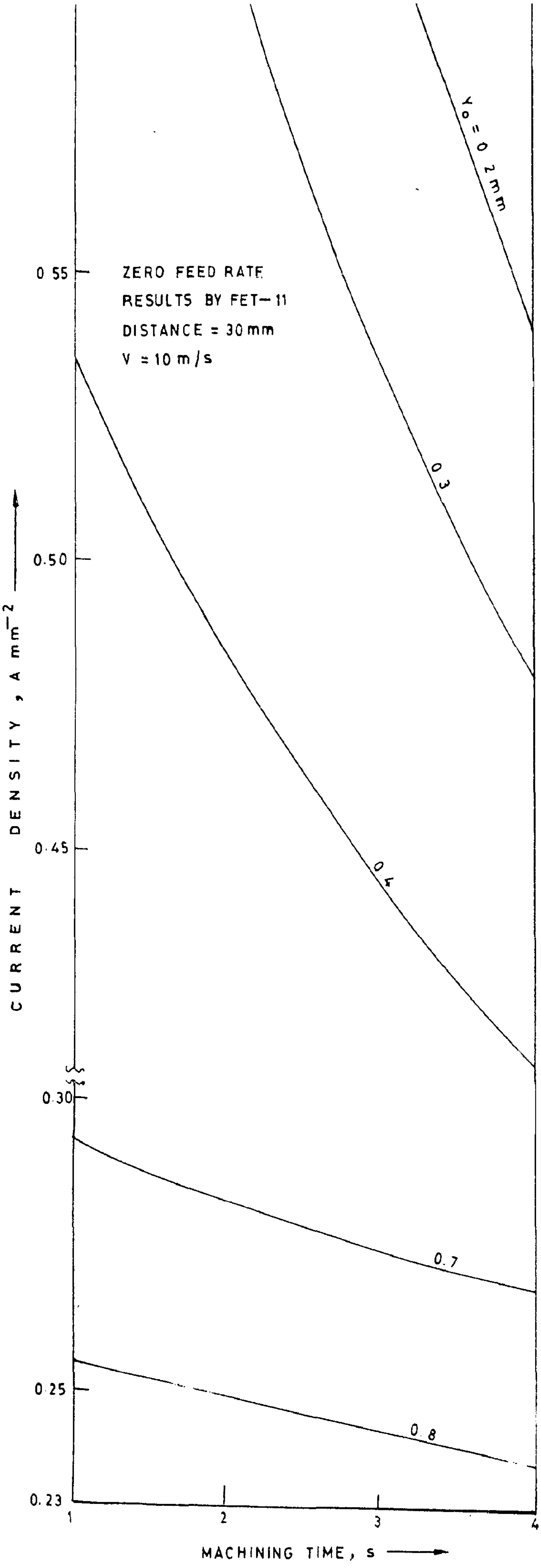

FIG 7.9 EFFECT OF MACHINING TIME ON CURRENT DENSITY AT DIFFERENT INTERELECTRODE GAPS

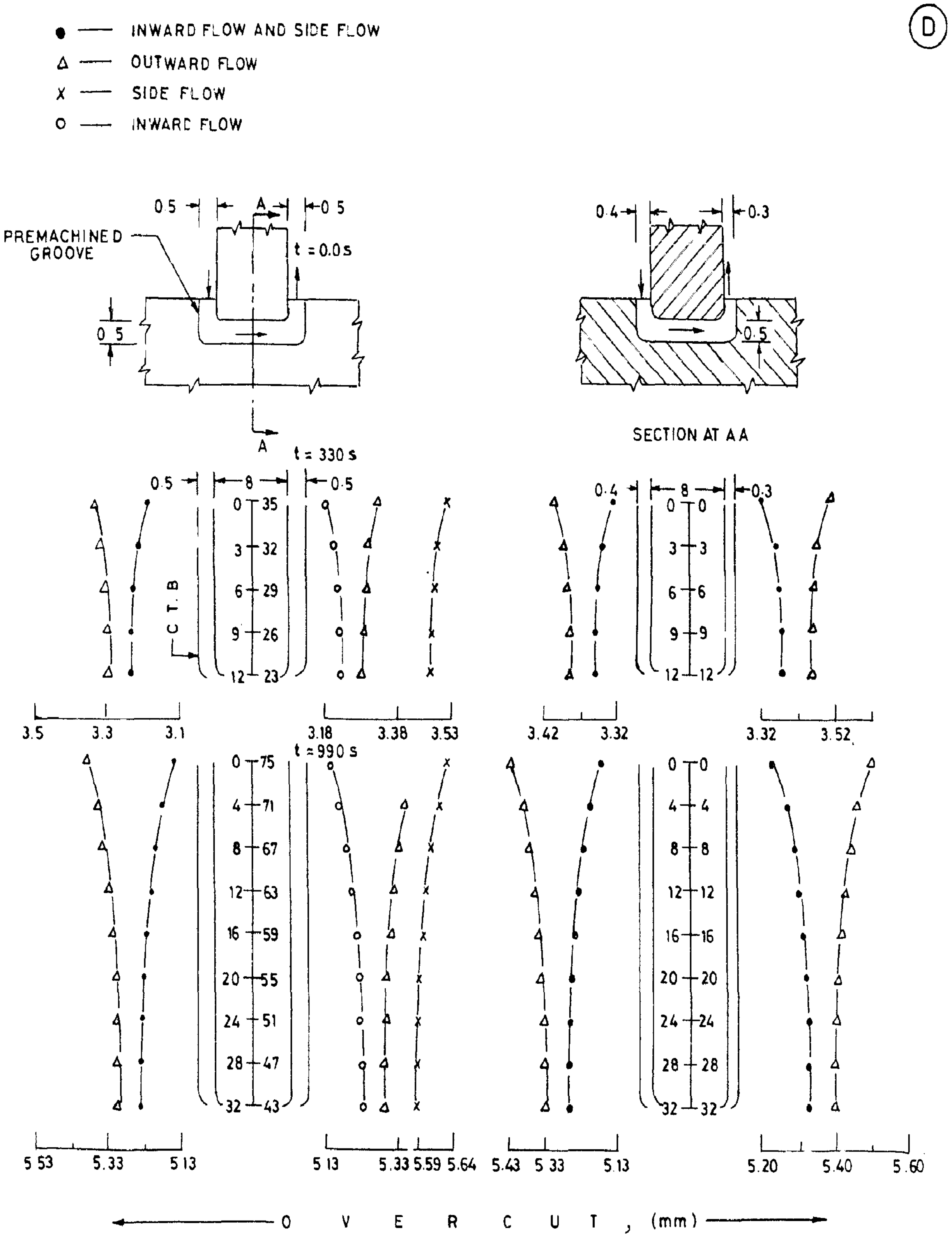
D
● — INWARD FLOW AND SIDE FLOW
Δ — OUTWARD FLOW
X — SIDE FLOW
O — INWARD FLOW
PREMACHINED GROOVE
0.5
A
0.5
t = 0.0s
0.5
A
0.4
0.3
0.5
SECTION AT AA
t = 330 s
0.5
8
0.5
C.T.B
0 35
3 32
6 29
9 26
12 23
0.4
8
0.3
0 0
3 3
6 6
9 9
12 12
3.5
3.3
3.1
3.18
3.38
3.53
3.42
3.32
3.32
3.52
t = 990 s
0 75
4 71
8 67
12 63
16 59
20 55
24 51
28 47
32 43
0 0
4 4
8 8
12 12
16 16
20 20
24 24
28 28
32 32
5.53
5.33
5.13
5.13
5.33
5.59
5.64
5.43
5.33
5.13
5.20
5.40
5.60
OVERCUT, (mm)

FIG. 7.9 EFFECT OF INITIAL INTERELECTRODE GAP AND MODE OF ELECTROLYTE FLOW ON ANODE PROFILE

Ⓐ

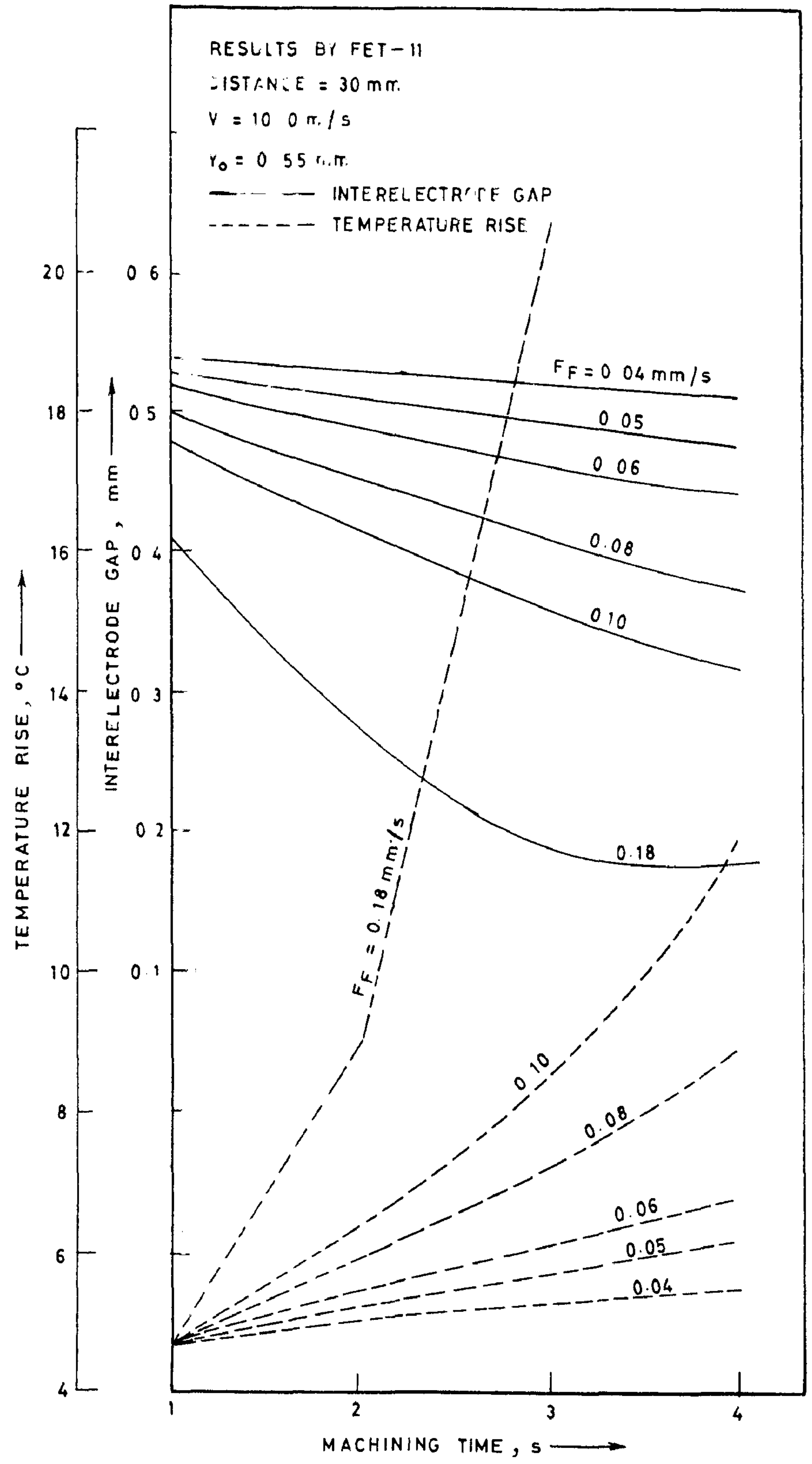

FIG.7.10 EFFECT OF MACHINING TIME ON INTERELECTRODE GAP AND TEMPERATURE RISE AT DIFFERENT FEED RATES

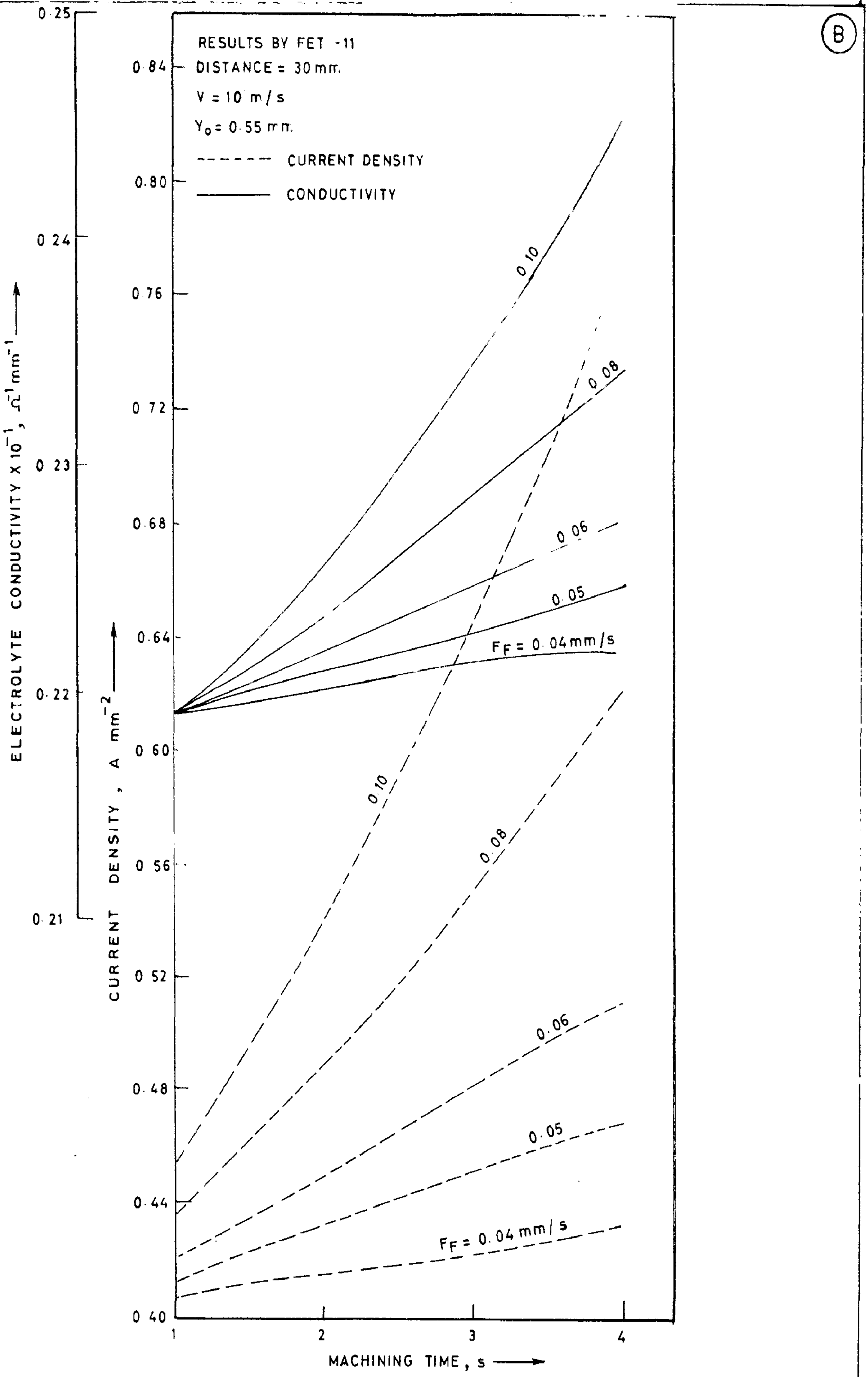

FIG. 7.10 EFFECT OF MACHINING TIME ON CURRENT DENSITY AND ELECTROLYTE CONDUCTIVITY AT DIFFERENT FEED RATES

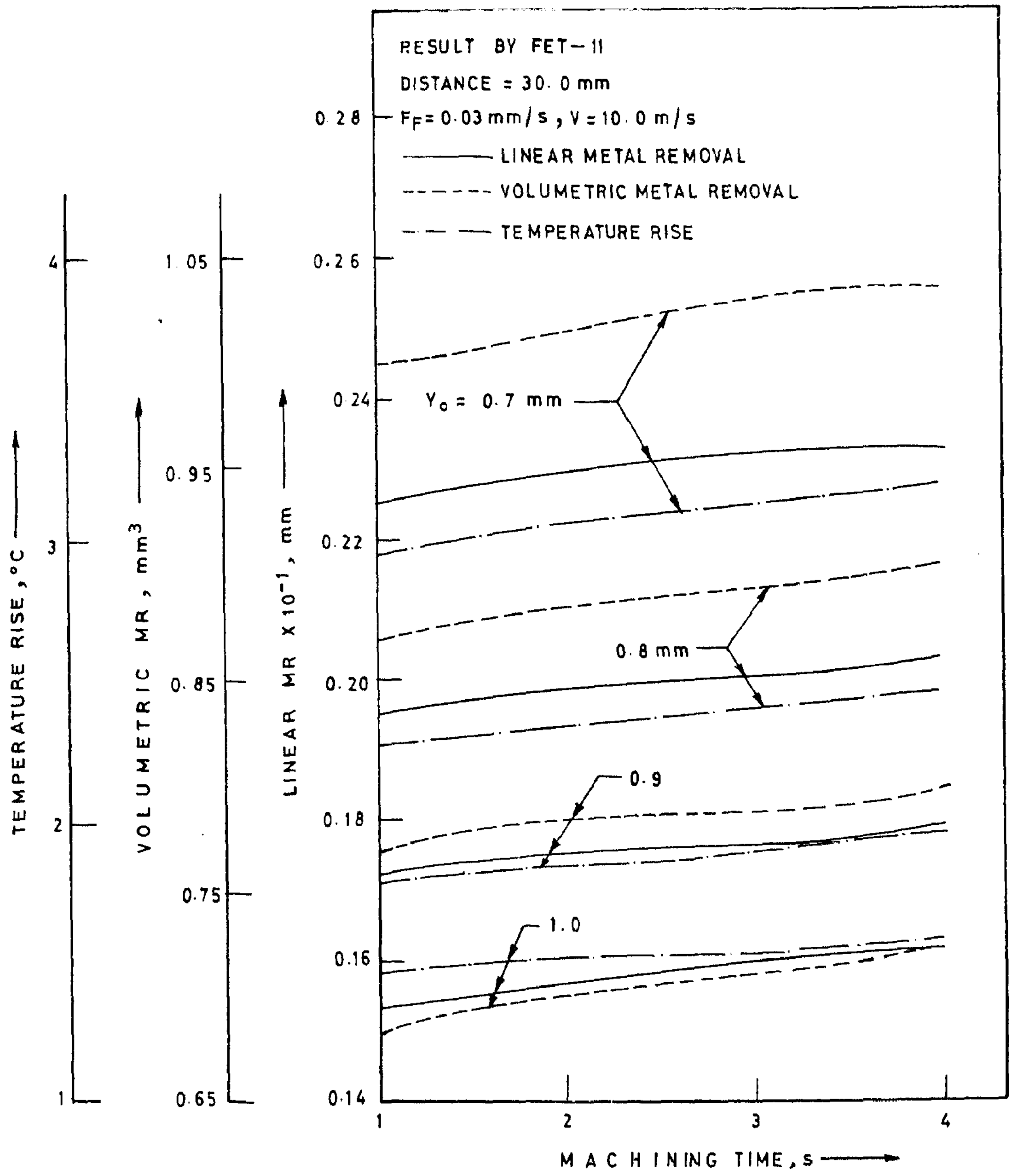

FIG. 7.11 EFFECT OF MACHINING TIME ON METAL REMOVAL AND TEMPERATURE RISE FOR DIFFERENT INTERELECTRODE GAPS

Ⓑ

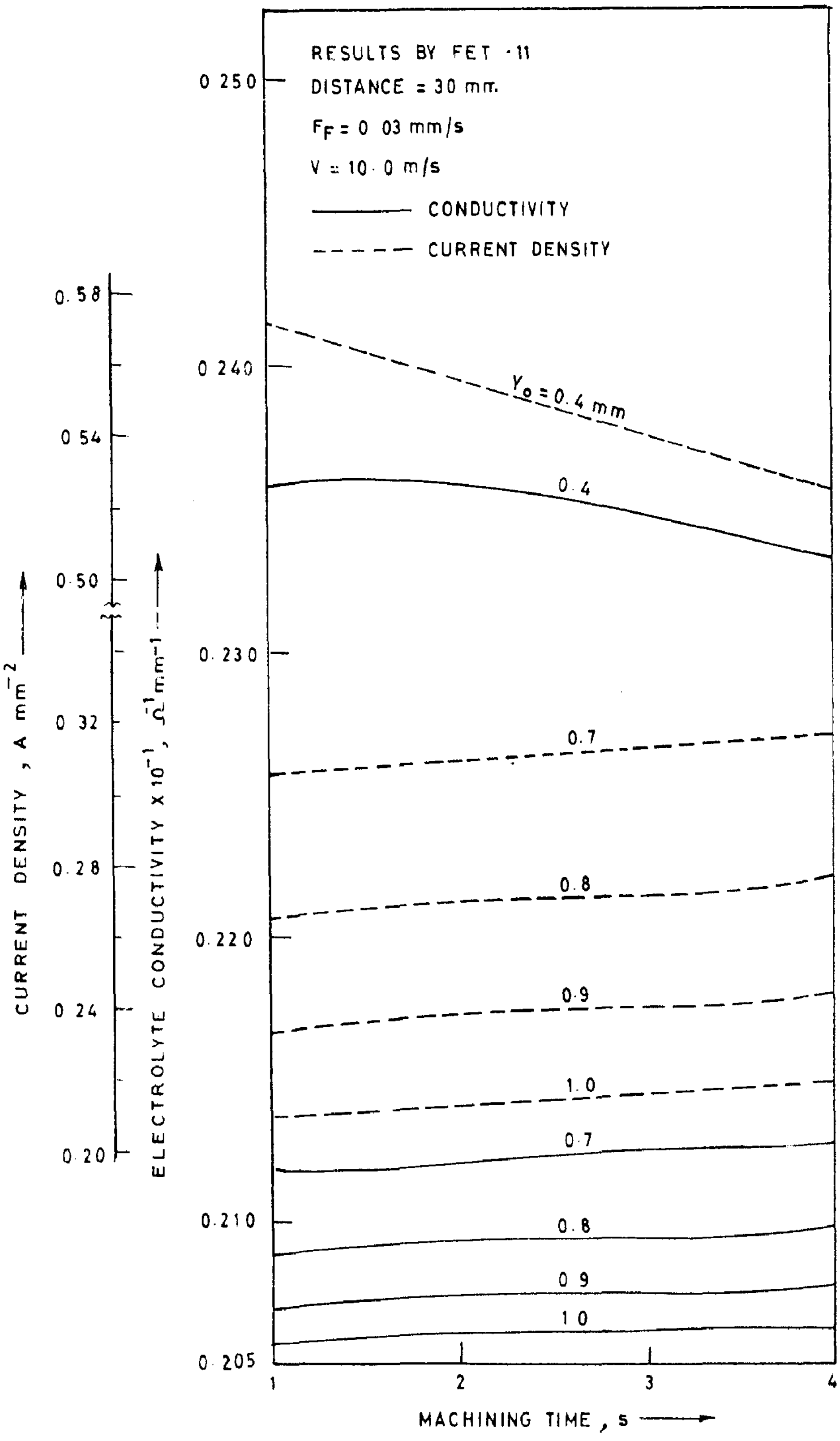

FIG 7 11 EFFECT OF MACHINING TIME ON ELECTROLYTE CONDUCTIVITY AND CURRENT DENSITY AT DIFFERENT INTERELECTRODE GAPS

Ⓐ

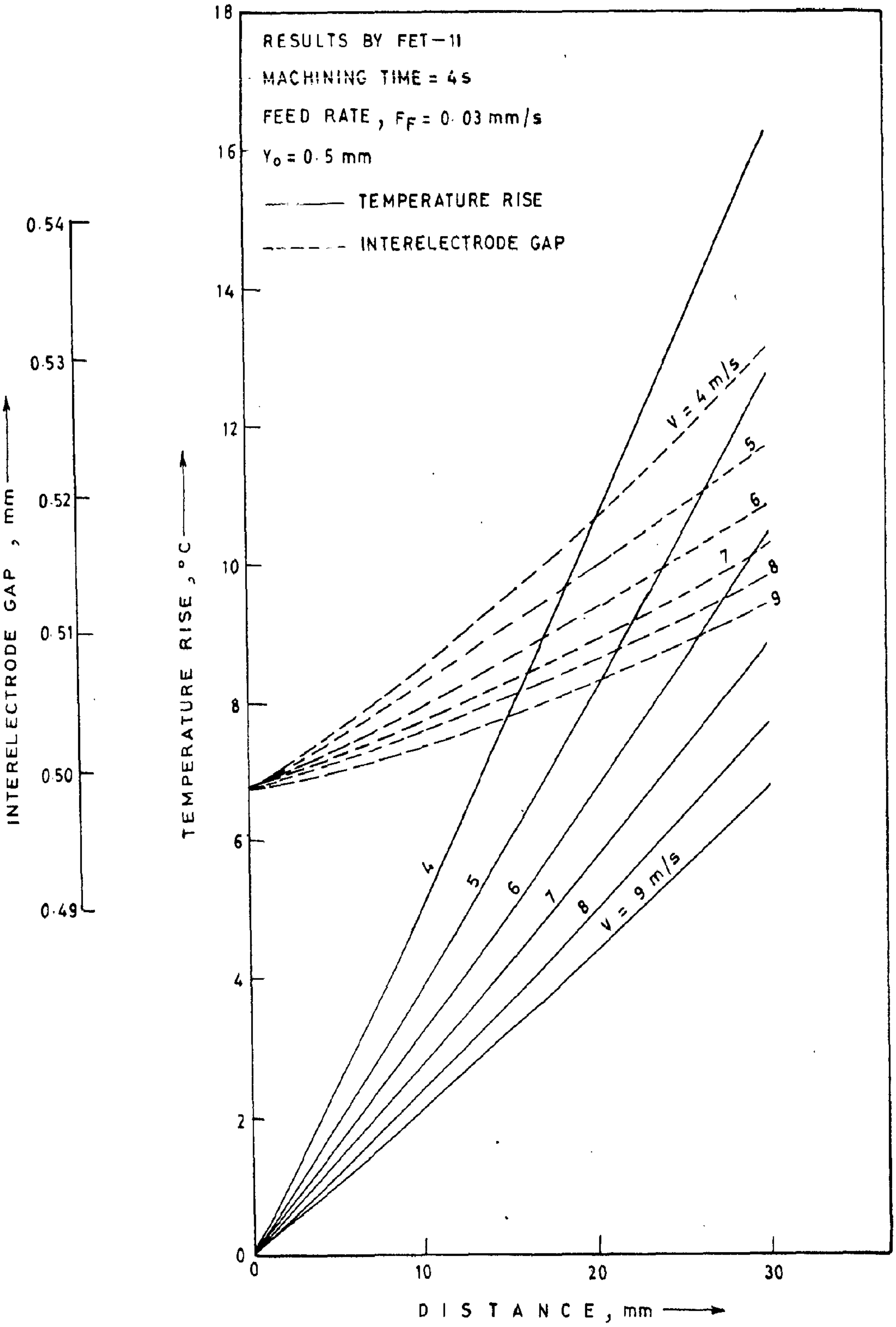

FIG. 7.12 EFFECT OF ELECTROLYTE FLOW DISTANCE ON TEMPERATURE RISE AND INTERELECTRODE GAP AT DIFFERENT ELECTROLYTE FLOW VELOCITIES

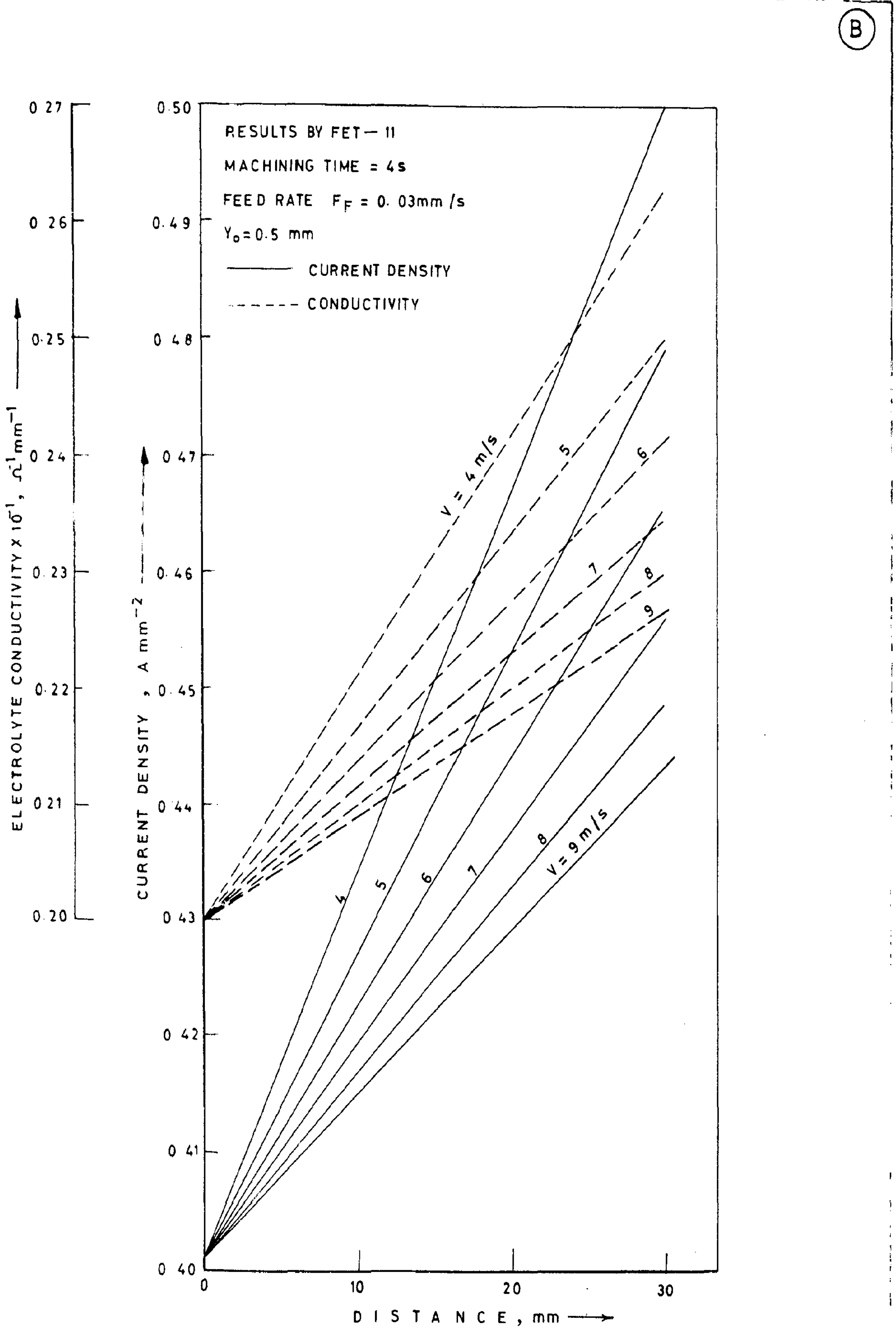

FIG 7 12 EFFECT OF ELECTROLYTE FLOW DISTANCE ON CURRENT DENSITY AND ELECTROLYTE CONDUCTIVITY AT DIFFERENT FLOW VELOCITIES

Ⓒ

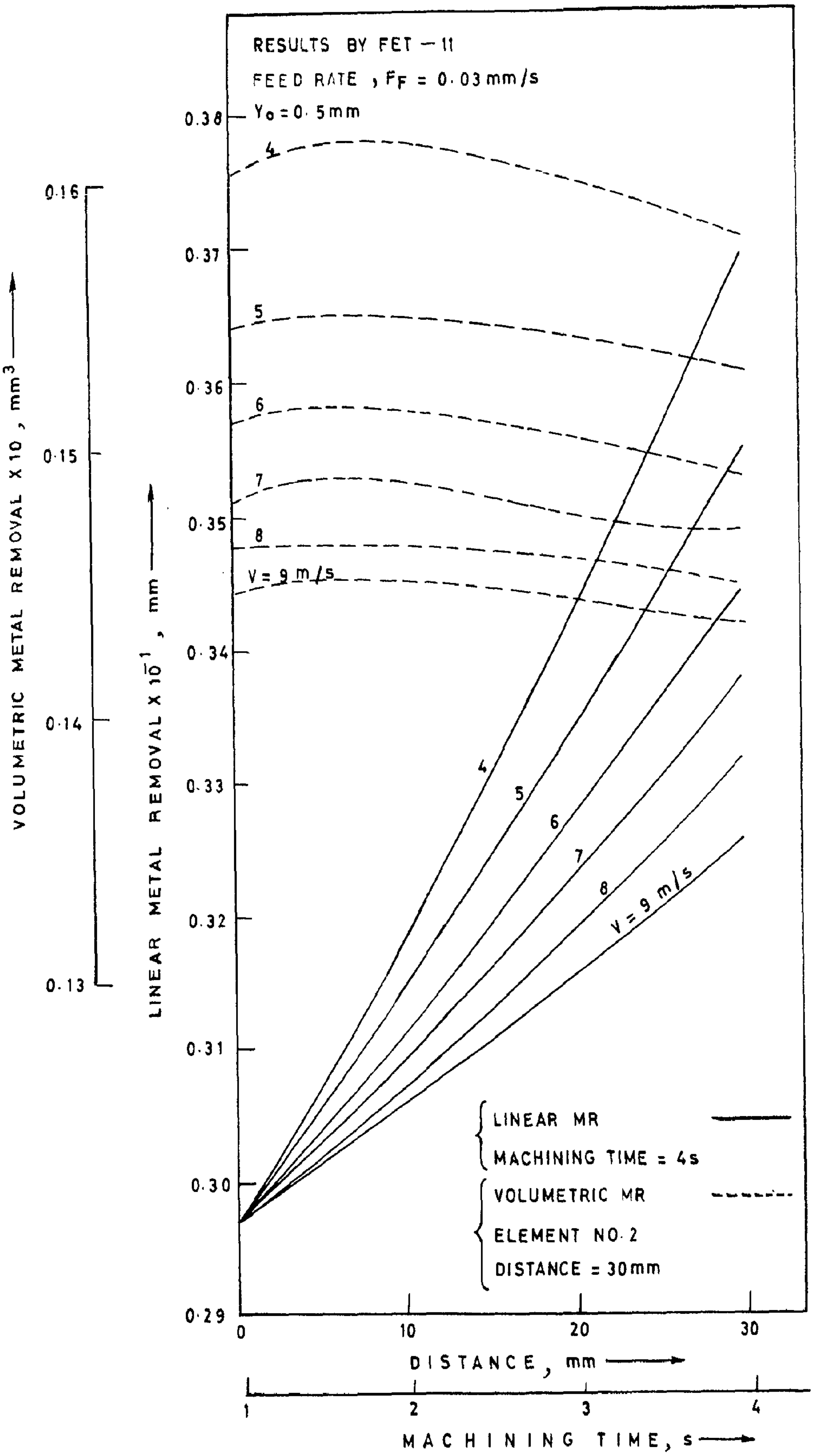

FIG. 7.12 EFFECT OF MACHINING TIME ON LINEAR AND VOLUMETRIC METAL REMOVAL AT DIFFERENT FLOW VELOCITIES

7.3 ELECTROCHEMICAL DRILLING (ECD) WITH BARE TOOL

For ECD, three types of anode materials viz., mild steel, low alloy steel in cast and forged conditions were used. The cathode in all the cases was made of brass however, tools with different diameters and geometries were used. Test conditions for ECD experiments are given in Table-12 (Mild steel), Table-13 (Cast low alloy steel) and Table-14 (Forged low alloy steel) and for calculating the anode profile, modified Eq(3.2) has been used. It is to be noted that during the computation of anode profile, overcut in transition zone was calculated using equation (3.4) derived on the basis of regression analysis. The values of its constants for different sets have been evaluated from the figures of type of 3.2. In few cases during ECM of mild steel applied voltage across the electrodes was found to vary during the cut. Hence the effective voltage E_V i.e., the voltage which prevailed for the machining period of time more than 66% was chosen. During ECM of M.S., the mean voltage and current were measured at an intervals of about 300 seconds, whereas for tests on low alloy steels, the observed modal values and in some cases mean values of current and voltage over a period of 30 s and in some cases 60 seconds was employed (Fig.7.13). The average of the modal/mean values was used as the effective voltage. Similarly, effective current was evaluated from the current variation with time curves (Fig. 7.14).

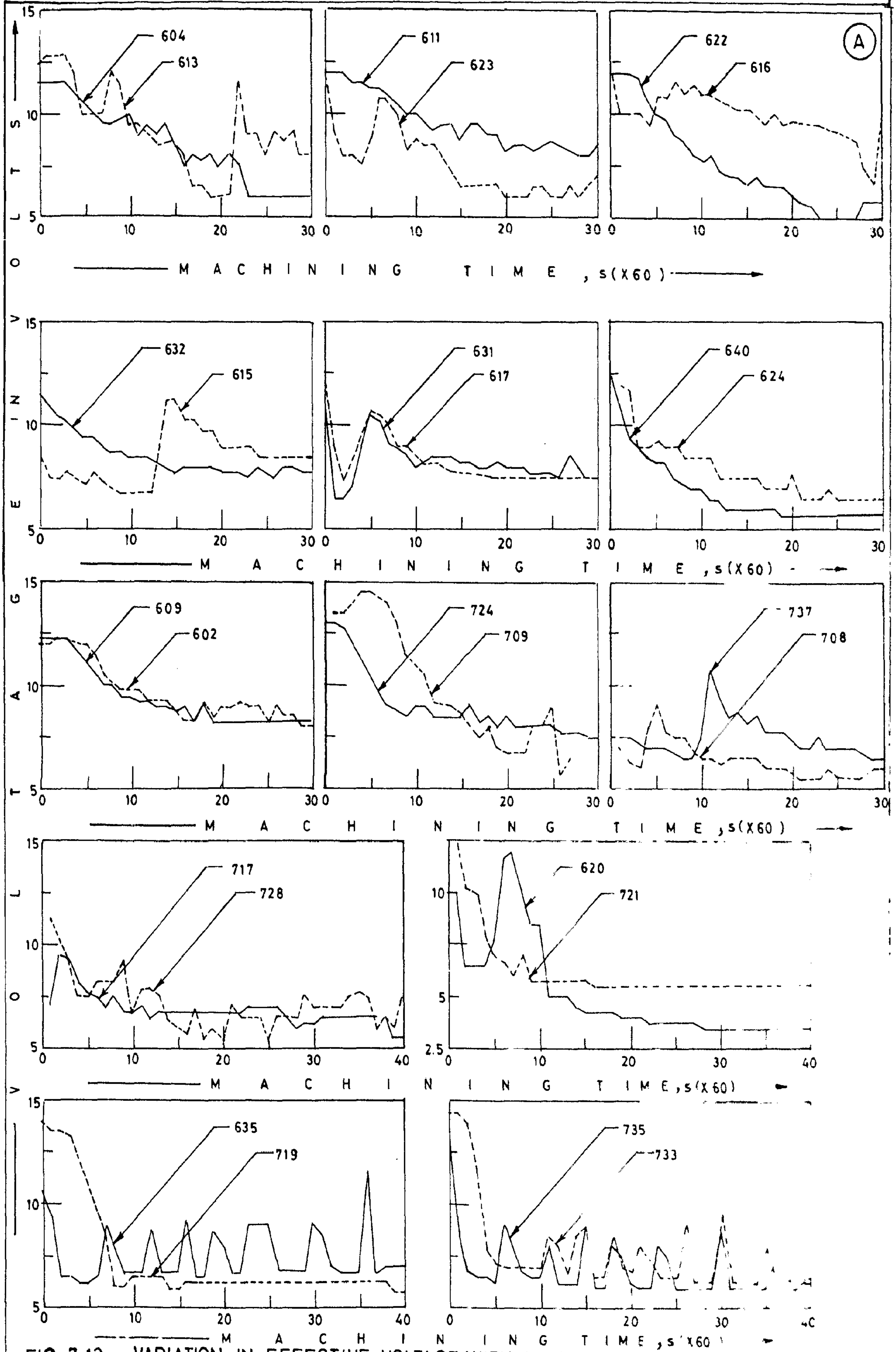

FIG. 7.13 VARIATION IN EFFECTIVE VOLTAGE WITH MACHINING TIME

Ⓑ

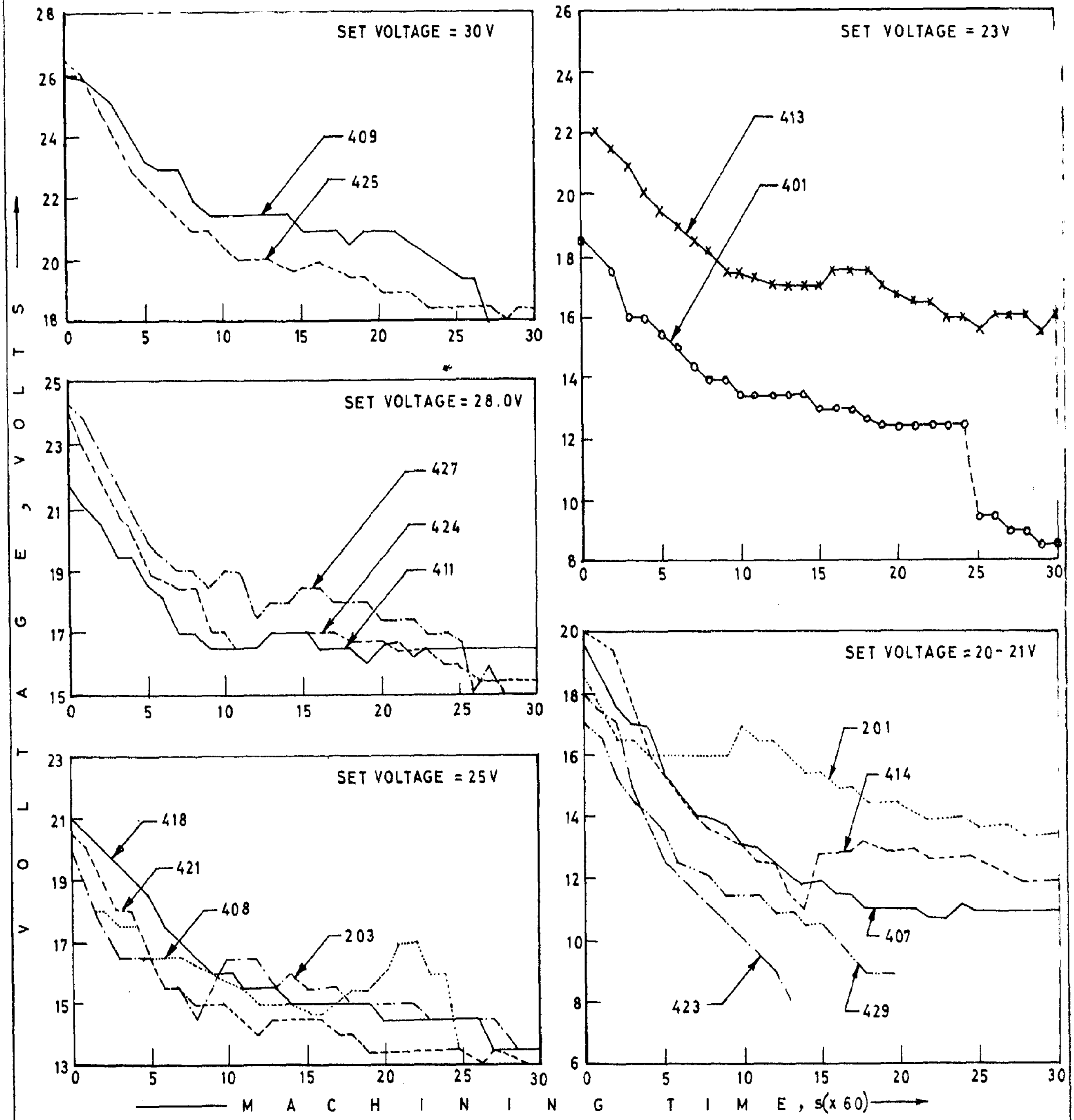

FIG.7.13 VARIATIONS IN VOLTAGE WITH MACHINING TIME

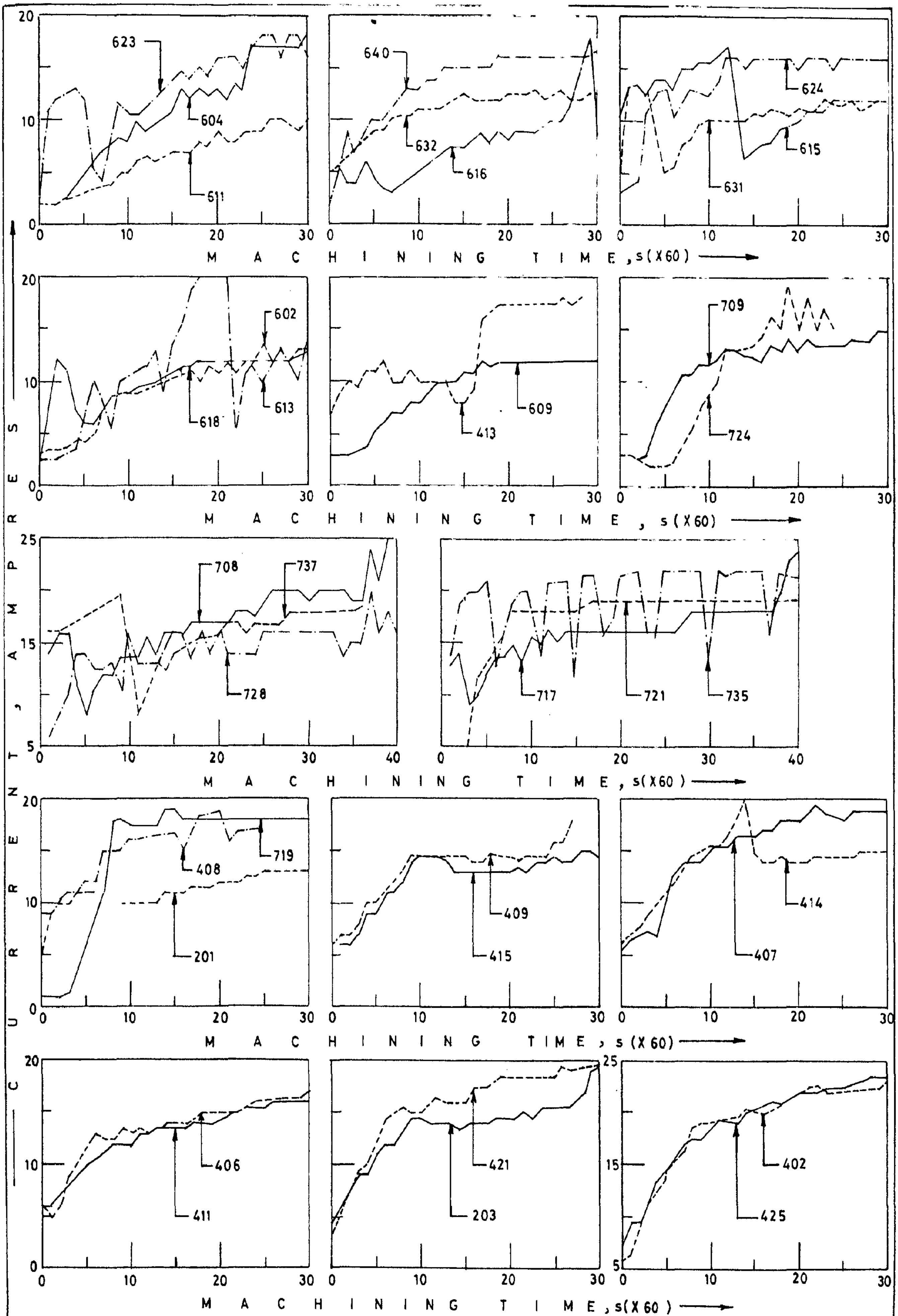

FIG. 7.14 CURRENT VARIATION WITH MACHINING TIME

To compute the anode profile and machining efficiency the effects of actual variation in voltage and current with time were taken into consideration (Figs. 7.13 & 7.14). During computation of anode profile, in majority of the cases, computational cycle time was used as 30 s whereas in some cases an interval of 60 s was also used to save the computation time. It should be noted that during the computation of anode profile heat transferred to electrodes was neglected and the void fraction was assumed to be negligible. This, however, would introduce some error in the calculations. Also univalency EC dissolution throughout the IEG during the process was assumed.

7.3.1 Effect of Voltage

To study the effects of voltage on anode profile, ECD tests were performed. For this purpose about 100 tests under different machining conditions (Table 12) were conducted on mild steel as the anode material and about 30 tests were conducted on cast low alloy steels (Table-13). As discussed earlier the form of the anode profile was measured using a replica technique and a tool makers microscope.

Fig. 7.15 shows the effect of voltage on the anode profile obtained. It is to be noted that in majority of the cases electrochemically drilled holes have the shape of an elongated S($\int$). However, the large overcut observed near the top of the machined hole extends only over a very small length as compared to the tapered part.

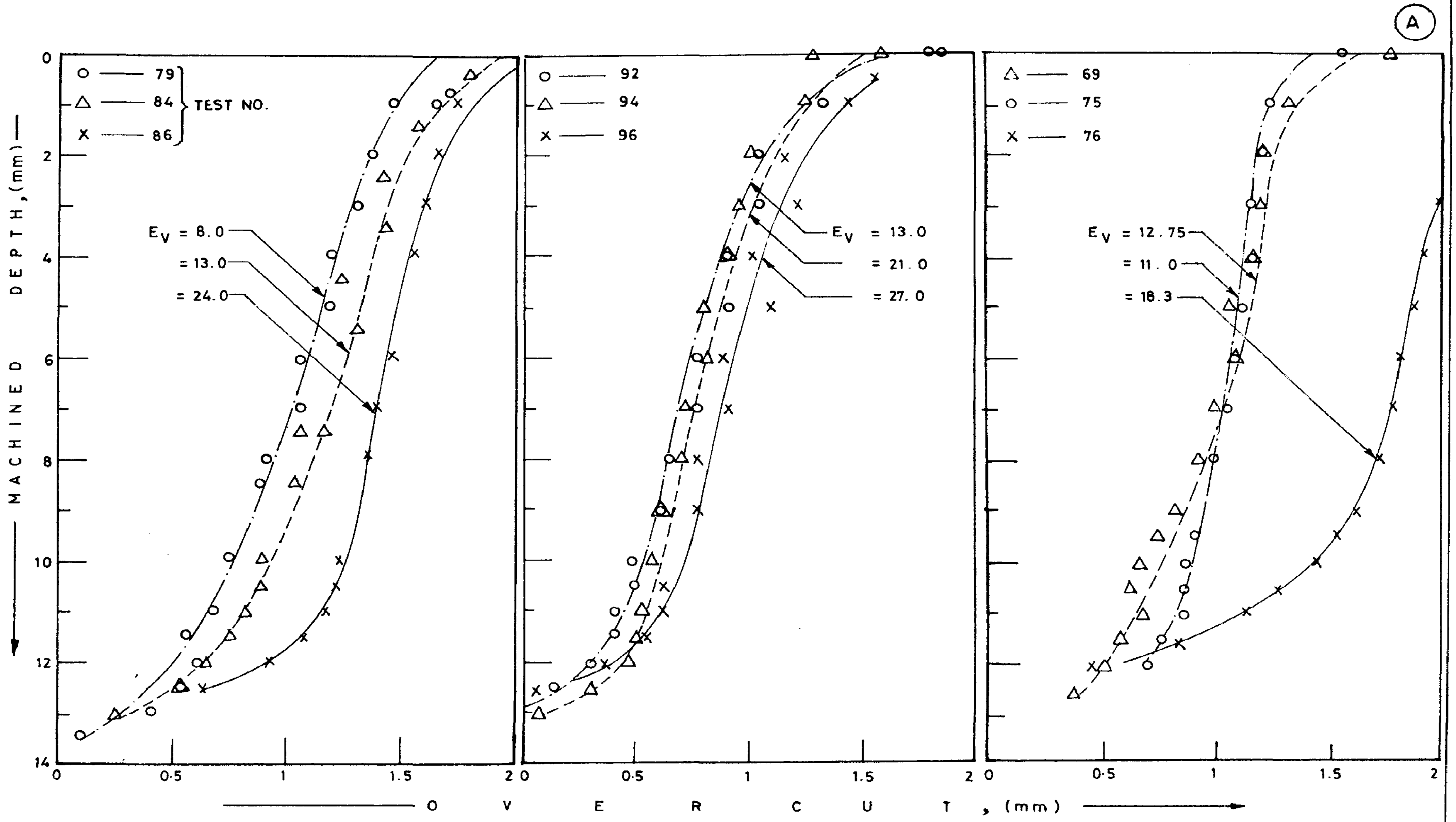

FIG. 7.15 EFFECT OF EFFECTIVE VOLTAGE ON ANODE PROFILE DURING ECD OF MILD STEEL

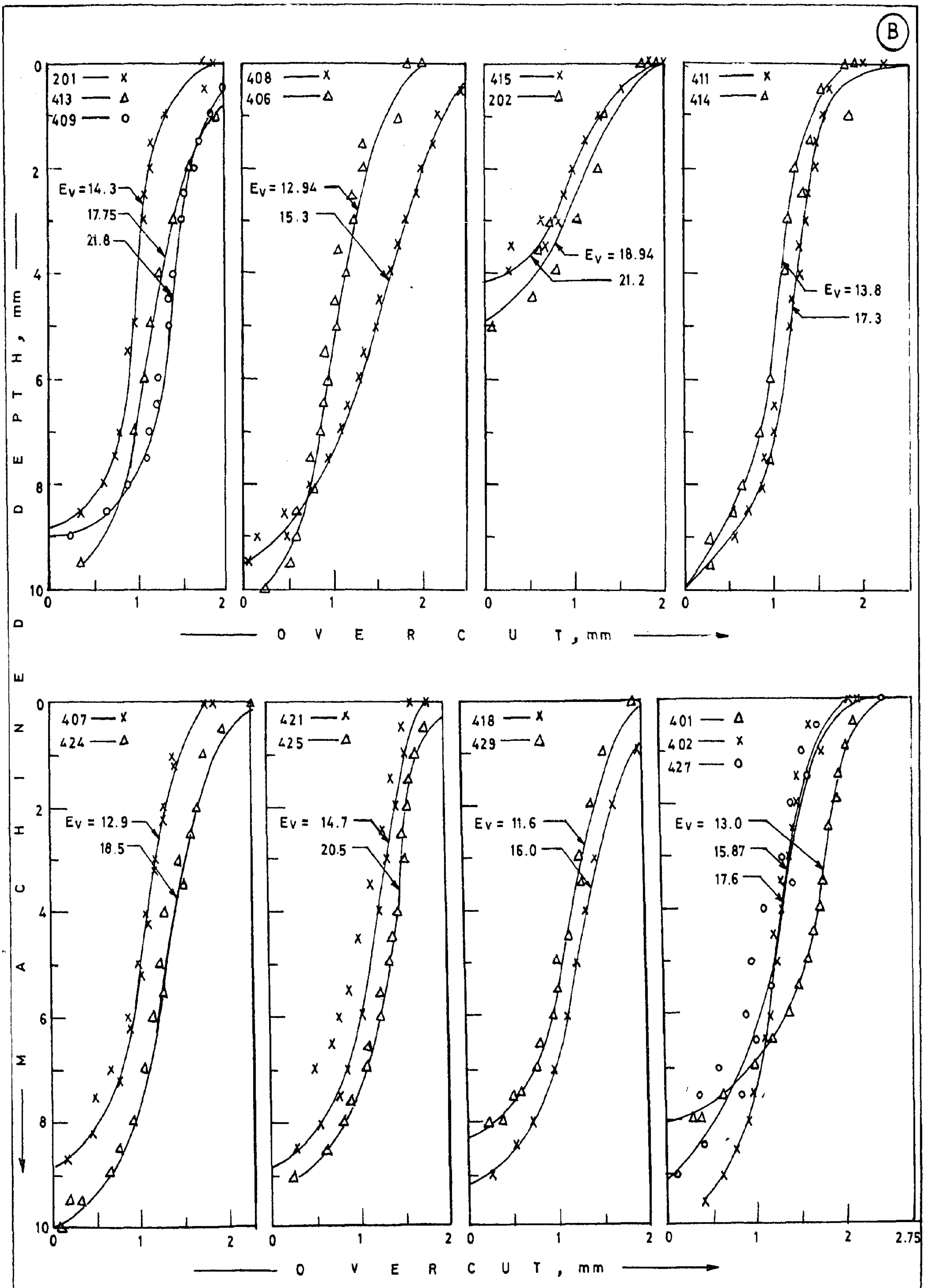

FIG. 7.15 EFFECT OF VOLTAGE ON ANODE PROFILES (WORK MATERIAL:— CAST LOW ALLOY STEEL)

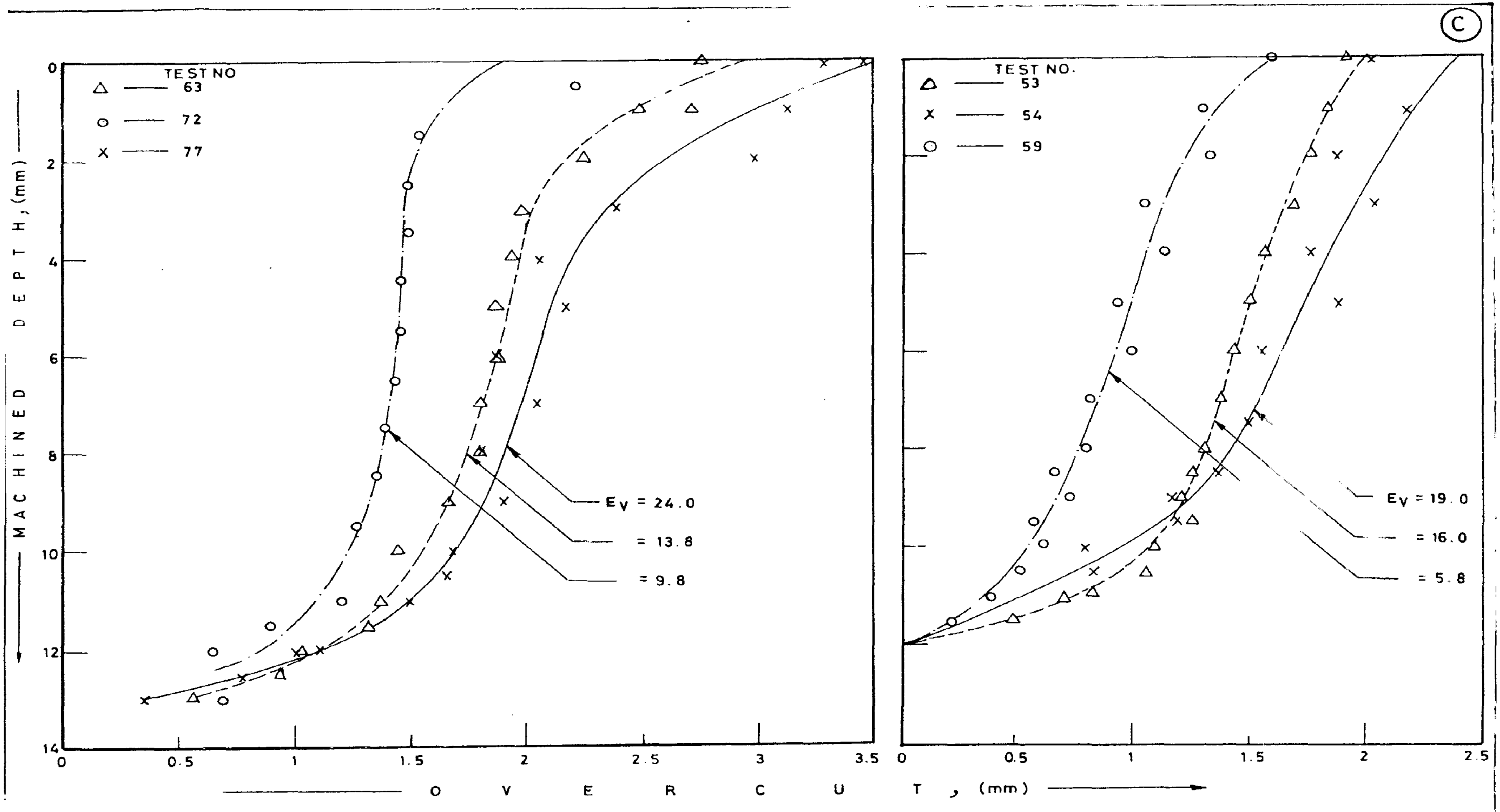

FIG. 7.15 EFFECT OF EFFECTIVE VOLTAGE ON ANODE PROFILE (WORK MAT.-MILD STEEL)

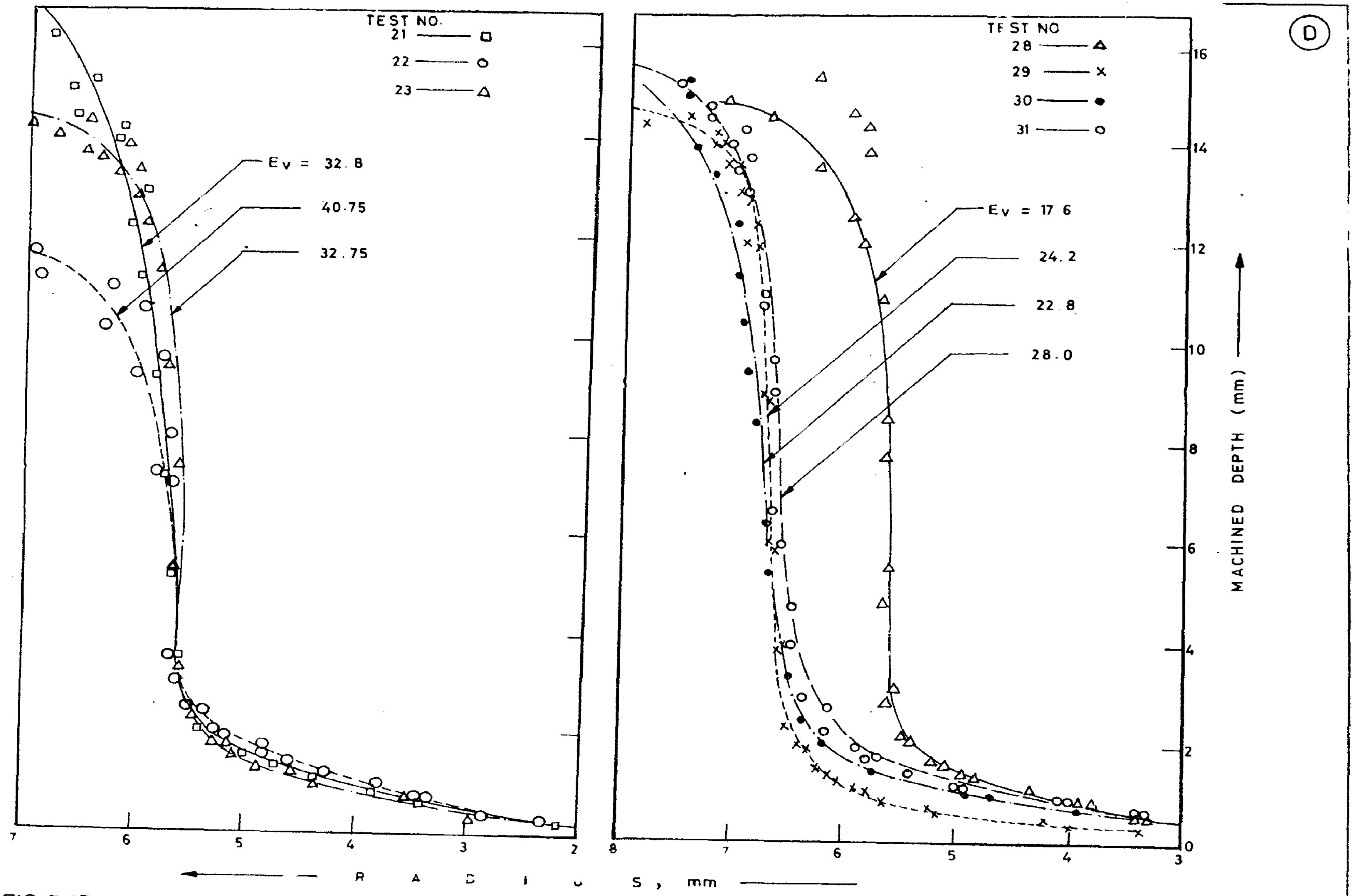

FIG. 7.15 EFFECT OF EFFECTIVE VOLTAGE ON ANODE PROFILE DURING E C D OF MILD STEEL

7.3.2 Effect of Tool-Diameter

The effect of tool diameter on overcut in ECM was also studied. For this purpose the effective voltage and other conditions were held constant whereas, the tool diameter was varied. The results are given in Fig. (7.16).

7.3.3 Machining Efficiency

To study of the effect of voltage on machining efficiency for otherwise similar machining conditions, the machining efficiency has been calculated from the following relationship.

$$\eta = \frac{m_a}{m_t} \qquad .. \qquad (7.2)$$

It is also to be noted that in few of the cases machining efficiency has crossed the threshold limit of 100% (Table 12 and Table 13).

7.3.4 Comparison of Experimental and Analytical Anode Profile

Using the model SGFET-11, the anode profile for different cases has been obtained (Fig. 7.17) assuming constant valency of EC dissolution of the anode and taking a mean value for the efficiency of machining. The value of α_v has also been assumed to be zero. It has also been assumed that the feed rate in the side gap is zero (i.e., F_s=0). But after the ECM starts, in case of bare tools or bare land width (b_b) with coated toolbit, the anode surface in side zone obtained

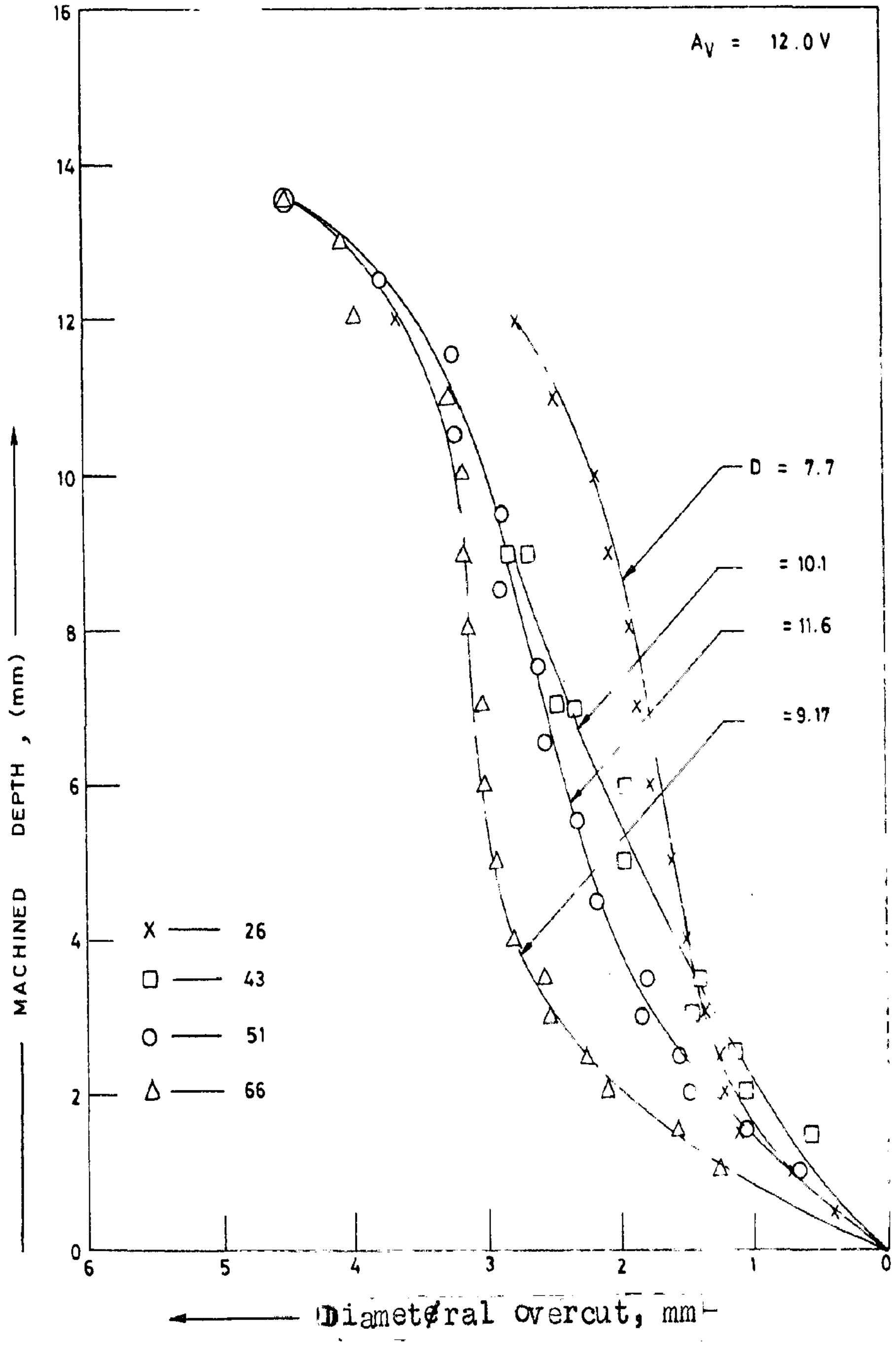

FIG. 7.16 EFFECT OF TOOL DIAMETER ON ANODE PROFILE

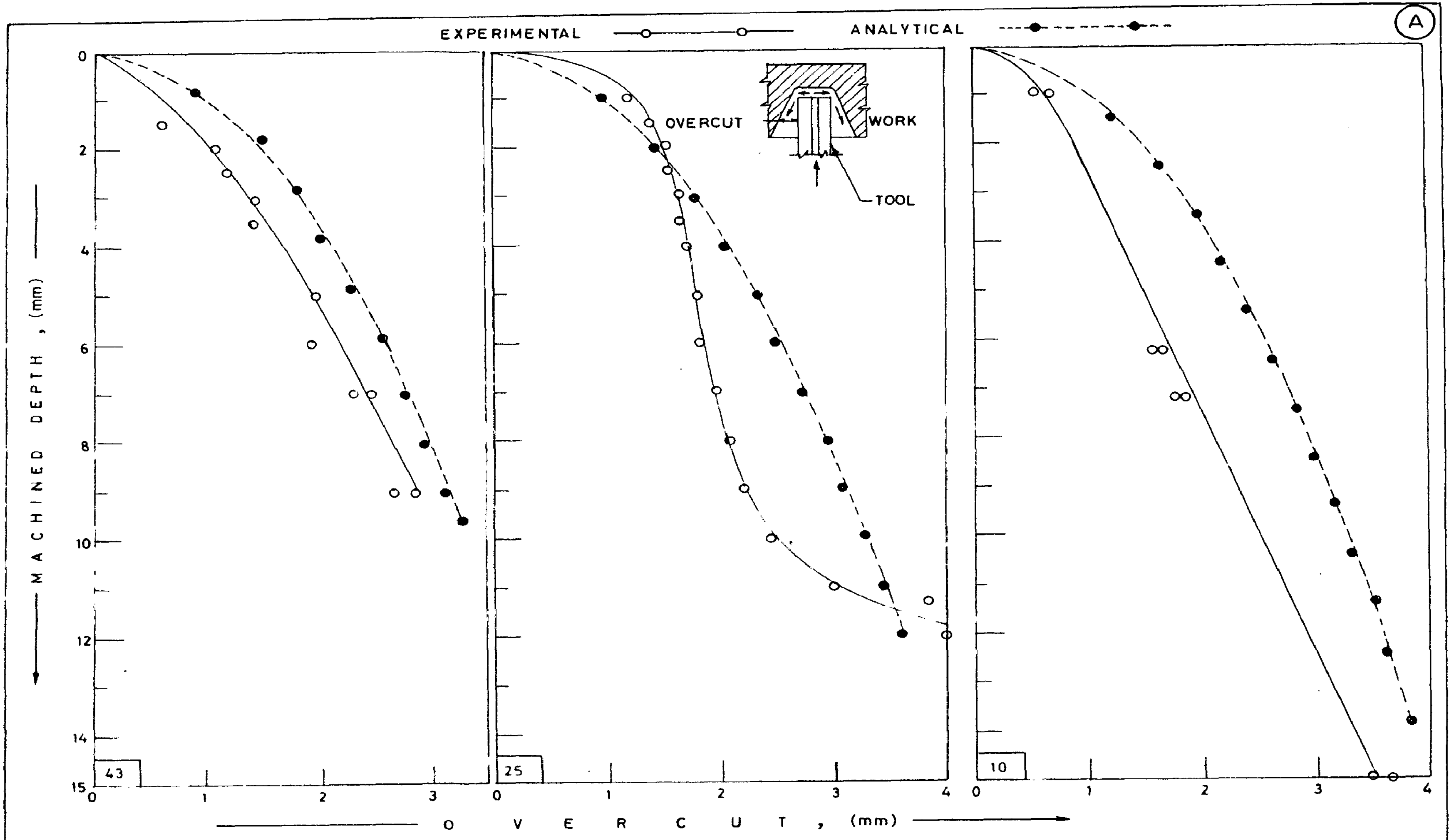

FIG. 7.17 COMPARISON OF ANALYTICAL (SGFET-11) AND EXPERIMENTAL ANODE PROFILES
(WORK MAT. – MILD STEEL)

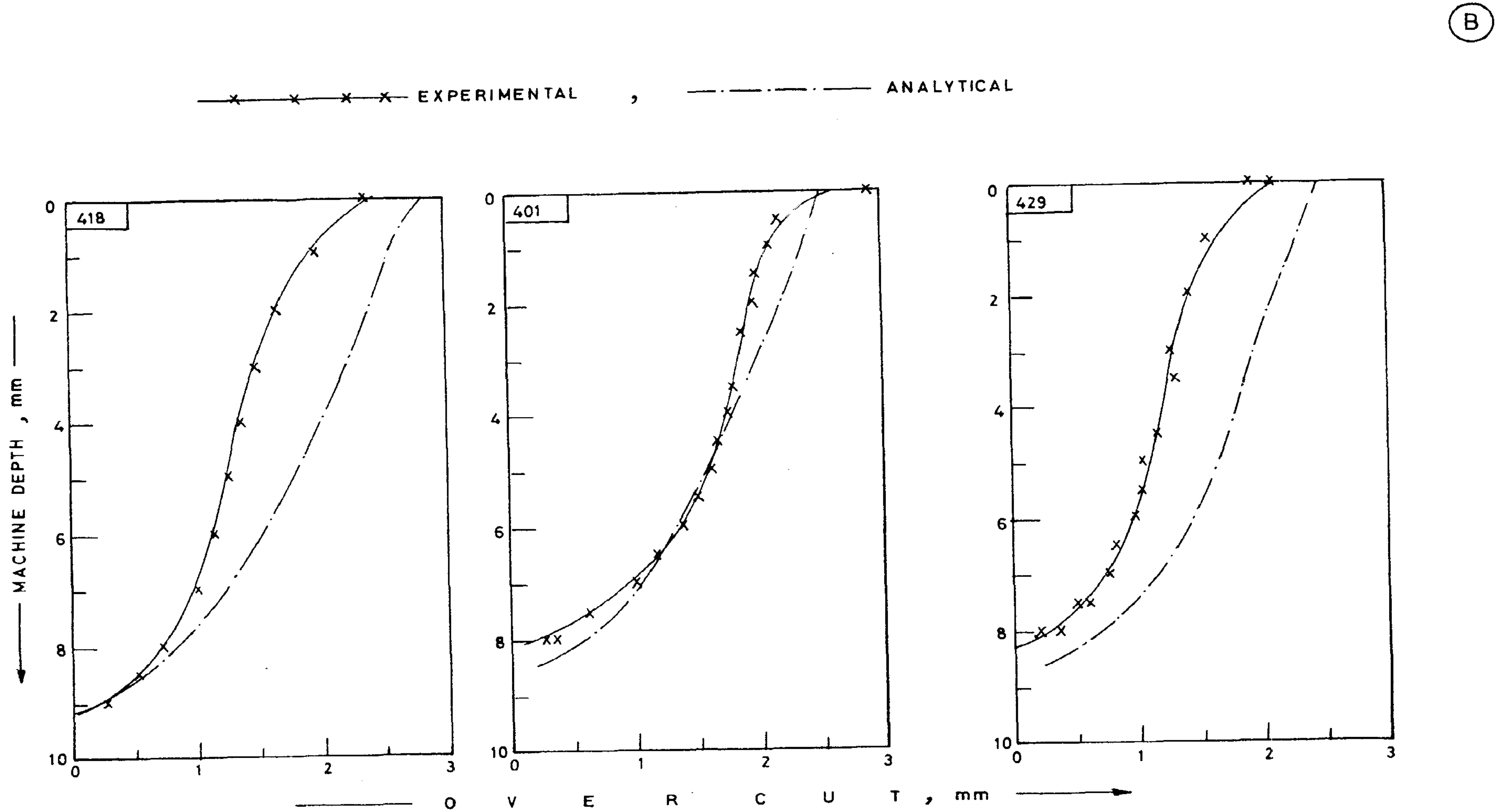

FIG. 7.17 COMPARISON BETWEEN ANALYTICAL (SGFET-11) AND EXPERIMENTAL ANODE PROFILES (WORK MAT:- CAST LOW ALLOY STEEL)

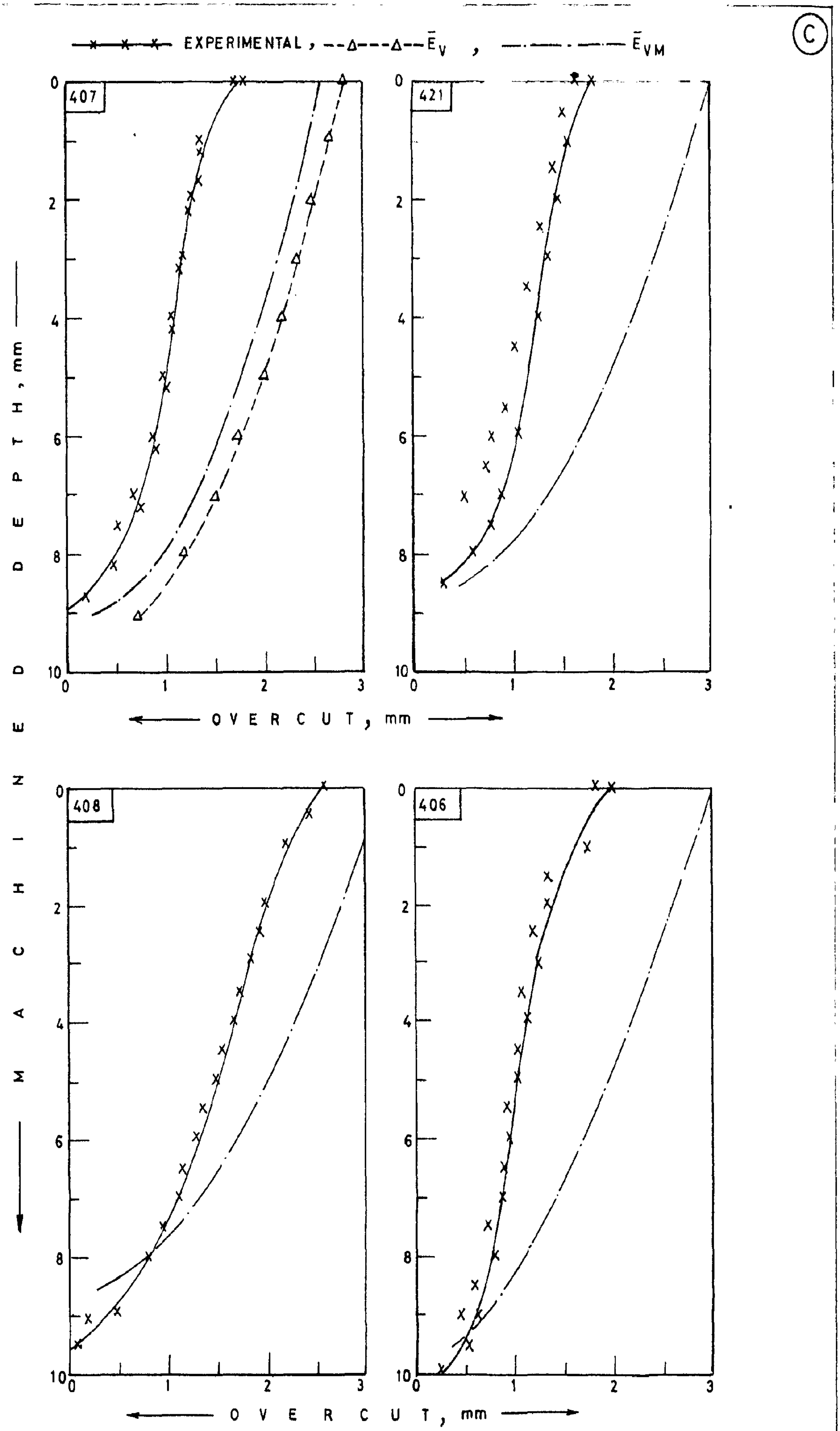

FIG. 7.17 COMPARISON BETWEEN ANALYTICAL (SGFET-11) AND EXPERIMENTAL ANODE PROFILES (WORK MAT. – CAST LOW ALLOY STEEL)

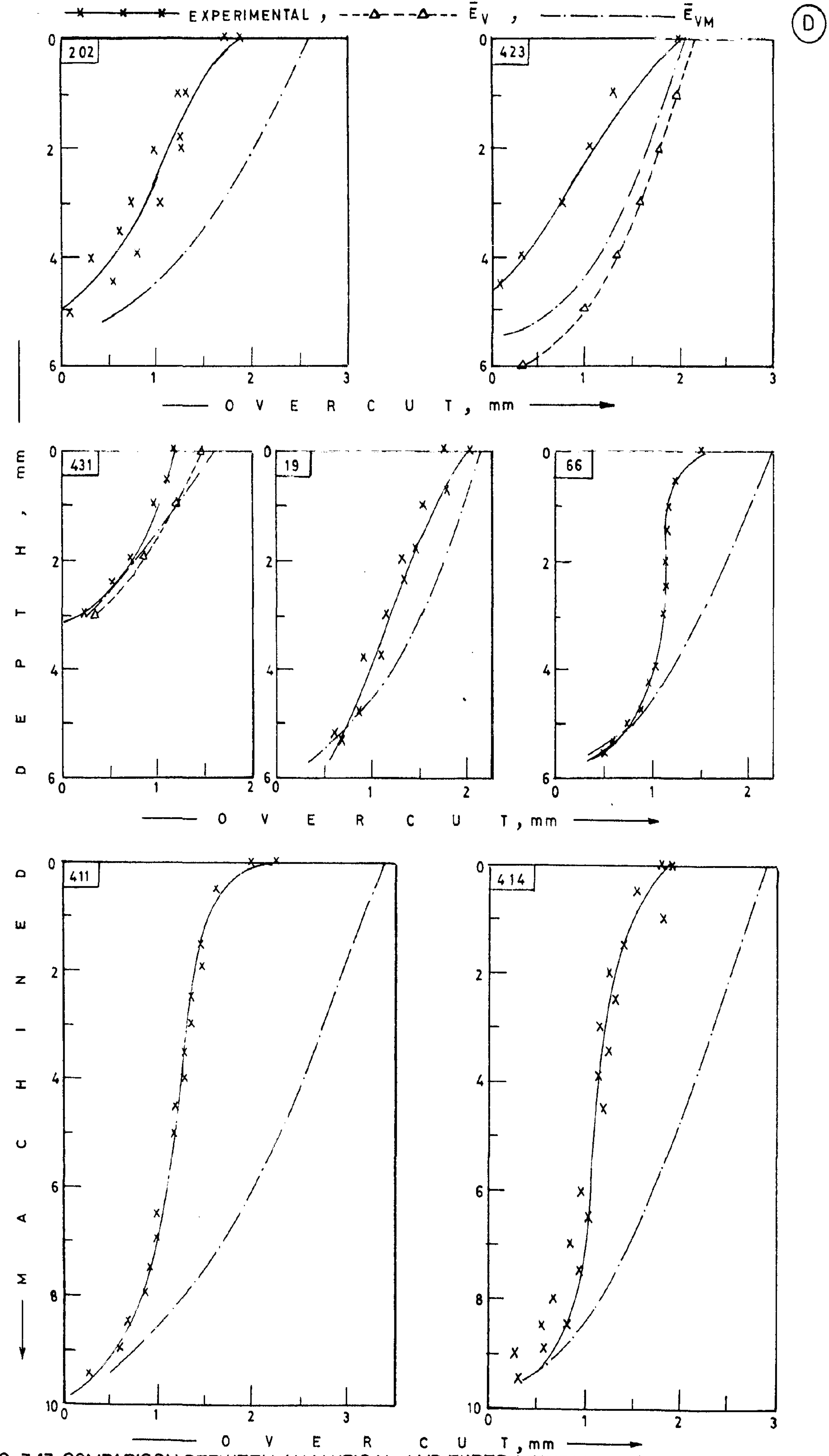

FIG. 7.17 COMPARISON BETWEEN ANALYTICAL AND EXPERIMENTAL ANODE PROFILES

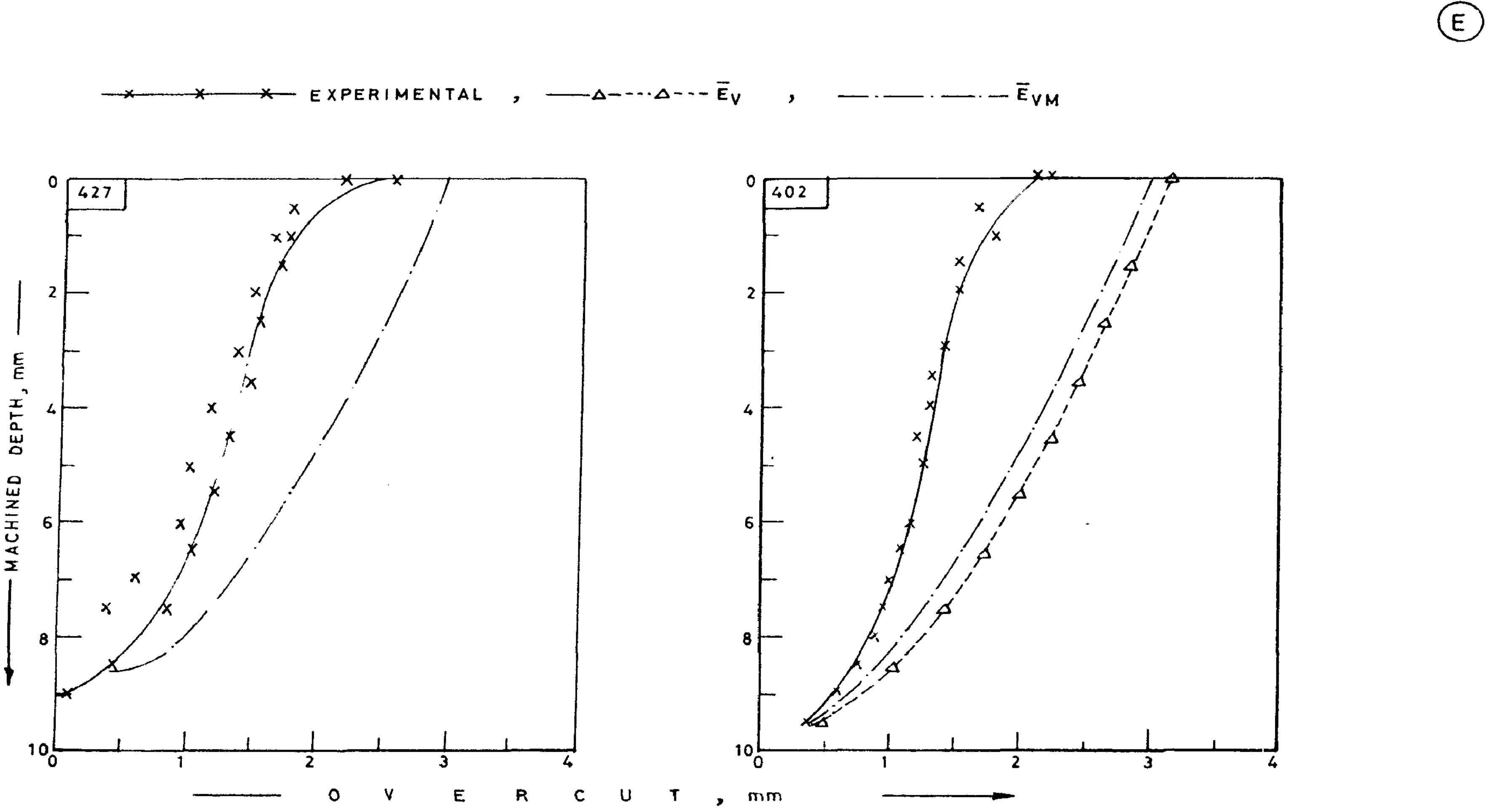

FIG. 7.17 COMPARISON BETWEEN ANALYTICAL (SGFET-11) AND EXPERIMENTAL ANODE PROFILES (WORK MAT. - CAST LOW ALLOY STEEL)

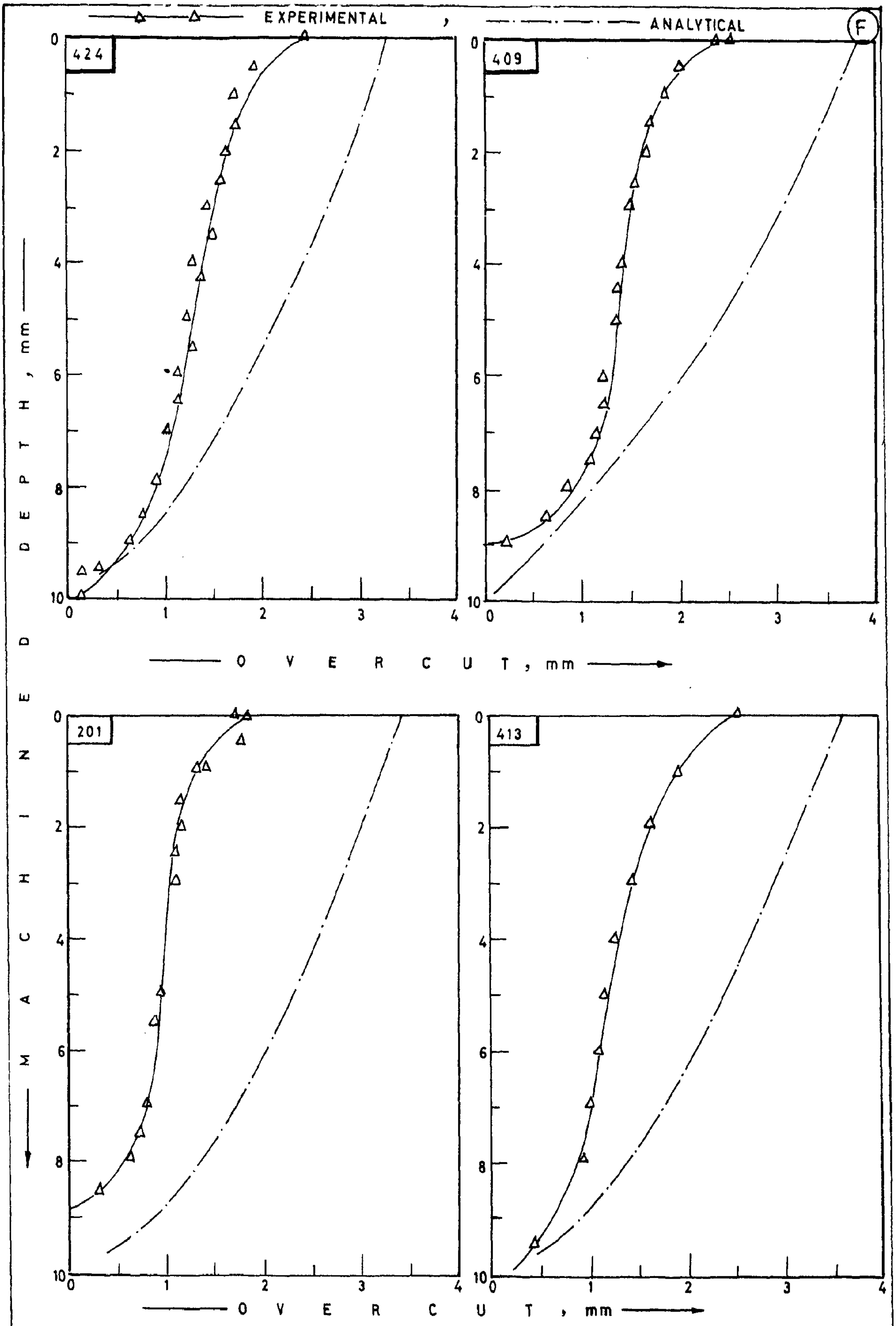

FIG. 7.17 COMPARISON BETWEEN ANALYTICAL (SGFET-11) AND EXPERIMENTAL ANODE PROFILES (WORK MAT.—CAST LOW ALLOY STEEL)

will be inclined at an angle to the feed direction. Hence, a component of feed will be acting on the work in the side zone that means $F_s \neq 0$ condition exists.

7.3.5 Experimental Observations

Plaster of paris replicas of drilled holes were prepared. In few cases, the hole shapes were distorted and some of representative magnified photographs of these are shown in Fig. 7.18. The conditions that led to the production of distorted holes are stated in the appropriate tables. This is caused mainly due to the effect of electrolyte flow velocity specially in case of outward mode of flow. Fig. 7.19 shows that top face views of some of the EC drilled holes.

7.3.6 Overcut in Transition Zone in ECD

Overcut in transition zone during ECD has been measured from the replica of the drilled hole. The equilibrium gap, Y_e was evaluated corresponding to the effective voltage using Eq(2.5). Fig.(7.20) shows the relationship between overcut, a_o and equilibrium gap, Y_e. In some cases, a scatter between line of best fit (obtained by applying regression analysis technique) and experimental values was observed. Therefore, for improving the degree of correlation, dimensional analysis (Appendix-III) was conducted. Fig. 7.21 shows the nature of relationship between the dimensionless parameters π_1 and π_2. But coefficient of correlation found was low. It was, however,

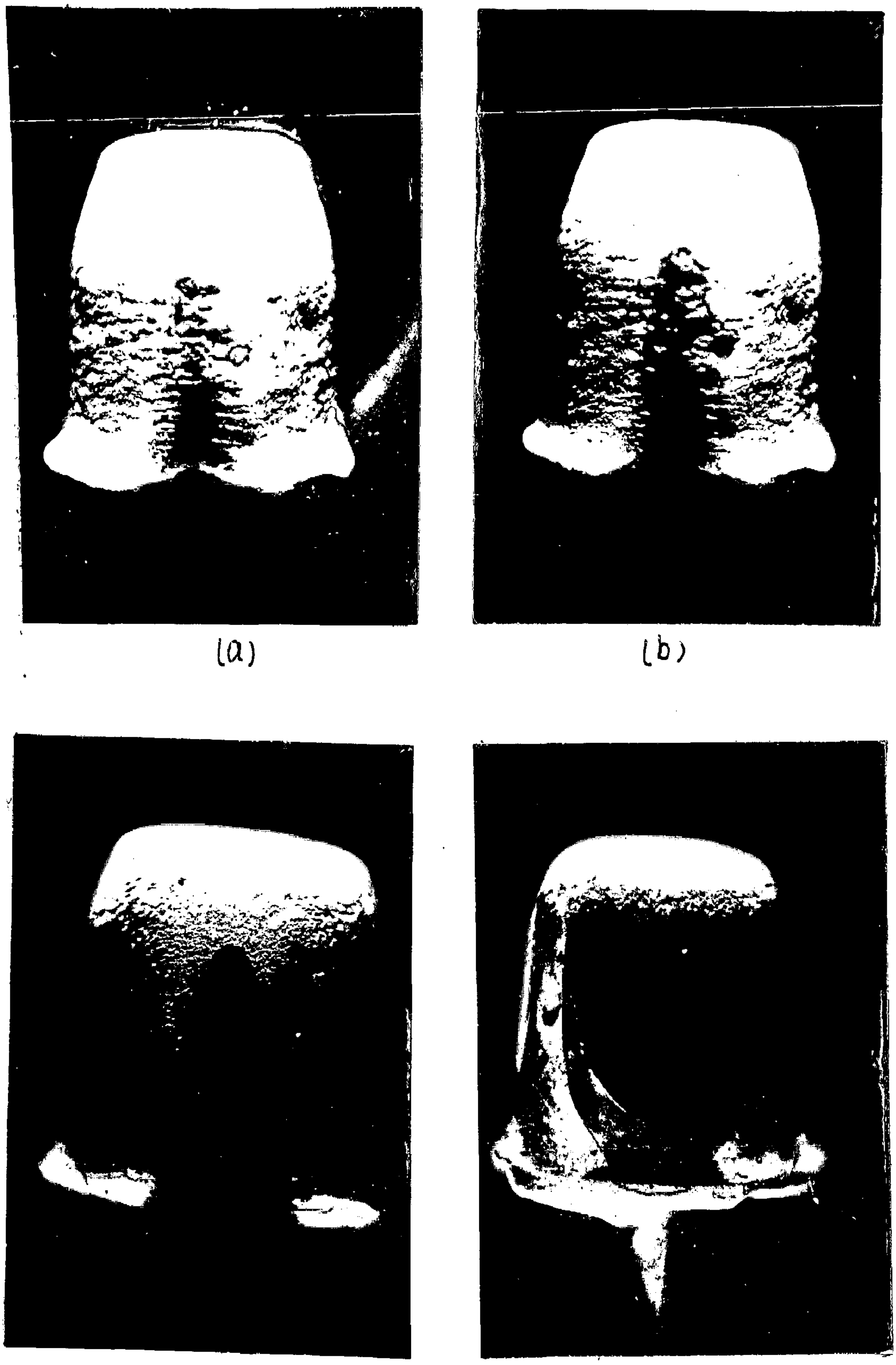

(a) (b)

(c) (d)

Fig.7.18: EC drilled hole-replicas. (X13). Test pieces - series numbers (a) 52 (b) 57 (c) 58 (d) 77

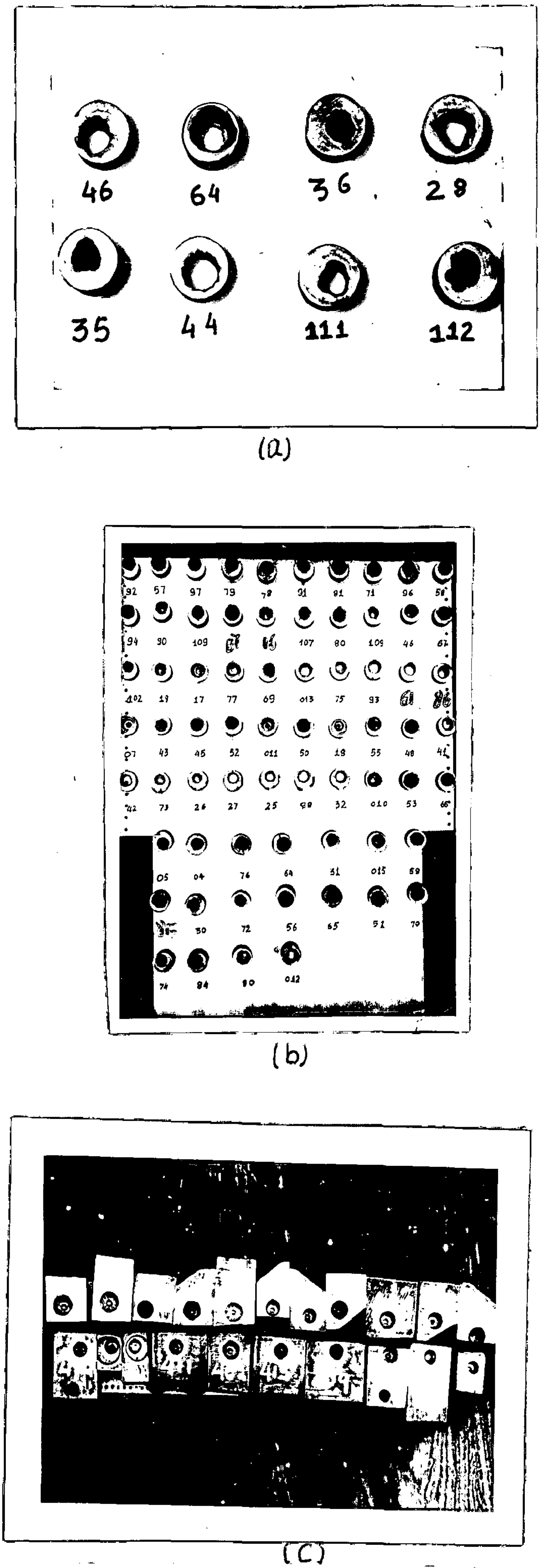
46
64
36
28
35
44
111
112
(a)
(b)
(c)

Fig.7.19: Top face views of EC drilled holes
(a) Mild steel (b) Mild Steel (c) Low Alloy Steel

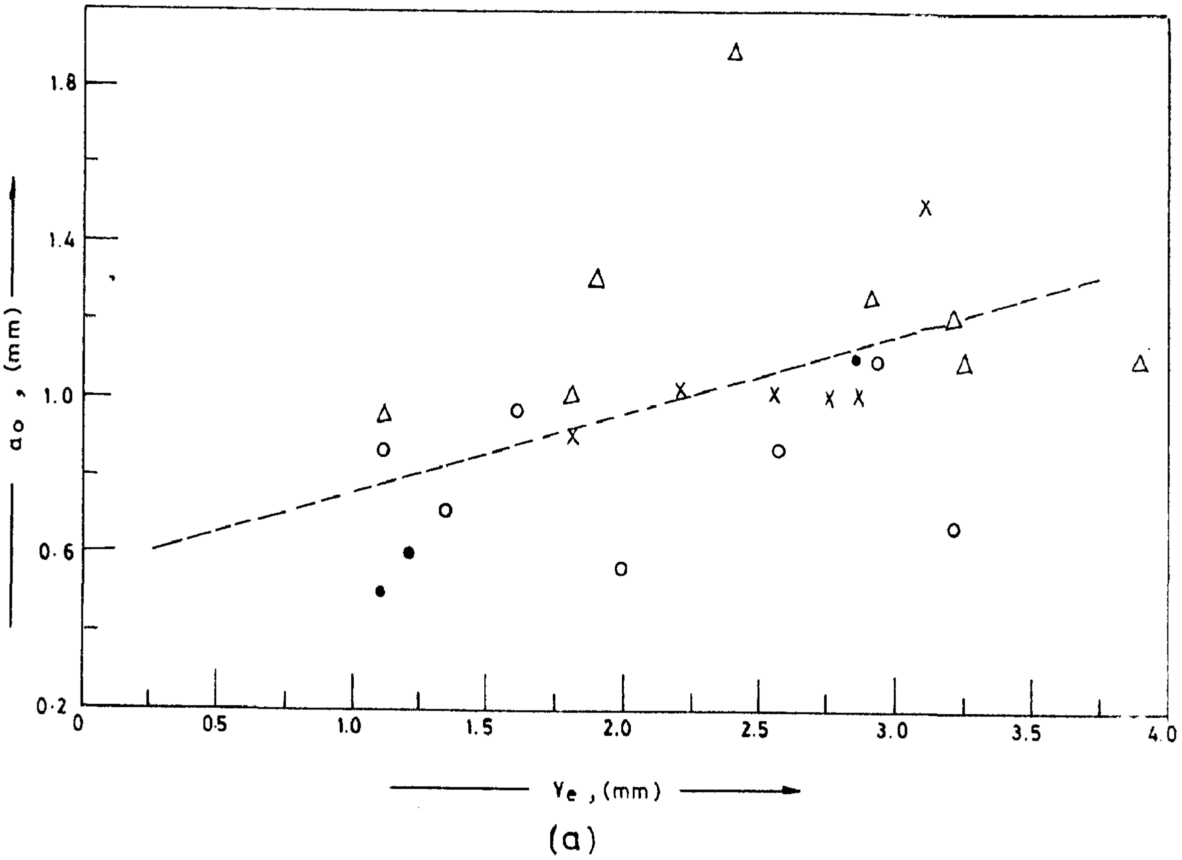

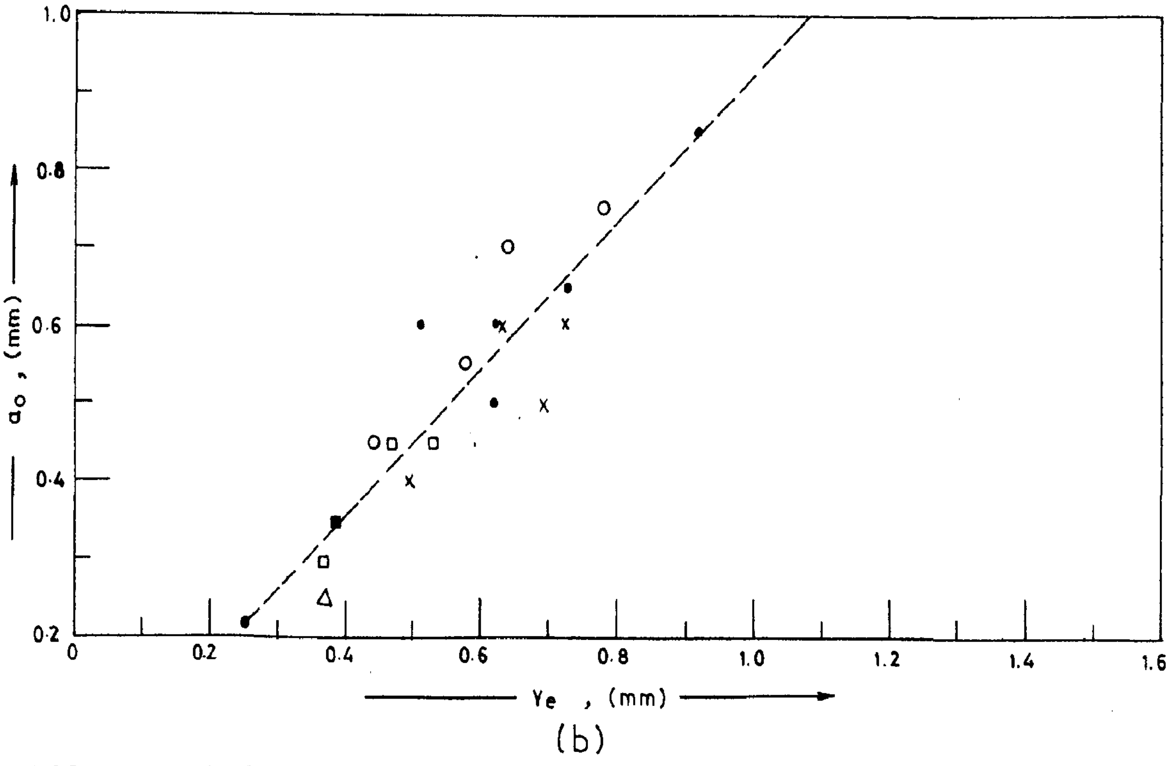

FIG. 7.20 RELATIONSHIP BETWEEN EQUILIBRIUM GAP (Ye) AND OVERCUT IN TRANSITION ZONE DURING ECD OF (a) MILD STEEL (b) CAST LOW ALLOY STEEL

found (Fig. 7.22) that tool diameter has got its independent influence on a_o. Later on, a relationship between D and C_d' was established through Fig.7.22. Finally the Eq(3.5) was obtained in the final form. This gives a better fit as shown in Fig. 7.22D. Based on Fig. 7.22 the values of constants C_d, n_1 and n_2 have been derived.

7.4 ELECTROCHEMICAL DRILLING WITH BARE TOOL USING "DESIGN OF EXPERIMENT" TECHNIQUE

To study the effects of machining parameters on metal removal rate and their interactions, ECD tests with bare tools were conducted in accordance with the details given in section 6.3.4 and experimental plan given in Table 6&7. This could help in evaluating the constants of a response surface equation (6.6) which can be used to predict the rate of metal removal.

7.5 ELECTROCHEMICAL WIRE CUTTING PROCESS (ECWCP)

A parametric study of ECWCP using rectangular wires has been made with a view to obtain a clear understanding of the process. Results have been computed by three different methods. Model-1 is based on the application of classical ECM theory, model-2 by the use of resistances in parallel model and model-3 based on finite elements technique (FET-1). The results have been computed for two different conditions viz., zero feed rate and finite feed rate. For the model FET-1, Fig. 7.23 shows the scheme of discretization for a 30 mm long wire.

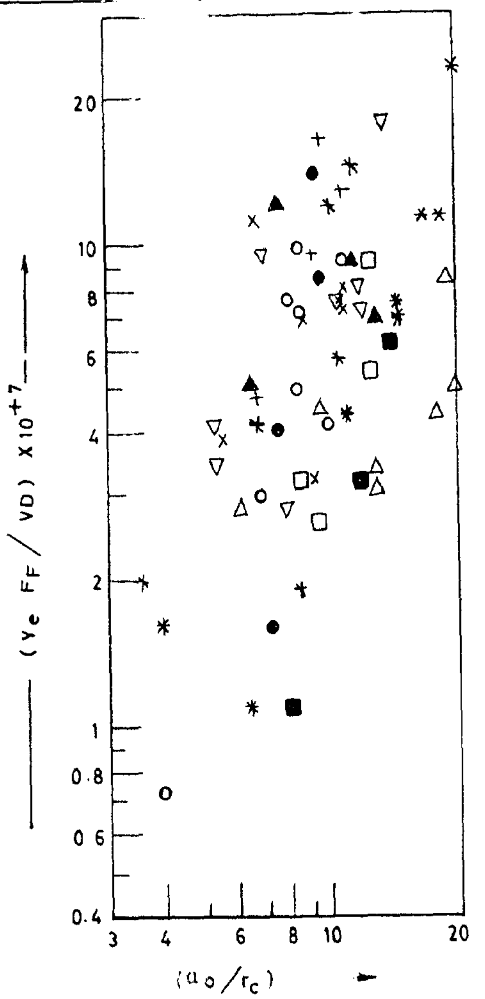

FIG.7.21 RELATIONSHIP BETWEEN TWO DIMENSIONLESS QUANTITIES

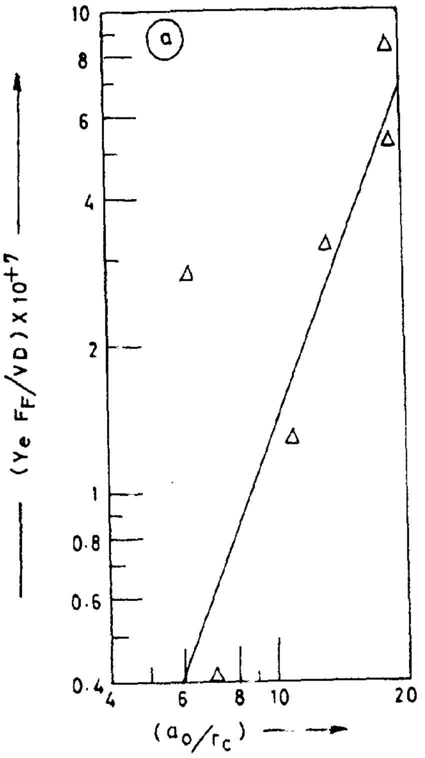

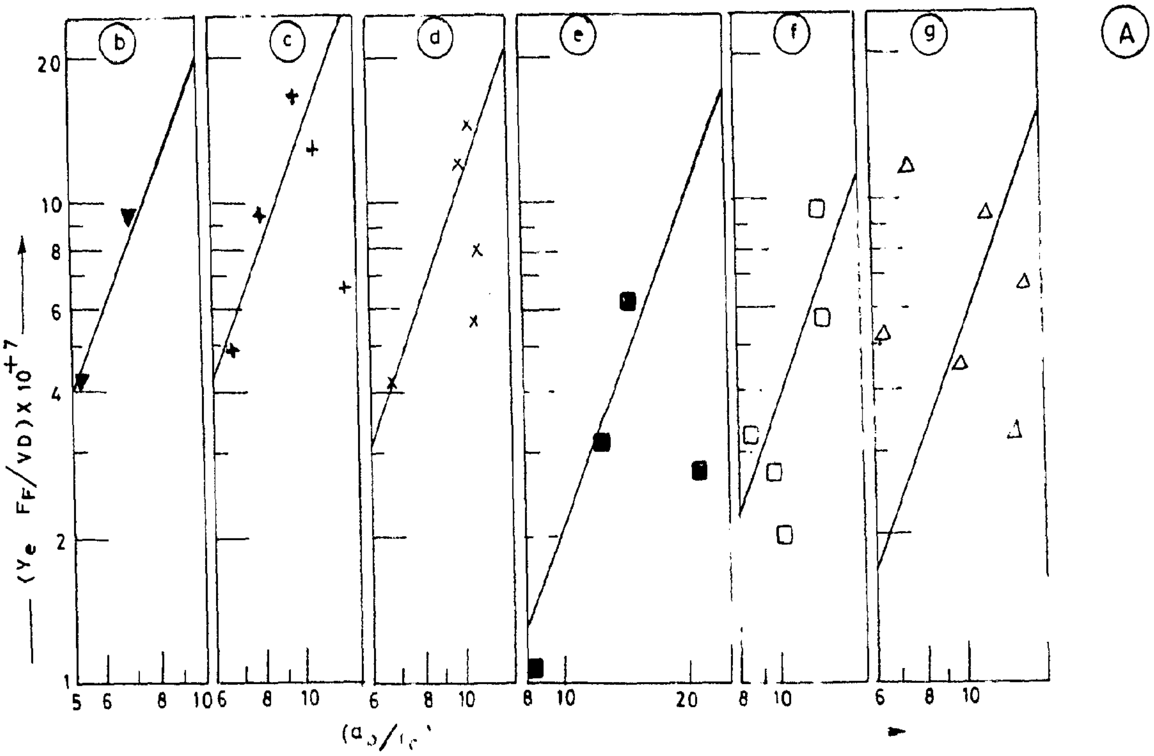

FIG.7.22 RELATIONSHIP BETWEEN TWO DIMENSIONLESS QUANTITIES IN (EQN. A.5)
(a) TEST GROUP VIII (b) XII (c) V (d) IV (e) X (f) IX (g) VII
(SEE TABLE 12)

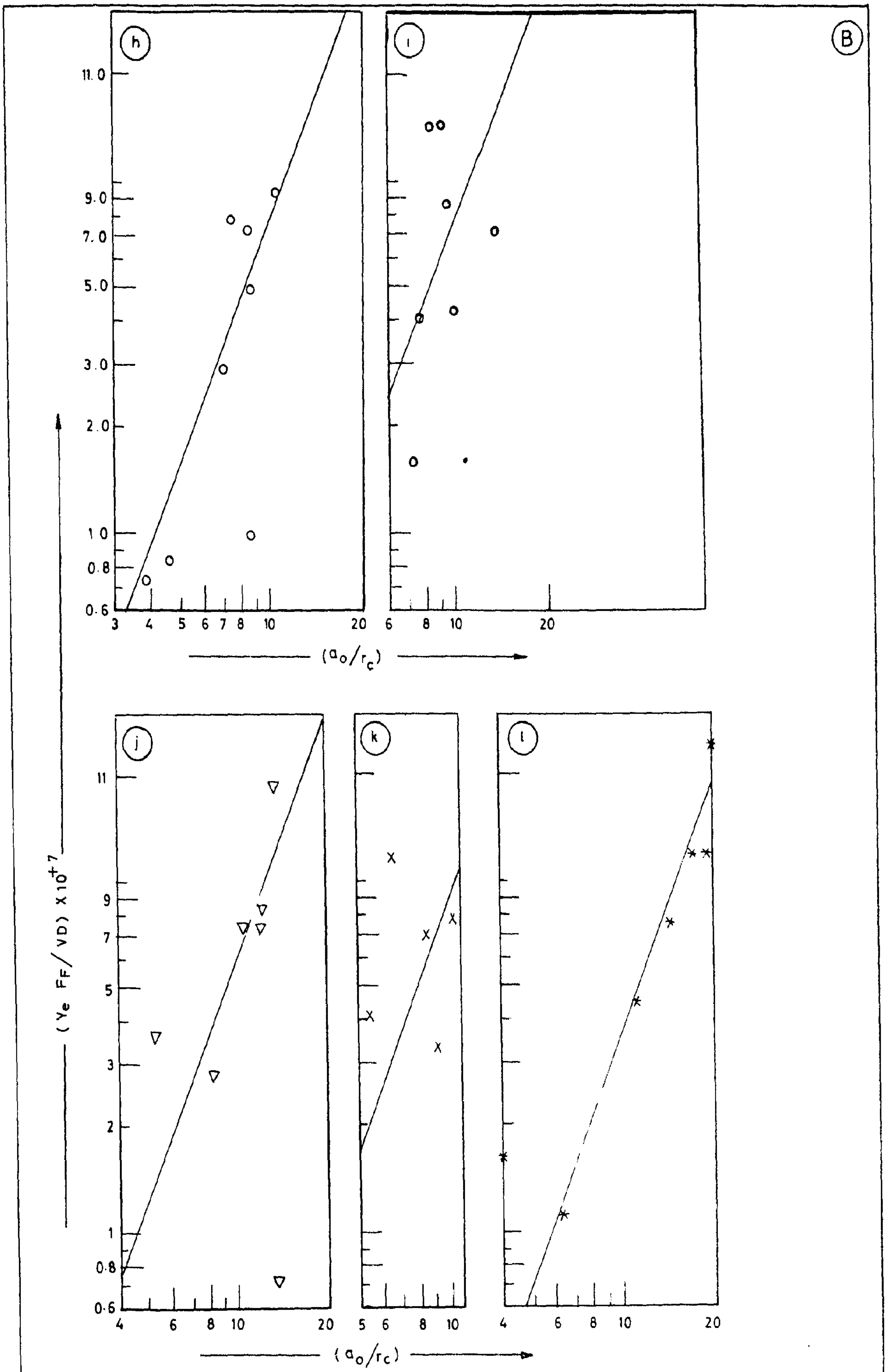

FIG.7.22 RELATIONSHIP BETWEEN TWO DIMENSIONLESS QUANTITIES FOR TEST GROUPS (h) I (i) II (j) XI (k) III AND (l) VI (SEE TABLE 12)

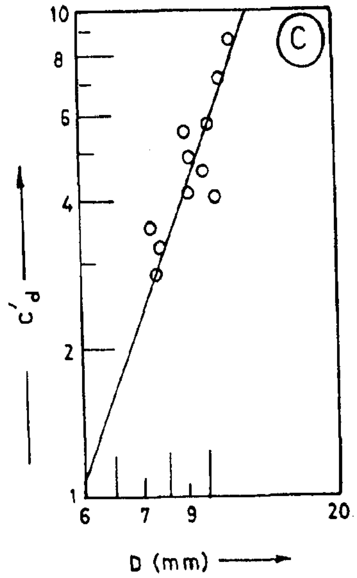

FIG.7.22 RELATIONSHIP BETWEEN TOOL DIAMETER D AND A CONSTANT C'd (EQN. A.7)

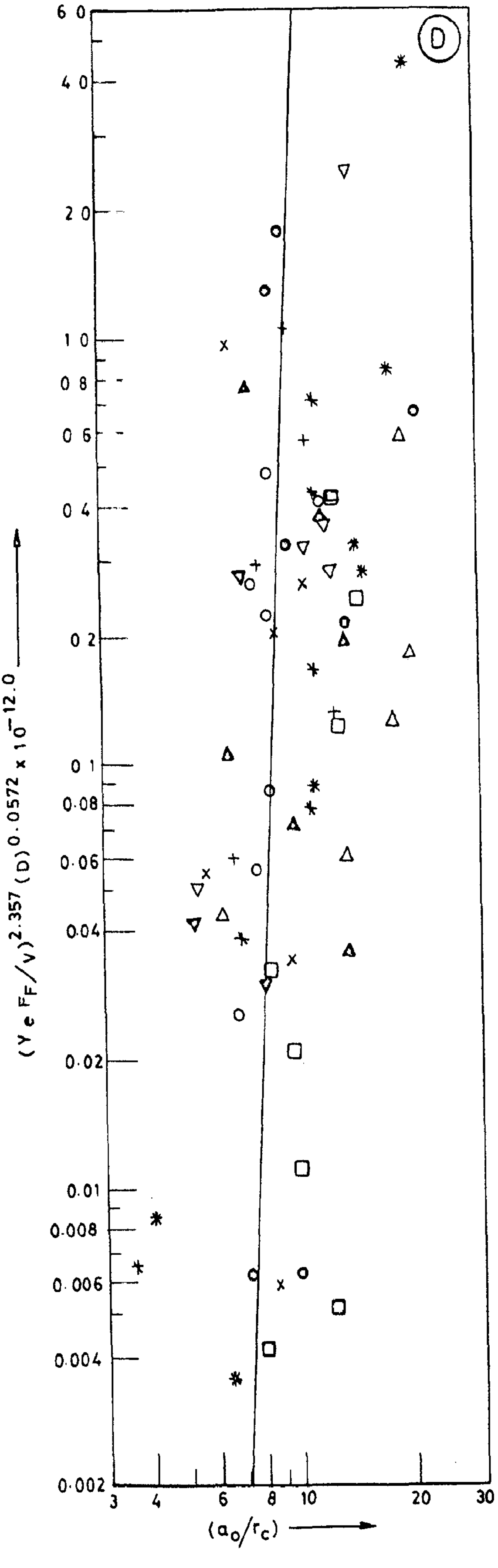

FIG.7.22 RELATIONSHIP BETWEEN (a_o/r_c) AND $(Y_e F_F/V)^{n_1}(D)^{n_2}$ [EQN.A.8]

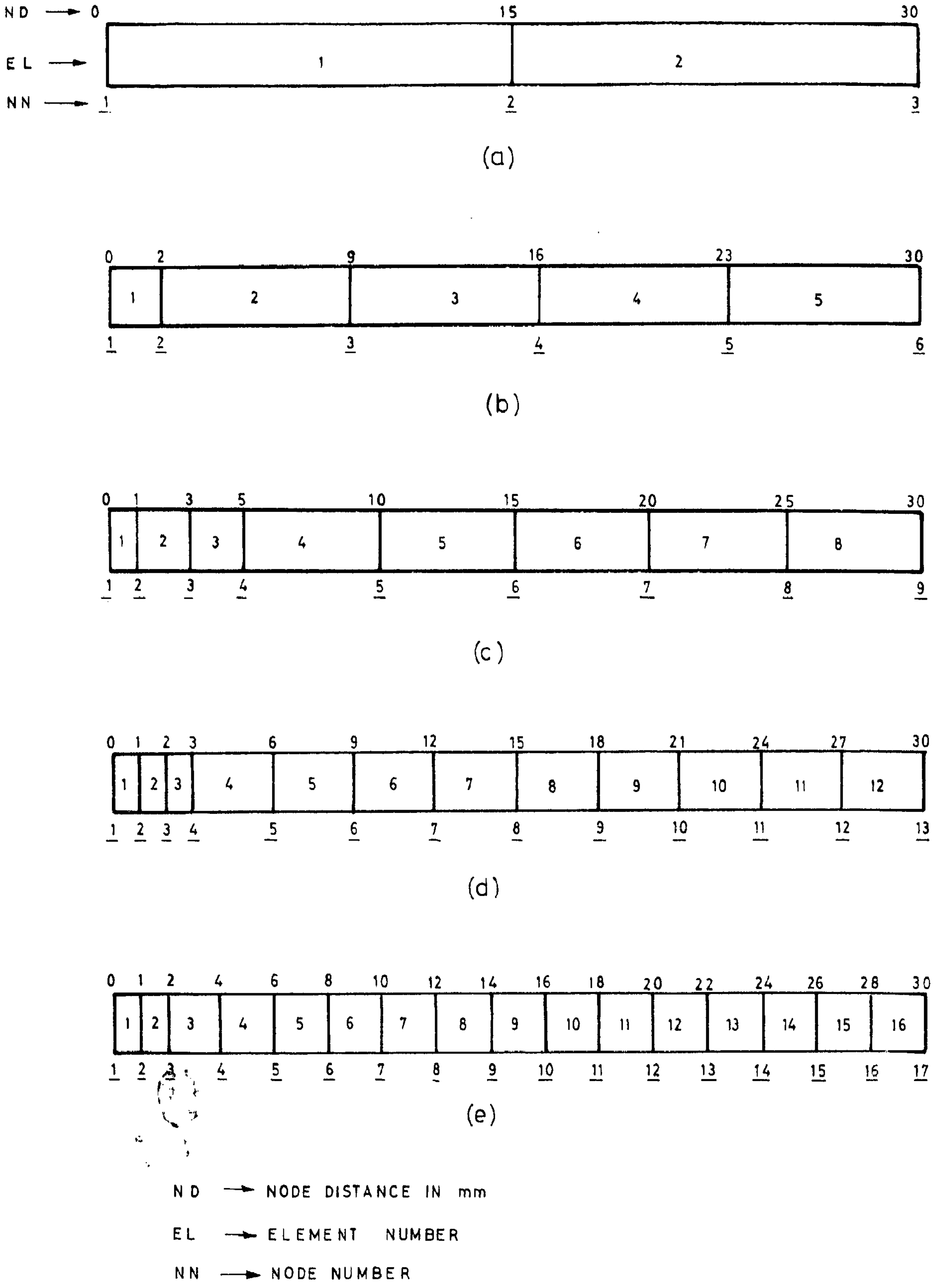
ND → 0 15 30
EL → 1 2
NN → 1 2 3
(a)
0 2 9 16 23 30
1 2 3 4 5
1 2 3 4 5 6
(b)
0 1 3 5 10 15 20 25 30
1 2 3 4 5 6 7 8
1 2 3 4 5 6 7 8 9
(c)
0 1 2 3 6 9 12 15 18 21 24 27 30
1 2 3 4 5 6 7 8 9 10 11 12
1 2 3 4 5 6 7 8 9 10 11 12 13
(d)
0 1 2 4 6 8 10 12 14 16 18 20 22 24 26 28 30
1 2 3 4 5 6 7 8 9 10 11 12 13 14 15 16
1 2 3 4 5 6 7 8 9 10 11 12 13 14 15 16 17
(e)
ND → NODE DISTANCE IN mm
EL → ELEMENT NUMBER
NN → NODE NUMBER

FIG.7.23 INTERELECTRODE GAP DISCRETIZATION SCHEME

7.5.1 Zero Feed Rate ($F_F=0$)

Fig. 7.24 shows the temperature distribution within the electrolyte along the wire and change in electrolyte temperature at different nodes with machining time. It (Fig.7.24A) also shows a comparison between the temperatures obtained by model-1, model-2 and FET-1. Fig. 7.25A gives the change in electrolyte conductivity with flow distance whereas, Fig. 7.25B shows the change in electrolyte conductivity with machining time. The variation in current density, J, within IEG with machining time are given in Fig. 7.26. Fig.7.27 shows the variation in metal removal rate with machining time at different nodes and elements.

7.5.2 Finite Feed Rate ($F_F \neq 0$)

Figs (7.28) to (7.30) show the analytical results obtained for the EC wire cutting with the finite feed rate. Results have been computed assuming computational cycle time of $\Delta t=1$ second because it has also been found that the accuracy of the results is dependent upon the computational time interval Δt.

7.6 ELECTROCHEMICAL DRILLING WITH BARE TOOL-BITS

These experiments were conducted to know the nature of anode profile obtained by using tool bits having a finite corner radii and a sharp corner. The results are shown in Fig. 7.31 and the machining conditions are given in Table-14.

Ⓐ

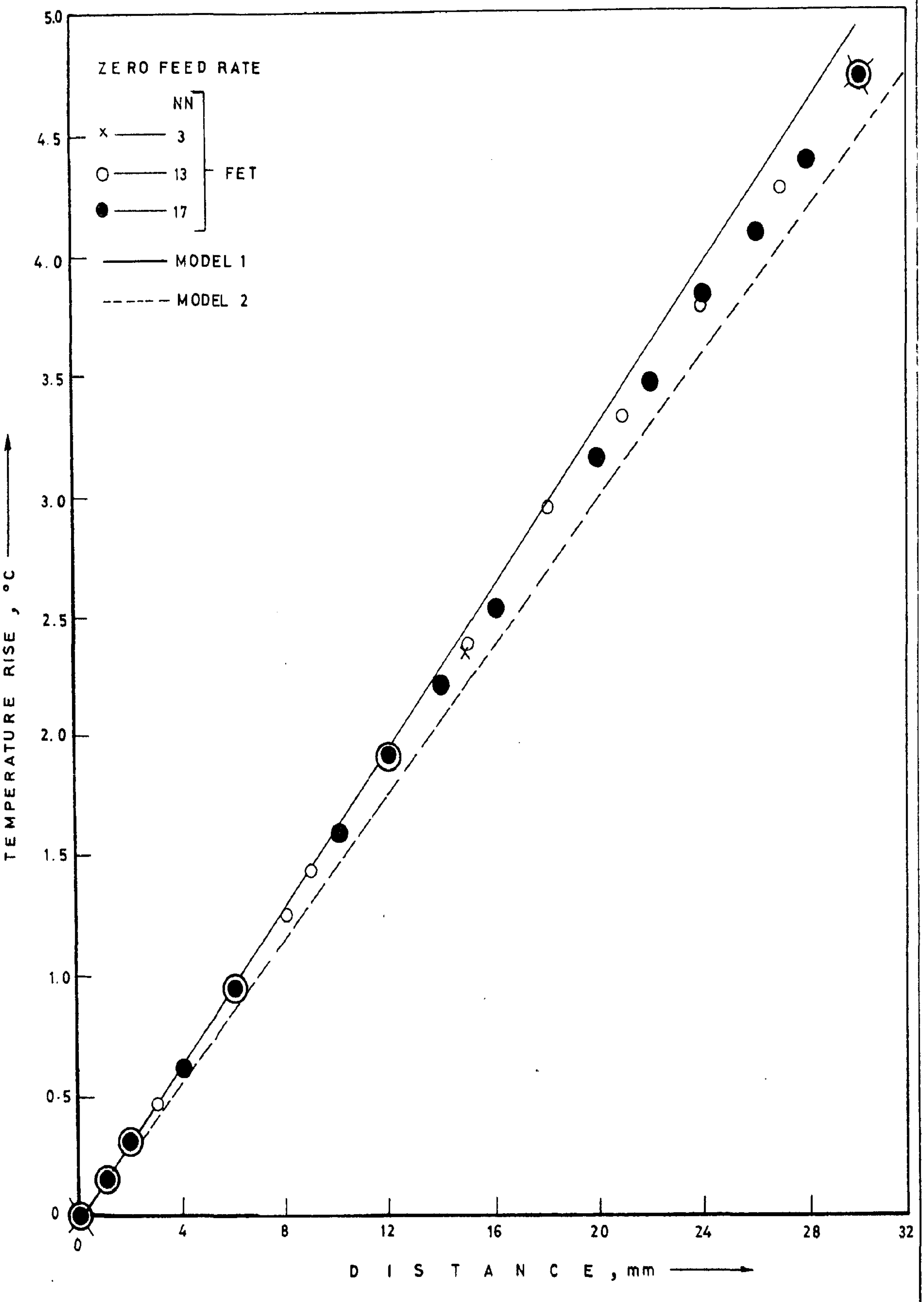

FIG. 7.24 COMPARISON OF RESULTS OBTAINED FROM MODEL-1, MODEL-2 AND FET-1

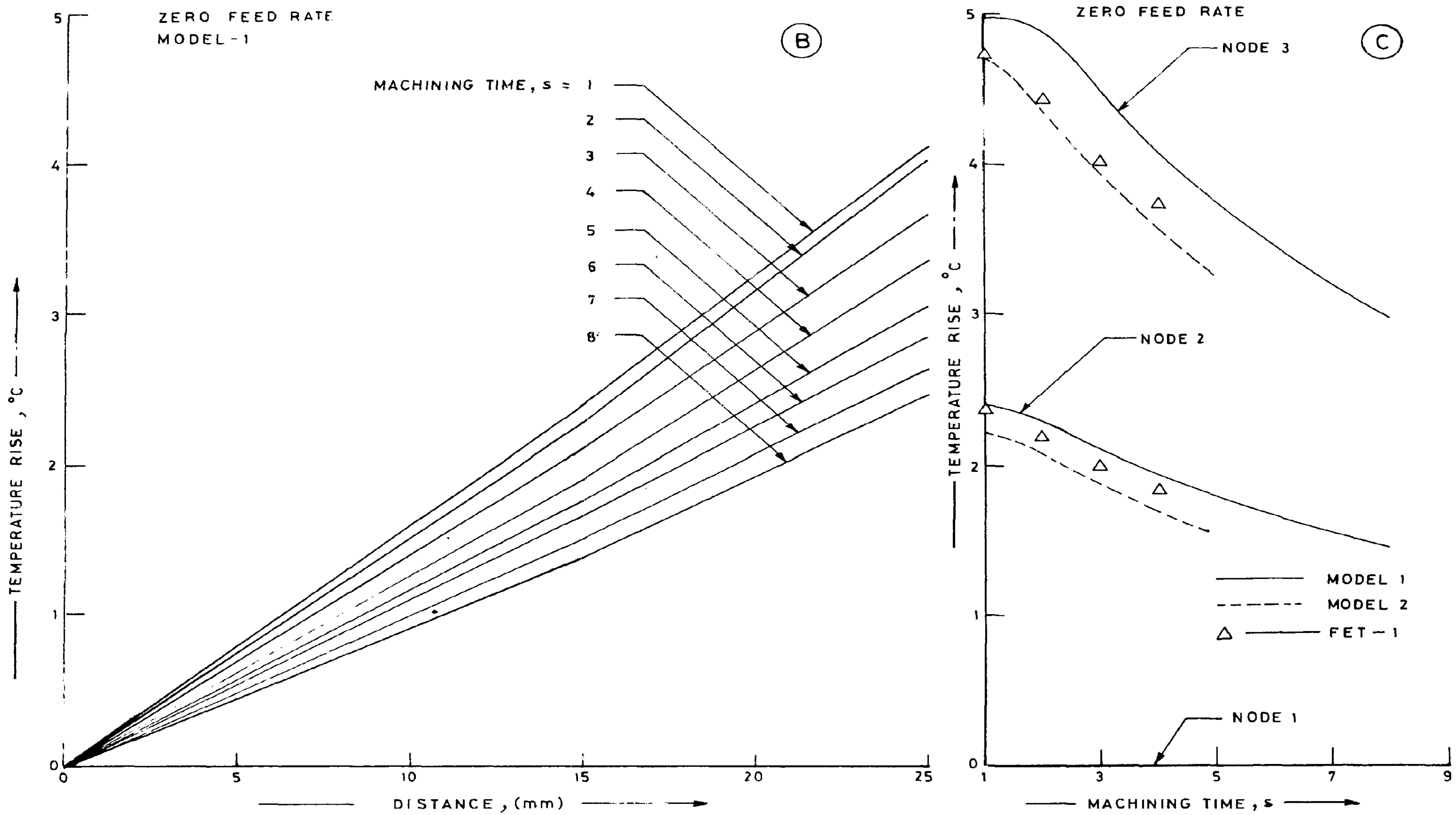

FIG. 7.24 EFFECT OF DISTANCE & MACHINING TIME ON TEMPERATURE RISE

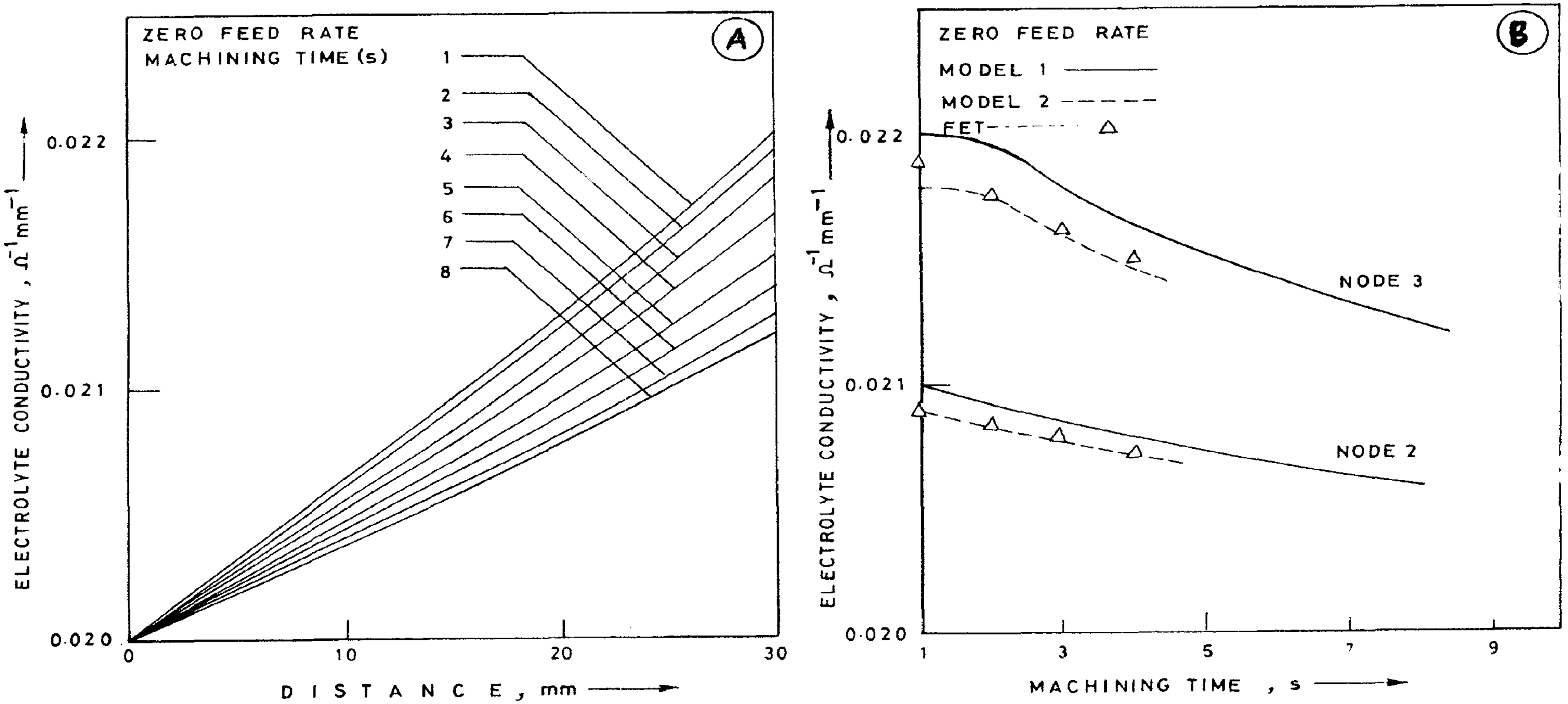

FIG. 7.25 EFFECT OF FLOW DISTANCE OR MACHINING TIME ON ELECTROLYTE CONDUCTIVITY

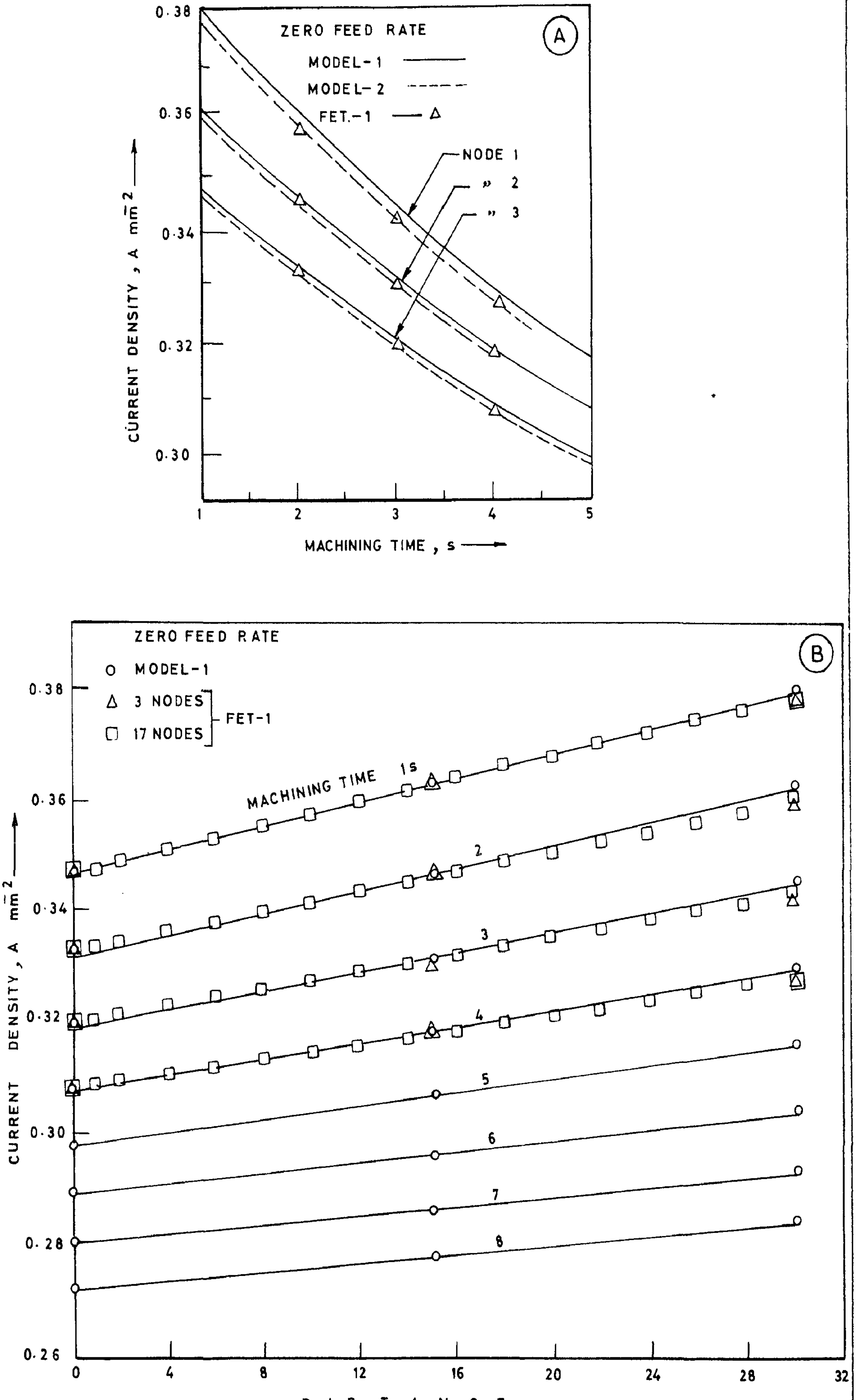

FIG. 7.26 EFFECT OF FLOW DISTANCE, MACHINING TIME ON CURRENT DENSITY

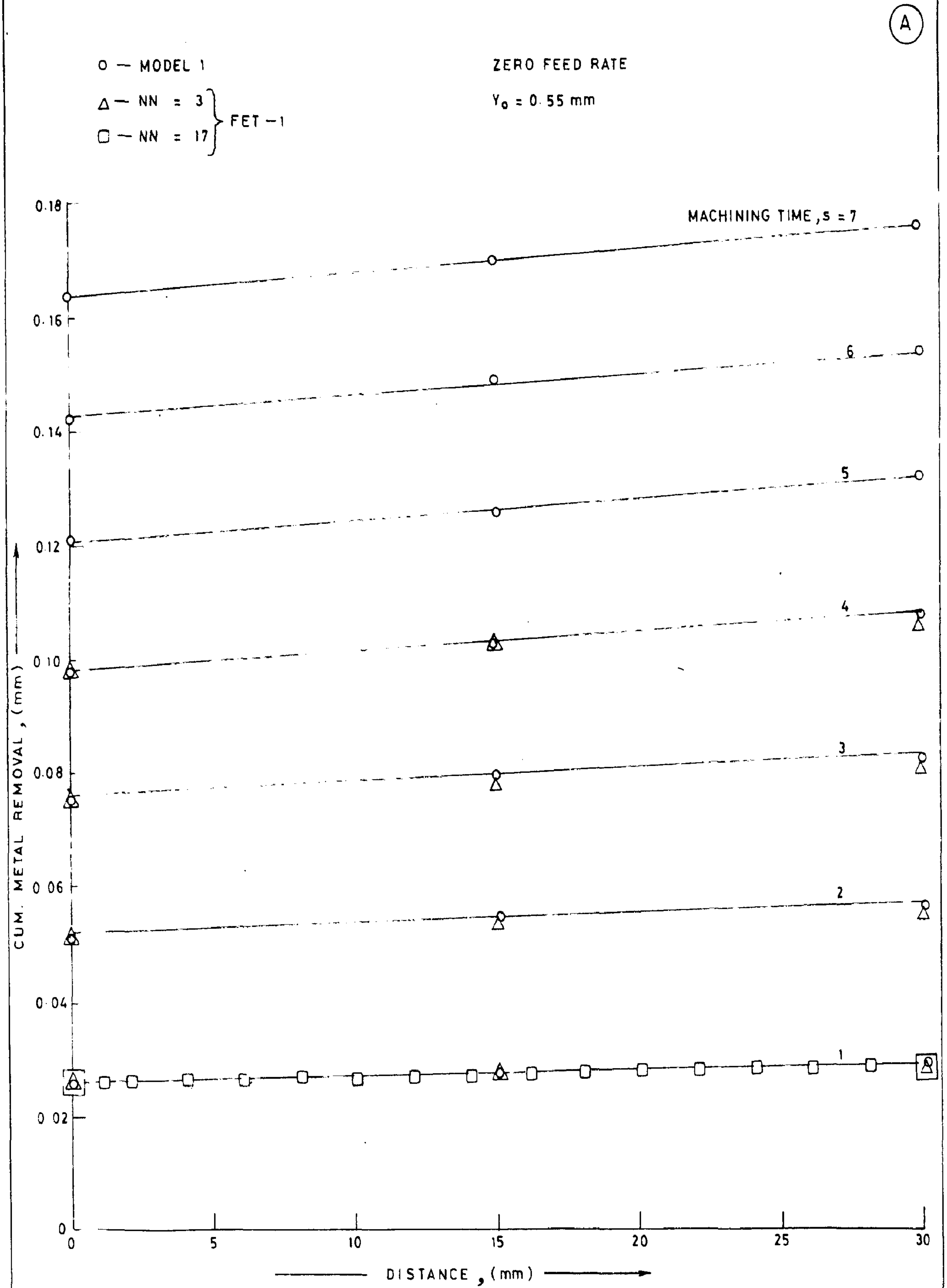

FIG. 7.27 VARIATION IN CUMULATIVE METAL REMOVAL WITH ELECTROLYTE FLOW DISTANCE FOR DIFFERENT MACHINING TIME

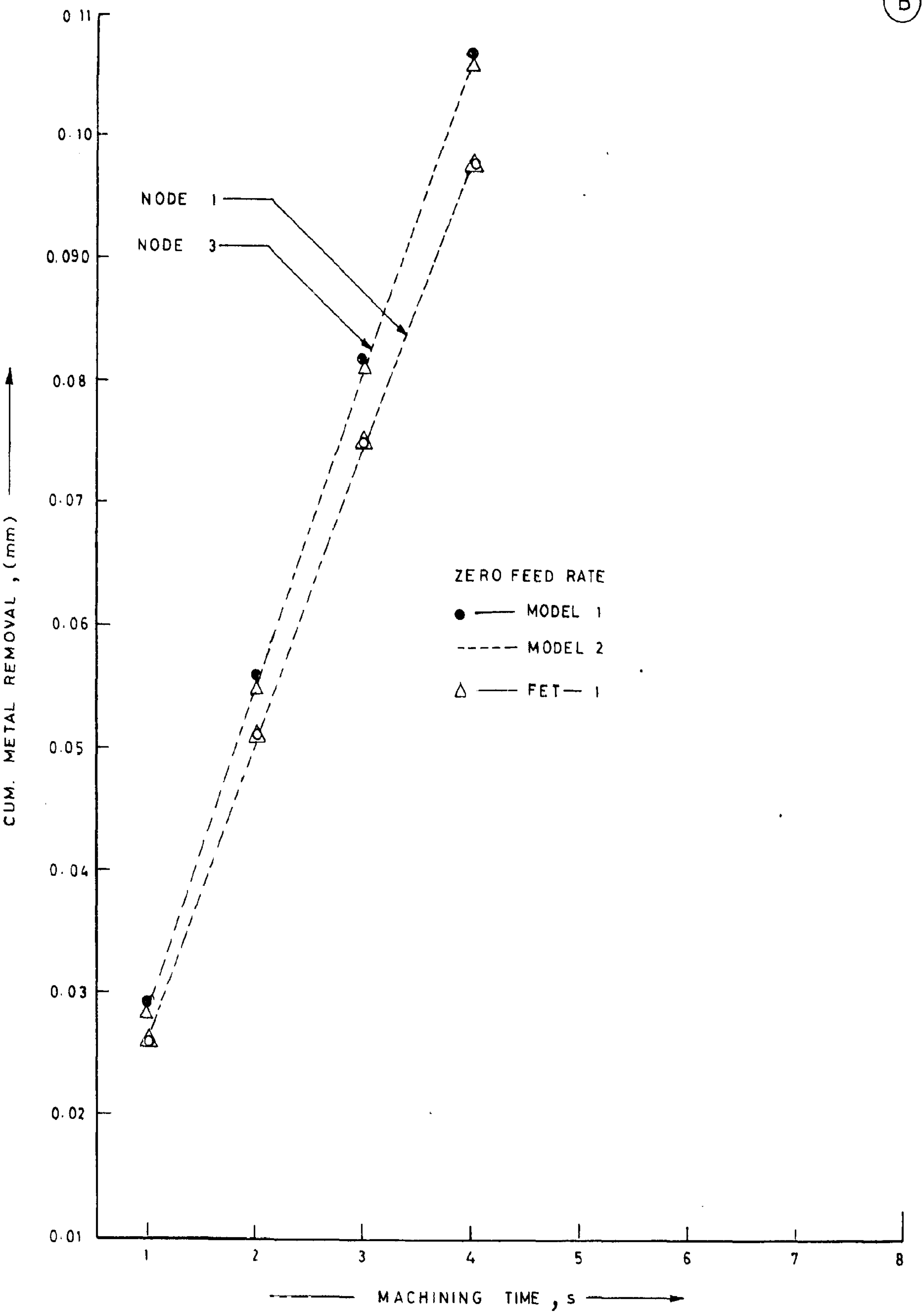

FIG 7. 27 EFFECT OF MACHINING TIME ON CUMULATIVE METAL REMOVAL AT DIFFERENT NODES

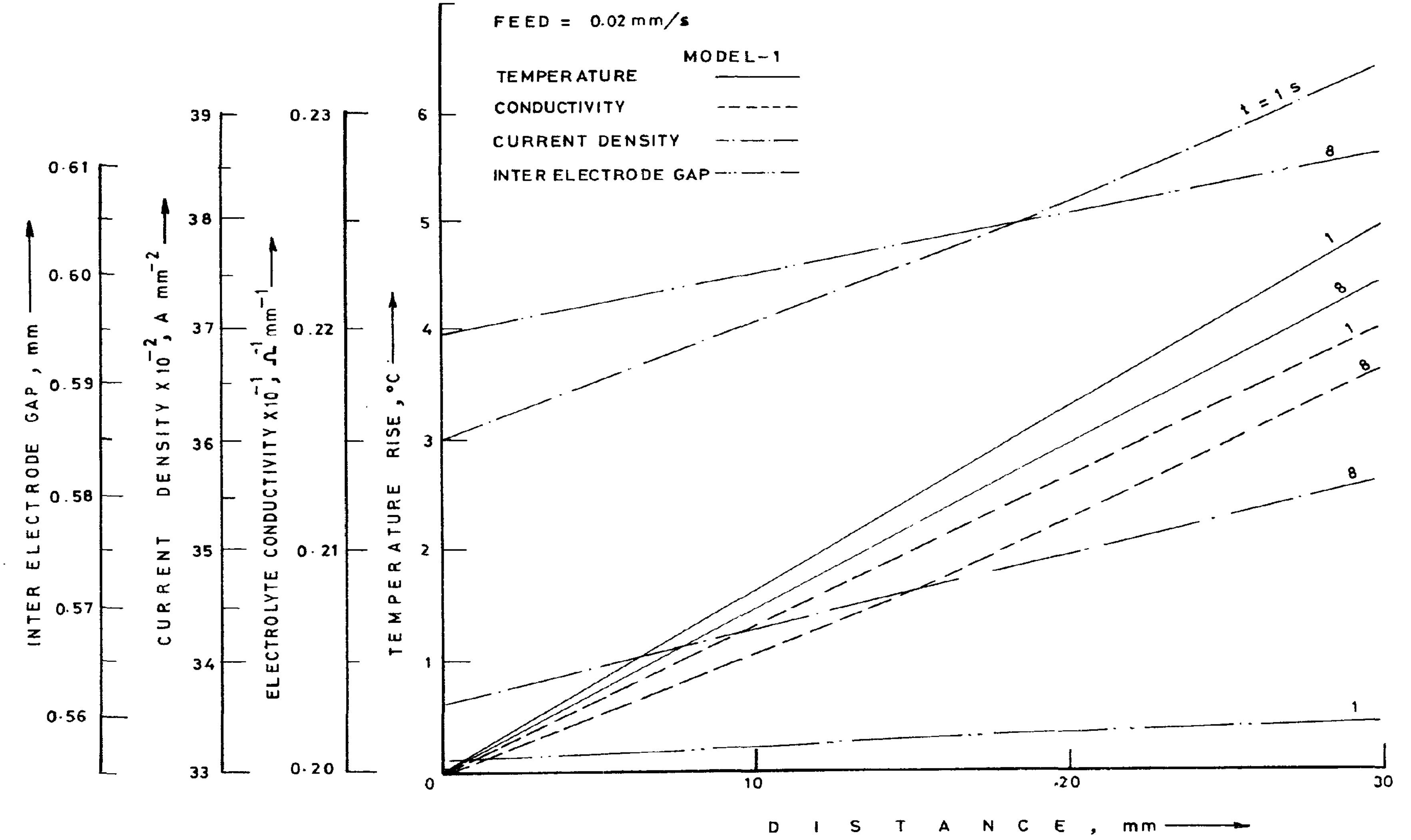

FIG.7.28 VARIATION IN ECM PARAMETERS ALONG THE ELECTROLYTE FLOW DISTANCE AT DIFFERENT MACHINING TIME

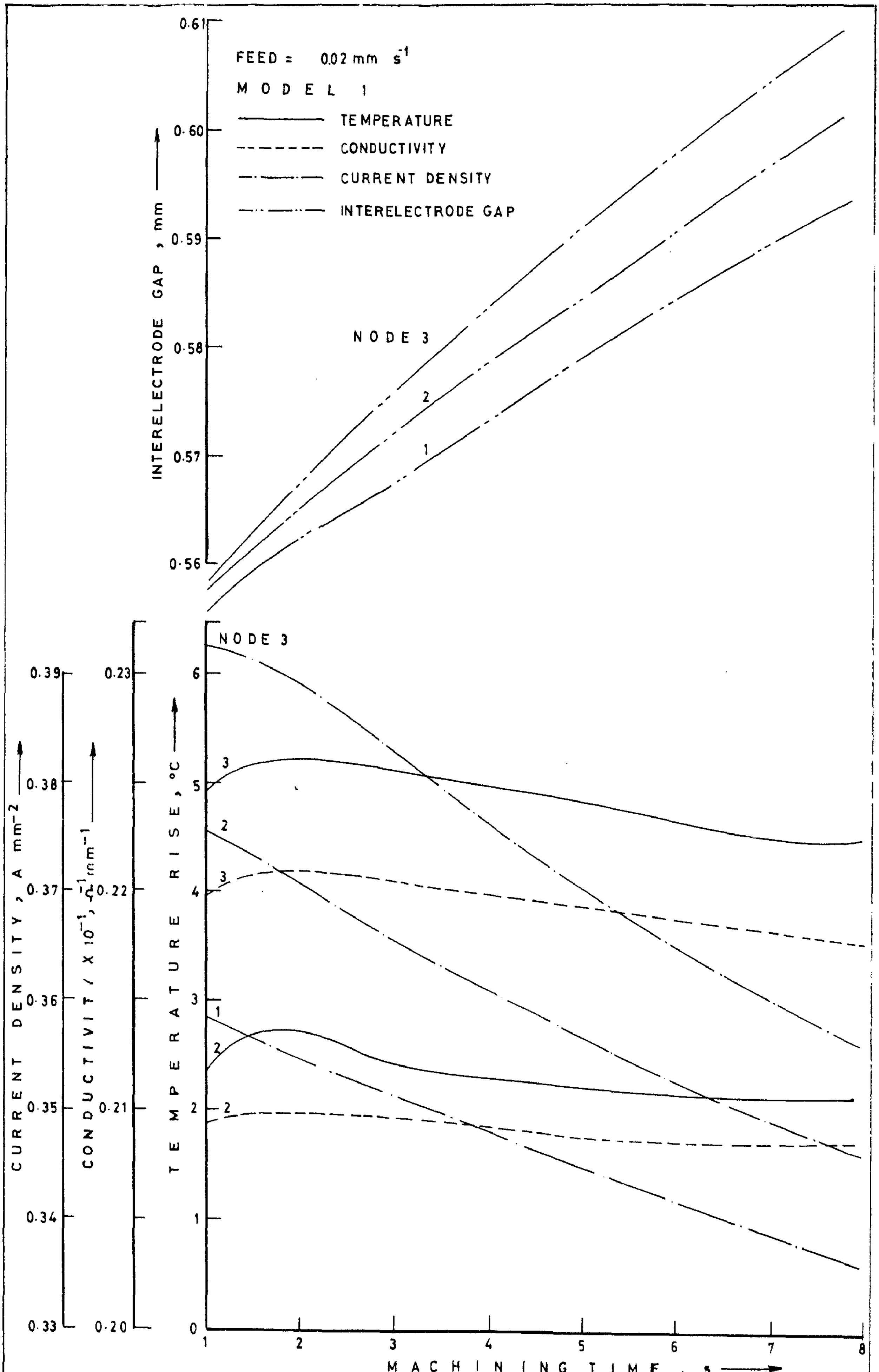

FIG.7.29 VARIATIONS IN ECM PARAMETERS WITH MACHINING TIME

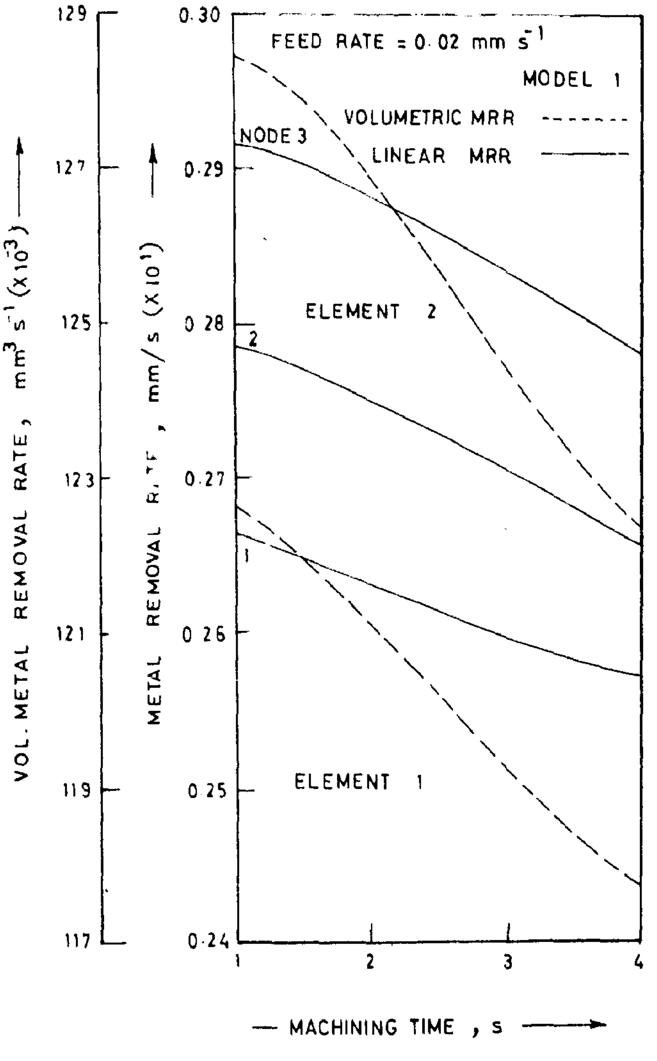

FIG.7.30 EFFECT OF MACHINING TIME ON METAL REMOVAL

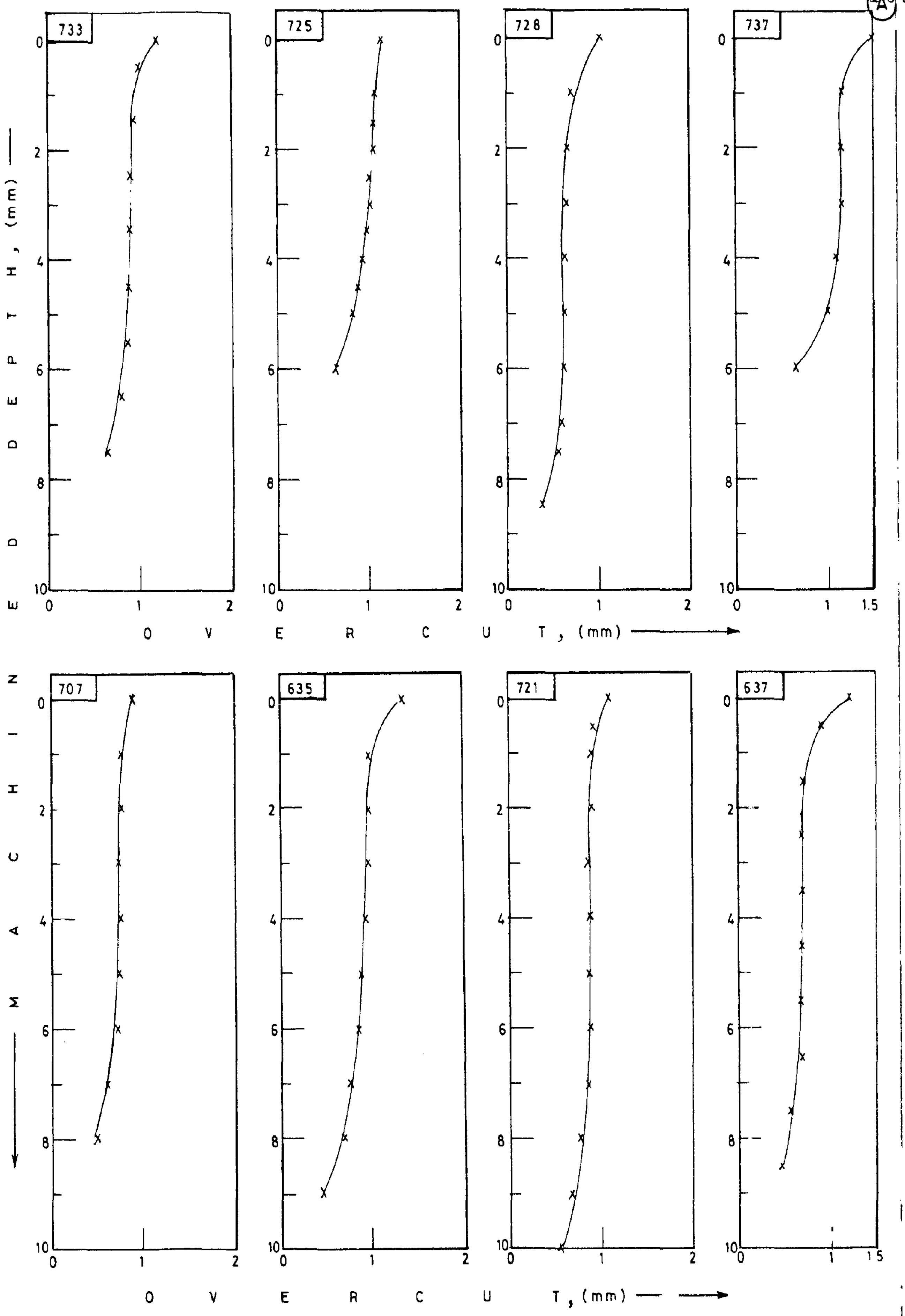

FIG.7.31 ANODE PROFILE IN ELECTROCHEMICAL BIT DRILLING

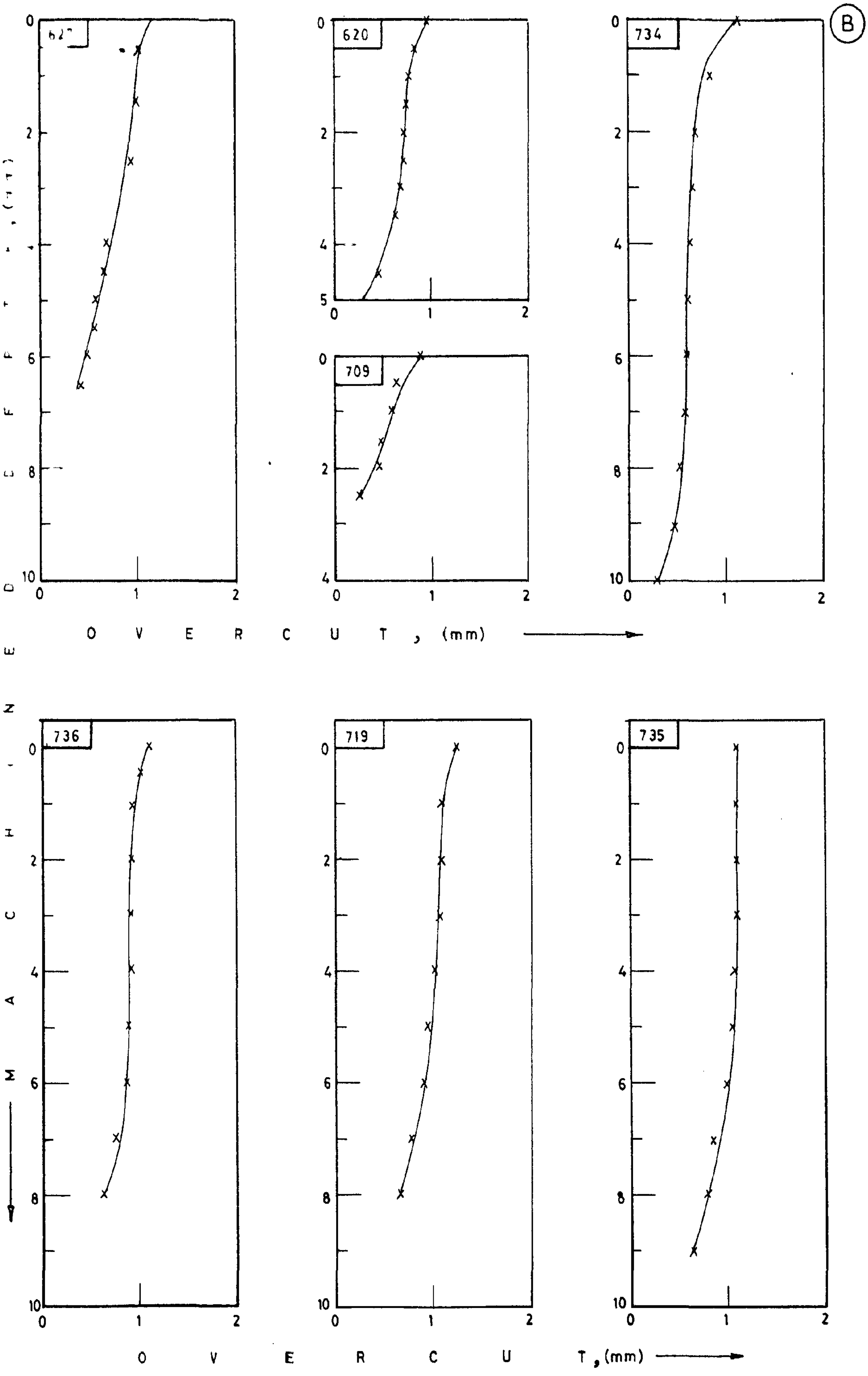

FIG. 7.31 ANODE PROFILE IN ELECTROCHEMICAL BIT DRILLING

Ⓒ

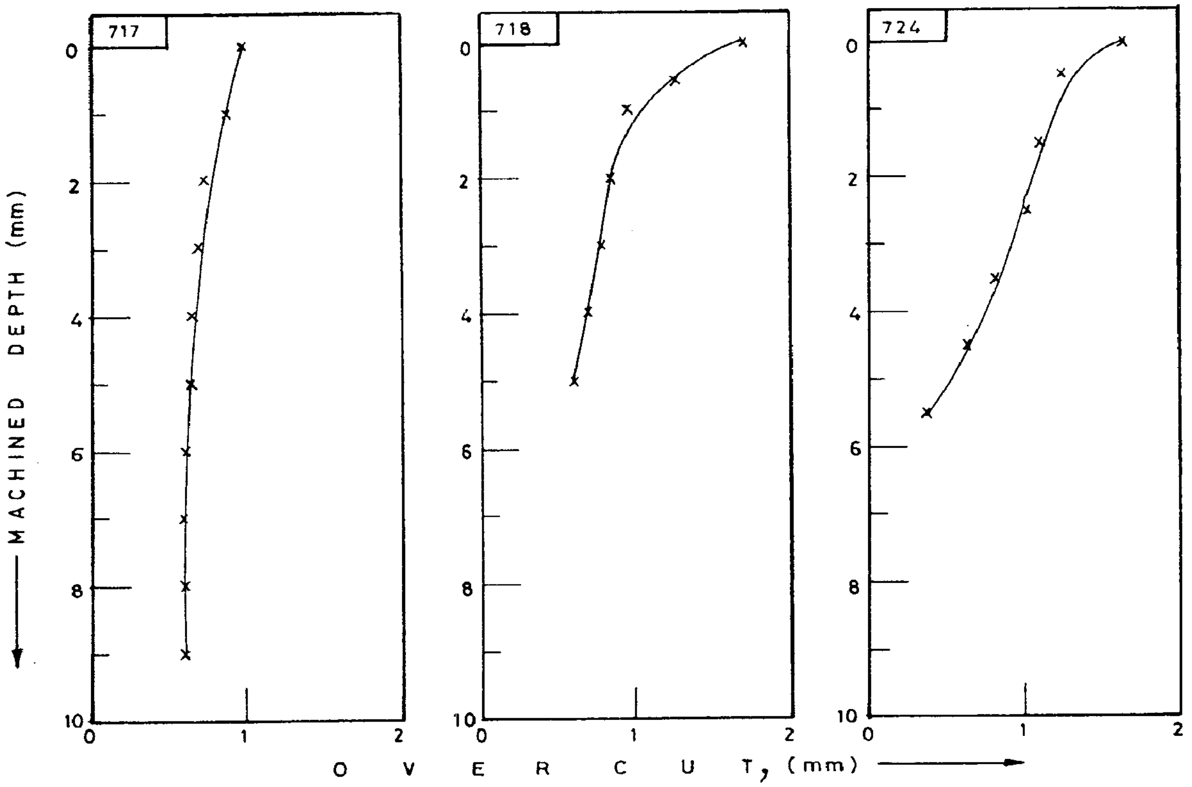

FIG. 7. 31 ANODE PROFILE IN ELECTROCHEMICAL BIT DRILLING

7.7 ELECTROCHEMICAL BORING WITH BARE TOOL-BITS

For the purpose of experimentation, workpieces with predrilled holes were bored by means of bare tool bits. The original hole in most of the cases was produced by ECD employing bare tools. The anode profile of the holes before and after boring have been compared in Fig. 7.32. It can be seen that the bored holed profile is more accurate in comparison to EC drilled hole.

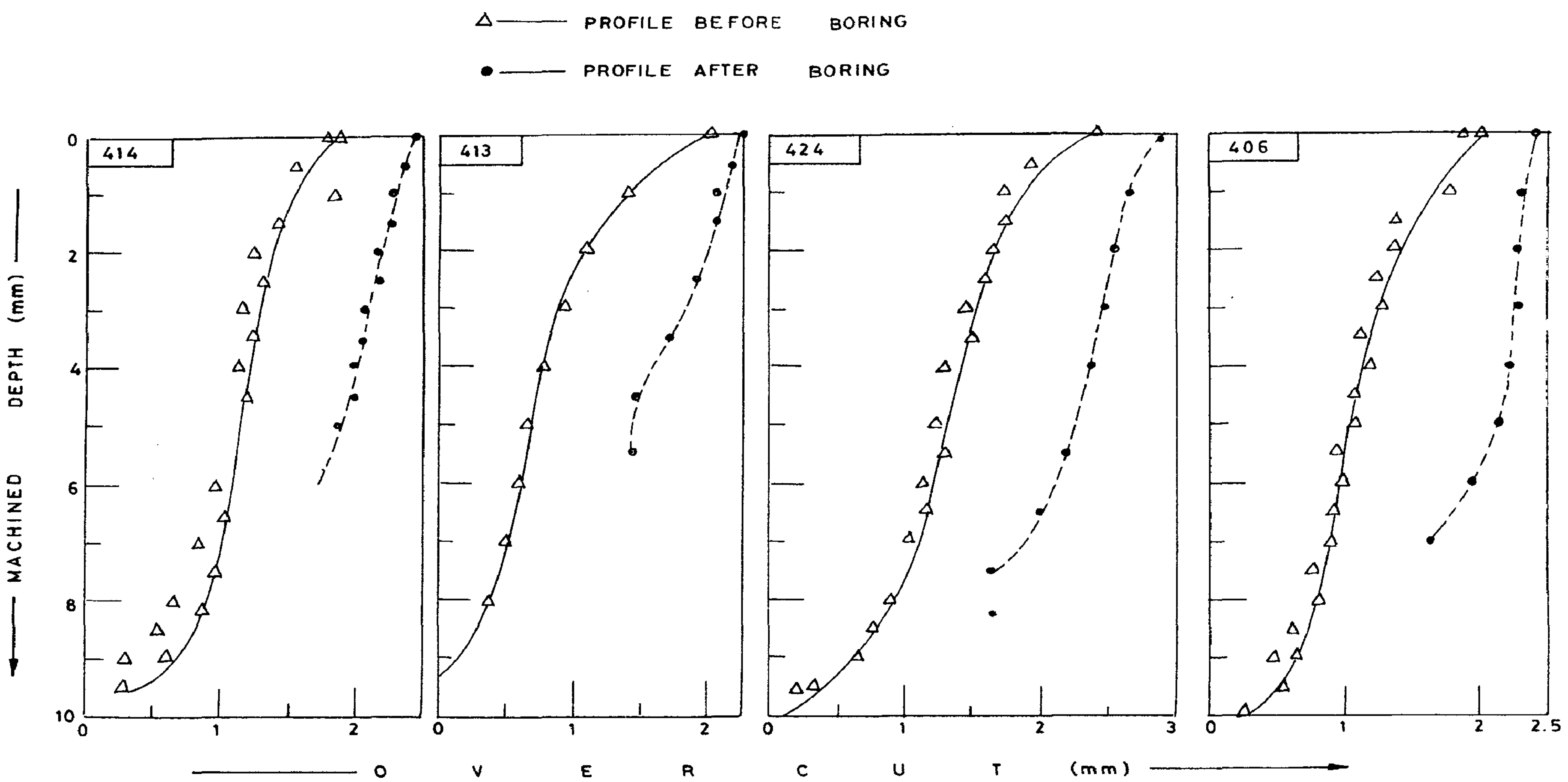

FIG. 7. 32 ANODE PROFILE IN ELECTROCHEMICAL BORING

CHAPTER - 8

DISCUSSION

This chapter presents a detailed discussion on the experimental and analytical results reported by the author. In order to facilitate the discussion it has been presented under the following heads.

8.1 ECM WITH PLANE PARALLEL ELECTRODES

8.1.1 Zero Feed Rate

(a) Current density

The analytical results obtained from model FET-11 have been compared with experimental data (106) (Fig. 7.1). It can be noticed that the model FET-11 yields current density and machining accuracy values that are slightly lower than the corresponding experimental values. This is mainly due to erroneous assumption made about the magnitude of current efficiency. In actual machining, this usually lies between 75 to 100%. Some error is also introduced due to the fact that over potential, ΔA_V in Eq(2.4) has been assumed to be zero. Slight improvement in analytical values in Fig. 7.1 could also be achieved if the heat transferred from the IEG to the tool and work electrodes is accounted for and the actual value of void fraction constant is taken rather than assuming it as zero.

(b) Machining accuracy

Fig. 7.1 also compares the experimental and analytical values of the machining accuracy. In this case, a slight discrepancy exists between the two which can be attributed to the approximations made in arriving at the analytical results and discussed above.

8.1.2 Finite Feed Rate

Figs (7.2) and (7.3) show a comparison between the analytical and experimental results. There is a good agreement between the two for the results obtained by model FET-11 (Figs. 7.2A to 7.2D) and model FET-22 (Figs. 7.3A to 7.3C). However, results by FET-22 give better agreement with experimental data because in this case Laplace's equation (2.15) was employed to evaluate the electric field potential distribution within the IEG. FET-11 on the other hand is based on the assumption that Ohm's law applies to the electrolyte within the IEG. The difference in the results given by these two models is evident when a comparison between the analytical and experimental data specially in the corner region is made. At corners, the current density is very high compared to the central region. Still better agreement between the analytical and experimental points near the corners can be achieved if the finite elements near the corners of the tool are taken to be smaller. Presence of high current density at corners has also been reported by Cuthbertson and Turner (52). Nature of current density distribution given by FET-22 compares favourably with the data of Cuthbertson et al. (Fig.4.5).

It is to be noted (Fig. 7.4A) that after a machining time of 210 s the ECM process parameters viz., K, IEG, J, volumetric metal removal and penetration alter only slightly meaning thereby that the equilibrium state has almost been attained. This is confirmed further by the fact that beyond 210 seconds the ratio Y_t/Y_e approaches a unit value (Fig. 7.4B). Under these conditions the volumetric metal removal also becomes virtually constant.

Discrepancy between analytical and experimental results can be attributed to the fact that experimental data is likely to be in error because of ineffective filtration of the electrolyte, limitations of the temperature measuring device, etc. Contamination of the electrolyte with reaction products has been known to influence the electrolyte conductivity. But the major factors responsible for discrepancy is the assumption of $\eta = 100\%$, neglecting the effect of void fraction ($\alpha_v = 0$) and assuming no heat transfer to the electrodes. These assumptions have been made due to non-availability of sufficient information for their evaluation. As is shown in next subsection if heat transferred to electrodes is considered the trend of the temperature distribution within the IEG changes to a certain extent.

8.1.3 Complex Shaped Electrodes

FET-11 has been applied to analyse sinusoidal wave form sinking (Fig. 7.5A). From the figure it is evident that MRR at the crests is very high compared to that at the troughs.

The feed rate at different points in this case has been calculated using cosine component of feed (i.e. $F_F \cos \theta$), where θ is the angle between feed direction and a normal on the work surface at a point under consideration.

Two dimensional model (FET-22) has been applied for the analysis of complex shaped cathode machining under zero feed rate. Fig. 7.5B gives the IEG discretization and table-10 shows the IEG values obtained at different intervals of machining.

These two examples have been chosen to show the versatility of the FET for application to complex shaped IEG.

8.1.4 Effect of Tool Material on Temperature Distribution

Fig. 7.6 shows a comparison between the experimental results (23) and those obtained from model FET-11. In majority of the cases, analytical values are slightly higher than the experimental data when a current efficiency η = 100% is assumed. However, for the case, η = 95%, a reverse trend can be noticed. Secondly near the inlet, electrolyte temperature in almost all the cases, is higher than the values obtained analytically whereas this is not true near the outlet end. The reason for this being that, one dimensional heat transfer model used in the present case considers the heat transfer in the direction normal to electrolyte flow only whereas in actual practice, heat transfer, within the electrodes itself could take place. The final temperature distribution would have higher temperature at the inlet side and lower at the outlet side.

However, it should be noted that in the present case the total heat going to the electrodes is about 13.0% for M.S. as the anode and copper as the cathode. The effect of tool material on temperature distribution within the IEG is shown in Fig. 7.6. It is also evident from Eqs (3.14-3.20) that heat transferred from or to the electrolyte is mainly a function of thermal conductivity of the electrodes, forced and natural convective heat transfer coefficients and the difference between IEG and the ambient temperature.

8.2 PARAMETRIC STUDY OF ECM PROCESS

Based on the results obtained in this thesis a parametric study of the ECM process has been presented. This has been divided under two headings viz., zero feed rate and finite feed rate.

8.2.1 Zero Feed Rate

Study of the side surface generation in ECM is important and this occurs under zero and finite feed conditions both. During hole sinking operation with straight sided tool, it is normally assumed that the side surface is produced under zero feed conditions. This situation has been analysed by the FET-11.

8.2.1.1 Effect of electrolyte flow velocity

Lowering the electrolyte flow velocity within the IEG leads to higher temperatures, consequently the electrolyte

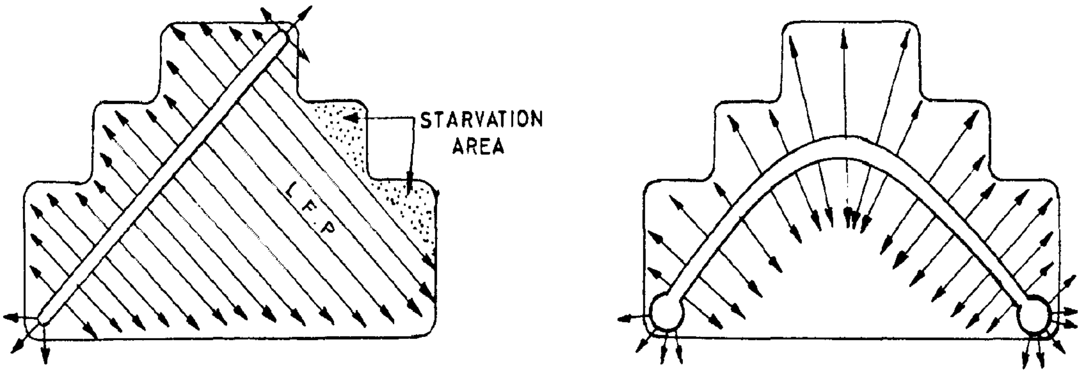
STARVATION AREA
L.F.P.

INCORRECT CORRECT

ELECTROLYTE FLOW SLOT PATTERNS

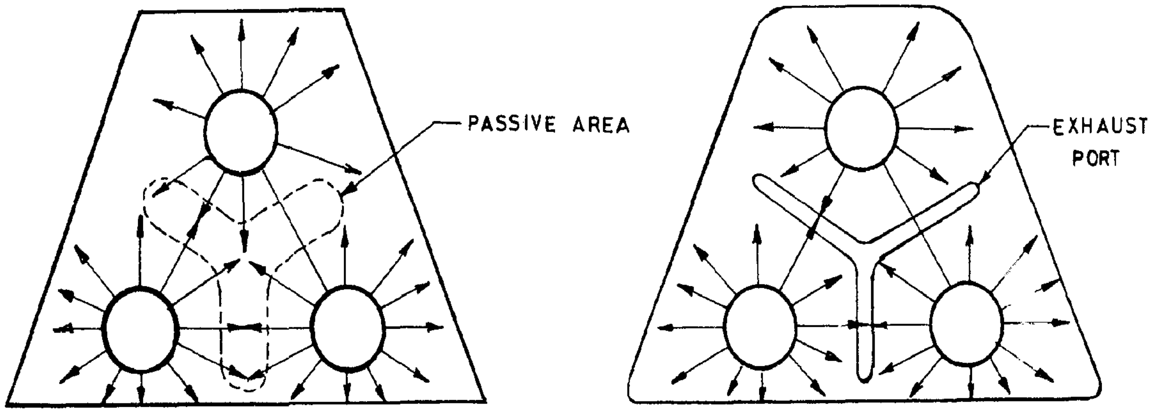
PASSIVE AREA
EXHAUST PORT

INCORRECT CORRECT

ELECTROLYTE SUPPLY AND EXHAUST SLOTS

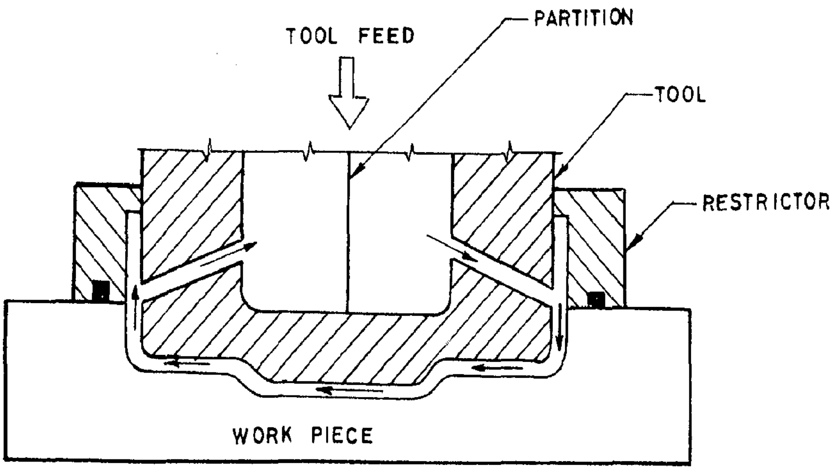
TOOL FEED
PARTITION
TOOL
RESTRICTOR
WORK PIECE

USE OF RESTRICTOR

FIG. 8.1 ELECTROLYTE SUPPLY AND EXHAUST SYSTEMS

conductivity and current density both increase (Figs.7.7A and 7.7B). As a result, faster metal removal rates and larger overcuts are obtained.

From the view point of an ECM tool designer, a high MRR with minimum of overcut would be an ideal situation. The former condition would be satisfied at lower flow velocities whereas, the latter would require the electrolyte to flow at higher velocities. In view of the conflicting requirements above the following guide lines are suggested.

(i) Length of the electrolyte flow path (i.e., the distance between inlet and outlet of the electrolyte) should be kept to its minimum. This would minimize the increase in conductivity due to temperature rise, ΔT. For this, Kuhn (120) has suggested use of electrolyte supply and exhaust slots as shown in Fig. 8.1.

(ii) Electrolytes with low value of temperature coefficients of conductivity (α) should be used. This can be achieved by the use of certain additives as discussed in chapter-2.

(iii) The electrolytes to be used should possess a high electrical conductivity. In this connection use of electrolytes either with certain additives or at elevated temperatures is recommended.

(iv) Use of tool in BIT form with coated sides has been proposed in this thesis by the author. This is expected to result into almost zero overcut.

8.2.1.2 Effect of electrolyte flow mode (side surface generation)

Electrolyte for use in ECM can be supplied in a number of ways (120) viz., inward flow, outward flow, side flow or mixed flow. However, the overcut, current density (J) and temperature distribution depend upon the mode of electrolyte supply (Fig. 7.8A). Minimum deviations in dimensions and minimum overcut can be seen to occur in the case of inward flow. It is further evident (Fig. 7.8B) that coated tool bits result in no overcut whereas bare tool bits lead to small overcut as compared to that obtainable from bare tools. It should, however, be noted that the results presented in Fig. 7.8 are based on the assumption that throughout the transition zone, the overcut remains uniform. The assumption has certain limitations and can lead to a descrepancy, in case of some electrolyte, between the analytical and experimental shapes produced.

8.2.1.3 Interelectrode gap

When IEG is small, T and K both increase due to increased Joule's heating. In the initial stages of machining, it leads to larger overcut compared to a case with initially large IEG. Linear and volumetric metal removal (Fig. 7.9A), temperature rise, conductivity (Fig. 7.9B) and current density (Fig. 7.9C) increase with the decrease in IEG. As an illustration, Fig. (7.9D) shows the effect of initially set IEG on predicted anode shapes. It should also be noted that in addition to the effect of IEG, the accuracy of the anode shape obtained in ECM is also affected by several other parameters such as form error in the tool itself, inaccurate fixing of the tool and workpiece, presence of vibration during cutting, etc. Therefore, for high precision in ECM, fixing of electrodes should be done with care and tool and/or workpiece vibrations should be maintained to the minimum possible level. Error in the tool form should be known before hand so that it can be accounted for during operations planning before using it for actual machining of the works.

8.2.2 Machining With Finite Feed Rate ($F_F \neq 0$)

Electrochemical dissolution occuring ahead of the tool face and that within the curved portion of the IEG can be treated as a case of cutting with finite feed rate. To be very exact machining within initially plane parallel side-gap would also occur with finite feed after a time interval of Δt seconds, since with passage of time the newly generated worksides would become inclined to the feed direction.

8.2.2.1 Effect of feed rate

Use of high feed rates results into higher temperatures due to decreased IEG (Fig. 7.10A). Feed also affects the electrolyte conductivity, current density and metal removal (or IEG) (Fig. 7.10B and 7.10A). The rate of MR changes along the direction of electrolyte flow and is non-uniform due to high temperature gradient. However, very high feed rates can result into tool damage on account of sparking (63) and may lead to frequent short circuits.

Low feed results into lower MRR while high feed rate impairs the machining accuracy and it may also lead to arcing and tool damage which can prove to be costly. Efforts should, therefore, be made to evaluate the optimum feed rate under the given conditions. The analysis for optimization of feed rate(25) could be of some use in this respect.

8.2.2.2 Interelectrode gap

Fig. (7.11A) shows the temperature distribution and MR within the working gap while Fig. (7.11B) shows the variation in electrolyte conductivity and current density with machining time for different IEG. If the initial IEG (Y_0) is larger than the corresponding equilibrium gap value (Y_e), the working gap would decrease with time resulting into increase in temperature, conductivity and current density. For minimum dimensional deviation the rules as discussed in section 'Effect of electrolyte flow velocity' would also apply to the case of machining with finite feed. If possible, the initial IEG should be chosen close to the equilibrium value corresponding to the entry conditions which can easily be evaluated. On the other hand, the initial gap should not be very small otherwise electrolyte boiling can take place.

8.2.2.3 Electrolyte flow velocity

Higher flow velocity of the electrolyte results into a reduction in its temperature rise and the IEG (Fig. 7.12).

Effect of electrolyte flow velocity on the current density and electrolyte conductivity can also be seen (Fig. 7.12B). For higher flow velocities, the penetration decreases (Fig. 7.12C) in a manner almost similar to temperature rise. Reduction in flow velocity impairs the dimensional accuracy and may lead to electrolyte boiling. Therefore, attempts be made to achieve an optimum flow velocity in ECM.

8.3 ELECTROCHEMICAL DRILLING (ECD)

8.3.1 Effective Voltage and Anode Profile

Fig. (7.15) shows the effect of effective voltage on anode shape produced during EC drilling. As the effective voltage is increased the overcut also increases and only in few of the cases during ECD of mild steel highly distorted shaped holes are produced (Fig. 8.2). Secondly, it is very essential to know the voltage and current history (Fig. 7.13 and Fig. 7.14) of the process during ECM of any test piece to explain the superimposition of two anode profiles (Fig. 7.15). Because the voltage variation with time may cross each other even though their effective voltage may be the same. From such crossing it is evident that in one case MRR at the beginning is more and at later part of machining it has dropped down considerably while in other case the MRR has been changing slowly. Due to this, high overcut has been obtained at the top while low overcut in the bottom part giving large taper angle. In the second case MRR has been maintained at the normal rate. Due to this type of voltage vs time history, in few cases anode profiles have crossed each other.

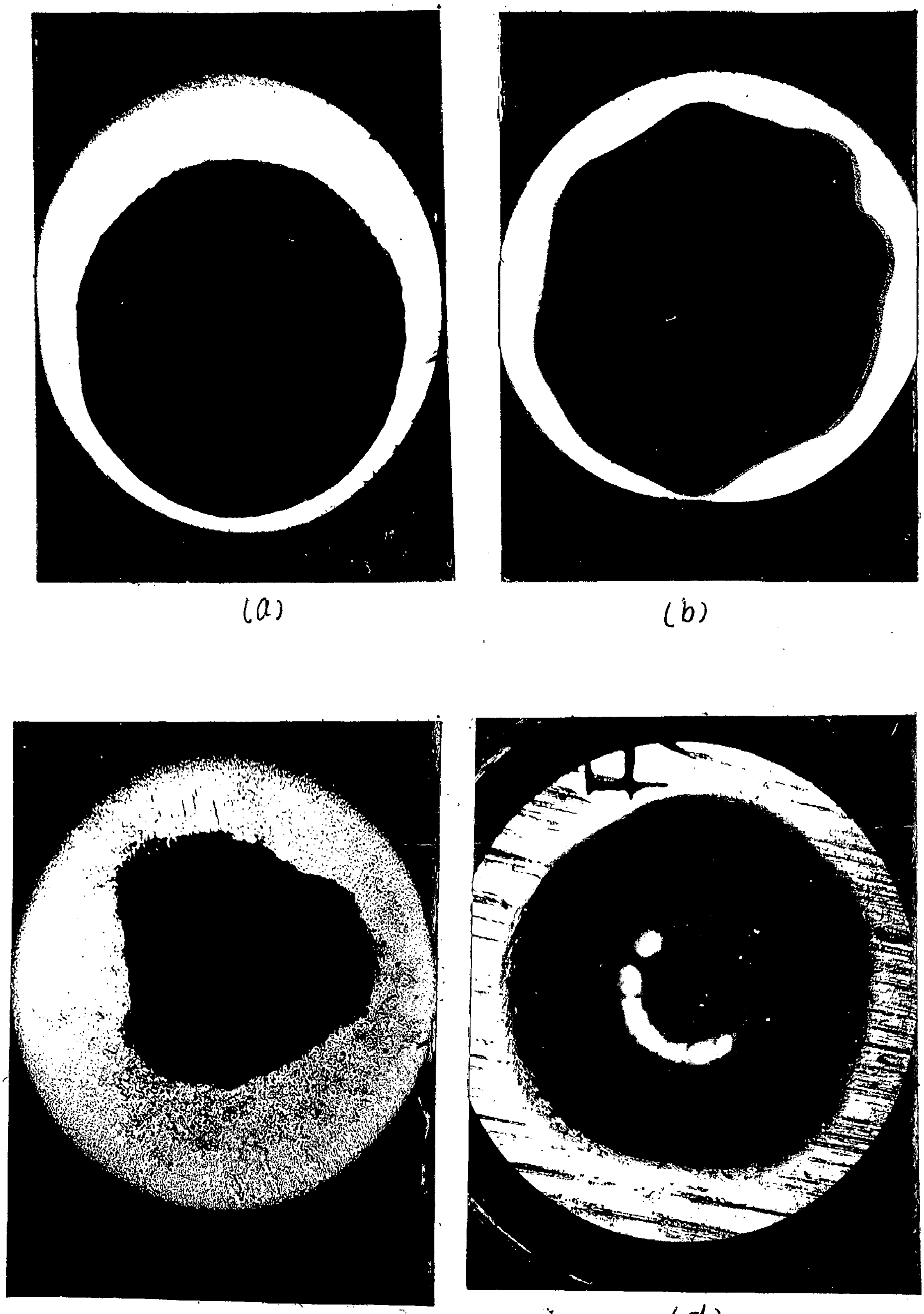

(a) (b)

(c) (d)

Fig.8.2: Top face view of EC drilled holes (X13).
Test piece series (a) 32 (b) 47 (c) 64 (d) 401

It is also to be noted that irrespective of the magnitude of effective voltage, the shape of the anode profile obtained is of $\int$ (elongated S) type.

At the top portion of the profile obtained, a sudden increase in the overcut can be seen to occur (Fig. 7.15). This is attributed partly to the stray current effect and partly due to the fact that this section of the workpiece is subjected to EC dissolution throughout the period of drilling. Fig. 8.3 shows EC dissolution time variation with machined depth. This increases the overcut at the top face. The overcut also increases as the initial IEG is increased. Let 'Y' be the initial IEG between tool and work. Then approximately Y_0/F_F is the extra time of machining for which top part of the anode has been subjected additionally to EC dissolution.

At the bottom, due to large equilibrium gap, specially in case of low feed rate the current density in the part of the transition zone would decrease considerably with the result that comparatively lower overcut (or lower MRR) is observed and hence the profile gets twisted towards the centre. With low equilibrium gap, this difference in overcut in zone 2 and zone 3 would also decrease.

It is also to be noted that the anode profile has been measured along two or more directions displaced each other by about 45°. Due to this, in many cases, different overcut at the same machined depth has been reported in Fig. 7.15.

In some of the tests, the process had to be stopped due to sparking or due to foam collected in the machining box or due to some other unavoidable reasons. This could happen even more than once during ECM of a test piece. Sometimes readjustment of the IEG had to be made. This would have also changed the history of the current and voltage variations with time, as a result, in some cases non-uniform anode profiles were obtained.

8.3.2 Tool Diameter and Anode Profile

Fig. (7.16) shows the effect of tool-diameter on overcut in ECD. It has been reported (110) that the anode profile (or overcut) is not affected by changing the tool-diameter keeping all other conditions the same. However, this conclusion does not seem to be valid because at the same voltage across the electrodes but varying the tool diameter, the current density changes. It is obvious that different current densities would give different overcut (Eq 3.9) and hence different anode profiles.

Considering two tools having tool diameters D_1 and D_2, the current density for the case of cylindrical hole drilling would be given by Eqs (8.1) and (8.2).

$$J_{r1} = \frac{K \cdot E_V}{r_1' \ln(r_1' / r_2')} \quad .. \qquad (8.1)$$

$$J_{r2} = \frac{K \cdot E_V}{r_2' \ln(r_2' / r_2)} \quad .. \qquad (8.2)$$

r_1' and r_2' are the values after drilling and r_1 and r_2 are the values before drilling.

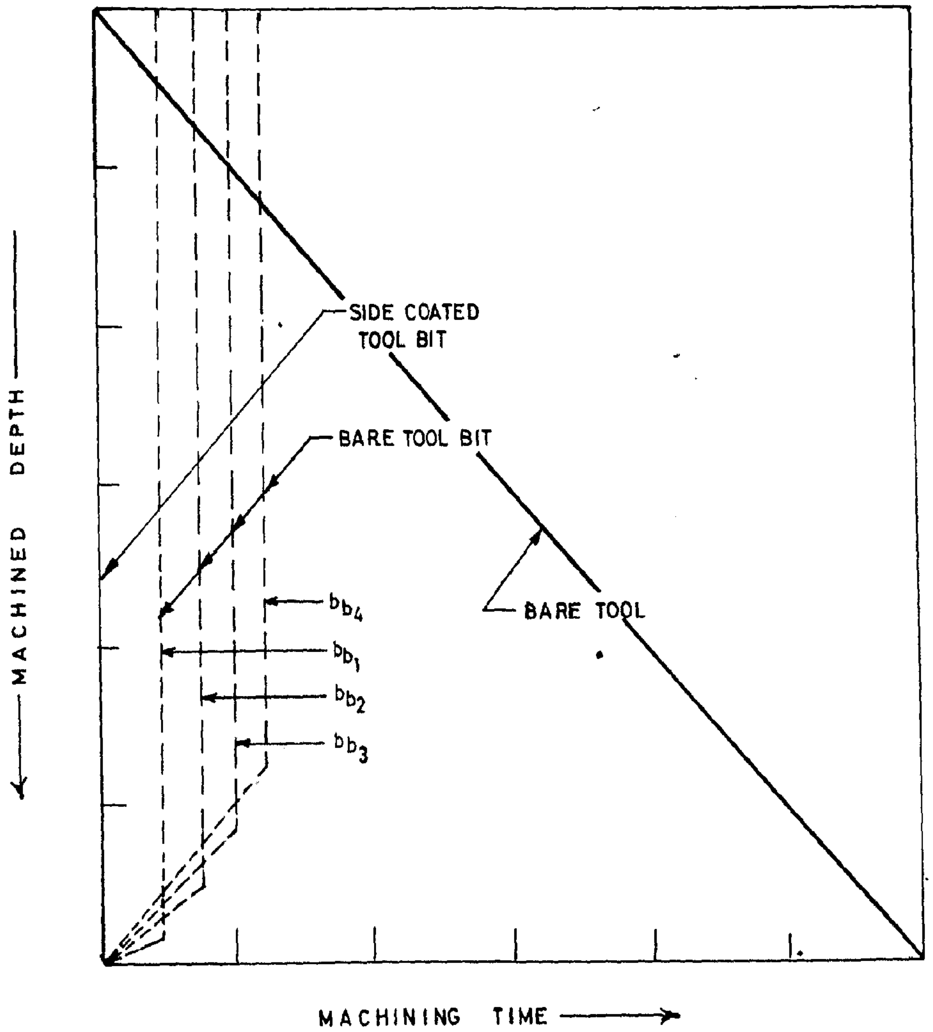

FIG. 8.3 VARIATION OF MACHINING TIME (OR EFFECTIVE ANODE DISSOLUTION TIME) FOR DIFFERENT TYPES OF TOOLS

The condition for equal overcut at a point in the side gap in ECM with two different tools would therefore be given by Eq(8.3).

$$\frac{J_{r1}}{J_{r2}} = \frac{r_2'}{r_1'} \; \frac{\ln(r_2'/r_2)}{\ln(r_1'/r_1)} = 1 \qquad .. \qquad (8.3)$$

or

$$r_2' \ln(r_2'/r_2) = r_1' \ln(r_1'/r_1) \qquad .. \qquad (8.3a)$$

It means that the condition given by (8.3) is not satisfied unless the two tools have the equal diameters. That is why higher overcut is obtained in case of smaller diameter tool (Fig. 7.1B). In few cases, the overcut obtained from small diameter tool is smaller than the higher diameter tool and it can very well be explained with the help of current and voltage history of the process during the test.

8.3.3 Machining Efficiency

As is evident from the Table-12, a systematic effect of different parameters on the machining efficiency could not be obtained. Similar results have also been obtained by McGeough during ECM of mild steel (149).

8.3.4 Analytical and Experimental Anode Profile During ECD

Fig. 7.17 shows a comparison between analytical and experimental anode profiles obtained during ECD using different machining conditions and work materials. It is evident that in majority of the cases, deviation between the experimental and analytical points is minimum within and near the transition zone and increases towards the top surface of the EC drilled hole. This discrepancy has been attributed to the following:

(i) For the purpose of computation of the anode profile a mean current efficiency of 85% was assumed however, in practice (59) its value often lies between 75-100% (Table-12).

(ii) In the present case, a value of $\Delta A_V=2.0$ (fixed) volts was assumed if $E_V \geq 10.0$ volts and $\Delta A_V=1.0$ volts if $E_V < 10.0$ volts. However, the value of ΔA_V could sometimes be high (59), upto 5.0 volts in certain cases. On the other hand, minimum potential needed across the cell, for machining to proceed should be about 2.5 volts. Thus, the value of E_V used in the present case seems to be higher than the effective working voltage in IEG. This also leads to the higher value of the computed overcut.

(iii) During the computation of metal removal, valency of iron was assumed as 2. This implies that the iron is being removed as ferrous hydroxide. However, visual examination of the reaction products confirmed (in case of ECM of M.S.) that part of the iron was being removed as ferric hydroxide (148,222) and hence a more appropriate value of the valency of iron under the present circumstances would lie between the calculated value and measured overcut.

It has also been shown (157) that during ECM of carbon steels, the parameter given by Eq(8.4) can be employed to decide about the mode of iron hydroxide formation

$$C_V = J_i(x_i/v^2Y_e^{0.25})^{0.33} \quad .. \quad (8.4)$$

when iron is removed predominently due to formation of ferric hydroxide the parameter C_V tends to become constant. In Fig. 8.4 the computed value of the parameter C_V have been plotted against the machined depth. It can be noticed that C_V assumes virtually a constant value after the tool has penetrated to a certain distance indicating that at large depths iron is being removed as ferric hydroxide. In case of deep penetration (or large depth), the effective electrolyte velocity reduces towards the exit - a situation which favours (157) the formation of ferric hydroxide rather than ferrous hydroxides.

(iv) Feed rate is the relative movement between tool and work-surface and in the begining of a cut its value is zero (i.e. $F_s=0$) in zone 4 provided vertical straight sided tools are used. As the cut proceeds the generated work surface no longer remains parallel to the feed direction and is inclined with respect to both the tool surface and feed direction. Thus, the assumption of zero feed rate in zone 4 is no longer valid. This has the effect of overestimating the IEG as in Fig. (7.17).

(v) During computation, effect of void fraction on electrolyte conductivity has been neglected and this results into higher values of the computed overcuts.

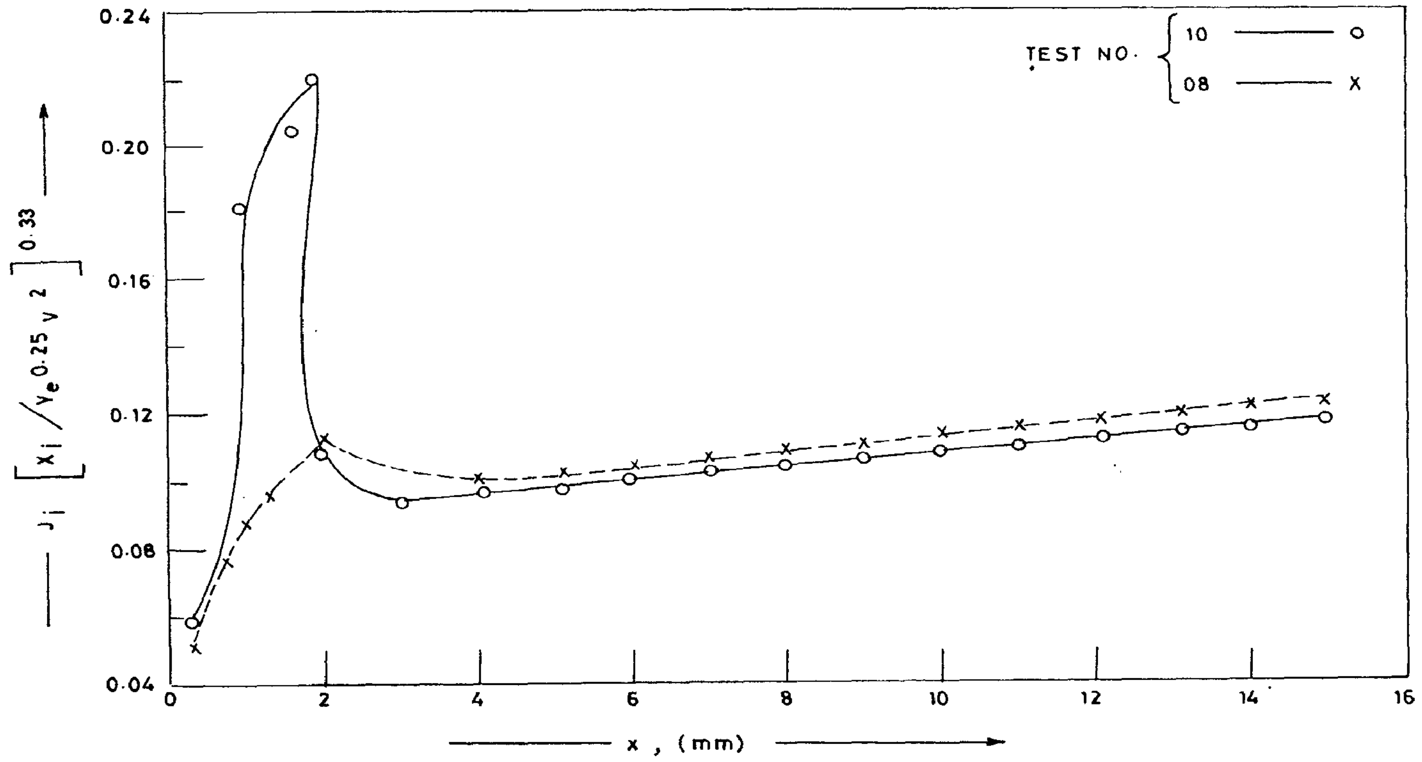

FIG. 8.4 RELATIONSHIP BETWEEN x AND $J_i \left[X_i / Ye^{0.25} v^2 \right]^{0.33}$

This is also to be noted that computation cycle time should be as low as possible because as shown in Fig. 8.5, it has got an effect on the computed values. Although very small value of Δt cannot be selected otherwise computer time will increase. On the other hand, large value of Δt will impair the accuracy. Hence, a compromise between accuracy and economy is always sought.

It is also to be noted that anode profile predicted by the use of actual voltage ($\vec{E}_v$) vs time curve is more accurate as compared to those predicted by the use of mean voltage ($\vec{E}_{vm}$). It shows the importance of voltage vs time variation (or voltage history) curves.

8.3.5 Presence of Striations on Work Surface

From Fig. 7.18, it is evident that drilled hole has the shape of $\int$ (elongated S) type and reasons of the same have been explained in section 8.3.1.

Fig. 7.19 shows the machined top surface of a few representative EC drilled holes. It is evident that in these cases, the hole shape gets distorted. Such distortion has been termed as 'Striations'. The striation formation phenomenon has not been understood well and several explanations have been given for this. Fluerenbrock (70,71) has explained the presence of flow lines on the basis of ECM sonic velocity theory. According to him alternating layers of high and low void concentration,

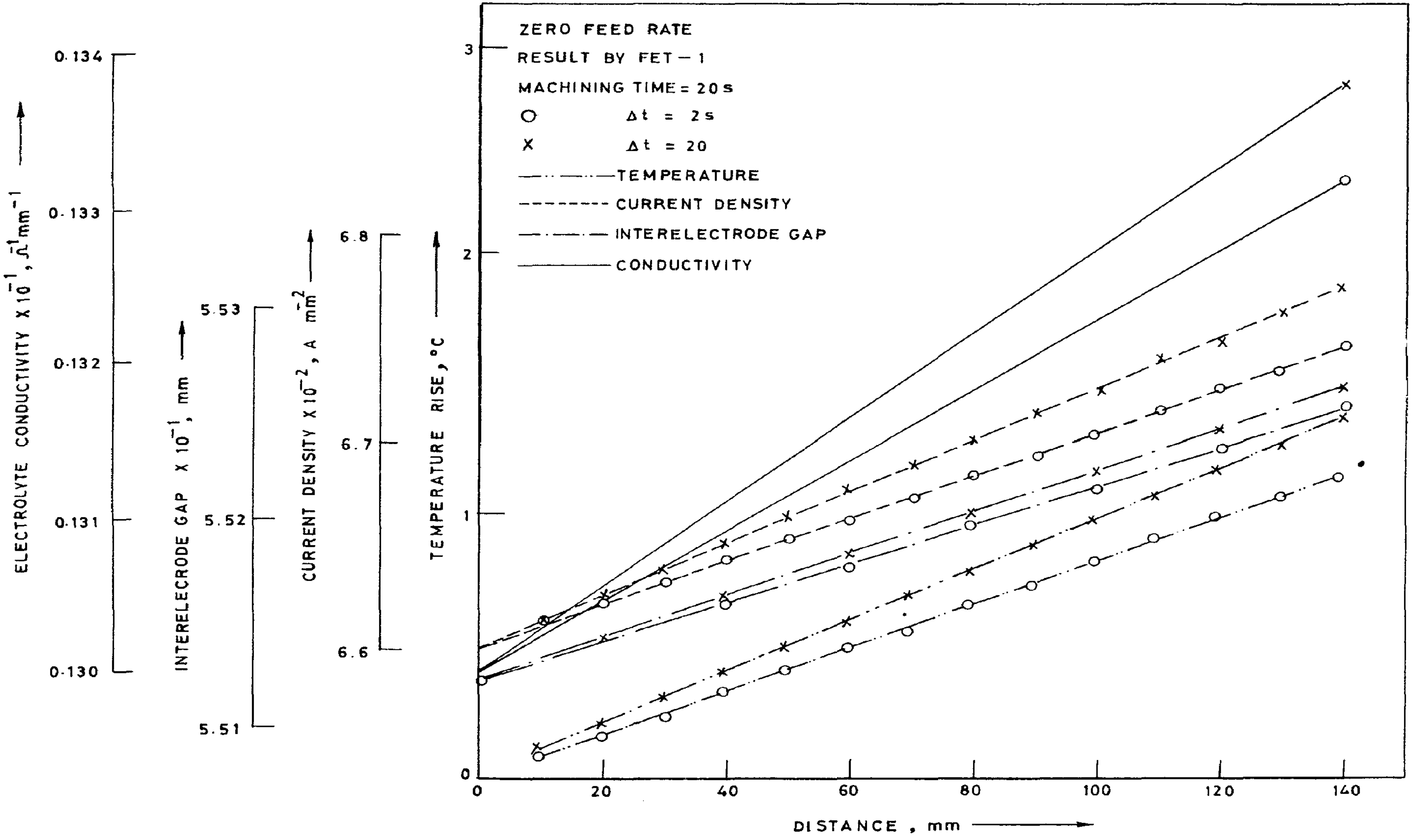

FIG. 8.5 EFFECT OF COMPUTATIONAL CYCLE TIME (Δt) ON COMPUTED VALUES OF DIFFERENT PARAMETERS

with orientation in the flow direction are produced. The layer with high void fraction produces a gap of small thickness whereas, the low void layers, creat a wide gap. Cole (48) has attributed the formation of striations to a certain combination of electrolyte pressure and flow rate; not yet fully analysed. Opitz (176) has also observed similar phenomenon and he has explained it as grooves in the work surface running in the direction of electrolyte flow. According to him the resulting cavitation phenomenon (97) act to break up the electrolyte flow into individual streams and led to non-uniform material removal. One of the remedies suggested for this is to inject gases like N_2 into the electrolyte; this helps to agitate the electrolyte and avoids the formation of streaks or striations. The conditions under which striations were observed in the present case are given in Table-12. It is evident that their formation is observed at very high velocities.

8.3.6 Overcut in Transition Zone in ECD

Fig. 7.20 shows a relationship between experimental observations of overcut (a_o), in transition zone and the best line of fit derived from linear regression technique (101). A good correlation is seen between the two. In few of the cases, a poor correlation coefficient (0.8 or less) was also obtained specially when attempts were made to derive a generalized equation involving very large number of points. Dimensional analysis of the parameters governing the overcut,

a_o was therefore conducted and yielded the final relationship (Eq 3.5). The values of C'_d, n_1 and n_2 for different tool-work material combinations have been derived from the Figures of the type (7.22). A knowledge of the parameter a_o is important for accurate prediction of anode profile in ECD. Deviations between the line of best fit and the actual overcut in Fig. 7.20 can be attributed to the fact that it is difficult to locate exactly the boundary between side region and transition region. Hence, an estimation about the boundary had to be made. Secondly, equilibrium gap (Y_e) has been calculated using the effective voltage whereas it would depend upon the voltage which persisted at the end of machining.

8.3.7 Study of Electrochemical Drilling with Bare Tools Using 'Design of Experiments'.

As, discussed in earlier chapter, experiments were conducted, in accordance with the design of experiment - plan (Table-6), to study the effects of various parameters on metal removal rate, in ECD, using bare tools. The observations were then analysed and the following constants for the response surface equation have been obtained.

$\beta_0 = 5.43409$; $\beta_{11} = 0.2544$; $\beta_{12} = 0.24256$; $\beta_{25} = 0.40206$

$\beta_1 = 0.15779$; $\beta_{22} = 0.12347$; $\beta_{13} = -0.33894$; $\beta_{34} = 24056$

$\beta_2 = 0.22529$; $\beta_{33} = 0.03031$; $\beta_{14} = -0.21644$; $\beta_{35} = 0.06069$

$\beta_3 = 0.56770$; $\beta_{44} = -0.12706$; $\beta_{15} = -0.0978$; $\beta_{45} = -20231$

$\beta_4 = -0.36521$; $\beta_{55} = -0.06331$; $\beta_{23} = -0.16468$;

$\beta_5 = 0.82705$; $\beta_{24} = -0.20219$;

To test the adequacy of the above model, analysis of variance was made and the following results obtained using the equations given in section 6.3.3.

	Sum of squares	Degrees of freedom
First order term	29.1678	5
Second order term	12.1588	15
Lack of fit	1.36523	6
Experimental error	1.02007	5
Total	43.7118	31

Then, the value of 'F' ratio from the table above was calculated as 1.3384. The tabulated value for the conditions of the experiment and for 95% confidence is equal to 5 which means that the model proposed above is 'adequate'.

8.3.8 Study of Electrochemical Bit Drilling Using 'Design of Experiments'

To study the effect of tool bit diameter and bare height of the tool bit on metal removal rate, experiments were conducted in accordance with the design of experiments plan given in table-7. The following response surface equation was obtained.

$$Y^* = 11.903 + 0.797\, x_1^* + 0.64024\, x_2^* - 0.55994\, x_1^{*2} + 0.02581\, x_2^{*2} - 0.4205\, x_1^* x_2^* \quad .. \quad (8.5)$$

The analysisis of variance has yielded the following results:

	Sum of squares	Degrees of freedom
First order terms	8.3601	2
Second order terms	2.958	3
Lack of fit	13.1933	3
Experimental error	3.24268	4
Total	27.755	12

The calculated value of 'F' ratio was 4.0686 while that obtained from Table (95% confidence limit) was 6.6. Thus, the calculated value of 'F' ratio does not exceed the value obtained from the table; this means the model presented by above equation (8.5) is adequate.

8.4 ELECTROCHEMICAL WIRE CUTTING

8.4.1 Zero Feed Rate (F_F=0)

Fig. 7.24A shows the temperature rise in the electrolyte along the flow direction, computed by three different methods. It is evident from this figure that as the mesh is refined the results of FET-1 approach to the values given by model-1. Since the results obtained by FET-1 are almost the same as by exact formulae hence significant effect of mesh refinement is not apparent. Fig. 7.24B also shows the temperature distribution within IEG along the electrolyte flow direction for different machining time. With increasing machining time the temperature rise between two points is decreasing because the IEG increases (Fig. 7.28). Fig.(7.24C) shows that the temperature varies at different nodes as the machining progresses. Since these results pertain to zero feed rate condition hence a constant drop in temperature with increase in machining time for a particular node is observed. Results given by the model-1 and model-2 and the FET-1 show similar trend. Fig. 7.25A shows the change in electrolyte conductivity along the flow direction whereas, Fig. 7.25B shows the change in K with machining time t. All the results have same trend and the linear dependence of K on Δt (Eq 2.6) is confirmed. Figs. (7.26A) and (7.26B) show the current density distribution along the IEG and at different machining times. The current density at a particular node can be seen to decrease with increase in machining time this is because at zero feed the IEG increases with time. Fig. (7.27) shows the variation of cumulative and volumetric MR(in mm) along the wire and with machining time at different nodes respectively. At the node near the electrolyte exit, cumulative MR (MR_c) is more than at the node near the electrolyte entry because K is increasing along the length of the wire (Fig. 7.25).

8.4.2 Feeding Electrodes (F_F=0)

Fig. (7.28) shows temperature, conductivity, current density and IEG variation along the length of the wire during the first and eighth seconds of machining. The electrolyte temperature can be seen to increase non-linearly along the wire length and decreases gradually with machining time. This is because the IEG increases with machining time for the feed rate chosen. This also is responsible for a decrease in the electrolyte conductivity and current density values as the machining proceeds.

Fig. 7.29 shows the variations in T, K, J and Y at different nodes for different machining time. Fig. 7.30 shows the linear MRR at nodes and volumetric MRR in elements obtained.

8.5 ELECTROCHEMICAL DRILLING WITH BARE TOOL BIT (ECBD)

Fig. 7.31 shows the anode profile obtained during ECBD. It is evident by comparison of figures (7.17) and (7.31) that a significant improvement in the dimensional tolerance can be attained by means of a bit tool. This can well be explained with the help of machined depth vs machining time curve (Fig. 8.3). It is to be noted that experimentally obtained anode profile is very much similar to the one predicted analytically in Fig. 3.5. The process has been observed (Figs. 7.13 and 7.14) to be more stable as compared to the cases when using bare tools. It is to be mentioned that in majority of the cases the difference between maximum and minimum overcut is about $\frac{1}{2}$ mm. It can, however, further be reduced by decreasing the bare land width, b_b, and maintaining constant voltage across the electrodes.

8.6 ELECTROCHEMICAL BORING WITH BARE TOOL BIT

Only few tests were conducted for electrochemical boring with the use of bare tool bit (See Fig. 7.32). It is evident that dimensional variation from top to bottom has decreased in case of ECB with bare tool bit. However, this effect is not reflected to the expected extent because total penetration depth of the bit is quite low because bit effect will appear only when it has penetrated to a depth much more than its bare land width, b_b. Secondly, for better accuracy side coated tool bit should be used and not the bare tool bit as done in the present case. It is to be noted that large sized holes drilled with the use of tool bit would require comparatively lower power machine . If such holes are drilled in steps then still lower power machines would serve the purpose.

However, it is evident that this new concept of bits to the ECM tools is highly promising for best possible precision in ECM.

CHAPTER-9

CONCLUSIONS AND SCOPE FOR FUTURE WORK

9.1 CONCLUSIONS

(i) The thesis has demonstrated the capability of the Finite Element Technique for the analysis of simple and complex shaped anode profiles obtainable in ECM. This has also enabled a detailed study of the nature of interaction between the ECM process parameters.

Development of the analytical model is based on the approximation of interelectrode gap both as an unidimensional and two dimensional continuum. The two dimensional approximation, in general, has been found to give better results. The effect of computational cycle time on the accuracy of the results obtained was studied in detail. For simple shaped IEG, in majority of the cases, a value of 20s-30s was found to be satisfactory whereas, for complex shaped workpieces the computational cycle time should be low.

However, the success of the analytical method proposed in this thesis, under the given conditions, depends to a certain extent on a prior knowledge of the values of machining efficiency, void fraction, electrochemical equivalent, current and voltage fluctuations, etc., during the period of cut. Experimental data concerning the above must be available so as to make a generalized application of the technique developed.

(ii) Heat transfer analysis of the ECM process reveals that the tool and work electrode materials have a controlling effect on the proportion of total heat transferred from the electrolyte to the environment and hence on the electrolyte temperature.

(iii) When cylindrical holes are drilled by Electrochemical method using bare tools, the longitudinal profile of the hole produced in majority of the cases is that of an elongated S ($\int$).

(iv) Use of tool bits, for drilling and boring operation, in ECM can result into a substantial reduction in power consumption and overcut. Tool bits with insulated sides and low operating voltage lead to practically zero overcut and hence is recommended for drilling and boring of precision holes.

(v) The overcut in transition zone, during EC drilling, can be computed accurately by the use of dimensional analysis (Eq 3.5) and is a function of a_o, Y_e, F_F, D, r_c and V. In few of the cases the overcut has also been found to depend linearly on the equilibrium gap, Y_e (Eq 3.4).

(vi) The tool diameter has its independent effect on the overcut, in ECM, under identical condition. Large sized tools produce more accurate holes.

(vii) For an accurate analysis of the electrochemical wire cutting process, considerations be given to the electrical resistance of the electrolyte within the side gaps i.e., use of 'Resistances in parallel' model (i.e. model-2) is recommended.

(viii) The analytical models proposed in this thesis are capable of explaining analytically, the nature of current density, temperature, electrolyte conductivity distribution,etc., within the IEG and lead to accurate computation of both the volumetric and linear metal removal rates in drilling, boring and wire cutting operations. The models are also capable of predicting accurately the anode profile obtained under the given set of working conditions.

(ix) Equation (3.2) is recommended for calculating interelectrode gap, metal removal rate and anode profile for both zero and finite feed rate. This equation gives results that are closer to experimental data, requires less computational time, simple to understand and easy to use.

9.2 SCOPE FOR FUTURE WORK

The work embodied in this thesis can be extended in the following directions:

(i) For better accuracy, two and three dimensional analysis of the ECM and other related processes can be developed using isoparametric and higher order elements.

(ii) Two and three dimensional heat transfer analysis of the process could give more accurate results.

(iii) Extensive data should be collected about the machining efficiency η, E, etc. of different materials under different situations, so that accurate prediction about anode profile could be made possible.

(iv) Theoretical analysis of ECWCP developed in this thesis should be tested experimentally.

(v) Experimental and analytical studies should be conducted to predict the profile in stagnation zone, so far ignored by most of the researchers.

(vi) Optimization of process parameter in different processes based on EC dissolution principle may be done with a view to obtain minimum overcut or best possible dimensional accuracy.

(vii) Theoretical models should be modified to account for the metallurgical and other parameters as discussed in chapter 2.

(viii) Extensive analytical and experimental work is needed to explore the feasibility of the use of tool bits for industrial problems.

REFERENCES

1. Adler, Yu.P. et al., The design of experiments to find optimal conditions, Mir Publishers, Moscow (1975).

2. Albal, S.V., Analysis and parametric study of machine tool columns using the finite element method, Thesis (Ph.D), I.I.T. Bombay (1977).

3. Alekseev, G.A. et al., Determining cathode shape for electrochemical machining, Machines & Tooling, 39, 6 (1976) 15-17.

4. Arantsev, V.A. et al., New electrolyte delivery method in electrochemical machining, Russ. Engg. J. 52, 11 (1972) 48-49.

5. Atkinson, J. and C.F. Noble, Residual stresses in workpiece after peripheral electrochemical grinding, Proc. Int. MTDR Conf. pp 525-532.

6. Bahl, R.C., Rigidity analysis and optimization of machine tool structures, Thesis (Ph.D), University of Roorkee, India (1977).

7. Bannard, John, Electrochemical machining - useful corrosion, Trans. SAEST 12, 1 (1977) 1-13.

8. Idem, Electrochemical machining, J. App. Electrochem. 7 (1977) 1-29.

9. Idem, Effects of surface finish obtained by electrochemical machining on the fatigue life of some titanium alloys, ibid 4 (1974) 229-234.

10. Idem, The effect of a surface-active additive on the dissolution efficiency and surface finish in ECM, ibid 7 (1977) 189-195.

11. Idem, Effect of flow on the dissolution efficiency of mild steel during ECM, ibid 7 (1977) 267-270.

12. Idem, The use of surface active additives in electrochemical machining electrolytes, ibid 4 (1974) 117-124.

13. Idem, The use of electrochemical machining in biomedical engineering, ibid 5 (1975) 89-90.

14. Bannard, John, Effect of density of the electrical conductance of aqueous sodium chloride solutions, J. App. Electrochem. 5 (1975) 43-53.

15. Idem, Fine hole drilling using electrochemical machining, Proc. 19th Int. MTDR Conf. (1978) 503-510.

16. Bannard, J.E., J.R. Treble and P.A. Brook, The electrochemical machining of titanium in non-aqueous electrolytes (Private communication).

17. Bannard, J. and L. Bannard, Bibliography of electrochemical machining, Department of Metallurgy and Material Science, University of Nottingham, (U.K.), 1975.

18. Bannard, J.E., P.J. Boden and P.A. Brook, The workpiece/electrolyte interaction during electrochemical machining, Proc. Conf. Electrical Methods of Machining, Forming and Coating 18-20 Nov. (1975) 147-153.

19. Bathe, K.J. and E.L. Wilson, Numerical methods in finite element analysis, Prentice Hall of India Pvt. Ltd., New Delhi (1978).

20. Bathe, K.J. et al. (Ed.), Preface in Proc. U.S. - German symposium on formulation and computational algorithms in finite element analysis (1978) ix-xii.

21. Bergsma, F., Electrochemical machining of metals, Annals CIRP 16 (1968) 93-99.

22. Bewley, L.V., Two dimensional fields in electrical engineering, Dover (1963).

23. Bhatia, S.M., Effects of electrolyte conductivity on ECM process, M. Tech. Dissertation, IIT Bombay (1971).

24. Bhatia, S.M. et al., Effect of some variables on ECM accuracy, J. Inst. Engrs(I) 58, Pt ME 2-3 (1977) 84-87.

25. Bhattacharyya, A., B. Sur and S.K. Sorkhel, Analysis for optimum parametric combination in electrochemical machining, Annals CIRP 22/1 (1973) 59-60.

26. Bhirud, L.L., Matrix operations on the computer, Oxford and IBH Pub. Co. New Delhi (1975).

27. Boden, P.J. and P.A. Brook, Electrochemical principles of ECM, The Production Engineer, (Sept. 1969) 408-417.

28. Box, G.E.P. and K.B. Wilson, On the experimental attainment of optimum conditions, J. Royal Stat. Soc. Sr. B 13, 1 (1951) 1-45.

29. Box G.E.P. and J.I. Hunter, Multifactorial experimental design, Ann. Math. Stat. 28 (1957).

30. Capello, G., et al., A new approach by electrochemical finishining of hardened cylinderical gears tooth face, Annals CIRP 28/1 (1979) 103-107.

31. Chetty, O.V., S.C.Das and G. Ramakrishnan, Some aspects of electrochemical machining, J. Inst. Eng.(I), ME 3, 55 (1975) 180-183.

32. Chetty, O.V. and S.C. Das, Electrochemical machining, ibid, ME 5, 52 (1972) 316-319.

33. Chetty, O.V. et al., A study of surface production in ECM, Proc. 8th AIMTDR Conf. (1978) 562-565.

34. Chetty, O.V. et al., Surface studies in ECM using a relocating machining fixture, Int. J. Mach. Tool Des. & Res. 18 (1978) 1-8.

35. Chikamori, K., Cell voltage vs current density curves during electrolysis of NaCl solution, Denki Kagaku 41, 4 (1973) 275-280.

36. Idem, Improvements in a $NaNO_3$ electrolyte for electrochemical machining by the addition of $(NH_4)_2SO_4$, $NaBrO_3$, $NaClO_3$, etc., ibid 39, 6 (1971) 493-496.

37. Chikamori, K. and S. Ito, Electrolyte dissolution of mild steel in high current density region, ibid 38, 7 (1970) 492-495.

38. Idem, Electrochemical machining in stagnant electrolyte, Int. Conf. Prod. Engg., New Delhi (1977) viii 31 - viii 39.

39. Chikamori, K., S. Ito and F. Sakurai, Flow of electrolyte in electrochemical die sinking, Bull. Japan Soc. Prec. Engg. 2, 4 (1968) 318-324.

40. Chin, D.T., Dissolution of mild steel with a rotating ring hemispherical electrode, J. Electrochem. Soc. 121, 12 (1974) 1592-1595.

41. Idem, Characterization of the deposition of iron-oxide on a platinum ring electrode, ibid 124, 4 (1974) 528-531.

42. Chin D.T., Anodic films and ECM dimensional control: A study of steel electrodes in solutions containing Na_2SO_4 and $NaClO_4$, ibid 119, 8 (1972) 1043-1048.

43. Chin D.T., Anodic mechanism of electrochemical machining: Study of current transient on a rotating electrode, ibid 118, 1 (1971) 174-179.

44. Chin, D.T. and A.J. Wallace, Anodic current efficiency and dimensional control in electrochemical machining, ibid 120, 11 (1973) 1487-1493.

45. Christiansen, S. and H. Rasmuseen, Numerical solutions for two dimensional annular electrochemical machining problems, J. Inst. Maths. Applics. 18 (1976) 295-307.

46. Clark, W.G. and J.A. McGeough, Temperature distribution along the gap in electrochemical machining, J. App. Electrochem. 7 (1977) 277-286.

47. Cochran, W.G. and G.M. Cox, Experimental design, Asia Publishing House, New Delhi (1962).

48. Cole, R.R., Basic research in electrochemical machining - Present status and future directions, Int. J. Prod. Res. 4, 2 (1965) 75-85.

49. Collett, D.E., R.C. Hewson Browne and D.W. Windle, A complex variable approach to electrochemical machining problems, J. Engg. Math. 4, 1 (1970) 29-37.

50. Cook, N.H., G.B. Foote, P. Jordan and B.N.Kalyani, Experimental studies in electrochemical machining, J. Engg. Ind., Trans. ASME (Nov. 1973) 945-950.

51. Cornor, J.J. and C.A. Brebbia, Finite elements technique for fluid flow, Newnes Butterworths, London (1976).

52. Cuthbertson, J.W. and T.S. Turner, Electrochemical machining - Some further studies of process variables, The Production Engineer 46(1976) 24-31.

53. Davies, O.L. (Editor), The design and analysis of industrial experiments, Longman Group Ltd., London (1956).

54. Davies, O.L. and W.A. Hay, The construction and uses of fractional factorial design in industrial research, Biometrika (Sept. 1950) 233-249.

55. Datta, M. and D. Landolt, On the influence of electrolyte concentration, pH and temperature on surface brightening of nickel under ECM conditions, J. App. Electrochem. 7 (1977) 247-252.

56. Idem, Stoichiometry of anodic nickel dissolution in NaCl and $NaClO_3$ under active and transpassive conditions, Corrosion Science 13 (1973) 187-197.

57. Datta, M. and D. Landolt, Film breakdown on nickel under transpassive dissolution conditions in sodium nitrate solutions, J. Electrochem. Soc. 124, 4 (1977) 483-489.

58. Idem, Surface brightening during high rate nickel dissolution in nitrate electrolytes, ibid 122, 11 (1975) 1466-1472.

59. De Barr, A.E. and D.A. Oliver (Ed.), Electrochemical machining, Macdonald and Co. Ltd. 1975 (Reprint).

60. Desai C.S. and J.F. Abel, Introduction to the finite element method, Affiliated East West Press Pvt.Ltd., New Delhi (1977).

61. Dietz, H., K.G. Gunther and K. Otto, Reproduction accuracy with electrochemical machining: Determination of the side gap, Annals CIRP 22/1 (1973) 61-62.

62. Dietz, H., et al., Electrochemical turning considerations on machining rates which can be attained, Annals CIRP 28/1 (1979) 93-97.

63. Ebeid, S.J., E.M. Baxter and C.N. Larsson, Further effects of process parameters on the incidence of sparking in electrochemical machining, Proc. 19th Int. MTDR Conf. (1978) 511-516.

64. Egorov, A.M. and A.S. Titov, Electrochemical machining for rounding-off complex shaped workpiece, Russ. Engg. J. 52 (1972) 44-46.

65. Evans, J.M., P.J. Boden and A.A. Baker, Effects of surface finish produced during ECM upon the fatigue life of nimonic 80A, Proc. 12th Int. MTDR Conf. (1972) 271-277.

66. Federer, W.T., Experimental design, Oxford and IBH Pub. Co., New Delhi (1963).

67. Fitz-Gerald J.M. and J.A. McGeough, A model for the mechanism controlling surface finish in electrochemical machining, Proc. Conf. Electrical Methods of Machining, Forming and Coating, London (1970) 72-81.

68. Flatt, R.K. and P.A. Brook, The effect of anion concentration on the anodic polarization of copper, zinc and brass, Corr. Sci., 11 (1971) 185-196.

69. Flatt, R.K., R.W. Wood and P.A. Brook, The concentration profiles in solution at dissolving anode surfaces (1) zinc, copper and brasses by the freezing technique, J.App. Electrochem. 1 (1971) 35-39.

70. Fluerenbrock, F., R.D. Zerkle and J.F. Thorpe, Verification of a one dimensional two phase flow model of the frontal gap in electrochemical machining, J. Engg. Ind., Trans. ASME 98, 2 (1976) 431-437.

71. Idem, Compressibility effects in electrochemical machining, ibid 423-430.

72. Ganesh, S. and T.S. Ranjan, Nomographic approach for planning in ECM, J. Inst. Eng (I) ME 4, 59 (1979) 200-204.

73. Gupta, C.P. and R. Prakash, Engineering heat transfer, Nemchand & Bros., Roorkee, India (1971).

74. Heitman, H., Surface roughness formation and determination of optimum working conditions in electrochemical die sinking, Proc. 2nd AIMTDR Conf. (1968) 41-47.

75. Hewson-Browne, R.C., Further applications of complex variable methods to electrochemical machining problems, J. Engg. Math. 5, 4 (1971) 233-240.

76. Hoare, J.P., Oxide film studies on iron in electrochemical machining electrolytes, J. Electrochem. Soc. 117, 1 (1970) 142-145.

77. Idem, Anodic polarization studies on soft iron in some concentrated salt solutions, Nature 219, 5158 (1968) 1034-1035.

78. Hoare, J.P., A.J. Chartrand and M.A. LaBoda, Electrochemical machining of high temperature alloys in NaClO$_3$ solutions, ibid 120, 8 (1973) 1072-1077.

79. Hoare, J.P. and C.R. Wiese, Current efficiency during the electrochemical machining of iron and nickel, Corr. Sci. 15 (1975) 435-440.

80. Hoare, J.P. and K.W. Mao, Anion effects on the dissolution of steel in ECM binary electrolyte systems, J. Electrochem. Soc. 120, 11 (1973) 1452-1456.

81. Hoare, J.P., K.W. Mao and A.J. Wallace, ECM behaviour of steel in NaClO$_4$ electrolytes, Corrosion 27, 5 (1971) 211-215.

82. Hoare J.P. and M.A. LaBoda, Electrochemical machining, Res. Pub. General Motors Research 2427 (11 May 1977) 1-35.

83. Idem, Electrochemical machining, Scientific American 230, 1 (1974) 30-37.

98. Jain, V.K. and P.C.Pandey, Technical report of 8th AIMTDR Conference, Precision Engineering 1,4 (1979) 246.

99. Jain, V.K. and S.B.L.Garg, Application of dimensional analysis to the determination of mean width of primary shear deformation zone size, J. Inst. Engr.(I) ME 2, 59 (1978) 70-74.

100. Jackson, C., An ECM process for drilling deep hole, Met. Progr. 97 (March 1970) 106,108,110

101. Kapur, J.N. and S.C. Saxena, Mathematical statistics, S. Chand & Co., New Delhi (1970) 205-228.

102. Kapustin,V.A. et al., Machine for internal electrochemical machining of tubes, Machines and Tooling 48, 4 (1977) 37-38.

103. Kargin, G.V., Electrochemical machining of shaped surfaces on round components by tubular shaped cathode tools, Russ. Engg. J. 55, 116 (1975) 63-66.

104. Kargin, G.V., Electrochemical shaping using tubular section cathode tool, Russ. Engg. J. 55 (1975) 73-74.

105. Kawafune, K., Studies of electrochemical machining, Bull. Japan Soc. Mech. Engr. 11, 45 (1968) 554-569.

106. Kawafune, K., T. Mikoshiba and K. Noto, Effect of the working parameters on the working gap during electrochemical machining, Annals CIRP 18 (1970) 305-317.

107. Idem, Study on shape processed by ECM, ibid 16 (1968) 345-352.

108. Kawafune, K., T. Mikoshiba, K. Noto and K. Hirata, Accuracy in cavity sinking by ECM, ibid 15 (1967) 443-455.

109. Kinoshita, K., D. Landolt, R.H., Muller and C.W. Tobias, Stoichiometry of anodic copper dissolution at high current densities, J. Electrochem. Soc. 117, 10 (1970) 1246-1251.

110. König, W. and D. Pahl, Accuracy and optimal working conditions in ECM, Annals CIRP 18 (1970) 223-230.

111. Idem, Electrochemical machining of heat resistant alloys, ibid, 21 (1972) 43-44.

112. König, W. and H. Degenhardt, The influence of process parameters and tool electrode geometry on the development of the overcut in ECM with high current densities, Principles of Electrochemical Machining (Ed. C.L. Faust) Pub. Electrochem. Soc., N.J. (1971) 63-83.

70. Fluerenbrock, F., R.D. Zerkle and J.F. Thorpe, Verification of a one dimensional two phase flow model of the frontal gap in electrochemical machining, J. Engg. Ind., Trans. ASME 98, 2 (1976) 431-437.

71. Idem, Compressibility effects in electrochemical machining, ibid 423-430.

72. Ganesh, S. and T.S. Ranjan, Nomographic approach for planning in ECM, J. Inst. Eng (I) ME 4, 59 (1979) 200-204.

73. Gupta, C.P. and R. Prakash, Engineering heat transfer, Nemchand & Bros., Roorkee, India (1971).

74. Heitman, H., Surface roughness formation and determination of optimum working conditions in electrochemical die sinking, Proc. 2nd AIMTDR Conf. (1968) 41-47.

75. Hewson-Browne, R.C., Further applications of complex variable methods to electrochemical machining problems, J. Engg. Math. 5, 4 (1971) 233-240.

76. Hoare, J.P., Oxide film studies on iron in electrochemical machining electrolytes, J. Electrochem. Soc. 117, 1 (1970) 142-145.

77. Idem, Anodic polarization studies on soft iron in some concentrated salt solutions, Nature 219, 5158 (1968) 1034-1035.

78. Hoare, J.P., A.J. Chartrand and M.A. LaBoda, Electrochemical machining of high temperature alloys in $NaClO_3$ solutions, ibid 120, 8 (1973) 1072-1077.

79. Hoare, J.P. and C.R. Wiese, Current efficiency during the electrochemical machining of iron and nickel, Corr. Sci. 15 (1975) 435-440.

80. Hoare, J.P. and K.W. Mao, Anion effects on the dissolution of steel in ECM binary electrolyte systems, J. Electrochem. Soc. 120, 11 (1973) 1452-1456.

81. Hoare, J.P., K.W. Mao and A.J. Wallace, ECM behaviour of steel in $NaClO_4$ electrolytes, Corrosion 27, 5 (1971) 211-215.

82. Hoare J.P. and M.A. LaBoda, Electrochemical machining, Res. Pub. General Motors Research 2427 (11 May 1977) 1-35.

83. Idem, Electrochemical machining, Scientific American 230, 1 (1974) 30-37.

84. Hoare J.P. and M.A. LaBoda, Some effects of solution flow rate on the stability of anodic films on steel, Corrosion paper No. 108 (1976) 108/1-108/7.

85. Hoare, J.P., M.A. LaBoda, M.L. McMillan and A.J. Wallace, An investigation in the differences between NaCl and $NaClO_3$ as electrolytes in electrochemical machining, J. Electrochem. Soc. 116, 2 (1969) 199-203.

86. Hofstede, A. et al., Some remarks on electrochemical turning, Annals CIRP, 18 (1970) 93-106.

87. Hopenfield, J. and R.R. Cole, Electrochemical machining - prediction and correlation of process variables, J. Engg. Ind., Trans. ASME 88 (1966) 1-7.

88. Idem, Prediction of the one dimensional equilibrium cutting gap in electrochemical machining, J. Engg. Ind., Trans. ASME 91 (1969) 755-765.

89. Huebener, K.H., The finite element method for engineers, John Willey and Sons, New York (1975).

90. Hümbs, H.J., Electrochemisches senkin experimentelle und analytische Untersuchung der Prozeßzusammenhange Thesis (Ph.D.) T.H. Aachen, Germany (1975).

91. Ippolito, R., Effect of fluidodinamic conditions on the gap resistivity in ECM, Annals CIRP 24/1 (1975) 115-119.

92. Ippolito, R. and G. Fassolio, The workpiece shape in electrochemical machining of external profiles using coated electrodes, Int. J. MTDR 16 (1976) 129-136.

93. Isachenko, V.P. et al., Heat transfer, Mir Publishers, Moscow (1977).

94. Isaev, A.J., Electrochemical shaping of high strength bodies of rotation, Russ. Engg. J. 52, 5 (1972) 40-42.

95. Ito, S., H. Yamamoto and K. Chikamori, Study on electrolytic machining process (XII), J. Mech. Lab., Japan 13, 1 (1967) 15-24.

96. Ito, S., K. Chikamori and T. Hayashi, Studies on electrolytic machining process (IV), J. Mech. Lab., Japan 10, 2 (1964) 33-41.

97. Ito, S. and K. Seimiya, Hydraulic approach to electrolyte flow in electrochemical machining, Proc. 12th Int. MTDR Conf. (1972) 259-263.

98. Jain, V.K. and P.C.Pandey, Technical report of 8th AIMTDR Conference, Precision Engineering 1,4 (1979) 246.

99. Jain, V.K. and S.B.L.Garg, Application of dimensional analysis to the determination of mean width of primary shear deformation zone size, J. Inst. Engr.(I) ME 2, 59 (1978) 70-74.

100. Jackson, C., An ECM process for drilling deep hole, Met. Progr. 97 (March 1970) 106,108,110

101. Kapur, J.N. and S.C. Saxena, Mathematical statistics, S. Chand & Co., New Delhi (1970) 205-228.

102. Kapustin,V.A. et al., Machine for internal electrochemical machining of tubes, Machines and Tooling 48, 4 (1977) 37-38.

103. Kargin, G.V., Electrochemical machining of shaped surfaces on round components by tubular shaped cathode tools, Russ. Engg. J. 55, 116 (1975) 63-66.

104. Kargin, G.V., Electrochemical shaping using tubular section cathode tool, Russ. Engg. J. 55 (1975) 73-04.

105. Kawafune, K., Studies of electrochemical machining, Bull. Japan Soc. Mech. Engr. 11, 45 (1968) 554-569.

106. Kawafune, K., T. Mikoshiba and K. Noto, Effect of the working parameters on the working gap during electrochemical machining, Annals CIRP 18 (1970) 305-317.

107. Idem, Study on shape processed by ECM, ibid 16 (1968) 345-352.

108. Kawafune, K., T. Mikoshiba, K. Noto and K. Hirata, Accuracy in cavity sinking by ECM, ibid 15 (1967) 443-455.

109. Kinoshita, K., D. Landolt, R.H., Muller and C.W. Tobias, Stoichiometry of anodic copper dissolution at high current densities, J. Electrochem. Soc. 117, 10 (1970) 1246-1251.

110. König, W. and D. Pahl, Accuracy and optimal working conditions in ECM, Annals CIRP 18 (1970) 223-230.

111. Idem, Electrochemical machining of heat resistant alloys, ibid, 21 (1972) 43-44.

112. König, W. and H. Degenhardt, The influence of process parameters and tool electrode geometry on the development of the overcut in ECM with high current densities, Principles of Electrochemical Machining (Ed. C.L. Faust) Pub. Electrochem. Soc., N.J. (1971) 63-83.

113. König W. and H.J. Hümb, Mathematical model for the calculation of the anode in electrochemical machining, Annals CIRP 25 (1977) 83-87.

114. König, W. and P. Lindenlauf, Surface generation in electrochemical machining, Annals CIRP 27/1 (1978) 97-100.

115. Kops, L., Effect of pattern of grain boundary network on metal removal rate in electrochemical machining, ibid 25/1 (1976) 125-130.

116. Kops, L. and V.B. Quach, Investigation on the role of workpiece grain size in electrochemical machining process, J. Engg. Ind., Trans. ASME 98 (1976) 360-368.

117. Krabacher, E.J., W.A. Hoggerty, C.R. Allison and M.F. Davis, Electrical methods of machining, Proc. Int. Con. Prod. Res. (ASME) (1962) 232-241.

118. Krylov, A.L., The Cauchy problem for the Laplace equation in the theory of electrochemical metal machining, Soviet Physics-Dokledy 13,1 (1968) 15-17.

119. Kuo, H.C. and D. Landolt, Rotating disc electrode study of anodic dissolution of iron in concentrated chloride media, Electrochemica Acta 20 (1975) 393-399.

120. Kuhn, A.T. (Ed), Industrial electrochemical processes, Elsevier Publishing Co. (1971) 263-326.

121. Kumar, B., Study of ECM process, Proc. 8th AIMTDR Conf. (1978) 550-553.

122. Kuppuswamy, G., Magnetic field on electrolytic grinding, Proc. 8th AIMTDR Conf. (1978) 546-549.

123. Idem, Electrochemical grinding: An investigation of the metal removal rate, Proc. 7th AIMTDR Conf. (1976) 337-340.

124. LaBoda M.A. and J.P. Hoare, Intricate pattern ECM on ferrous alloys, J. Electrochem. Soc. 122, 11 (1975) 1489-1491.

125. LaBoda, M.A., J.P. Hoare and S.E. Beacam, The importance of the electrolyte in electrochemical machining, Collection of Czechoslovak communication 36 (1971) 680-688.

126. Landolt, D., Throwing power measurements during high rate nickel dissolution under active and transpassive conditions, ibid 119, 6 (1972) 708-712.

113. König W. and H.J. Hümb, Mathematical model for the calculation of the anode in electrochemical machining, Annals CIRP 25 (1977) 83-87.

114. König, W. and P. Lindenlauf, Surface generation in electrochemical machining, Annals CIRP 27/1 (1978) 97-100.

115. Kops, L., Effect of pattern of grain boundary network on metal removal rate in electrochemical machining, ibid 25/1 (1976) 125-130.

116. Kops, L. and V.B. Quach, Investigation on the role of workpiece grain size in electrochemical machining process, J. Engg. Ind., Trans. ASME 98 (1976) 360-368.

117. Krabacher, E.J., W.A. Hoggerty, C.R. Allison and M.F. Davis, Electrical methods of machining, Proc. Int. Con. Prod. Res. (ASME) (1962) 232-241.

118. Krylov, A.L., The Cauchy problem for the Laplace equation in the theory of electrochemical metal machining, Soviet Physics-Dokledy 13,1 (1968) 15-17.

119. Kuo, H.C. and D. Landolt, Rotating disc electrode study of anodic dissolution of iron in concentrated chloride media, Electrochemica Acta 20 (1975) 393-399.

120. Kuhn, A.T. (Ed), Industrial electrochemical processes, Elsevier Publishing Co. (1971) 263-326.

121. Kumar, B., Study of ECM process, Proc. 8th AIMTDR Conf. (1978) 550-553.

122. Kuppuswamy, G., Magnetic field on electrolytic grinding, Proc. 8th AIMTDR Conf. (1978) 546-549.

123. Idem, Electrochemical grinding: An investigation of the metal removal rate, Proc. 7th AIMTDR Conf. (1976) 337-340.

124. LaBoda M.A. and J.P. Hoare, Intricate pattern ECM on ferrous alloys, J. Electrochem. Soc. 122, 11 (1975) 1489-1491.

125. LaBoda, M.A., J.P. Hoare and S.E. Beacam, The importance of the electrolyte in electrochemical machining, Collection of Czechoslovak communication 36 (1971) 680-688.

126. Landolt, D., Throwing power measurements during high rate nickel dissolution under active and transpassive conditions, ibid 119, 6 (1972) 708-712.

127. Landolt, D., R. Acosta, R.H. Muller and C.W. Tobias, An optical study of cathodic hydrogen evolution in high rate electrolysis, J.Electrochem. Soc., 117, 6(1970) 834-845.

128. Landolt, D., R.H. Muller and C.W. Tobias, Anode potentials in high rate dissolution of copper, ibid 118, 1 (1971) 40-46.

129. Idem, Crystallographic factors in high rate anodic dissolution of copper, ibid 36-40.

130. Idem, High rate anodic dissolution of copper, ibid 116, 10 (1969) 1384-1390.

131. Lapides, L.M. et al., A control system for electrochemical machining processes under cylic operating conditions, Machines and Tooling 49, 4 (1978) 32-36.

132. Larsson, C.N. and E.M. Baxter, Tool damage by sparking in ECM, Proc. 18th Int. MTDR Conf. (1977) 499-505.

133. Idem, Electrochemical drilling- tool life and feed rate, Proc. IEE Conf. on Electrical Methods of Machining, Forming and Coating (1975) 161-168.

134. Larsson, C.N. and K. Muzaffaruddin, Electrochemical effects on shape reproduction in ECM, Proc. 19th Int. MTDR Conf. (1978) 533-540.

135. Levy, S. Forced convection subcooled boiling - prediction of vapour volumetric fraction, Int. J. Heat & Mass Transfer 10 (1967) 951-965.

136. Loutrel, S.P. and N.H. Cook, Sodium chloride electrolyte data at high temperature and pressure, J. Engg. Ind., Trans. ASME 95 (1973) 997-1002.

137. Idem, A theoretical model for high rate electrochemical machining, ibid, 1003-1008.

138. Idem, High rate electrochemical machining, ibid, 992-996.

139. Maeda, S., N. Saito and S. Arai, Studies on electrochemical machining (1st report) - apparent specific resistance and machining accuracy, Bull. JSPE 2, 2 (1967) 126-131.

140. Mahalingam, V. and V.C. Venkatesh, Measurement of anodic potential in ECM and its relation to surface finish, Proc. 7th AIMTDR Conf. (1976) 341-344.

141. Mao, K.W., M.A. LaBoda and J.P. Hoare, Anodic film studies on steel in nitrate based electrolytes for electrochemical machining, J. Electrochem. Soc. 119, 4 (1972) 419-427.

142. Martin, H.C. and G.F. Carey, Introduction to finite element analysis, Tata McGraw Hill Pub. Co., New Delhi (1975).

143. Mashnostroeniya, V., Electrochemical shaping using tubular section cathode tools, Russ. Engg. J. 55, 4 (1975) 73-74.

144. Idem, Electrochemical machining of shaped surfaces on round components by tubular shaped cathode tools, ibid 55, 11 (1975) 65-66.

145. Idem, Methods of cleaning ECM electrolytes, ibid 54, 4 (1974) 77-78.

146. Idem, Electrochemical piercing of holes in mono and polycrystalline alloys, ibid 75-76.

147. McCormick, J.M. and M.G. Salvadori, Numerical methods in fortran, Prentice Hall of India Pvt. Ltd., New Delhi (1971).

148. McGeough, J.A., Principles of electrochemical machining, Chapman & Hall, London (1974).

149. McGeough, J.A., Some effects of carbon content on the efficiency of electrochemically machined carbon steels and cast iron, Int. J. Prod. Res. 9, 2 (1971) 311-316.

150. McGeough, J.A. and H. Rasmuseen, Theoretical analysis of electrochemical machining process, J. Engg. Ind., Trans. ASME Paper No. 69-WA/Prod-10.

151. Idem, A perturbation analysis of the electroforming process, J. Mech. Engg. Sci. 18, 6 (1976) 271-278.

152. Idem, On the derivation of the quasi steady model in electrochemical machining, J. Inst. Maths. Appls. 13 (1974) 13-21.

153. Meleka, A.H., The applications of electrochemical machining, Proc. Conf. Machinability, Iron & Steel Institute (1965) 221-224.

154. Merchant, M.E., Newer methods for the precision working of metals - research and present status, Proc. Int. Conf. Prod. Res. (ASME) (1962) 93-107.

156. Moir, P.J. and S.J. Harvey, Electrochemical machining of curved long flow path profiles, Proc. 16th Int. MTDR Conf. (1976) 283-289.

157. Idem, Some effects of the electrolyte flow rates on the electrochemical machining process, ibid 275-281.

158. Molloy, J., Comparison between electrochemical and conventional methods of machining complex shapes, Machinery and Production Engg. (Jan. 5, 1966) 13-17.

159. Idem, Electrochemical machining, ibid 107 (1965) 1027-1034.

160. Idem, Electrochemical machining of a turbine blade, ibid 1198-1203.

161. Moore, A.I.W., Have you considered ECM?, Electrical Review 198, 1 (1976) 19-21.

162. Moroz, I.I., Recommendations for selecting electrolytes for electrochemical machining, Machines & Tooling 49 1 (1978) 43-45.

163. Idem, Basic problems and development trends of electrochemical machining methods, ibid, 48, 1 (1977) 36-37.

164. Morozov, B.I., Electrolyte regeneration in vibrating cathode electrochemical machining equipment, Machines & Tooling 45, 6 (1974) 27-28.

165. Mukherjee, S., Electrochemical turning, J. Inst. Eng (I) ME 4, 57 (1977) 210-211.

166. Mukherjee, S.K., et al., Analysis of electrochemical turning, Proc. 8th AIMTDR Conf. (1978) 554-557.

167. Muller, H.H., The state of the art in the Chem-Milling technique for refractory alloys, Machinery (July 1963) 105-109.

168. Nanyakkara, M.B. and C.N. Larsson, Computation and verification of workpiece shape in electrochemical machining, Proc. 20th Int. MTDR Conf. (1979) 617-623.

169. Nastasii, V.K. and A.N. Safronov, Power supplies, control systems and protective devices for electrochemical diesinking machines, Machines and Tooling 48, 9 (1977) 40-42.

170. Nilson, R.H. and Tsuei, Y.G., Free boundary problem of ECM by alternating field technique on inverted plane, Comp. Meth. App. Mech. and Eng. 6 (1975) 265-282.

171. Idem, Free boundary problem for the Laplace equation with application to ECM tool design, J. App. Mech., Trans. ASME 98, 1 (1976) 54-58.

172. Idem, Inverted Cauchy problems for the Laplace equation in engineering design, J. Eng. Math. 8, 4 (1974) 329-337.

173. Noto, K., H. Okudaira and K. Kawafune, The working gap in electrochemical machining using sodium nitrate solution, Annals CIRP 22, 1 (1973) 63-64.

174. Olenchich, V.P., et al., Electrochemical machining of gears, Machines and Tooling 46, 7 (1975) 59-60.

175. Olsen, G.H., Field plotting, Wireless World 168, 2 (1962) 58-64.

176. Opitz, H., Electrochemical machining processes, Proc. Int. Conf. on Prod. Res. (ASME) (1962) 225-231.

177. Oswal, A.K., Some investigations on metal removal in electrochemical machining at low current densities, Thesis (M.E.), University of Roorkee, India (1973).

178. Paustovskii, A.V. et al., How ECM affects the surface layer of steel, Machines & Tooling 44, 12 (1973) 52-54.

179. Petrov, Yu. N. et al., Electrochemical piercing of holes in V.K. type cemented carbides, Russ. Engg. J. 52, 10 (1972) 54-57.

180. Petrusenka, V.S. et al., Electrochemical diamond grinding of HSS tools, Machines & Tooling 48, 10 (1977) 42-43.

181. Plackett, B.R. and J.P. Burman, The design of optimum multifactorial experiments, Biometrika, 33 (1943-1946) 305-325.

182. Pramanik, D.K., Effect of heat treatment on ECM productivity, Machinery & Prod. Engg. (March 1975) 224-226.

183. Idem, Anode efficiency of materials in different heat treated condition in ECM, Proc. 8th AIMTDR Conf. (1978) 558-561.

184. Pramanik, D.K. and A.K. Dey, Determination of the relative influence of the process variables on overcut in ECM, Proc. 7th AIMTDR Conf. (1976) 349-351.

185. Pramanik, D.K. et al., Studies in the electrolytic pressure distribution in the working gap in ECM using plane parallel electrodes, J. Inst. Eng.(I) ME 5, 57 (1977) 250-253.

186. Ramani, A. V. et al., Electroforming - A process to form complex shapes, Proc. 7th AIMTDR Conf. (1976) 53/ 56.

187. Ramani, A.V. et al., Electrochemical machining - Developments in N.A.L., Proc. 7th AIMTDR Conf. (1976) 357-360.

188. Ranganathan,V., Electrochemical grinding of titanium, Proc. 7th AIMTDR Conf. (1976) 365-368.

189. Rasch, F.O., Recent developments in electrochemical machining, Mecanique No. 303 Mars (1975) 12-14.

190. Rasch, F.O., K.G. Günther and W. König, Summary report of cooperative research, Annals CIRP 27/2 (1978) 561-564.

191. Rasmuseen, H. and S. Christiansen, A perturbation solution for a two dimensional annular electrochemical machining problem, J. Inst. Math. Applics 18 (1976) 149-153.

192. Rolsten, R.F. and E.J. Manning, Electrochemical deburring, The Tool and Manufacturing Engineer (1969) 14-16.

193. Rourke J.W. and D.C.Kennedy, Electrochemical turning - a general purpose machine, Proceeding 2nd Int.Conf. on Development of Production Systems held at Copenhegan Denmark 27-31 (Aug. 1973) 161-172.

194. Segerlind, J., Applied finite element analysis, John Wiley & Sons Ltd. New York (1976).

195. Seimiya, K. and S. Ito, A control system for electrochemical machining using a mini computer, Proc. 14th Int. MTDR Conf. (1974) 575-578.

196. Idem, Characteristics of ultrasonic waves evolved by cavitation in electrochemical machining, Proc. Int. Conf. Prod. Eng. held at Tokyo (1974) 62-67.

197. Shaw, M.C., Analysis and lubrication of bearings, McGraw Hill Book Co. (1949) CH.3.

198. Simpson, J.P. and P.A. Brook, The anodic dissolution of iron chromium alloys, J. App. Electrochem. 4 (1974) 163-167.

199. Smith, H. and A. Rose, Subjective response in process investigations, Industrial and Engg. Chemistry 55, 7 (1963) 25-28.

200. Sorkhel, S.K., Analysis of various process parameters of electrochemical machining, Thesis (Ph.D.), Jadavpur University (1979) India.

201. Sorkhel, S., et al., Electrochemical machining, Proc. 5th AIMTDR Conf. (1972) 651-656.

202. Idem, Passivity reduction in ECM process, Proc. 7th AIMTDR Conf. (1976).

203. Stronach, A.F. et al., Experimental and numerical analysis of the pressure distribution in electrochemical machining, Int. J. Mech. Scie. 18 (1976) 261-268.

204. Teterev, A.G. et al., Assessing errors in the electrochemical machining of curvilinear slots, Machines & Tooling 41, 7 (1970) 43-46.

205. Thorpe, J.F., Operating characteristics of electrochemical machining, Fertingung 6, 2 (1975) 47-50.

206. Thorpe, J.F. and R.D. Zerkle, A theoretical analysis of the equilibrium sinking of shallow, axial symmetric cavities, Fundamentals of Electrochemical Machining (Ed. C.L. Faust) Pub. Electrochem. Soc., N.J. (1971) 1-39.

207. Idem, Analytical determination of the equilibrium electrode gap in electrochemical machining, Int.J. Mach. Tool Des. Res. 9 (1969) 131-144.

208. Tipton, H., The detemination of tool shape for electrochemical machining, Machinery & Production Engg. (Feb. 14, 1968) 325-328.

209. Idem, Metal machining improved by electrical methods, Electrical Review (12 March, 1965) 404-406.

210. Idem, The determination of shape of tools for use in electrochemical machining, Res. Report No. 40 (1971) MTIRA (U.K.).

211. Idem, The calculation of tool shapes for electrochemical machining, Fundamentals of Electrochemical Machining (Ed. C.L. Faust) Pub. Electrochem. Soc., N.J. (1971) 87-102.

212. Idem, The dynamics of electrochemical machining, Proc. 5th Int. MTDR Conf. (1964) 509-522.

213. Tipton, H., Tool design for electrochemical machining, Machinery & Production Engg. (1968) 869-871.

214. Tsuei, Y.G. et al., Theoretical and experimental study of workpiece geometry in electrochemical machining, (Private communication).

215. Tsuei Y.G. and R.H. Nilson, Effects of variable electrolyte conductivity on side gap geometry in ECM, Int. J. Mach. Tool Des. Res. 17 (1977) 169-178.

216. Turner, M. and P.A.Brook, The anodic behaviour of copper in static and flowing hydrochloric acid solutions, Corr. Sci. 13 (1973) 973-983.

217. Idem, Some observations on electropolishing of copper, electroplat. and Sur. Treat. 2 (1973/74) 245-248.

218. Turner, M., G.E. Thompson and P.A. Brook, The anodic behaviour of nickel in sulphuric acid solution, Corr. Sci. 13 (1973) 985-991.

219. Vasileve, V.V., Optimizing the conditions for the electrochemical machining of medium carbon steel, Machines & Tooling 46, 9 (1975) 43.

220. Vestnik Mashino Stroeniya, Electrochemical shaping using tubular section cathode tools, Russ. Engg. J. 55, 4 (1975) 73-74.

221. Vitkovitch, D. (Ed), Field analysis, experimental and computational methods, Van Nostrand (1966).

222. Vogel, A.I., A text book of qualitative analysis, Longmans Green and Co., London (1951), 3rd Ed.

223. Volkov, Yu. S., The laws governing contactless electrochemical forming, Machines & Tooling 48, 9 (1977) 38-39.

224. Walton, M.E. and P.A. Brook, The dissolution of Cu-Ni alloys in hydrochloric acid-1 rotating disc electrode measurements, Corr. Sci. 17 (1977) 317-328.

225. Idem, The dissolution of copper nickel alloys in hydrochloric acid-II stationary electrodes and impedance measurements, ibid 593-602.

226. Wicks, C.H., Electrical and chemical machining methods, Machinery & Prod. Engg. 116 (11th Feb. 1970) 212-215.

227. Wicks, C.H., Advances in electrochemical machining, ibid, (25th Feb. 1970) 288-291.

228. Wilkinson, B.H. and P. Warburton, Electrochemical machining, Proc. Machinability Conf., Iron & Steel (1965) 215-220.

229. Wilson, J.F., Practice and theory of electrochemical machining, Wiley Interscience, New York (1971).

230. Yuan, S.W., Fundamentals of Fluid Mechanics, Prentice Hall of India Pvt. Ltd., New Delhi (1976).

231. Zienkiewicz, O.C., The finite element method, McGraw Hill Book Co., London (1977).

232. Zienkiewicz, O.C. and Y.K. Cheyung, Finite element in the solution of field problems, The Engineer (Sept. 24, 1965).

233. Zompi, A. and R. Ippolito, Voltage current relationships in ECM analysis of experimental data and model evaluation, Proc. Int. Conf. Prod. Engg., New Delhi (1978) vii20-viii-30.

234. Anon, Precision comes to electrochemical machining, Published by Technical Information Department, General Motor Research Laboratories Warren, Michigan.

235. Anon, ECM constant current machining, Machine Tool Review 63, 67 (1975).

236. Anon, Sizing forgings with electrochemical machining, Am. Mach. 111 (1967) 158-159.

237. Anon, ECM - not only for aerospace, Machine Tool Review 63, 363 (1975).

238. Electrochemical Machining - PERA Report No. 145, 1965.

TABLE-1

Comparison of Eq(2.10), Eq(3.2) and Experimental data for Anode Shape Prediction, t=300 s, Δt=30 s , *x=21.5 mm

Test No.	x mm	Y(mm) x10^{-1} Eq(2.10)	Y(mm) x10^{-1} Eq(3.2)	Temperature rise in °C. Eq(2.10) Y_o=0.8	Temperature rise in °C. Eq(3.2) Y_o=0.8	Expt.	J(Am/mm^2) Eq(2.10)	J(Am/mm^2) Eq(3.2)	K(Ω-mm)$^{-1}$ x 10^{-1} Eq(2.10)	K(Ω-mm)$^{-1}$ x 10^{-1} Eq(3.2)	MR$_1$(mm) Eq(2.10)	MR$_1$(mm) Eq(3.2)
6	7.0	7.8500	7.8477	5.2595	5.2623	5.0	0.3709	0.3712	0.1560	0.1561	0.4408	0.4410
	17.0	9.0419	9.0452	13.7024	13.6954	11.625	0.3706	0.3704	0.1799	0.1799	0.4415	0.4410
	22.0	9.7153	9.7192	18.4565	18.4422	15.0*	0.3711	0.3708	-	0.1933	0.4413	0.4410
7	7.0	3.4808	3.3670	5.7189	5.3100	-	0.5034	0.4854	0.1573	0.1567	0.6000	0.6050
	17.0	4.0584	4.0890	14.9660	15.0073	15.8687	0.5023	0.5060	0.1834	0.1840	0.6000	0.6058
	22.0	4.3841	4.3980	20.1821	20.4389	22.45*	0.5024	0.5039	0.1982	0.1983	0.6000	0.6030
8	7.0	5.0027	5.0018	6.3056	6.3067	11.8875	0.4687	0.4687	0.1590	0.1590	0.5640	0.5640
	17.0	5.9176	5.9177	16.6205	16.6175	-	0.4676	0.4675	0.1881	0.1881	0.5640	0.5639
	22.0	6.4426	6.4434	22.5309	22.5336	23.6*	0.4679	0.4680	0.2048	0.2048	0.5640	0.5641
9	7.0	5.9083	5.9097	7.4490	-	9.9375	0.4994	0.4995	0.1622	0.1622	0.6089	0.6090
	17.0	7.1881	7.1877	19.9007	-	22.5	0.4978	0.4977	0.1974	0.1974	0.6090	0.6089
	22.0	7.9424	7.9452	27.2433	-	26.0*	0.4985	0.4988	0.2181	0.2182	0.6090	0.6095
10	7.0	4.6961	4.6955	7.0750	-	10.2375	0.5015	0.5016	0.1612	0.1612	0.6089	0.6099
	17.0	5.6616	6.6587	18.8207	-	23.0	0.5001	0.4997	0.1943	0.1943	0.6090	0.6084
	22.0	6.2235	6.2265	25.6587	-	28.4*	0.5005	0.5008	0.2136	0.2137	0.6090	0.6093

TABLE -2

Identification number and Hardness of Work-materials.

Work material	Identification No.	Average hardness (BHN)
Mild steel	1-110	-
Low alloy steel(castings)	100-199	218
"	200-299	239
"	300-399	163
"	400-499	187
Low alloy steel(forgings)	500-599	168
"	600-699	218
"	700-799	220

TABLE - 3

WORK MATERIAL COMPOSITION

Test Pieces Numbers

Alloying element	100-199	200-299	300-399	400-499	500-599	600-699	700-799
	Low alloy steel castings				Low alloy steel forging		
C	0.135	0.094	0.223	0.234	0.202	0.379	0.535
S	0.012	0.018	0.015	0.011	0.072	0.017	0.016
P	0.017	0.020	0.020	0.014	0.016	0.018	0.018
Si	0.327	0.317	0.338	0.500	0.227	0.280	0.301
Mn	0.588	0.400	1.680	1.44	0.691	0.800	0.805
Ni	0.171	-	-	0.095	0.093	-	0.065
Cr	1.072	0.760	-	0.260	0.212	1.020	0.039
Mo	0.985	0.920	-	0.073	0.049	0.278	0.076
Cu	-	-	-	0.065	-	-	-
Al	0.004	-	-	0.055	-	-	-
Va	Very small	Very small	-	-	-	-	-
Other Impurities.	-	-	-	5 to 6			

TABLE - 4

Experimental Conditions Used During ECM Tests by Author

Work material	M.S., low alloy steel casting and low alloy steel forgings
Tool material	Brass
Tool diameter	7 mm to 18 mm
Mode of electrolyte supply.	Radial outward flow
Applied voltage	10-60 V
Electrolyte flow rate	6.7×10^{-5} to 15×10^{-5} $m^3.s^{-1}$
Electrolyte conductivity	0.003 to 0.011 $(\Omega\text{-mm})^{-1}$
Machining time	600 to 3600 s

TABLE - 5

Properties of Tool-materials

No.	Properties*	Material			
		Copper	Brass	Stainless steel	Titanium
1.	Electrical resistivity	1.0	4.0	53.0	48.0
2.	Stiffness	1.1	1.0	1.9	1.1
3.	Machinability	6.0	8.0	2.5	1.0
4.	Thermal conductivity	25.0	7.5	1.0	1.6

*Properties are given in relative terms.

TABLE 6

5 $\overset{*}{X}$- variables N = 32 treatment combinations

$\frac{1}{2}$ replicate of a 2^5 factorial + star design + 6 points in the center.

x_1^*	x_2^*	x_3^*	x_4^*	x_5^*	Y^*	x_1^*	x_2^*	x_3^*	x_4^*	x_5^*	Y^*
-1	-1	-1	-1	1	6.285	-2	0	0	0	0	6.140
1	-1	-1	-1	-1	4.365	2	0	0	0	0	7.010
-1	1	-1	-1	-1	4.775	0	-2	0	0	0	5.565
1	1	-1	-1	1	7.820	0	2	0	0	0	6.534
-1	-1	1	-1	-1	4.565	0	0	-2	0	0	4.017
1	-1	1	-1	1	7.135	0	0	2	0	0	7.34
-1	1	1	-1	1	7.025	0	0	0	-2	0	5.573
1	1	1	-1	-1	6.085	0	0	0	2	0	4.525
-1	-1	-1	1	-1	3.215	0	0	0	0	-2	3.77
1	-1	-1	1	1	5.223	0	0	0	0	2	6.838
-1	1	-1	1	1	4.473	0	0	0	0	0	5.623
1	1	-1	1	-1	5.075	0	0	0	0	0	5.190
-1	-1	1	1	1	7.885	0	0	0	0	0	5.00
1	-1	1	1	-1	4.310	0	0	0	0	0	5.825
-1	1	1	1	-1	5.474	0	0	0	0	0	4.915
1	1	1	1	1	5.731	0	0	0	0	0	5.995

solutions

$$b_o = 0.159091(0\overset{*}{y}) - \Sigma 0.034091 \; (ii\overset{*}{y})$$

$$b_i = 0.041667(i\overset{*}{y})$$

$$b_{ii} = 0.031250(ii\overset{*}{y}) + 0.002841 \Sigma (ii\overset{*}{y}) - 0.034091(0\overset{*}{y})$$

$$b_{ij} = 0.0625(ij\overset{*}{y})$$

TABLE - 7

Central Composite Rotatable Design in Two

	Design		$\overset{*}{x}$-variables			
$\overset{*}{x}_0$	$\overset{*}{x}_1$	$\overset{*}{x}_2$	$\overset{*}{x}_1^2$	$\overset{*}{x}_2^2$	$\overset{*}{x}_1\overset{*}{x}_2$	$\overset{*}{Y}$
1	-1	-1	1	1	1	8.801
1	1	-1	1	1	-1	12.830
1	-1	1	1	1	-1	11.660
1	1	1	1	1	1	14.007
1	-1.414	0	2	0	0	8.690
1	1.414	0	2	0	0	11.965
1	0	-1.414	0	2	0	11.115
1	0	1.414	0	2	0	11.883
1	0	0	0	0	0	12.850
1	0	0	0	0	0	11.165
1	0	0	0	0	0	12.900
1	0	0	0	0	0	11.500
1	0	0	0	0	0	11.100

Solutions

$b_o = 0.2(0\overset{*}{Y}) - 0.1 \Sigma (ii\overset{*}{Y})$; where $\Sigma (ii\overset{*}{Y}) = (11\overset{*}{Y}) + (22\overset{*}{Y})$

$b_i = 0.125(i\overset{*}{Y})$

$b_{ii} = 0.125(ii\overset{*}{Y}) + 0.01875 \Sigma(ii\overset{*}{Y}) - 0.1(0\overset{*}{Y})$

$b_{ij} = 0.25(ij\overset{*}{Y})$

TABLE-8

Experimental Conditions for Results Given in Fig. 7.1

Initial interelectrode gap	0.5 mm
Width of work	40.0 mm
Length of work	140.0 mm
Electrolyte flow velocity	10.0 m/s (Fig.7.1B) 21.0 m/s (Fig.7.1A)
Electrolyte temperature at inlet	$(20 \pm 1)^\circ$ C
Electrolyte conductivity	0.013 $(\Omega\,\mathrm{mm})^{-1}$
Applied voltage	2.8 volts
Workpiece thickness	$(20.9 \pm 1\times10^{-2})$mm
Machining time	300 s
Concentration of electrolyte	11.0%
Surface temperature of electrodes	8° C
Feed rate	0.0 mm/s

TABLE-9

Machining Conditions Used for Computing Results in Fig.(7.5a)

Work material	Mild steel
F_F	= 0.015 mm/s
E_V	= 10.0 volts
Q	= 50.0×10^3 mm^3/s
ΔT	= 30 s
K_o	= 0.02 $\mho$ mm^{-1}

TABLE - 10

Machining Conditions Used for
Computing Results Given Below
(Fig. 7.5b)

E_V = 10.0 volts
F_F = 0.0 m/s
K_o = 0.01412 ℧ mm^{-1}
Q = 31.25 x 10^{-6} m^3/s
T_o = 30.0^oC
$\dot{m}$ = 7.87 x 10^3 kg/m^3

Sl. no.	Node No.	y_o (m)x10^{-3}	Interelectrode gap in m x10^{-3} after time				
			120 s	240 s	360 s	480 s	600 s
1	1	5.0	5.1238	5.2446	5.3627	5.4783	5.5915
2	4	5.0	5.1241	5.2452	5.3635	5.4793	5.5926
3	7	5.0	5.1247	5.2467	5.3657	5.4822	5.5962
4	10	7.25	7.3361	7.4213	7.5056	7.5889	7.6712
5	12	14.0	14.0446	14.0890	14.1332	14.1774	14.2214
6	15	7.0	7.0897	7.1782	7.2657	7.3522	7.4376
7	18	5.0	5.1257	5.2485	5.3684	5.4856	5.6003
8	20	5.0	5.1257	5.2485	5.3683	5.4855	5.6001
9	23	5.0	5.1283	5.2537	5.3761	5.4956	5.6123
10	26	7.5	7.5843	7.6678	7.7504	7.8321	7.9129
11	28	14.0	14.0446	14.0890	14.1333	14.1774	14.2214
12	31	6.5	6.5977	6.6941	6.7890	6.8826	6.9749
13	34	5.0	5.1276	5.2523	5.3738	5.4927	5.6089
14	36	5.0	5.1274	5.2516	5.3729	5.4914	5.6073
15	39	5.0	5.1275	5.2519	5.3733	5.4919	5.6080

TABLE - 11

Feed rate = 0.0, 0.02, 0.03, 0.04, 0.05, 0.06, 0.08, 0.10 (mm/s)

Electrolyte conductivity = 0.02 Ω^{-1} mm^{-1}

Temperature coefficient of specific electrical conductivity = 0.02/deg.C

Specific heat of the electrolyte = 4.18×10^{-3} watts/kg.^{o}C

Electrolyte density = 1.0×10^{3} kg/m^{3}

Work material density = 8.93×10^{3} kg/m^{3}

Electrochemical equivalent of work material. = 63.57×10^{-3} kg

Effective applied voltage = 10.0 volts

Faraday's constant = 96500.0 coulombs

Computation cycle time = 1.0 s

Initial temperature of electrolyte = 25.0^{o}C

Electrolyte flow velocity = 10.0, 9.0, 8.0, 7.0, 6.0, 5.0, 4.0 (m/s)

Initial inter-electrode gap = 0.2, 0.3, 0.4, 0.5, 0.6, 0.7, 0.8, 0.9, 1.0 (mm)

TABLE - 12

Mode of Electrolyte Flow - Outward

C_e	4.18×10^3 watts/kg.°C
F	96500.0 coulombs
F_F	0.00571 mm/sec
K_o	0.011 $(\Omega\,\text{mm})^{-1}$
T_o	30°C
Δt	30 s

Test Group	Test No.	Machined depth (mm)	$\bar{E}$ (volts)	$\bar{I}$ (Amperes)	η %
			$D_t=9.1$ mm, $r_c=0.13$ mm, $Q=140 \times 10^3$ mm^3/s		
	3	20.6	27	20.25	76.75
	4	14.9	52.7	20.6	92.20
	6	14.1	31.3	29.0	65.80
	8	12.8	8.7	17.7	84.15
I	9	9.1	30.0	20.0	55.6
	10	15.0	8.3	-	-
	11	21.5	26.0	19.2	102.60
	13	21.0	21.25	18.2	109.0
	14	23.9	16.5	21.1	95.3
			$D_t=9.04$ mm, $Q=110.0 \times 10^3$ mm^3/s, $r_c=0.13$mm		
	15	14.2	17.0	18.5	95.9
	16	12.0	11.3	19.5	96.8
	17	10.75	18.0	21.7	-
II	19	14.75	23.4	16.0	-
	20	15.38	25.6	18.25	99.0
	21	15.74	32.8	17.6	86.7
	22	12.3	40.75	18.0	-
	23	14.98	32.75	17.0	-

contd...

Test Group	Test No.	Machined depth (mm)	$\bar{E}_v$ (Volts)	$\bar{I}_c$ (Amperes)	η %
		D_t=10.5 mm, Q=110.0x10^3 mm^3/s, r_c=0.1 mm			
	24	7.8	5.5	20.0	77.56
	25	14.14	8.2	25.8	83.22
	26	14.24	15.0	25.4	-
III	27	13.16	15.8	25.0	83.51
	28	15.0	17.6	29.4	-
	29	15.04	24.2	35.0	-
	30	14.88	22.8	37.0	-
	31	15.8	28.0	34.5	-
		D_t=7.36 mm, Q=110.0x10^3 mm^3/s, r_c=0.19 mm			
	28A	14.8	36.8	16.6	87.8
	29A	15.84	33.6	17.4	90.0
	30A	15.5	24.6	16.0	101.2
IV	31A	14.36	30.2	17.2	86.0
	36	10.8	18.0	12.0	115.85
	37	16.12	12.0	13.0	98.1
	39	15.34	21.0	13.2	95.5
		D_t=7.7 mm, Q=120.12x10^3 mm^3/s, r_c=0.17 mm			
	3A	14.5	15.0	12.0	98.15
	25A	12.0	10.0	12.2	91.8
	26A	13.5	6.5	12.75	69.8
	27A	14.5	23.6	14.1	97.8
V	32	14.50	28.0	15.4	95.6
	33	13.2	20.0	13.0	106.1
	40	14.7	12.4	-	126.5
	41	13.9	32.4	-	95.75
	42	12.5	37.0	16.0	99.9

contd...

Test Group	Test No.	Machined depth (mm)	$\overline{E}_v$ (volts)	$\overline{I}_c$ (Amperes)	η %
			D_t=10.13 mm, Q=121.12x10^3 mm^3/s, r_c=0.1 mm		
	43	8.24	8.5	16.0	91.2
	44	13.5	14.0	19.0	100.0
	45	10.5	7.0	20.0	78.16
	46	14.32	14.5	25.0	83.6
VI	47	15.10	22.5	25.5	92.1
	48	9.16	17.8	27.2	84.1
	49	12.7	22.6	28.86	99.4
	50	9.2	32.25	21.0	100.8
			D_t=11.63 mm, Q=120.0x10^3 mm^3/s, r_c=0.1 mm		
	51	14.14	10.3	26.3	97.5
	53	14.08	16.0	31.8	92.6
	54	14.6	19.0	30.0	101.60
	55	5.5	18.0	23.75	88.6
VII	56	14.0	20.6	32.5	86.0
	57	12.6	23.0	-	-
	59	11.0	5.8	21.6	82.7
			D_t=9.17 mm, Q=120.0x10^3 mm^3/s, r_c=0.13 mm		
	61	16.28	12.0	17.0	102.6
	62	13.3	9.8	24.3	80.10
	64	14.2	16.5	24.4	89.8
VIII	65	14.36	20.7	26.2	75.8
	66	12.34	6.0	22.0	59.1
	67	13.4	23.0	18.0	98.15
	68	13.0	31.5	23.0	78.7
	70	14.0	20.0	28.5	68.0

contd...

Test Group	Test No.	Machined depth (mm)	$\overline{E}_v$ (volts)	$\vec{I}_c$ (Amperes)	η%
		$D_t=9.15$ mm, $Q=40.0\times10^3$ mm^3/s, $r_c=0.13$ mm			
IX	63	13.5	13.8	22.9	96.7
	69	13.4	12.75	-	-
	71	11.8	6.0	23.0	90.6
	72	14.2	9.8	27.0	62.8
	75	14.0	11.0	15.0	88.0
	76	13.5	18.3	22.4	92.33
	77	13.2	24.0	24.2	84.87
		$D_t=11.0$ mm, $Q=90.0\times10^3$ mm^3/s, $r_c=0.1$ mm			
X	79	14.0	6.0	22.5	96.1
	81	15.0	17.0	34.5	82.8
	82	14.7	15.6	37.2	93.0
	83	13.4	14.0	26.0	81.5
	84	14.7	13.0	23.3	87.7
	85	14.5	16.6	38.0	77.9
	86	14.2	10.0	17.0	112.4
	87	13.5	24.0	39.0	67.4
		$D_t=10.0$ mm, $Q=90.0\times10^3$ mm^3/s, $r_c=0.13$			
XI	88	11.5	8.0	17.6	77.5
	91	14.0	14.5	25.0	76.4
	92	13.6	13.0	20.0	97.7
	93	13.7	21.5	23.0	97.4
	94	15.2	21.0	20.75	87.2
	96	14.5	27.0	24.5	91.2
	97	13.7	22.2	28.0	67.2
		$D_t=7.62$ mm, $Q=90.0\times10^3$ mm^3/s, $r_c=0.2$ mm			
XII	98	14.4	10.25	15.5	92.7

.. ..

TABLE - 13

Experimental Conditions Used During ECD of Cast low alloy steel

F_F = 0.00571 mm/s, Y_0 = 1.0 mm

Workpiece No.	$\bar{K}(\mho\, mm^{-1})$	$\bar{E}_v^*$ (Volts)	$\bar{I}_c$ (Amperes)	η%
Tool-1, $\bar{r}_t$= 3.79 mm, $\bar{r}_c$= 1.246 mm, V=5.69 m/s				
201	0.00790	14.348	12.52	83.70
413	0.00725	17.75	13.1	90.15
408	0.00725	15.31	16.24	91.70
409	0.00725	21.84	14.14	95.00
406	0.00725	12.94	13.28	86.9
Tool-2, $\bar{r}_t$= 3.783 mm, $\bar{r}_c$=1.43 mm, V = 5.70 m/s				
414	0.00655	13.78	13.62	98.68
203	0.00680	15.58	13.40	99.40
202	0.00640	18.94	10.54	89.75
411	0.00640	17.30	12.90	96.9
Tool-3, $\bar{r}_t$= 4.54 mm, $\bar{r}_c$= 1.57 mm, V = 5.263 m/s				
407	0.0063	12.93	15.0	93.15
421	0.0070	14.89	16.4	96.20
424	0.0060	18.5	19.86	92.0
425	0.0066	20.49	18.80	91.86
Tool-4, $\bar{r}_t$= 5.03 mm, $\bar{r}_c$= 2.13 mm, V = 5.37 m/s				
429	0.0060	11.57	18.53	94.0
401	0.00547	12.975	22.15	91.82
418	0.00532	15.95	18.4	92.5
427	0.00532	17.62	-	-
402	0.006000	15.87	18.4	93.7
Tool-5, $\bar{r}_t$=6.03 mm, $\bar{r}_c$= 4.51 mm, V = 4.56 m/s				
423	0.00600	11.53	18.24	87.17
431	0.00600	11.30	18.04	88.7

*Overpotential is inclusive.

TABLE - 14

Experimental Conditions Used During ECBD and ECB of Forged Low Alloy Steel

$K = 0.007 \mho\, mm^{-1}$, $Y_o = 1.0$ mm, $A_V = 15.0$ V

Work-piece No.	$\bar{E}_V^*$	I_c	F_F mm/s(x10^{-3})	$\bar{r}_t$ (mm)	$\bar{r}_c$ (mm)	b_b (mm)	t (s)
707	6.54	20.46	6.19	6.03	2.386	5.22	2100
637	7.64	17.17	6.19	5.52	1.500	3.80	2400
717	6.88	16.34	5.33	5.52	1.500	3.80	2400
728	7.24	14.3	4.5	5.52	1.500	3.80	2400
718	8.23	11.4	3.7	5.52	1.500	3.80	2400
705	6.62	13.16	3.0	8.85	Sharp corner	3.94	2400
736	6.4	19.98	3.0	8.85	"	3.94	1440
620	5.07	22.8	3.7	8.85	"	3.04	2400
627	3.88	25.675	3.7	8.92	"	5.02	2400
628	4.27	23.3	4.5	8.92	"	5.90	1260
724	8.52	12.66	3.7	6.03	2.386	5.22	2400
709	10.08	11.16	4.5	6.03	2.386	5.22	1620
737	7.325	16.49	4.5	6.03	2.386	5.22	2160
708	6.034	17.22	3.7	6.03	2.386	5.22	2400
736	6.47	15.75	4.5	6.0	Sharp corner	2	2400
721	6.18	17.025	5.33	6.0	"	3	2400
726	8.88	10.98	3.70	6.0	"	3	900
725	7.55	13.80	3.70	6.0	"	3	2400
619	7.58	12.54	3.00	6.0	"	4	2400
635	7.36	17.7	4.50	6.0	"	4	2400
719	7.18	15.775	4.50	6.0	"	4	2400
734	6.23	20.36	6.18	6.0	"	4	2400
729	7.09	16.09	3.7	6.0	"	5	2400
735	6.75	19.41	5.33	6.0	"	5	2400
733	7.60	16.70	4.50	6.0	"	6	2400
413	8.07	12.793	4.50	5.5	"	2	1800
406	7.30	13.66	4.50	5.5	"	2	2400
414	6.3	15.77	5.33	5.5	"	3	2400
424	6.77	15.07	6.18	5.5	"	3	2400
427	8.23	13.4	4.5	5.5	"	3	2400

*Overpotential is inclusive.

APPENDIX-II

```
C         COMPUTER PROGRAM DEVELOPED BY JAIN

C         MAIN
C***      ØMEAN ALPHABETIC LETTER'O'***
1000      CALL DATIN
          IF(EV.EQ.Q.0) GØ TØ 9998
          IPATH=1
          INN1 = INN+1
          AJI=EV*AKI/YI
          IF(IPPE.LT.1)GØ TØ 301
          CALL AGNC
C
301       CØNTINUE
          IF(CIRCL.EQ.1.0) W=PI*(R1+(YI/2.))
          CALL INIT
          CALL AGCSM
          IF(IOW)38,39,38
C
39        KNN=INN+2*KADD
          GØ TØ 57
C
38        KNN=INN+KADD

57        SA=0.0
          NC=NTST/KSTC
          XEM=X(2)-X(1)
          XTØT=0.0
          DØ 160 KIN=1,NC
          EV=EVV(KIN)
C
          NN=KNN
          NE=KNN-1
          XTØT=XTØT+A*AKSTC
          KNE=KNN-1
          JJ=KIN-1
C
          CALL REVEC
          CALL GET
          AKSTC=KSTC
          DØ 150 I=1,KNN
          TA(I)=TI+T(I)
          AK(I)=AKI*(1.0+(ALF*T(I)))
          YYY=Y(I)
          KKK=KNN-INN
          IF(IOW) 651,652,651
C
652       I11=(KNN-INN)/2
          I13=I11+INN
C
651       CØNTINUE
          IF(IOW)777,886,888
```

```
886        IF(I-I11)55,55,556
556        IF(I-I13) 1,1,55
888        IF(I-INN) 1,1,55
777        IF(I-KKK) 55,55,1
55         CALL ZEFR
           GØ TØ 149
1          CALL BIR
C
149        CØNTINUE
           WY=PI*(R1+(Y(I)/2.))
           AV(I)=Q/(WY*Y(I))
           AJ(I)=EV*AK(I)/Y(I)
           IF(KIN-1) 904,904,905
           FPYT(I)=Y(I)
905        AMRR(I)=A*AKSTC+Y(I)-FPYT(I)
           GØ TØ 600
904        AMRR(I)=A*AKSTC+Y(I)-YI
600        CØNTINUE
150        CØNTINUE
           IF(W) 601,601,603
603        DØ 606 J=1,KNE
           IF(CIRCL.EQ.1.0) TØ TØ 7
           AMRV(J)=W*(AMRR(J)+AMRR
         1 (J+1)*((X(J+1)-X(J))/2.)
           GØ TØ 8

7          YMV=(Y(J+1)+Y(J))/2.
           RIS=R1**2
           AMRV(J)=1.5708*(YMV**2-RIS)*
         1 (X(J+1)-X(J))
C
606        CØNTINUE
601        CØNTINUE
3          CALL PRNTOT
6          SA=SA+A*AKSTC
           IF(SA-XEM) 1311, 312,312
312        KNN=KNN+1
           IF(IOW) 3131,314,313
314        CALL SIDFLO
           GØ TØ 3141
313        CALL OUTFLO
3131       CØNTINUE
3141       SA=0.0
1311       CØNTINUE
           DØ 160 L=NN,KNN
           WY=PI*((Y(L)/2.)+R1)
           AV(L)=Q/(WY*Y(L))
           X(L)=X(L-1)+XEM
160        CØNTINUE
           GØ TØ 1000
9998       CØNTINUE
           STØP
           END
```

```
          SUBROUTINE AGNC
          X(1)=0.0
          IF(AND)15,15,25
25        X(2)=AIE/AND
          GØ TØ 70
15        X(2)=X(1)+AIE
70        CØNTINUE
          DØ 60 J=3,NN
          KN=J-1
          IF(J-NNSD) 1,1,2
C
1         X(J)=X(KN)+(AIE*AM/AND)
          GØ TØ 60
2         X(J)=X(KN)+AIE
60        CØNTINUE
          RETURN
          END

          SUBROUTINE AGCSM
          SK(I,1)=1.0
          SK(I,2)=0.0
          SK(NN,1)=1.0
          SK(NN,2)=0.0
          JJ=NN-1
C
          DØ52 I=2,JJ
          SK(I,1)=2.0
          SK(I,2)=-1.0
52        CØNTINUE
          RETURN
          END

          SUBROUTINE REVEC

          DØ 30 I=1,NE
          V=AV(I)
14        IF(CIRCL.LT.1.0)GØTØ12
          IF(IOW)777,886,888
886       IF(I-I11) 55,55,556
556       IF(I-I13) 12,12,55
888       IF(I-INN) 12,12,55
777       CØNTINUE
55        R2=Y(I)+R1
C
          H(I)=((EV**2*AK(I)*(X(I+1)-X(I))*
        1 PI)/ALØG(R2/R1)))
          D(I)=2.0/((PI)*(R2**2-R1**)*V*DE*C)
          GØ TØ 13
C
12        H(I)=(EV*EV*AK(I)*(X(I+1)-X(I)))/Y(I)
          D(I)=1.0/(Y(I)*DE*V*C)
11        H(I)=H(I)*D(I)
30        CØNTINUE
```

```
          N1=NN-1
          DØ 50 I=2,N1
          J=I-1
          HM(I)=H(J)-H(I)
50        CØNTINUE
          HM(1)=0.0
          HM(NN)=H(N1)
          RETURN
          END

          SUBROUTINE BIR

          CHEK=0.00000001
1         NPATH=1
          AYT=Y(I)
          BINT=SINT
          J=1
          A=Z(I)
          YE=EV*E*AK(I)*ETA/(F*DW*A)
C
          IF(YSUG.GE.1.0)GØ TØ 188
          IF((YE-AYT).EQ.0.0)GØ TØ 199
2         AA=Y(I)-AYT+(YE*AIØG((YE-Y(I))/
     1    (YE-AYT)))-A*AKSTC
          GØ TØ 3
199       AA=Y(I)-AYT-A*AKSTC
3         IF(YE-AYT) 91,91,331
91        BYT=AYT-BINT
          IF(YE-BYT) 65,63,65
65        CHEN=YE(YE-Y(I))/(YE-BYT)
          IF(CHEN) 63,63,64
63        BINT=BINT/2.
          IF(BINT.LT.CHEK) GØ TØ 64
          GØ TØ 91
C
64        CØNTINUE
          GØ TØ 56
331       BYT=AYT+BINT
          IF(YE-BYT) 66,61,66
66        CHEP=(YE-Y(I))/(YE-BYT)
          IF(CHEP) 61,61,62
C
61        BINT=BINT/2.
          IF(BINT.LT.CHEK) GØ TØ 62
          GØ TØ 331
62        CØNTINUE
56        CØNTINUE
          IF((YE-BYT).EQ.0.0) GØ TØ 666
          IF(((YE-Y(I))/(YE-BYT)).LE.0.0) GØ TØ 666

          BB=Y(I)-BYT+(YE*AALØG((YE-Y(I)))/
     1       (YE-BYT)))-A*AKSTC
          GØ TØ 667
```

```
C
666         BB=Y(I)-BYT-A*AKSTC
667         J=J+1
            IF(J-100) 9,9,12
9           IF(AA*BB) 5,5,4
4           AYT=BYT
            AA=BB
            IF(BINT.LT.CHEK) GØ TØ 13
            GØ TØ (3,5), NPATH
C
5           BINT=BINT/2.
            NPATH=2
            IF(BINT-EPS) 11,11,3
11          CØNTINUE

            IF(AA*BB) 900,900,901
900         CC=ABS(AA)+ABS(BB)
            RA=ABS(AA)/ABS(CC)
            Y(I)=AYT+RA*BINT
            GØ TØ 9999
C
901         IF(AA-BB) 903,903,902
902         Y(I)=BYT
            GØ TØ 9999
903         Y(I)=AYT
            CYE(I)=Y(I)/YE
188         Y(I)=Y(I)+((E*EV*AK(I)*ETA)/
     1      (F*DW*Y(I))-A)*AKSTC

9999        CØNTINUE
            RETURN
            END

            SUBROUTINE GET

            DØ 70 I=1,NN
            DØ 70 J=1,KBH
            A(I,J)=S(I,J)
70          CØNTINUE
            NBH=KBH-1
            N1=N-1
            DØ 40 I=1,N1
            II=I+1
            IF(A(I,1)) 11,96,11
11          RATIO=1./A(I,1)
            IHR=I+NBH
            IF(IHR-NN) 14,14,13
13          IHR=NN
14          DØ 30 J=II,IHR
            L=J-I+1
            B(J)=B(J)-A(I,L)*B(I)*RATIO
            DØ 20 K=1,NBH
            JK=J+K-1
            IF(JK-N) 15,15,20
```

```
15      M=J-I+K
        IF(M-KBH) 16,16,20
16      TERM=A(I,L)*A(I,M)*RATIO
        A(J,K)=A(J,K)-TERM
        DIF=10000.0*ABS(A(J,K))-ABS(TERM)
        IF(DIF) 18,18,20
18      A(J,K)=0
20      CØNTINUE
30      CØNTINUE
40      CØNTINUE
        IF(A(N,1)) 41,96,41
C
41      X(N)=B(N)/A(N,1)
        DØ 60 L=1,N1
        I=N-L
        X(I)=B(I)
        DØ 50 M=2,KBH
        K=I+M-1
        IF(K-N) 46,46,50
46      X(I)=X(I)-A(I,M)*X(K)
50      CØNTINUE
        X(I)=X(I)/A(I,1)
60      CØNTINUE
        RETURN
96      PRINT 97
97      FØRMAT (10X,11HNO SOLUTION)
        RETURN
        END
```

```
C     MAIN

C     MODEL FET-22
C     THIS PROGRAMME HAS BEEN RUN ON IBM 370 AT ONGC DEHRADUN (INDIA)
C     * * * *   *  *  *   *  *  * *
C     *Ø - MEAN ALPHABETIC LETTER O*
C     *  * * *  *    *  * * * * *  *

      SINT=0.004
      EPS=0.00001

 1000 CALL DATIN
      IF(EV.EQ.0.0) GØ TØ 9998
      AKSTC=KSTC
      NC=NTST/KSTC
      DØ 110 I1=1,NNW
      YII(IW(T1) )=Y(IW(I1))
      AK(IW(I1) )=AKI
      AV(IW(I1))=Q/(W*Y(IW(I1)))

  110 CØNTINUE
      XTØT=0.0
      ZZ=Z
      DØ 150 KIN=1,NC
      XTØT=XTØT+ZZ*AKSTC
      CALL BWD
      CALL ZER
      IF(KIN.EQ.1)GØ TØ 4
      DØ 3 I1=1,NNW
      Y(IT(I1))=Y(IW(I1))/2.

    3 CØNTINUE

    4 CØNTINUE

      KTC=KIN*KSTC
      CALL AGCSG
      CALL ABC
      CALL BANSØL
      CALL CDTC
      CALL INELGP
      CAL METR
      CALL PRINTOT
  150 CØNTINUE
      GØ TØ 1000

 9998 CØNTINUE
      STØP
      END
```

```
C     * * * Ø MEAN ALPHABETIC LETTER 'O'
      SUBROUTINE ABC
      KF=MB-1
      DØ 300 K=1,NNUS
      N5=IBC(K)
      DØ 400 K= 1,KF
      IR=N5-K1
      IF(IR.LT.1) GØ TØ 450
      B(IR)=B(IR)-A(IR,(K1+1))*VIBC(K)
      A(IR,(K1+1))=0.0

  450 IR=N5+K1
      IF(IR.GT.NN) GØ TØ 400
      B(IR)=B(IR)-A(N5,(K1+1))*VIBC(K)
      A(N5,(K1+1))=0.0

  400 CØNTINUE
      A(N5,1)=1
      B(N5)=VIBC(K)

  300 CØNTINUE
      RETURN
      END

      SUBROUTINE AGCSG
      DØ 101 K=1,NE
      DELT=(X(I(K,2))*Y(I(K,3))+X(I(K,1))*Y(I(K,2))
     1 +X(I(K,3))*Y(I(K,1)))-(X(I(K,2))*Y(I(K,1))
     2 +X(I(K,3))*Y(I(K,2))+X(I(K,1))*Y(I(K,3)))
      B1=(Y(I(K,2))-Y(I(K,3)))/DELT
      B2=(Y(I(K,3))-Y(I(K,1)))/DELT
      B3=(Y(I(K,1))-Y(I(K,2)))/DELT
      A1=(X(I(K,3))-X(I(K,2)))/DELT
      A2=(X(I(K,1))-X(I(K,3)))/DELT
      A3=(X(I(K,2))-X(I(K,1)))/DELT
      S(1,1)=(B1*B1+A1*A1)*DELT/2.0
      S(1,2)=(B2*B1+A2*A1)*DELT/2.0
      S(1,3)=(B3*B1+A3*A1)*DELT/2.0
      S(2,2)=(B2*B2+A2*A2)*DELT/2.0
      S(3,3)=(B3*B3+A3*A3)*DELT/2.0
      S(2,1)=S(1,2)
      S(3,1)=S(1,3)
      S(3,2)=S(2,3)
      DØ200 IM=1,3
      IR=I(K,IM)
      DØ200 IN=1,3
      IC=I(K,IN)
      ID=IC-(IR-1)
      IF(ID.LT.1) GØ TØ 200
      A(IR,ID)=A(IR,ID)+S(IM,IN)
```

```
200   CØNTINUE
101   CØNTINUE
      RETURN
      END

      SUBRØUTINE BANSØL
      N=NN
      DØ10 K=1,NN
      B(K)=B(K)/A(K,1)
      IF(K.EQ.N) GØ TØ 100
      DØ 20 J=2,MB
      C(J)=A(K,J)
      A(K,J)=A(K,J)/A(K,1)

 20   CØNTINUE
      DØ 30 L=2,MB
      I=K+L-1
      IF(N.LT.I) GØ TØ 30
      J=0
      DØ 40 LL=L,MB
      J=J+1
      A(I,J)=A(I,J)-C(L)*A(K,LL)

 40   CØNTINUE
      B(I)=B(I)-C(L)*B(K)

 30   CØNTINUE

 10   CØNTINUE

100   K=K-1
      IF(K.EQ.0) GØ TØ 200
      DØ 50 J=2,MB
      L=K+J-1
      IF(N.LT.L) GØ TØ 50
      B(K)=B(K)-A(K,J)*B(L)
 50   CØNTINUE
      GØ TØ 100

200   CØNTINUE
      RETURN
      END

      SUBROUTINE BWD
      IX=0
      DØ 100 K=1,NE
      IY1=IABS(I(K,1)-I(K,2))
      IY2=IABS(I(K,2)-I(K,3))
      IY3=IABS(I(K,3)-I(K,1))
      IF(IY1.GE.IY2.AND.IY1.GE.IY3) IY=IY1
      IF(IY2.GE.IY3.AND.IY2.GE.IY1) IY=IY2
      IF(IY3.GE.IY1.AND.IY3.GE.IY2) IY=IY3

100   IF(IY.GT.IX) IX=IY
      MB=IX+1
      RETURN
      END
      SUBROUTINE CDTC

      DØ10 I1=1,NNW
      IF(I1.EQ.NNW) GØ TØ 12
      I2=I1+1
      AC=(Y(IT(I2))-Y(IT(I1)))
      BC=(X(IT(I1))-X(IT(I2)))
      CC=-X(IT(I1))*AC-Y(IT(I1))*BC
      DELN=ABS((AC*X(IW(I1))+BC*Y(IW(I1))+CC)/SQRT(AC**2+BC**2))
      IF(I1.EQ.1) AK(IW(I1-1))=AKI

 12   AJ(IW(I1))=((B(IW(I1))-B(IT(I1)))/DELN)*
     1AK(IW(I1-1))

 10   CØNTINUE
      DØ15 I1=1,NNW
      V=AV(IW(I1))
      TAA=(AJ(IW(I1))**2)/(DE*V*C*AK(IW(I1)))
      EXI=EXP(TAA*ALF*(X(IW(I1))-X(IW(I1))))
      T(IW(I1))=(EXI-1.)/ALF
      TA(IW(I1))=T(TI+T(IW(I1))
      AK(IW(I1))=AKI*(1.0+ALF*T(IW(I1)))
 15   CØNTINUE
      RETURN
      END
      SUBROUTINE INELGP
      AKSTC=KSTC
      DØ 100 I1=1,NNW
      IND=IW(I1)
      Z=AZ(IW(I1))
      IF(Z),1,55,1

 55   BT=E*EV*AK(IW(I1))/(F*DW)
      IF(YSUG.GE.1.0) GØ TØ 186
      Y(IW(I1))=SQRT(Y(IW(I1))**2+2.*BT*AKSTC)
      GØ TØ 8888

  1   NPATH=1
      IF(YSUG.GE.1.0) GØ TØ 186
      AYT=Y(IW(I1))
      BINT=SINT
      J=1
      YE=EV*E*AK(IW(I1))/(F*DW*Z)
      EY(IW(I1))=YE

  2   AA=Y(IW(I1))-AYT+(YE*ALØG((YE-Y(IW(I1)))/(YE-AYT)))-Z*AKSTC

  3   IF(YE-AYT) 91,91,33

 91   BYT=AYT-BINT
      IF(YE-BYT) 65,163,65

 65   CHEN=(YE-Y(IW(I1)))/(YE-BYT)
      IF(CHEN) 163, 163, 64
```

```
163  BINT=BINT/2.
     GØ TØ 91

 64  CØNTINUE

     GØ TØ 56

 33  BYT=AYT+BINT
     IF(YE-BYT) 66,61,66

 66  CHEP=(YE-Y(IW(I1)))/(YE-BYT)
     IF(CHEP) 61, 61, 62

 61  BINT=BINT/2.
     GØ TØ  33

 62  CØNTINUE

 56  BB=Y(IW(I1))-BYT+(YE*ALØG((YE-Y(IW(I1)))/(YE-BYT))-Z*AKSTC

667  J=J+1
     IF(J-100) 9,9,12

  9  IF(AA*BB) 5,5,4

  4  AYT=BYT
     AA=BB
     GØ TØ (3,5), NPATH

  5  BINT=BINT/2.0
     NPATH=2
     IF(BINT-EPS) 11,11,3

 11  CØNTINUE
     GØ TØ 19

 12  PRINT 994

994  FØRMAT (10X, 18HWRONG VALUE ØF GYT)

 19  CØNTINUE
     IF(AA*BB) 900,900,901

900  CC=ABS(AA)+ABS(BB)
     RA=ABS(AA)/ABS(CC)
     Y(IW(I1))=AYT+RA*BINT
     GØ TØ 9999

901  IF(AA-BB) 903,903,902

902  Y(IW(I1))=BYT
     GØ TØ 9999

903  Y(IW(I1))=AYT
     GØ TØ 9999
 186  Y(IND)=Y(IND)+((E*FV*AK(IND))/(Y(IND)*F*DW)-Z)*AKSTC
      GØ TØ 8888

9999  CØNTINUE

8888  AV(IW(I1))=Q/(W*Y(IW(I1)))

 100  CØNTINUE
      RETURN
      END

      SUBROUTINE METR
      DØ 4 I1=1,NNW
      Z=AZ(IW(I1))
      IF(KIN.GT.1) GØ TØ 5
      AMRR(IW(I1))=Z*AKSTC+Y(IW(I1))-YII(IW(I1))
      GØ TØ 41

   5  AMRR(IW(I1))=Z*AKSTC+Y(IW(I1))-FPY(IW(I1))

  41  CØNTINUE
      FPY(IW(I1))=Y(IW(I1))

   4  CØNTINUE
      DØ 6 I1=1,NELW
      AMRV(IW(I1))=W*(AMRR(IW(I1))+AMRR(IW(I1+1)))*((X(IW(I1+1))-X(IW(I1)))/2.)
      SMRR(IW(I1))=AMRV(IW(I1))/((AJ(IW(I1+1))+AJ(IW(I1)))/2.)

      RETURN
      END
```

APPENDIX - 3

ANALYSIS OF OVERCUT IN TRANSITION ZONE

Due to low correlation coefficient (0.8 or less) obtained during regression analysis dimensional analysis was conducted to formulate a relationship between the overcut in transition zone (a_o) and the variables that govern its magnitude. The relevant variables and their dimensions have been listed in chapter-3. The dimensionless groups π_1 and π_2 corresponding to the variables are:

$$\pi_1 = a_o(r_c)^a(V)^b \qquad .. \qquad (A.1)$$

$$\pi_2 = \left(\frac{Y_e F_F}{D}\right)(r_c)^c(V)^d \qquad .. \qquad (A.2)$$

Solving for a,b,c and d leads to following relationships:

$$\pi_1 = (a_o/r_c) \qquad .. \qquad (A.3)$$

$$\pi_2 = (Y_e F_F/DV) \qquad .. \qquad (A.4)$$

Relationship between π_1 and π_2 has been assumed as follows:

$$\pi_1 = f(\pi_2) \qquad .. \qquad (A.5)$$

Values of π_1 and π_2 have been plotted in Fig. 7.21 but on account of large scatter it was not possible to evaluate the nature of functional relationship between them. Therefore, π_1 and π_2 for tools having different diameters, were plotted (Fig. 7.22A and 7.22B). Wherefrom the following power law equation has been derived.

$$\left(\frac{a_o}{r_c} \right) = C'_d \left(\frac{Y F_F}{.D} \right)^{n_1} \qquad (A.6)$$

CENT OF ROORKEE

From Fig. 7.22, it is evident that

(i) Value of n_1 is found to be almost constant for a specified combination of tool-work materials and different machining conditions.

(ii) Value of a constant C'_d for a combination of tool-work material differs when tools of different diameters are employed.

It is evident (Fig. 7.22) that power law Eq(A.6) is closely obeyed by experimental results however, few deviations are apparent.

It can thus be concluded that the tool diameter D, has got an independent effect on a_o in Eq(A.6). To evaluate this effect of tool diameter D on (a_o/r_c), Fig. 7.22C has been plotted showing a relationship between the tool diameter D and the constant C'_d given by Eq(A.6); this yields Eq(A.7)

$$C'_d = C_d (D)^{n'_2} \qquad .. \qquad (A.7)$$

Substitute the value of C'_d from Eq(A.7) in Eq(A.6), we obtain,

$$\left(\frac{a_o}{r_c} \right) = C_d \left(\frac{Y_e F_F}{VD} \right)^{n_1} D^{n'_2}$$

or

$$\left(\frac{a_o}{r_c} \right) = C_d \left(\frac{Y_e F_F}{V} \right)^{n_1} D^{n_2} \qquad .. \qquad (A.8)$$

where $n_2 = n'_2 - n_1$

Now (a_o/r_c) and $(Y_e F_F/V)^{n_1} D^{n_2}$ have been plotted in Fig. 7.22D and better correlation has been observed, thus validating ~~the~~ Eq(A.8).

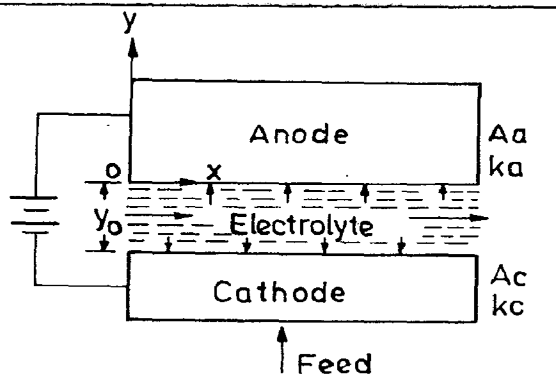
y
Anode
Aa
ka
o
x
y_o
Electrolyte
Cathode
Ac
kc
Feed

SCHEMATIC DIAGRAM OF ECM PROCESS

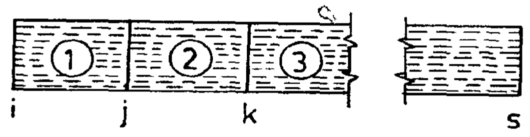

INTERELECTRODE GAP AS AN UNIDIMENSIONAL CONTINUM

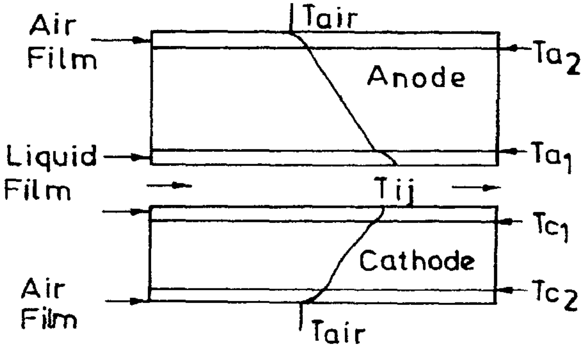
Air Film
Tair
Anode
T_{a2}
Liquid Film
T_{a1}
Tij
T_{c1}
Cathode
Air Film
T_{c2}
Tair

TEMPERATURE GRADIENT IN TOOL WORK ELECTROLYTE SYSTEM

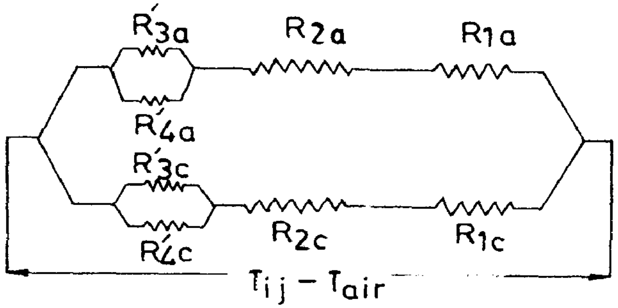
R'_{3a}
R_{2a}
R_{1a}
R'_{4a}
R'_{3c}
R'_{4c}
R_{2c}
R_{1c}
$T_{ij} - T_{air}$

THERMAL RESISTANCE MODEL OF IEG IN ECM

FIG. 3.6

Let $*q_a$ and $*q_c$ be the heat transferred from anode and cathode respectively to the air. It can then be shown (73,93) that heat transferred through anode, $*q_a$, would be equal to

$$*q_a = \frac{(T_{ij} - T_{air})}{*R_a} \quad .. \qquad (3.14)$$

where,

$$*R_a = *R_{1a} + *R_{2a} + *R_{3a} = \frac{1}{A_a}\left[\frac{1}{h_{fa}} + \frac{1}{k_a}\right] + \left(\frac{R'_{3a} \cdot R'_{4a}}{R'_{3a} + R'_{4a}}\right) \qquad (3.14a)$$

Also,

$$R'_{3a} = \frac{1}{A_a \cdot h_{na}} \text{ and } R'_{4a} = \frac{(T_{a2} - T_{air})}{A_a\, \epsilon_a\, \sigma^*_a F_a\, (T'_{a2} - T'_{air})} \qquad (3.14b)$$

where,

T'_{a2} and T'_{air} are the temperatures in Kelvin. Similarly, heat transferred through cathode to the atmosphere is obtained as follows:

$$*q_c = \frac{(T_{ij} - T_{air})}{*R_c} \quad .. \qquad (3.15)$$

where,

$$*R_c = *R_{1c} + *R_{2c} + *R_{3c} = \frac{1}{A_c}\left[\frac{1}{h_{fc}} + \frac{1}{k_c}\right] + \left(\frac{R'_{3c} \cdot R'_{4c}}{R'_{3c} + R'_{4c}}\right) \qquad (3.15a)$$

Also,

$$R'_{3c} = \frac{1}{A_c\, h_{nc}} \text{ and } R'_{4c} = \frac{(T_{c2} - T_{air})}{A_c\, \epsilon_c\, \sigma^*_c \cdot F_c (T'_{c2} - T'_{air})} \qquad (3.15b)$$

The thermal conductance k_a and k_c of electrodes is a function of the temperature and can be evaluated from Eq(3.16).

$$k_a = k_{ao}\,(1 + \alpha'_a \Delta T) \quad .. \qquad (3.16)$$